THE EFFECT OF COMPRESSION RATIO ON THE PERFORMANCE OF A DIRECT INJECTION DIESEL ENGINE

A Thesis submitted for the degree of Doctor of Philosophy

by

Razmik Aivaz Balian

Department of Mechanical Engineering, Brunel University, Uxbridge

March 1990

Brunel University
Uxbridge
Department of Mechanical Engineering

Razmik Aivaz Balian

The Effect of Compression Ratio on the Performance of a Direct Injection Diesel Engine

March 1990

ABSTRACT

This thesis considers the effect of compression ratio on the performance of a direct injection diesel engine.

One aspect of engine performance is considered in great detail, namely the combustion performance at increased clearance volume. This aspect was of particular interest because variable compression ratio (VCR) systems normally operate by varying the clearance volume.

The investigation relied upon results obtained both from experimental and computer simulating models. The experimental tests were carried out using a single-cylinder direct-injection diesel engine, under simulated turbocharged conditions at a reduced compression ratio. A number of one-dimensional computer models were developed; these simulate the induction and compression strokes, and the fuel spray trajectories in the presence of air swirl.

The major objectives of the investigation were: to assess the benefits of VCR in terms of improvements in output power and fuel economy; to assess the effects on combustion of increased clearance volume, and investigate methods for ameliorating resulting problems; develop computational models which could aid understanding of the combustion process under varying clearance volume conditions.

It was concluded that at the reduced compression ratio of 12.9:1 (compared to the standard value of 17.4:1 for the naturally-aspirated engine), brake mean effective pressure (BMEP) could be increased by more than 50%, and the brake specific fuel consumption (BSFC) could be reduced by more than 20%. These improvements were achieved without the maximum cylinder pressure or engine temperatures exceeding the highest values for the standard engine. Combustion performance deteriorated markedly, but certain modifications to the injection system proved successful in ameliorating the problems. These included: increase in the number of injector nozzle holes from 3 to 4, increase in injection rate by about 28%, advancing injection timing by about 6°CA. In addition, operation with weaker air fuel ratio, in the range of 30 to 40:1 reduced smoke emissions and improved BSFC.

Use of intercooling under VCR conditions provided only modest gains in performance.

The NO_x emission was found to be insensitive to engine operating conditions (fixed compression ratio of 12.9:1), as long as the peak cylinder pressure was maintained constant.

Engine test results were used in order to assess the accuracy of four published correlations for predicting ignition delay. The best prediction of ignition delay with these correlations deviated by up to 50% from the measured values.

The computer simulation models provided useful insights into the fuel distribution within the engine cylinder. It also became possible to quantify the interaction between the swirling air and the fuel sprays, using two parameters: the crosswind and impingement velocities of the fuel spray when it impinges on the piston-bowl walls. Tentative trends were identified which showed that high crosswind velocity coincided with lower smoke emissions and lower BSFC.

ACKNOWLEDGEMENTS

The author wishes to acknowledge Dr. Nicos Ladommatos for his guidance, support, and patience during the supervision of this project. He would also wish to thank Dr. Richard Stone for his ever constructive criticisms and comments during the course of this study.

The author also wishes to thank Mr. Godfrey Reading, Mr. John Langdon and all the laboratory and workshop technicians for their technical advice and support.

Finally, I would like to specially thank my parents, Emik and Avo Aivaz Balian for their immense help, and their endless moral and financial support without which, my studies would have been impossible. With this, I would like to dedicate this thesis to my parents, specially my mother Emik, who died on 14th of January 1989 with her only wish being the successful completion of this project and with it my studies.

NOMENCLATURE

A	Area.	m^2
A_c	Cylinder cross-sectional area.	m^2
A_L	Effective leakage area.	m^2
A_o	Orifice area.	m^2
A_{sq}	Percentage squish area.	m^2
ATDC	After top dead centre.	
B	Cylinder bore.	m
BDC	Bottom dead centre.	
BMEP	Brake mean effective pressure.	bar
BSAC	Brake specific air consumption.	kg/kWh
BSFC	Brake specific fuel consumption.	kg/kWh
BTDC	Before top dead centre.	
C_d	Discharge coefficient.	
CI	Compression ignition.	
CR	Compression ratio.	
d	Nozzle hole diameter.	m
D	Combustion bowl diameter.	m
DI	Direct injection.	
F	Constant defined by Eq 5.13.	
f_{cyl}	Skin friction coefficient for the cylinder walls.	
f_{pc}	Skin friction coefficient for the piston crown and cylinder head.	
HSDI	High speed direct injection.	
IC	internal combustion.	
IDI	In-direct injection.	
IVC	Inlet valve closure.	
l	Valve lift.	m
L	Characteristic length.	m

LDV	Laser doppler velocimeter.	
m	mass.	kg
m_{ivc}	Trapped air mass at inlet valve closure.	kg
m_{max}	Maximum trapped air mass during induction.	kg
$\dot{m}$	mass flow rate.	kg/s
$\dot{m}_{av}$	Average air mass flow rate during time interval δt.	kg/s
$\dot{m}_{t}$	Air mass flow rate at time t.	kg/s
$\dot{m}_{tt}$	Air mass flow rate at time t + δt.	kg/s
n	Number of nozzle holes.	
N	Engine speed.	rev/min
P	Pressure.	bar
P_{amb}	Ambient pressure.	bar
P_{c}	Cylinder pressure.	bar
P_{o}	Manifold pressure.	bar
P_{t}	Cylinder pressure at time t.	bar
P_{tt}	Cylinder pressure at time t + δt.	bar
q	Volume of fuel injected per engine cycle.	m^3/s
Q_{a}	Momentum flux of the swirling air.	N/m^2
Q_{j}	Momentum flux of the fuel spray.	N/m^2
r	Radius.	m
R	Specific gas constant.	kJ/kgK
s	Distance between the piston crown and cylinder head at any crank angle.	m
S	Tangential displacement of the fuel spray tip.	m
SI	Spark ignition.	
SMD	Sauter mean diameter.	m
T	Temperature,	°C
	or Torque.	Nm
T_{o}	Manifold temperature.	°C

t	Time t.	
tt	Time t + δt.	
v	Combustion bowl volume.	m^3
V	Volume.	m^3
V_c	Cylinder volume.	m^3
V_{cw}	Crosswind velocity.	m/s
V_i	Impingement velocity.	m/s
V_{inj}	Mean injection velocity.	m/s
V_{sq}	Squish velocity.	m/s
W_t	Turbine power.	kW
X_t	Fuel spray tip penetration in quiescent air.	m/s
X_{tw}	Fuel spray tip penetration in a swirling air environment.	m/s
γ	Ratio of the specific heats of air.	
δt	Small time interval between time t and tt.	s
δP	Pressure drop across the injector nozzle.	bar
ρ	Density.	kg/m^3
ρ_a	Density of the compressed air within the cylinder.	kg/m^3
ρ_{atm}	Density of air at atmospheric conditions.	kg/m^3
ρ_d	Density of the standard diesel fuel.	kg/m^3
ρ_f	Fuel density.	kg/m^3
μ	Absolute viscousity of air.	m^2/s
θ	Measured injection period.	degree
τ	Shear stress.	N/m^2
ω	angular velocity.	rad/s
ω_i	Angular velocity of the swirling air during compression.	rad/s
ω_{av}	Average angular velocity of the swirling air during compression over interval δt.	rad/s

CONTENTS

Chapter 1: Introduction

1.1 - BACKGROUND

This thesis deals with the effects on engine performance of varying the clearance distance between the piston crown and cylinder head when the piston is at top dead centre (TDC).

Varying the clearance distance and, consequently, the clearance volume has historically been the most commonly adopted method of varying engine compression ratio. In the past, engine tests in both the UK and the US (Mansfield et al, 1965; Grundy et al, 1951), have shown that the major benefit of variable compression ratio (VCR) in diesel engines is a high brake mean effective pressure (BMEP), without excessive cylinder-gas pressure or deterioration in cold starting and idling performance (Kamo, 1978).

The specific power output from diesel engines has been gradually increased over the last 30 years (Ladommatos and Stone, 1988). This has been achieved mainly through a gradual increase in BMEP (see Fig 1.1). In some applications, such as road trucks and rail locomotives, higher BMEP is needed in order to satisfy increasing power demands without excessive increase in size and weight of the engine. Currently, many diesel engines operate at BMEP levels of around 15 bar, whilst several experimental engines have run at levels of 30 and even 40 bar.

The gradual increase in BMEP has been obtained by increasing the air mass trapped in the cylinder, chiefly by turbocharging. However, the disadvantage of higher trapped mass is increasing peak cylinder pressure, Fig 1.2. Strengthening the combustion chamber to contain the higher peak pressure is not an easy solution; it adds to the weight, bulk and the cost of the engine. The problem of greater bulk is at odds with the need for extra cooling in order to cope with the increased

thermal loading. The alternative to containing the higher peak cylinder pressure is to lower the compression ratio, or to retard the injection timing.

Undesirable side effects of retarding the injection timing, by more than about 5° crank angle (CA) are: a lower thermal efficiency, an increase in smoke and hydrocarbon emissions (Heywood, 1988), although a benefit is that NO_x emissions tend to decline. Alternatively, adopting a lower fixed compression ratio would also have several disadvantages. These include lower thermal efficiency, increased unaided cold starting difficulties, and detonation at light load conditions (Osborne, 1985).

The preferred solution would be a low compression ratio at medium and high loads, and a high compression ratio for starting and low load conditions. This would necessitate a system capable of varying the compression ratio during engine operation.

Expected engine operation with VCR is summarised in Fig 1.3. The rise in peak firing pressure (accompanying increasing BMEP) is halted by progressively lowering the compression ratio using a suitable system. The reverse process takes place when load is removed; the compression ratio is progressively returned to its highest value for good light load performance and better fuel economy. During starting, the VCR mechanism chosen should adopt the highest compression ratio available.

Numerous mechanisms for varying the compression ratio whilst the engine is running have been conceived over the years. The great majority of these rely on altering the clearance volume at TDC.

Fig 1.4 shows a number of VCR systems. In the first system, the movement of the contra-piston varies the clearance volume. In a series of tests by Volkswagen of West Germany this movement was controlled by

an electric servomotor (Walzer et al, 1986). The second system is utilised in the Co-operative Fuel Research engine which is used for Cetane-rating tests on diesel fuels. The contra-piston in this engine is controlled by a handwheel (ASTM, 1963). The third system allows two sizes of clearance volume to be selected. In diesel engines, only the main chamber would be used during starting; after this has been achieved the passage between the main and auxiliary chambers would be opened (Barber, 1987). In the fourth system, upward or downward displacement of the pivot varies the position of the piston at TDC and the clearance volume (US patent 4538557, 1985). In the fifth system, rotation of the eccentric pivots increases the separation of the pistons and the clearance volume at TDC (Mech. Eng. publications, 1984). In the sixth system, displacement of the main pivot varies the piston position at TDC (US patent 4112826, 1978). The mechanical output is in the form of an oscillatory motion, although a similar system (US patent 4270495, 1981), is arranged so as to deliver rotational output. The seventh system uses a rotational sleeve which varies the piston stroke and, therefore, the clearance volume. The sleeve can be rotated relative to the crankpin by means of the sleeve gears, and this allows continuous variation of the combustion chamber volume during the engine cycle (Rychter and Teodorczyk, 1985). The eighth system, which has been produced commercially in small numbers, relies on a two-part piston. Variation of the clearance volume is achieved by movement of the outer shell relative to the inner shell. This movement is controlled by a system of hydraulic valves which control a flow of oil from the engine lubrication system through the piston (Ladommatos et al, 1989, Wirbeleit et al, 1990). The last system shown in Fig 1.4 also relies on a two part piston. This

system would be controlled pneumatically using the gas in the engine crank case. The flow of gas would be controlled by a number of passages within the piston which also facilitate lubrication of the moving surfaces (Eureka magazine, 1989).

The variation in the clearance volume associated with the systems shown in Fig 1.4 affects the combustion process in diesel engines, but the effect is greater in the case of DI diesel engines. In this type of engine, good mixing of the fuel and air trapped in the cylinder is essential for efficient combustion. This is particularly important in the case of high speed direct injection (HSDI) diesel engines with bowl-in-piston combustion chambers. In this type of engine, the combustion process relies greatly upon air squish and swirl motion which can be severely reduced when clearance volume is increased.

Published information on the effect of varying the clearance volume in diesel engines is very limited. Wallace and Lux (1963) tested a VCR piston system (item 8 in Fig 1.4) in a single cylinder DI engine at 1600 and 2800 rev/min. The piston had a semi-quiescent toroidal combustion chamber. They found that poor combustion could be partially relieved by modifications to the injection system, combustion system geometry, and swirl induced by the inlet port. Osborne (1985) reported results of tests at engine speeds up to 1500 rev/min on a single-cylinder version of the Paxman Valenta DI engine (Osborne and Bhinder, 1982). A semi-quiescent toroidal combustion chamber was used, and the compression ratio was varied between 13:1 and 8:1 by increasing the clearance volume. Osborne's results did not show serious problems with combustion expect when increasing load from near-idling conditions. Grundy et al (1976) reported results of tests at speeds up to 1600 rev/min in a

single-cylinder DI engine with a semi-quiescent combustion chamber. In some tests the clearance volume was reduced so that the compression ratio was increased from 15:1 to 17:1. They found that modifications to the piston crown and injector nozzle geometry were necessary in order to avoid fuel impingement and high smoke emission at the higher compression ratio.

In recent years, increasing pressure for greater fuel economy, greater engine compactness, and lower weight, have led to intensive development of HSDI diesel engines with bowl-in-piston combustion chambers. Two examples of these engines are the Ford 2.5 HSDI and the Perkins Prima engine. Both are capable of speeds in excess of 4000 rev/min (previously the domain of the indirect injection (IDI) type of diesel engine) and have shown specific fuel consumption improvements of 10 to 15% over IDI engines of the same power output. To date no information has been published in the open literature on the performance of HSDI diesel engines using a VCR system of the type that varies the clearance volume.

1.2 - OBJECTIVES OF THE STUDY

The general aim of the work presented here was to study the effect of increase in clearance volume on the performance of an HSDI engine with a bowl-in-piston combustion chamber.

The specific objectives of the work presented in this thesis were:

i - To assess the benefits of VCR in terms of increased BMEP and improved fuel economy.

ii - To identify and quantify the effects on the combustion performance of increased clearance volume.

iii - To investigate methods for ameliorating the problems with combustion.

iv - To develop computer simulation models of the air flow structure at low compression ratio. These could be used in order to optimise the combustion process when VCR systems of the variable-clearance-volume type are applied to HSDI engines.

1.3 - OUTLINE OF THE THESIS

Chapter 2 presents a literature survey on combustion in DI diesel engines, with particular reference to the effect of air motion within the cylinder during compression and combustion. Published information on the effect of increased clearance volume on air motion and combustion is included in this chapter.

Chapter 3 describes the experimental facility set up for this study. It includes the results of commissioning and baseline tests.

Results from engine tests at a low compression ratio are presented and described in Chapter 4. This Chapter also includes an assessment of a number of published semi-empirical correlations for predicting ignition delay.

In Chapter 5, computer models are developed which predict the air

squish and swirl during compression in the engine used for the experimental work. These models are then used in order to interpret the results from the experimental work.

Chapter 6 brings together the conclusions that emerged from the work presented in this thesis, and includes recommendations for future work.

Chapter 2:
Literature Survey

2.1 - FUNDAMENTALS OF INTERNAL COMBUSTION ENGINES

One way of classifying internal combustion engines is according to the method used to ignite the air fuel mixture: spark ignition (SI) and compression ignition (CI).

The cylinders of conventional SI engines are supplied with premixed air and fuel. The mixture is prepared in the manifold, prior to being drawn into the cylinders, during the induction process. The mixture is prepared either by means of a carburettor or a fuel injection system. The mixture strength (air fuel ratio) is around stoichiometric. Most of the fuel is in the vapour state, and well mixed with air, by the time the spark is initiated. The mixture is ignited at a desired crank angle by a high energy spark. The power output of the engine is controlled by varying the amount of mixture supplied to the engine using a strangler (throttle).

In a CI engine, however, only air is drawn into the cylinders during the induction process. Towards the end of the compression stroke liquid fuel is injected into the trapped, compressed, hot air. Unlike SI engines, a heterogeneous mixture is formed within the combustion chamber, with a wide range of air fuel ratios. During compression, the pressure and temperature of the trapped air rises above the level required for spontaneous ignition of the diesel fuel. Thus, part of the air fuel mixture ignites (after a short delay period) in one or more locations within the combustion chamber. These ignition points are normally located where the mixture has attained, approximately, stoichiometric proportions. In CI engines, unlike SI engines, the location and, (to a some extent) the timing of ignition are not controllable.

In SI engines, the combustion proceeds by the propagation of a flame front initiated by the high energy spark. In a CI engine, however, combustion proceeds at a rate which is principally dependent on the fuel evaporation rate, its mixing with the surrounding air, and the rate of combustion of the premixed fuel and air after ignition. Once the combustion process is under way, the evaporation and mixing of the fuel is accelerated by the increasing temperature of the cylinder contents. In a large proportion of diesel engines, agitation of the air within the cylinder, in addition to the molecular diffusion, accelerates fuel air mixing. This higher air fuel mixing rate is achieved, because, mass of the various species in the cylinder is transferred towards (and away) from the burning regions by convection.

An approximately fixed amount of air is supplied to CI engines under all running conditions. The power output of the engine is controlled by varying the amount of fuel injected per cycle; that is, by varying the overall air fuel ratio.

2.1.1 - Diesel engine types

Diesel engines can be divided into two basic types according to their combustion chamber design:

1 - Direct injection (DI) engines.
2 - Indirect injection (IDI) engines.

DI engines have a single, open combustion chamber, into which fuel is injected directly, Fig 2.1(a). The combustion chamber in IDI engines is divided into two parts, the prechamber (which is located within the cylinder head) and the main chamber. Fuel is injected into the

prechamber which is connected to the main chamber via a throat, Fig 2.1(b). There are several variations for each type of combustion chamber.

Quiescent chambers (characterised by a shallow bowl in the crown of the piston) are traditionally used with large-bore low-speed DI engines. The mixing of the air and fuel is mainly promoted by a large number of high velocity, finely atomised fuel jets. Due to the lower engine speed, and more time available for combustion, additional agitation of the air is not required. A large number of sprays is necessary, in order to distribute the fuel evenly within the compressed air. The high velocity of the fuel jets also helps fuel penetration to the outer edges of these large-diameter combustion chambers.

In high-speed direct-injection (HSDI) diesel engines (operating at up to 4500 rev/min) high fuel air mixing rates are required. This is achieved by air swirl and turbulence. In these engines swirl is imparted during induction, usually by the inlet port (section 2.3.1). During compression, the displacement of the air into the bowl reduces the radius of gyration (and moment of inertia) of the trapped air, causing the swirl rate to increase (Fig 2.1a).

In IDI engines, during the compression stroke, air is forced at high speed through a small throat into the prechamber. This generates very high levels of air swirl and turbulence in the prechamber. This allows the engine to run at high speeds (up to 5000 revs/min). Fuel is injected into the prechamber, often through a single-hole nozzle. The fuel spray is usually coarser, and has a lower velocity than in DI engines. Despite the lower spray quality, good fuel air mixing is obtained, as a result of the higher swirl and turbulence in the

prechamber. The pressure rise, in the prechamber due to combustion, forces the burning mixture back into the main chamber, where the air in the main chamber completes the combustion. IDI engines have high heat loss rates to the prechamber walls and throat, arising from high flow velocity and turbulence. They also have additional pumping losses due to the transfer of air and burning gases between the prechamber and main chamber. These features partly account for the thermal efficiency of IDI engines being 5 to 15 percent lower than that of DI engines.

This thesis is concerned with combustion in a DI diesel engine, having a bowl-in-piston combustion chamber. For this reason, all subsequent sections in this chapter will deal only with the DI type of diesel engine.

2.2 - THE COMBUSTION PROCESS IN DI DIESEL ENGINES

In diesel engines, the mixture of vaporised liquid fuel and air must be within flammable limits, and must be raised to a sufficiently high temperature and pressure for autoignition to occur. For diesel fuel, the overall air fuel ratios that can support combustion are between 14.5:1 and over 100:1.

The combustion process can be divided into three distinct phases, Fig 2.2:

i - Ignition delay period
ii - Premixed combustion period
iii - Diffusion burning period

Ignition delay

The delay period is defined as the time between the start of injection and: either, first appearance of visible flame, or the start of pressure rise due to heat release. Before a significant proportion of the chemical energy of the fuel can be released through burning, certain physical and chemical processes take place during the delay period. The physical processes are: break up of the fuel jet into fine droplets (atomisation), evaporation of the fuel droplets, and mixing of the fuel vapour with the surrounding air. The chemical processes involve cracking of large fuel (hydrocarbon) molecules into smaller ones, and oxidation of the fuel vapour.

The delay period is dependent on the pressure and temperature of the air, also on the physical and chemical properties of the fuel. Constant-volume bomb tests by Taylor (1968), Spadoccini (1982), and Igura et al (1975), have shown that delay periods (measured in ms)

shorten as the pressure or temperature of the air increase, Fig 2.3. However, Fig 2.3 shows that a given percentage change in pressure has a smaller effect on the delay period than a corresponding change in the thermodynamic air temperature.

The delay period could also be influenced by the impingement of the fuel jets on the combustion chamber surfaces, for example, the sides of the piston bowl.

Premixed combustion

The delay period is followed by rapid premixed combustion. A certain amount of fuel and air, that has been premixed to within the flamability limits, ignites. The amount of premixed mixture burning is closely associated with the length of the delay period. If the ignition delay period is long, a greater amount of fuel will be prepared for ignition. The subsequent rate of combustion would, therefore, be greater, causing a more rapid pressure rise, and higher maximum cylinder pressure. The level of combustion noise emitted would also be greater, due to this high initial rate of pressure rise. This is noticeable shortly after a diesel engine is started from cold, when ignition delay is usually longer.

Diffusion burning

The third phase of combustion (diffusion burning period) follows the premixed combustion phase, and lasts until combustion is complete. During this phase, the rate of combustion is mainly governed by the droplet evaporation rate; and by the rate at which fuel vapour and oxygen molecules can diffuse towards the burning zone that surrounds

each fuel droplet. This is affected by the distribution of the fuel within the combustion chamber, and by the degree of air agitation during combustion.

Injection timing

The fuel injection timing controls the crank angle at which combustion starts. Varying the injection timing, affects the delay period. Changes in the delay occur because the compressed air temperature and pressure within the cylinder are different for different injection timings. As mentioned above, the delay period shortens with increasing air temperature and pressure.

If injection starts early (well before TDC), the ignition delay period will be longer. This will result in high rates of pressure rise and high cylinder pressures. If injection starts late (close to TDC), burning will continue well into the expansion, resulting in hot exhaust gases, worse fuel economy and higher emissions. Therefore an optimum injection timing can be found in between these two extremes.

Fig 2.4 shows the effect of injection timing on DI diesel engine performance and emissions. An optimum injection timing exists for minimum BSFC and maximum BMEP. The optimum timing for the lowest smoke level is somewhat advanced of that for optimum BSFC.

Injection timing has a strong effect on NO_x emission. Retarding the timing can result in a substantial reduction in NO_x, with only a moderate BSFC penalty.

The engine designer's goal is to achieve the best BSFC possible with emission levels low enough to meet the constraints imposed by the emissions legislation. This involves tradeoffs between BSFC and exhaust

emissions. Fig 2.5 shows tradeoffs between the two principal emissions, smoke and NO_x.

2.3 - BULK FLOW WITHIN THE CYLINDER

A principal requirement in DI diesel engines is rapid air fuel mixing during combustion. The mixing rate is dependent on several engine parameters. Mainly, it depends on the characteristics of the fuel injection system and on the air motion during injection and combustion. This section deals with the air motion. The effects of the injection system are dealt with in Chapter 5.

The air motion has the following principal features:

i - Swirl
ii - Squish
iii - Turbulence

Whilst swirl and squish involve bulk motion of the air, turbulence includes a wide range of smaller-scale motions, that occur within the bulk of the air. Turbulence is generated during both the induction and compression processes. During compression, the level and scales of turbulence are influenced by the levels of swirl and squish.

2.3.1 - Swirl

Swirl is the organised bulk rotation of the air within the cylinder, around the cylinder axis. Normally, the swirling motion of the air is generated during the induction stroke, and is enhanced during compression.

There are several ways of generating swirl during induction. One way, is to direct the incoming air tangentially to the cylinder axis, near the cylinder wall. This causes the incoming air stream to be deflected by the walls into a swirling motion, around the cylinder axis. Figs 2.6a and 2.6b show two typical directed port designs which achieve

this effect. In this approach, the flow rate around the flow annulus of the inlet valve, is highly non-uniform. This results in poor utilisation of the available valve annulus area, which usually reduces the volumetric efficiency of the engine. In another approach, the inlet port passage is arranged into the form of a helical ramp which forces the flow to rotate about the inlet valve axis prior to entry into the cylinder, Fig 2.6c and 2.6d. Helical ports usually present a smaller flow restriction, and thus have a greater flow discharge coefficient (C_d) than directed ports.

The above two approaches are commonly used in commercially available diesel engines. Another approach, which has been used mainly in lean-burn gasoline engines, involves masking part of the valve outlet as shown in Fig 2.7a. Yet another approach, having a similar effect as valve masking, involves the use of a shroud attached to the inlet valve as shown in Fig 2.7b. The shrouded valve has been used in experimental engines; it allows control of the amount of swirl, through the rotation of the valve. Some means of locking the valve at the desired rotational position is necessary. Both the masked-valve and the shrouded-valve present obstruction to the flow, and can reduce the volumetric efficiency of the engine.

Experimental investigation of swirl in an operating engine presents considerable practical difficulties. For this reason, steady-flow rigs are often used (section 3.3, Fig 3.10) in order to investigate the swirl induced by the inlet ports. Air is blown at a steady rate into the cylinder barrel, via the inlet port and valve assembly. The air flows out of the bottom of the cylinder barrel without any restrictions (the piston is absent). The air flow rate, the valve opening, and the

geometry of the port and valve assembly can be altered independently in order to study their effect on the air swirl within the cylinder. In conjunction with swirl studies, steady flow rigs are also used for the study of the flow restriction offered by the port and valve geometry, as this affects the volumetric efficiency of the engine. Various devices can be placed within the cylinder barrel for the measurement of the swirl rate, the air velocity distribution, and air turbulence levels. Two commonly used devices for measuring the level of swirl are the paddle wheel and the torque meter; these are shown in Fig 2.8. The paddle wheel has the disadvantage of underestimating the rotational speed of the air in the cylinder. This is mainly due to bearing friction causing slip between the paddle and the air flow. In order to estimate the swirl rotational speed from the torque meter, it is easiest to treat the swirling flow as a forced vortex (i.e. assume solid body rotation); this point is discussed in a latter part of this section.

Monaghan and Pettifer (1981) used both the paddle wheel and the torque meter. They compared the induction swirl, produced by both directed and helical inlet ports. Fig 2.9 shows their results. It can be seen that both instruments have shown that helical ports generate more swirl (for a given valve opening and pressure drop across the valve). It can also be seen that the swirl measured by the torque meter is between 25 to 50 percent greater than that measured by the paddle wheel. A measure of the swirl generated during induction is given by the swirl coefficient (C_s). C_s essentially compares the flow angular momentum with its axial momentum. This is defined in a number of different ways by various investigators. One commonly used definition, Heywood (1988), is:

$$C_s = \frac{\dot{m}B^2\omega}{\dot{m}V_o B} = \frac{B\omega}{Vo} \qquad \ldots\ 2.1$$

where $\dot{m}$ is the air mass flow rate, ω is the angular velocity of the swirling air assuming solid body rotation (forced vortex), B is the cylinder bore, and V_o is the calculated flow velocity through the valve that would result with a mass flow rate $\dot{m}$ if the flow through the valve was frictionless. V_o is given by:

For incompressible flow

$$V_o = \left[\frac{2\,(P_o - P_c)}{\rho_o}\right]^{1/2} \qquad \ldots\ 2.2$$

For compressible flow

$$V_o = \left\{\frac{2\gamma P_o}{(\gamma-1)\,\rho_o}\left[1 - (P_c / P_o)^{\frac{(\gamma-1)}{\gamma}}\right]\right\}^{1/2} \qquad \ldots\ 2.3$$

where P_o and P_c are the manifold and cylinder pressures respectively, ρ_o is the air density at inlet manifold conditions and γ is the ratio of the specific heats of air. The angular velocity (ω) can be estimated by either using a torque meter or a paddle wheel. In the case of the torque meter, (assuming a forced vortex) if T is the restraining torque on the flow straightener,

$$T = \frac{\dot{m}\,B^2\omega}{8} \qquad \ldots\ 2.4$$

hence $$\omega = \frac{8T}{\dot{m}B^2} \quad \ldots\ldots 2.5$$

In the case of the paddle wheel the estimated angular velocity is less than that estimated using the torque meter. This is because the paddle lags the flow, mainly due to slip arising from bearing friction.

Swirl coefficients (C_s) for three types of ports are shown in Fig 2.10, at different valve openings, Monaghan and Pettifer (1983). As the valve opens beyond 30% of maximum lift, the flow restriction offered by the valve diminishes, and the shape of the port begins to have a greater influence. At medium valve openings, the helical ports impart greater swirl than directed ports. At full opening, the swirl imparted by all port designs is of similar magnitude.

Steady-state flow rigs are useful in the sense that they allow various inlet ports, and other swirl generating devices, to be compared. The data obtained from these tests can also be used to predict the moment of momentum of the air at end of induction, i.e. at inlet valve closure (IVC), Fitzgeorge and Allison (1963), Dent and Derham (1974). The value of the moment of momentum at IVC could be used to predict the swirl during the compression stroke.

Monaghan (1981) used a Laser Doppler Velocimeter (LDV) to measure air velocities within the cylinder of a motored engine with a shallow-ramp helical port. Fig 2.11 shows the tangential air velocity at IVC; this is shown at various radii and different depths below the cylinder flame face. It is apparent that away from the cylinder head, the flow pattern resembles solid-body rotation (with velocity increasing in

direct proportion to the radius, i.e. in forced-vortex fashion). But close to the cylinder head, the velocity pattern is markedly different, and resembles more closely that of a free rather than forced vortex. Further results, obtained at a higher engine speed, Fig 2.12, show a drastic change in the flow pattern away from forced and towards free vortex flow pattern.

The results of several investigators show that with bowl-in-piston chambers, the swirl speed within the bowl increases when the piston approaches TDC. This occurs due to the fact that as air is forced from the squish area into the bowl, the radius of gyration (and moment of inertia) of the air is reduced. Thus, for given moment of momentum, the air rotational speed increases, as the overall moment of inertia reduces. There are many different shapes of bowl-in-piston combustion chambers. In general, they can be divided into cylindrical, toroidal, and re-entrant bowls, Fig 2.13. The bowl-to-cylinder diameter ratio is an important parameter controlling the rate and extent to which the moment of inertia of the swirling air is reduced during compression (at a given engine speed). The smaller the value of this ratio, the greater the increase in swirl during compression.

As explained before, with bowl-in-piston combustion chambers the swirl is modified during compression. This phenomenon was investigated by Fansler (1985) using LDV and a motored engine. The engine had a bowl-in-piston combustion chamber, centred around the cylinder axis, and a directed port. Fig 2.14 shows the flow pattern within the piston bowl during compression. This figure shows an increase in tangential velocity (or swirl), as the piston approached TDC. This is true for a number of locations below the head surface. Also, it shows that the air motion

within the cylinder continued to resemble solid-body rotation, throughout the compression stroke. The effect of squish (see next section) was first apparent at around 300 °CA (60 °CA BTDC), where the tangential component of the air velocity at the rim of the bowl was affected by the air rushing into the bowl, as a result of squish. The deformation of the swirl profile became more pronounced in the last 10-30°CA BTDC. Note that at lower locations in the bowl (half-way down the bowl depth), the flow pattern remained near solid body rotation. At upper locations in the bowl (near the rim) the swirl profile was distorted by the effect of squish. Note, also, that the centre of rotation did not coincide with the cylinder (and bowl) axis, and changed location during compression. Other investigators have also observed a similar movement of the centre of rotation.

Tindal (1982) found that in addition to the rotation about the cylinder axis, there was circulation in vertical planes; the air moves upwards near the wall and downwards along the axis of the cylinder.

The effect of the bowl shape on air motion (especially bowl entry diameter) was investigated by Williams and Tindal (1980), for re-entrant and toroidal bowls. The re-entrant bowl had a rim diameter one-half that of the toroidal chamber. At TDC, they found that just below the rim of the bowl, the air angular velocity was almost twice as high for the re-entrant chamber; however, the tangential velocity at the rim was about the same value.

An important feature of the combustion chamber is the clearance distance at TDC between the piston crown and the cylinder head. With a smaller clearance distance, a greater proportion of the air mass trapped in the cylinder will be forced into the bowl, and greater swirl and

squish velocities will result. No experimental results could be found in the literature which show the effect of clearance distance on swirl. However, this feature is of great interest to the investigation presented in this thesis. With variable compression ratio systems that vary the clearance volume, there will be a great effect on the swirl and squish levels, towards the end of the compression stroke.

Iijima and Bracco (1987) investigated the influence of bowl offset on air motion in a motored DI diesel engine, under a variety of operating conditions, using an LDV system. They used different pistons, all having the same overall diameter and bowl geometry. The bowl axis was progressively offset from the piston centre line, by up to 7.7 percent of the piston diameter. They found that the angular momentum of the trapped air at TDC was decreased by a maximum of 5.4 percent. The turbulence intensity remained almost unchanged by the degree of offset.

These results agree with those of Mckinley and Primus (1988), who used the KIVA fluid dynamic computer program, developed at the Los Alamos Laboratory in the US for study of flow in IC engines. Mckinley and Primus progressively offset the bowl axis by up to 9.6 percent of the piston diameter. They found that the angular momentum decreased by a maximum of 8 percent, whilst the turbulence intensity increased by a maximum of 10 percent, as a result of the bowl offset. Different swirl rates at IVC were used, between 2.6 and 4.27.

Mckinley and Primus also estimated that the decay in the IVC angular momentum during the compression stroke was less than 15 percent, and largely not affected by the bowl offset.

2.3.2 - Squish

Squish is defined as the radially-inward air motion that occurs towards the end of the compression stroke, when the piston crown approaches the cylinder head. Fig 2.15 shows how the air is displaced from the bump clearance region into the bowl, causing high squish velocities. Squish velocities are dependent on the fraction of the piston plan area not occupied by the bowl (shaded area on Fig 2.15).

$$A_{sq} = \left[\frac{B^2 - D^2}{B^2}\right] \times 100 \qquad \ldots\ldots 2.6$$

However, the ratio of the bowl diameter to the cylinder bore (D/B) is commonly referred to as the parameter controlling the squish velocity.

A theoretical squish velocity can be calculated by applying the conservation of mass to the instantaneous air displacement into the combustion bowl (bowl-in-piston chamber), Dent and Derham (1974):

$$V_{sq} = \frac{r\,[(B/2r)^2 - 1]}{2s}\left[\frac{v}{A_c\, s + v}\right]\frac{ds}{dt} \qquad \ldots\ldots 2.7$$

where r is the radius at which the squish velocity is required, s is the distance between the piston crown and the cylinder head, A_c is the cross sectional area of the cylinder, v is the combustion volume and $\frac{ds}{dt}$ is the piston speed.

The above equation does not take into account the reduction in squish velocity due to fluid friction , gas inertia, leakage past the piston rings, and heat transfer to the combustion chamber surfaces. Gas

inertia and fluid friction effects have been shown to be small, Heywood (1988). The effects of gas leakage past the piston rings and of heat transfer are more significant. Fig 2.16 (Shimamoto and Akiyama 1970) shows the decrease in squish velocity due to leakage and heat transfer for two bowl-diameter-to-bore ratios (D/B). The decrease in squish velocity is also shown to depend on a dimensionless leakage number defined as:

$$N_L = A_L \frac{\sqrt{\gamma R T_{IVC}}}{NV} \quad \ldots\ldots 2.8$$

where A_L is the effective leakage area, T_{IVC} is the temperature of the cylinder gases at inlet valve closure, N is the engine speed and V is the displaced cylinder volume.

The effect of clearance height and compression ratio are discussed in section 2.5.

2.3.3 - Turbulence

The interaction of the swirl and squish is responsible for the generation of turbulence during fuel injection and combustion. Turbulence is also generated by the high velocity fuel jets, which entrain the surrounding air. Some of the larger-scale turbulence, generated during induction, may also survive viscous dissipation during the compression process. The generation of turbulence, and the effect of combustion chamber geometry on the turbulence, are dealt with in this section.

Turbulence intensity is a measure of the magnitude of the instantaneous velocity fluctuations in a turbulent flow. It is defined,

by Bird et al (1960):

$$I_t = \frac{1}{\bar{u}} \left[\overline{(u')^2}\right]^{1/2} \quad \ldots\ldots 2.9$$

where u is the instantaneous flow velocity, $\bar{u}$ the mean flow velocity (time averaged), u' is the instantaneous velocity fluctuations (deviations of instantaneous velocity from the mean velocity) and $\left[\overline{(u')^2}\right]^{1/2}$ is the root-mean-square (time averaged) of the velocity fluctuations. When the fluctuations are not of the same value in all directions (i.e. non isotropic turbulence) a more general definition of turbulence fluctuations for three dimensional flow is as follows:

$$I_t = \frac{1}{\bar{u}} \left[\frac{\overline{(u')^2}}{3} + \frac{\overline{(v')^2}}{3} + \frac{\overline{(w')^2}}{3}\right]^{1/2} \quad \ldots\ldots 2.10$$

Brandle et al (1979), found that the turbulence intensity near the top of an off-centre toroidal combustion bowl, was much higher than that with a flat piston. However, at lower sections of the combustion bowl, the intensity level was similar to that obtained with a flat piston. Brandle et al concluded that the squish motion had little effect upon the flow in the lower parts of the combustion bowl.

Fansler (1985) studied the distribution of turbulence within the bowl of a motored DI engine using an LDV system. He concluded that the bowl diameter to bore ratio, and by implication the level of squish, affects this distribution. Fig 2.17a and 2.17b shows that the RMS fluctuation (defined above) near the rim of the bowl were dominated by squish when the piston approached TDC.

Fansler also showed that as the piston approached TDC, the RMS fluctuations were greatest near the cylinder head face; and it decreased as the measuring location was moved down the bowl, away from the cylinder head face, Fig 2.17c. This agrees with Brandle's observations, and confirms the effect of squish on turbulence generation in the upper strata of the bowl.

2.4 - EFFECT OF SWIRL, SQUISH, AND TURBULENCE ON AIR FUEL MIXING

This section deals with the effect of swirl, squish, and turbulence on the mixing process between the air and fuel during injection and combustion.

The air fuel mixing process is affected by several factors: the temperature and pressure of the air within the cylinder, the nature and level of the air motion, the fuel properties, and the fuel spray characteristics. In high speed DI Diesel engines, the motion of the air and its temperature and pressure, change as the piston approaches TDC. Thus, the timing of the fuel injection relative to the piston position is also an important parameter affecting air fuel mixing.

Shiozaki et al (1980) carried out tests on a DI Diesel engine in which three different inlet manifolds were fitted in turn. The aim of their tests was to investigate the effect on combustion of different levels of swirl and turbulence. Shiozaki et al state, that these manifold geometries provided different swirl levels and turbulence intensities during injection and combustion, as follows:

MANIFOLD	A	B	C
SWIRL RATIO	2.6	2.1	2.3
TURBULENCE	LOW	HIGH	MEDIUM

Shiozaki et al took both direct and Schlieren photographs of the cylinder contents. Fig. 2.18 shows the rate at which the area occupied by, (a) the spray (mixing area) and, (b) the flame, spread during combustion, in engine A and B. It can be seen from this figure, that manifold B promotes more rapid spread of the spray and flame. This rapid mixing and burning with manifold B was attributed by Shiozaki et al to higher turbulence intensity. They also found, that the ignition delay

period was generally shorter with manifold B, at both speeds of 1000 and 2400 rev/min. By comparing the engine performance with manifolds B and C, Shiozaki et al. reached the same conclusion: that the inferior performance with manifold C was due to lower turbulence intensity, despite its higher swirl ratio.

Kamimoto et al (1980) used a two zone combustion model for the calculation of the equivalence ratio in the flame region, and for the calculation of the rate of heat release due to fuel burning. The model relied on measured values of cylinder pressure (P). The pressure was measured from tests, during which the inlet manifold and piston-bowl geometry were altered systematically, in order to produce changes in swirl and squish during combustion. Some of their test data are summarized in Table 2.1.

Table 2.1 - Experimental Conditions, Exhaust Emissions and BMEP, Kamimoto et al (1980).

PISTON BOWL	SWIRL RATIO	SMOKE (Bosch)	NOx (ppm)	bmep (MPa)
SHALLOW	0	4.5	390	0.344
SHALLOW	2	2.9	530	0.394
SHALLOW	4	4.4	540	0.336
DEEP	0	2.6	490	0.404
DEEP	4	1.5	840	0.407

Generally, Kamimoto et al found that combination of a deep bowl with high swirl, produced high mixing and burning rates. These resulted in a higher bmep and a lower smoke emission, but the NOx emission was

highest. Conversely, a combination of shallow bowl and no swirl, produced the lowest burning rate and NOx emission, but the lowest BMEP and highest smoke.

Pischinger and Cartellieri (1972), obtained similar results: higher NOx and lower smoke emissions, when they reduced the bowl-to-cylinder diameter ratio from 0.62 to 0.51.

Brandle et al (1979), state that higher smoke concentrations could be expected in the centre of the bowl, where poor mixing occurs due to low air activity. They found correlations between the level of smoke and the level of air activity at the centre of the bowl, see Fig 2.19. It can be seen that smoke reduces as the air activity (described by turbulence velocity) is increased.

Dent (1980) analysed further the results presented by Brandle et al and came to the same conclusions. Dent argued, that at low air activity levels, the rate at which soot particles are oxidised during the final stages of combustion is reduced.

2.5 - EFFECT OF CLEARANCE HEIGHT ON SWIRL AND SQUISH

The compression ratio with many VCR systems, is varied by altering the clearance distance between the piston crown and the cylinder head at TDC. As explained elsewhere, this variation in clearance volume would reduce the levels of squish and swirl during combustion. Fig 2.20 shows the variation of squish velocity with varying clearance distance, measured by Shimamoto and Akiyama (1970). It can be seen that the squish velocity fell with increasing clearance, at a constant engine speed. This reduction in the squish velocity is due to reduced rate of change of cylinder volume as the piston approaches TDC.

The clearance height also affects the swirl in the piston bowl, as the piston approaches TDC. With a smaller clearance height, a greater proportion of the air mass trapped in the cylinder will be forced into the bowl, and a greater swirl velocity will result. No experimental results could be found in the literature which show the effect of clearance height on swirl. However, this feature is of great interest to the project presented in this thesis.

There are a number of ways of overcoming the problem of reduced mixing rate, arising from the reduction in the swirl and squish. One is to modify the injection system so as to match the lower air activity. This is dealt with in more detail in the next section. A complementary method is to operate with weaker air fuel mixtures, and restore the consequent reduction in power by supercharging or turbocharging the engine to higher boost pressures. There is an additional benefit from the latter method; the higher air flow velocity through the inlet system during induction, also raises the swirl at the end of the induction process, Dent and Derham (1974). However, since squish is

dependent on the rate of change of volume as the piston approaches TDC (regardless of gas density), turbocharging may not have much effect on the squish velocity. This is dealt with, in more detail, in Chapter 5.

Finally, higher air flow momentum through the inlet manifold, associated with turbocharging, increases the turbulence levels generated during induction. However, the turbulence generated during induction is largely dissipated during the compression process.

2.6 - MATCHING OF INJECTION SYSTEM WITH IN-CYLINDER AIR ACTIVITY

Engine performance is not only dependent on the air activity within the cylinder, but also on the fuel injection system characteristics. This was demonstrated convincingly by Monaghan and Pettifer (1981). These authors compared three different inlet port designs; after optimisation of the injector nozzle and an increase in injection rate, all the ports provided similar values of smoke emissions and ISFC, at high engine speeds, and at all injection timings. They reported that, at very high injection rates, most of the mixing energy is derived from the fuel jets, and that the detailed air motion becomes less significant.

2.6.1 - Fuel spray structure and its effect on combustion

In a Diesel engine, fuel is introduced into the combustion chamber through one, or more, small orifices at high velocity. The high velocity of the fuel jet is created by a large pressure difference across the nozzle orifice. The geometry of nozzle orifices can vary, depending on the needs of the combustion chamber design.

Fig 2.21 illustrates the structure of a typical DI Diesel spray. The fuel emerges from the orifice with a velocity of over 100m/s; the fuel jet then spreads into a cone, and continues spreading as injection proceeds. The outer regions of the spray cone break-up, close to the nozzle exit, into fine droplets. The core of the spray also disintegrates into droplets after a finite length, called the break up length, Fig 2.21. The droplets evaporate into the surrounding, high temperature, air.

Spray cone angle and spray penetration

Youl et al (1985), and Varde et al (1984), used rigs to investigate the fuel spray cone angle, and spray penetration, for a number of injectors. Both groups injected diesel fuel sprays into high pressure nitrogen, and used high-speed photography for their investigations. Their results show similar trends. It was found that the spray tip penetration reduced, and the cone angle increased, with increasing gas pressure (at a constant temperature). Youl et al ascribed these trends to the increase in gas density with increasing pressure. Varde et al reached the same conclusion, and correlated the spray cone angle (θ degrees) with the gas-to-fuel density ratio, as follows:

$$\theta \propto \left[\frac{\rho_g}{\rho_f}\right]^{0.33} \quad \ldots\ldots 2.11$$

Khan (1969) reported that as the nozzle hole length was reduced (for a given nozzle hole diameter), the spray cone angle increased. An increased spray cone angle tends to improve fuel distribution, but is normally accompanied by reduced spray tip penetration. Khan observed that at retarded injection timings, an increase in smoke level resulted with greater cone angles.

Investigations into the effect of gas temperature on the spray cone angle, led Youl et al (1985) to conclude that the cone angle reduces considerably with increasing gas temperature. They proposed that at elevated temperatures, rapid evaporation of smaller droplets at the spray periphery could reduce the observed cone angle.

Droplet size distribution

Varde et al (1984) obtained droplet photographs from which a Sauter mean diameter (SMD) and an average fuel droplet diameter were calculated :

$$SMD = \frac{\sum N_i D_i^3}{\sum N_i D_i^2} \quad \ldots\ldots 2.12$$

where N_i is the number of droplets with a diameter D_i. SMD, for a given nozzle hole geometry, was shown to decrease rapidly with increasing injection pressure, Fig 2.22, up to 100 MPa. Above this pressure SMD was reduced at a slower rate. Varde et al, using a number of nozzle geometries obtained similar trends.

Khan (1969) reported a sharp rise in droplet SMD as the nozzle hole diameter was increased from 0.28 to 0.33mm. The effect was a rise in the smoke concentration when the two nozzles were installed, in turn, in an engine. The possible reasons for this rise were said to be a reduction in the rate of the diffusion burning process, due to fewer larger droplets for a given amount of fuel. This reduced the evaporation and the combustion rates of the fuel trapped in the cylinder.

Osborne (1985), as well as Taylor and Wilsham (1969), also have shown that a better fuel atomisation is achieved with small nozzle holes; if the nozzle holes are excessively small, necessiating a high injection rate, undesirable secondary injections could result.

2.6.2 Optimisation of a fuel injection system

The basic requirements of an injection system are: fuel droplet

distribution to all parts of the combustion volume, atomisation of fuel into fine droplets, and correct interaction of the fuel jet and air so as to achieve rapid air fuel mixing and complete burning of the fuel. In practice, fuel injection system designers have at their disposal the following system parameters with which they can meet these requirements, Moris and Dent (1976), Kamimoto et al (1980), Varde et al (1984), Timoney (1985), Mehta and Gupta (1985), Kuo et al (1983):

a - injection pressure.
b - number of nozzle holes.
c - nozzle hole size and shape.
d - injector opening pressure.
e - injection timing.

Timoney attempted to rationalise the injection system optimisation process, and place it on more analytical foundations. He singled out a parameter, which he found to be of primary importance in injection system optimisation. This is the tangential velocity of the air, relative to the tangential velocity of the fuel spray tip, at the instant of fuel spray impingement with the combustion bowl sides. Timoney calls this parameter the crosswind velocity, V_{cw}. The definition of this parameter is illustrated in Fig 2.23. Detailed analysis of his results are included in Chapter 5.

Timoney's results showed that for a given injection system, there was an optimum air swirl value which maximised V_{cw}, see Fig 2.24. Timoney has demonstrated a good correlation between the maximum V_{cw}, and both smoke and ISFC, see Figs 2.25 and 2.26. Other researchers, for example Aoyagi et al (1980), have also shown that an optimum swirl value exists in a DI Diesel engine at a given running condition, but did not analyse their results in terms of V_{cw}.

Timoney also investigated the effect of impingement velocity on smoke and ISFC (impingement velocity is defined in Fig 2.23). His results showed that a correlation exists between impingement velocity, and both smoke and ISFC; the higher the impingement velocity, the lower the smoke and ISFC. The impingement velocity was increased, either by reducing the bowl diameter, or by increasing the fuel flow rate. A relevant question is whether spray impingement on the bowl sides occurs. Taylor and Wilsham (1969) reported that in the majority of medium-speed Diesel engines, spray impingement occurs. It could be concluded that, for low smoke and ISFC, both the crosswind velocity at impingement and the fuel spray impingement velocity, should be maximised. This could be done by appropriate adjustments to the swirl, combustion chamber geometry, and fuel injection system parameters.

2.7 - EXHAUST POLLUTANT EMISSIONS

The principal pollutants from a diesel engine are: soot (or smoke), which arises from unburned carbon in the fuel; unburned fuel (denoted by HC for hydrocarbons), and oxides of nitrogen, NO and NO_2 (collectively denoted by NO_x - NO is by far the major component). CO is not a problem in diesel engines, as it is present in much smaller quantities than in gasoline engines. This is due to the weak overall air/fuel ratios used in diesel engines.

The amount of NO_x and HC depends on engine design and on operating conditions. NO_x levels are of the order of 500 to 1000 ppm (parts NO_x per million parts of exhaust gas, by volume) or 20 g/kg of fuel consumption. HC levels are of the order of 600 ppm C_1 or 5 g/kg of fuel.

HC comprises a number of different hydrocarbons, some of which are responsible for the characteristic odour of diesel exhaust emissions. Smoke arises from small carbon particles bound together by higher molecular weight HC (about 0.1 fm) which remain unburned. Up to 0.5% of the fuel may be emitted as smoke at full load. Some HC is absorbed by the smoke particles, and emitted in the exhaust smoke.

NO_x formation requires high temperature, so it is formed mostly in the regions where the air/fuel ratio is close to stoichiometric. The rate of NO_x formation is highest during the period of 5 to 15 degrees crank angle after TDC. During this period, the gas temperature in the cylinder is at its highest levels, promoting formation of NO. The NO reactions are said to be frozen shortly after 20xCA after TDC, when the formation of NO and simultaneous dissociation into N_2 and O_2 stops. This is illustrated in Fig 2.27, Kamimoto et al (1980)

Greeves et al (1977), reported that some HC is formed in the outer

fringes of the fuel spray, and near the walls of the combustion chamber. At the outer spray fringes, the mixture becomes overdiluted, and fails to ignite; long ignition delays allow longer periods for the outer fringes of the spray to become overdiluted. Greeves et al have demonstrated this for a DI engine operating at 1800 revs/min, see Fig 2.28. In addition, fuel remaining in the holes of the injector nozzle, after injection is completed, vaporises late in the combustion process and fails to ignite. The effect of greater sac and hole volume in increasing HC emission has been clearly demonstrated experimentally by Greeves.

Near the chamber walls the fuel air mixture can be quenched, due to heat loss to the walls. As a result this mixtures can fail to burn. Experiments have been conducted, Heywood (1988), during which the ignition delay was kept constant and the coolant was maintained first warm and then hot. With the hot coolant, HC emissions were up to 30 per cent lower. This suggested that, due to heat loss, the mixture near the walls was quenched and failed to burn.

Soot (or smoke) forms in the fuel-rich core of the fuel spray, where the fuel vapour is heated by mixing with hot burned gases. The fuel cracks (decomposes) into its carbon, hydrogen and unsaturated hydrocarbons including polycyclic hydrocarbons. The soot burns in the flame region with a characteristic luminous yellow flame. Most soot comes from unburned fuel carbon; a small amount comes from the lubricating oil.

Measurements of the distribution of particulates within the combustion chamber have been made in an operating DI diesel engine by Aoyagi et al (1980). The highest concentration was found to be around

the core of the fuel spray, where the mixture was too rich. Soon after combustion started, the core of the fuel spray showed very high soot concentrations; these decreased rapidly once injection ended, when mixing of the spray core with the surrounding air took place. Over 90% of this soot eventually burned prior to the exhaust valve opening, Fig 2.27.

2.8 - CONCLUSIONS

For diesel engines to be able to operate at high engine speeds, the rate of air fuel mixing during combustion must be high. In DI engines, swirl and squish could be employed in order to generate turbulence and accelerate combustion.

In DI engines, swirl and squish can be generated by suitable design of inlet port and using bowl-in-piston combustion chambers. The variation in swirl and squish, which are inevitable with certain VCR systems, will have a substantial effect on the combustion process.

Injection timing is an important parameter affecting engine output, economy, and exhaust emissions. The change in combustion rate expected with some VCR systems may require optimisation of injection timing with varying compression ratio, during engine operation.

Experimental results by several investigators have shown that a forced vortex (solid body rotation) flow pattern exists in the cylinder at the end of induction (IVC). However, this is not the case close to the cylinder head face, as a result of fluid friction. With bowl-in-piston combustion chambers, the expected increase in swirl as the piston approaches TDC has been confirmed experimentally by several investigators. With bowl-in-piston combustion chambers, the flow structure within the bowl varies substantially with location, at a given crank angle during compression. With VCR systems which vary the clearance volume, the position of the spray in the piston bowl will vary with changing compression ratio. At a given crank angle, the interaction of the air and fuel spray will, therefore, change with compression ratio due to, both: change in spray position relative to the bowl, and changes in swirl and squish levels.

Experimental tests, and computational fluid dynamic models have shown that bowl offset from the piston axis up to 10% of the piston diameter, decreases the angular momentum of the air at TDC by less than 10%. The effect on turbulence intensity is an increase of similar magnitude. This conclusion is of practical value for modelling of in-cylinder air flows. One such model is presented later in Chapter 5; in common with other authors, the model is applied to a piston bowl whose axis is concentric with the piston axis.

With bowl-in-piston combustion chambers, the turbulence intensity near the bowl rim is much greater than at the bottom of the bowl. Squish appears to have little effect upon the turbulence intensity at the bottom of the bowl. The injection of the fuel should, therefore, be directed towards the upper part of the piston bowl. There is little doubt, that the reduction in squish that occurs with VCR systems at low compression ratios, will reduce the turbulence intensity near the bowl rim, where the fuel is injected. The level of turbulence has been shown to correlate well with smoke emission, over a wide range of engine operating conditions.

Experimental evidence in the literature demonstrated that with high injection rates the detailed air motion becomes less significant, (much of the air fuel mixing energy is derived from the fuel jets). This is relevant to VCR operation with high BMEP, where, the amount of fuel injected per cycle is higher than normal. The injection rate must be higher, if late burning, higher smoke levels, and lower fuel economy are to be avoided.

One important way in which air fuel mixing could be improved at lower swirl and squish levels is through changes in the fuel spray

characteristics. For example, a finer spray would be obtained by the use of higher injection pressure, although pressures above 100 MPa would provide little further reduction in average droplet diameter. A larger number of smaller nozzle holes could result in smaller droplets and also improve fuel distribution.

There is some evidence in the literature that smoke and ISFC, in DI engines with bowl-in-piston combustion chambers, correlate well with crosswind velocity. This is the relative velocity between: the tangential component of the spray tip velocity, and the swirling air tangential velocity, at the instant of spray impingement with the bowl sides.

Chapter 3:
Experimental System and Commissioning Tests

3.1 - DESCRIPTION OF THE EXPERIMENTAL SYSTEM

In order to carry out the experimental work described in this thesis, an engine test facility was installed and commissioned. This involved the installation of a single cylinder diesel engine, including fuel, air and electrical supplies, and the provision of an instrumentation system.

The test facility allowed engine operation under naturally aspirated, and simulated turbocharged conditions.

3.1.1 - Outline

Fig 3.1 shows the arrangement of the test facility which is based on a 0.5 litre single cylinder, high speed direct injection (HSDI) diesel engine manufactured by the Lister company. The engine specification is given in Table 3.1.

A DC motor / generator was connected to the engine via a toothed belt and was used for starting and loading the engine. Fuel flow to the engine could be controlled through the engine fuel-pump rack. The air supply to the engine could be heated using an electric heater, and it could also be pressurized using the laboratory compressed air supply system. Exhaust back pressure could be controlled using a gate valve installed in the exhaust system.

The compression ratio could be altered by raising or lowering the engine cylinder head using shims of different thicknesses in the form of rings.

Speed, torque, fuel consumption, exhaust emissions, gas inlet and outlet conditions and temperatures at several locations around the engine were measured. In addition, injector needle lift, fuel line

Table 3.1 - Standard Engine Specification

TYPE	Lister LV1. Four stroke, vertical, single cylinder, air cooled, direct injection, diesel engine.
ROTATION	Anti-clockwise looking at flywheel.
COOLING	Air circulated around cylinder head and barrel by flywheel mounted fan.
GOVERNING	Variable speed governor, any desired speed between 1100 and 3000 rev/min can be set. Governor maintains speed within +30 rev/min
COMPRESSION RATIO	17.41
BORE	85.73 mm
STROKE	82.25 mm
SWEPT VOLUME	0.4748 litre
FUEL PUMP	Bryce jerk pump with 7.5mm dia. plunger.
FUEL INJECTOR	Bryce high spring injector with three 0.25 mm diameter hole nozzle. Opens at 180 bar.
INJECTION TIMING	Static - 26° CA BTDC.
COMBUSTION CHAMBER ...	Bowl-in-piston, re-entrant, straight bowl sides. Piston crown to cylinder surface clearance (bumping clearance) 0.61 mm.
MAXIMUM SPEED	3000 rev/min.
MAXIMUM CONTINUOUS POWER OUTPUT	6.7 kW at 3000 rev/min.
TORQUE	23 Nm, approximately. Constant over 1700-3000 rev/min.
MINIMUM BRAKE SPECIFIC FUEL CONSUMPTION	0.282 kg/kWh approx. at 3000 rev/min.
LUBRICATING OIL CONSUMPTION	Less than 0.75 % of full load fuel consumption.
INLET PORT SHAPE	Helical

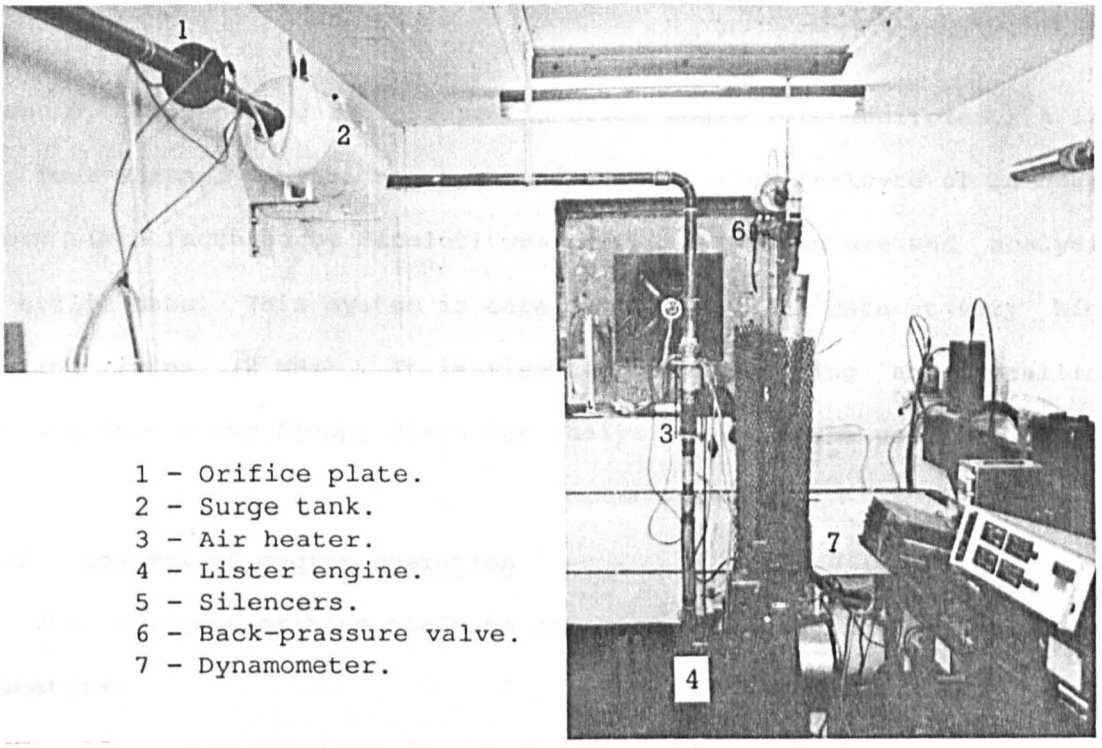

1 - Orifice plate.
2 - Surge tank.
3 - Air heater.
4 - Lister engine.
5 - Silencers.
6 - Back-prassure valve.
7 - Dynamometer.

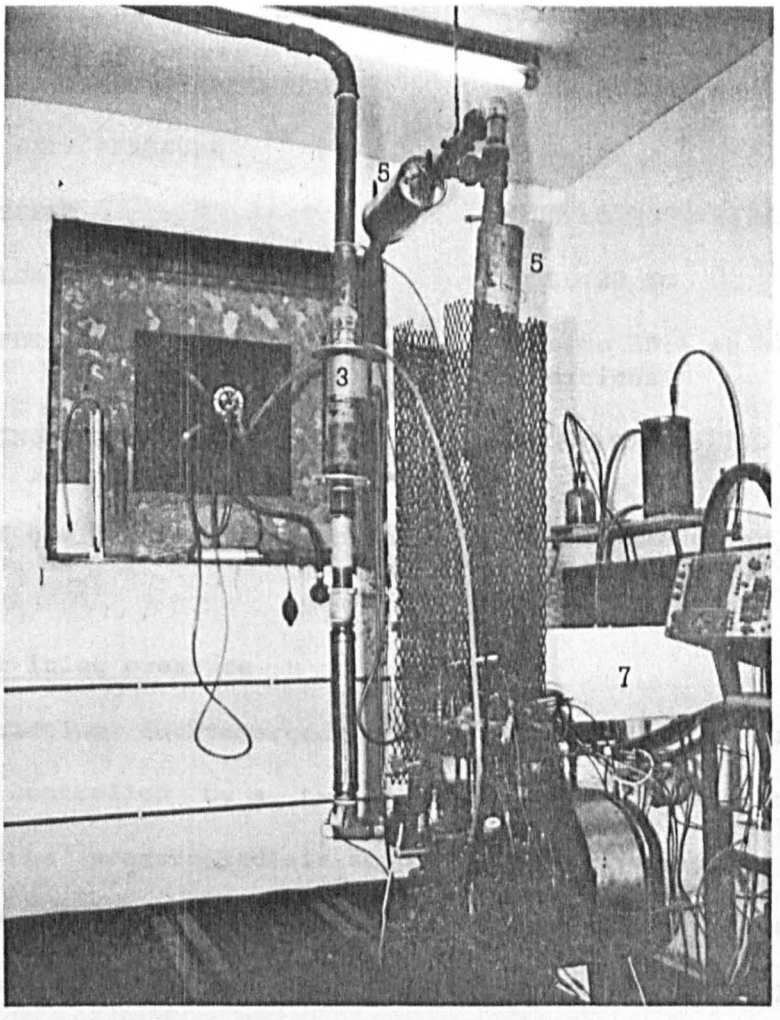

Photographs of the engine test facility.

pressure, cylinder gas pressure and crank angle were monitored. A 12-bit, four-channel digital storage oscilloscope with 16-kbyte of on-board memory (manufactured by Nicolet) was used for the capture and analysis of cyclic data. This system is capable of capturing data at very high sampling rates (2 MHz). It is also capable of storing and recalling captured data using floppy discs for analysis and future use.

3.1.2 - Control of engine operation

The engine operation could be controlled by varying the following parameters:

- ENGINE AIR INLET PRESSURE	1 to 3 bar abs.
- ENGINE AIR INLET TEMPERATURE	up to 120°C
- EXHAUST BACK PRESSURE	
- ENGINE SPEED	1100 to 3000 rev/min
- ENGINE LOAD	up to 23 Nm
- AIR TO FUEL RATIO	down to 20:1 at all running conditions
- STATIC INJECTION TIMING	50°CA BTDC to TDC

Details of how these parameters were controlled are given below.

Engine air inlet pressure

When simulating turbocharged conditions, the engine air inlet pressure was controlled by a two stage pressure regulator valve installed in the pressurised air supply line to the engine (see Fig 3.1). During engine tests, this system maintained a constant air supply pressure to the engine. Between the regulator valve and the engine there

was an air reservoir (surge tank) with a capacity of about 100 times the engine displacement volume; this provided a considerable degree of damping of the air flow pulsations created by the intermittent operation of the engine inlet valve.

Engine air inlet temperature

When simulating turbocharged conditions, the air supplied to the engine could be heated by a 2 kW electric heater installed about one metre upstream of the inlet manifold (see Fig 3.1). The temperature was controlled by an electronic feedback controller. This varied the electrical power supplied to the heater so that the temperature of the intake air was kept constant at the desired value.

Exhaust manifold pressure

When simulating turbocharged conditions, the pressure in the exhaust manifold was varied by means of a gate valve installed in the exhaust pipework (see Fig. 3.1). This simulated the pressure drop across the turbine of a turbocharger.

Engine speed

For small changes in the engine load, the engine speed was maintained nearly constant at the selected value by a mechanical centrifugal governor. The details of the governor are shown in Fig 3.2a. The original linkage between the governor and the fuel pump rack was extended, Fig 3.2.b, so as to allow an increase in fuel flow over the maximum flow rate that was possible with the standard naturally-aspirated engine. The extra fuelling was needed when turbocharging was

being simulated.

An electronic overspeed controller was installed in the fuel supply line to the engine; this could cut-off the fuel supply (using a solenoid valve) when the speed exceeded a selected safe limit (see Fig. 3.1). This solenoid valve could also be operated remotely, which provided an emergency fuel cut-off system.

Engine load

The engine load was controlled by altering the resistance offered to the engine via the DC motor/generator; this was done by varying the generator field current.

Air fuel ratio

The air fuel ratio was set to a desired value by varying the fuel flow and/or the air flow to the engine. The fuel flow rate was varied using the fuel pump rack. The air flow rate, however, could only be controlled independently when simulating turbocharging using the pressure regulator valve, see Fig 3.1. The effect of varying the fuel flow or the air flow rate to the engine was a change in engine speed and load which had to be compensated for by varying the load to the engine as described above.

Static injection timing

The fuel injection starts when the fuel line pressure reaches a preset value early in the stroke of the pump plunger (in the case of an in-line cam-driven fuel pump). Since in this case the camshaft was driven directly from the crankshaft via gears, the static injection

timing was varied by lowering or raising the fuel pump (using special shims). Thus varying the pump rotation prior to start of injection.

3.1.3 - Measured parameters and instrumentation system

The following parameters could be measured:

- Engine air inlet pressure
- Exhaust back pressure
- Air flow rate
- Fuel flow rate
- Engine speed
- Engine load
- Air temperature upstream of the orifice plate
- Ambient temperature
- Air inlet temperature
- Exhaust temperature
- Cylinder head temperature "Exhaust side"
- Cylinder head temperature "Inlet side"
- Cylinder barrel temperature "Exhaust side"
- Cylinder barrel temperature "Inlet side"
- Cylinder barrel temperature "Between valves"
- Cooling air in
- Cooling air out
- Sump oil temperature
- Cylinder gas pressure
- Injector fuel line pressure
- Injector needle lift
- Crank angle

- Volumetric percentage of NO_x in the exhaust gas

- Smoke concentration

Details of how these parameters are measured are given below:

Air inlet and exhaust back pressures

The air inlet pressure to the engine was measured at two locations: 1) upstream of the orifice plate and 2) at the surge tank. Both pressures were measured using U-tube mercury manometers. As a convention, the pressure within the surge tank was taken as the air inlet pressure to the engine. The pressure measured upstream of the orifice plate was used in order to estimate the air mass flow rate supplied to the engine.

The exhaust gas pressure was measured using a U-tube manometer installed just before the gate valve (used as a restrictor for turbocharging simulation, see Fig. 3.1). Between this measuring point and the exhaust manifold there were two silencers of combined capacity of about 20 times the engine displacement; these damped the pressure pulsations in the exhaust system at this measuring point. The smallest graduation on all the U-tube mercury manometers were 1 mm.

Air flow rate

The air flow rate supplied to the engine was measured using a 21.6mm (0.85 in) orifice plate constructed and installed upstream of the surge tank, according to British Standard BS1042. The parameters needed for the estimation of air flow rate were:

a) Orifice plate upstream pressure, measured by a U-tube mercury manometer.

b) Pressure difference across the orifice plate, measured in millimeters of water by an inclined, U-tube, paraffin filled manometer.

c) Orifice upstream air temperature, measured using a thermocouple.

d) Relative humidity of the air flowing through the orifice, measured using a sling hygrometer. When simulating turbocharging, air was blown on the hygrometer, from a tapping on the air supply line to the engine.

The design of the orifice plate is detailed in section A.1 of Appendix A. The orifice plate measurements were compared under steady flow conditions with the measurements of air flow rate using a positive displacement volumetric meter manufactured by Romet. Agreement in mass flow rate was within 3% for the range of 0 - 15 g/s. Details of this comparison are given in section A.1 of Appendix A. When the engine was operating the orifice plate could not be relied upon to give the correct value of air flow rate due to the air pulsations present at the plane of the orifice plate. The pulsations were considerably reduced by the presence of the surge tank, but still present. These pulsations were observed using a Lucas Dawe LAM1000 corona-discharge, instantaneous air mass flow meter. The orifice plate was calibrated for pulsating conditions, at different engine speeds, using the Lucas Dawe LAM1000 flow meter. Further details and the calibration curve can be found in section A.1 of Appendix A.

A listing of the program "MASSFLOW" (used for estimating the air mass flow rate supplied to the engine) written, according to BS1042, for a BBC microcomputer is also included in section A.1 of appendix A.

Fuel flow rate

The fuel flow was measured by an electronic system which timed the period required for the engine to consume 24.07 cm^3 of fuel. This was then converted to mass flow rate using the density of diesel fuel at the

measured fuel temperature, according to the following expression:

$$\rho_f = 844\,(\,1 - 0.818 \times 10^{-3}\,T\,) \qquad \ldots\ 3.1$$

where ρ_f is the density of the fuel in kg/m^3 at temperature T °C. Eq 3.1 was also incorporated in the program "MASSFLOW" in order to calculate the fuel flow rate and overall air fuel ratio. The fuel flow measuring system was calibrated prior to the start of the engine test program.

Engine speed

The engine speed was measured electronically using a digital frequency counter with a gate time of 10 seconds. Impulses were received by the counter once per revolution from an electromagnetic proximity detector installed on the engine. The resolution of the measurement was: ±1 revolution, or ±0.6 % at 1000 rev/min; and ±1 revolution, or ±0.2 % at 3000 rev/min.

Engine torque

The torque developed by the engine was measured by means of a swinging-beam and spring-balance system attached to the casing of the dynamometer. The smallest graduation on the spring balance was 1.0 lb (4.448 N) allowing a resolution of the measured torque of 0.7457 Nm or about 5.9 % at engine mid-load conditions.

Temperatures

Thermocouples were used at various positions around the engine. All

the thermocouples were connected to an amplifier via a twenty-one way selector switch. The readings were displayed in degree Celsius. The error of this system was measured using, first, melting ice and then steam. The system had an offset of +1°C at 100 and at 0°C. This corresponds to an error of 0.5% at 200°C and 2% at 50°C. Fig 3.3 shows in more detail the locations of these thermocouples which were installed around the combustion chamber.

Cylinder gas pressure

The cylinder gas pressure was measured using an AVL water-cooled piezoelectric pressure transducer (type 8QP500C) and a Kistler model 566 (S/N747) charge amplifier. The pressure transducer was connected to the charge amplifier using a teflon-coated low-capacitance (60pf/m) coaxial cable. The output from the pressure transducer was temperature compensated. The measuring range of the pressure transducer was 0-150 bar (dynamic pressure) with a gas temperature range of up to 2500°C when the transducer was water-cooled (water cooling was used during the tests described here). The pressure transducer was installed onto the engine, so that the sensing face of the transducer was almost flush with the inner surface of the cylinder head. This was necessary in order to avoid high frequency pressure pulsations being picked up by the transducer. If a cavity existed between the transducer sensing surface and the main combustion chamber space, high frequency acoustic waves could have been generated in the cavity and superimposed on the main chamber pressure signal.

The transducer, together with the amplifier, were calibrated under steady state conditions using a dead-weight tester and a digital

voltmeter. All the connecting plugs and sockets were regularly cleaned with Freon-113 to ensure that there was no leakage of charge due to dampness or dirt. The calibration curve is shown in section A.2 of appendix A.

Fuel line pressure

The fuel pressure in the high-pressure supply pipe between the fuel pump and the injector was measured using an 800 bar Honeywell strain-gauge pressure transducer. The transducer was connected to a Lucas-Dawe bridge amplifier. The pressure transducer forms the fourth leg of a 2 kΩ resistance bridge; the fuel line pressure changes the resistance of the 2 kΩ strain gauge in the pressure transducer. The result is that an out of-balance voltage is generated across the bridge which is amplified by the Lucas-Dawe bridge amplifier. The calibration factor, according to the manufacturer, was given as 52770.4 Pa / bridge amplifier gain.

Injector needle lift

The injector needle lift was detected using a variable inductance system connected to an FM oscillator/demodulator (type P4550/236) manufactured by Cussons Ltd. The engine injector was modified to allow a small coil to be installed inside the injector housing. The coil bobbin was turned from Nylon. The coil had 150 turns of 32 swg enamelled copper wire with a resistance of 9 and inductance of 200 mH. The injector needle was extended using a 1.5 mm brass rod which travelled half way up the bobbin. The details of the installation of the coil are shown in Fig 3.4. As can be seen from the figure, the available space for the installation of the coil was very restricted.

Crank angle

The crank angle was measured by a variable reluctance electromagnetic pick-up which is activated by the teeth of the starter gear ring on the engine flywheel. The pick-up consisted of a coil having a magnetic core. The passage of the flywheel starter ring induced a voltage through the coil which was shaped by a Schmidt trigger (housed within the sensor) into a TTL-compatible pulse, corresponding to the passage of the teeth. There were 108 teeth on the flywheel starter ring, so a pulse was generated every 3.33 °CA. The gap between the two teeth closest to TDC was filled to produce an extra pulse which marked the TDC position. Crank angle was recorded and displayed on the digital storage oscilloscope simultaneously with other signals such as cylinder pressure and injector needle lift.

Exhaust gas analysis

The exhaust gas was analysed using a chemiluminesence NO_x analyser manufactured by Thermoelectron Corporation. The exhaust gas was first passed through two ordinary engine oil filters in series. The filters were used to remove excess particulates which would have otherwise damaged the analyser. Before entering the analyser the gas was cooled by a refrigeration system down to 2°C, in order to remove water vapour from the sample gas. The analyser was switched on and allowed to warm up for at least 30 minutes, and was calibrated using a standard 240 ppm Nitrogen Oxide (NO) gas in Nitrogen before any readings were taken.

The principle of operation of the NO_x analyser is as follows. A small sample from the exhaust, containing NO, is drawn into the instrument. This reacts with Ozone (generated within the instrument) in

a darkened chamber. The reaction generates visible light whose power is related to the NO concentration in the darkened chamber. The light emitted is monitored by a photodetector, whose output is processed by the signal conditioning and display electronic circuits, so that the NO content is displayed in parts per million by an analogue meter.

Ozone is generated by passage of oxygen or zero-grade air through a tube in which a continuous spark is maintained by a high voltage electrical system. The small quantity of NO_2 present in the exhaust gases can also be measured. This is done by passing the sample gas through an oven, at 650 °C, which dissociates NO_2 into NO and O_2. An internal system of fine orifices maintains the flow rate of the sample into the darkened chamber constant so that only the NO_x concentration is measured. The smallest division on the analogue display meter was 2.5 % of the full scale value (i.e. 5 ppm in the range of 0-250 ppm NO_x, 25 ppm in the range of 0-1000 ppm NO_x, and 50 ppm in the range of 0-2500 ppm NO_x).

Exhaust smoke

Exhaust smoke was measured using a standard TI Dieseltune 114 smoke density tester. Smoke particulate samples were taken from the exhaust pipe (after the silencers and the gate valve) using the suction pump and standard filter papers. This position was chosen to allow good mixing of the exhaust stream and damping of pressure pulsations. Some loss of particles in the pipe work and silencers (before the sampling location) inevitably took place. The standard Bosch evaluation meter was then used to read out the Bosch values of the smoke particulate deposits on the filter paper. In principal, the evaluation meter measures the amount

of light reflected by the smoke deposited on the filter paper on an arbitrary scale of 0-10. Five, on this scale, corresponds to the amount of light reflected by a clean filter paper which has 50% of its surface area covered with a black, non reflective coating. The evaluation meter was calibrated, before a reading was taken, using the standard calibration paper, and according to the manufacturer's instructions. The smallest division on the analogue display of the evaluation meter was 2% of the full scale value (i.e. 0.2 Bosch unit), or 4 % of mid-range reading of 5 Bosch units.

3.1.4 - Cyclic data acquisition system

The data acquisition system was based around a Nicolet digital oscilloscope, capable of very fast data capture. Storage of data on floppy discs and limited data processing was also possible. Captured data could also be plotted using a digital plotter. The system consisted of the following items:

(i) - Nicolet 4094 digital oscilloscope
(ii) - Nicolet XF-44/2 dual disc recorder
(iii) - HP 7470A digital plotter
(iv) - IBM keyboard

The oscilloscope was used to capture signals of:

a - Cylinder gas pressure
b - Crank angle
c - Injector needle lift
d - Fuel line pressure

The oscilloscope had four channels and a total of 16 kbyte (16 bit per byte) RAM which could be allocated as follows: 16k as a whole to one

channel, 2 x 8k to two channels, and 4 x 4k to four channels. Each pair of two channels could sample simultaneously every 0.5 microsecond (at 2 million samples per second) using a 12 bit analogue to digital converter. The captured signals from all four channels could be displayed on a 5" high definition screen, and expanded both horizontally and vertically by up to 265 times. The co-ordinates of each individual sample could be found using vertical and horizontal cursors; these co-ordinates were displayed digitally at the bottom of the screen as voltage and time respectively. A variety of mathematical routines are available as software on floppy discs. The data processing routines used during this project were: differentiation, and calculation of signal minimum and maximum values between selected cursor positions.

The captured signals could be stored on 5.25" double-sided, double-density floppy discs. The stored data could be recalled for display and manipulation using the system software. There were options for output to digital and analogue plotters. A digital plotter was used for this project.

3.2 - BASELINE TESTS

3.2.1 - Purpose of baseline tests

The aims of the baseline tests were as follows: (a) to check correct operation of the experimental system and provide experience in using the system; (b) to provide the operating limits of the engine in terms of maximum cylinder gas pressure and maximum metal temperatures around the combustion chamber; and (c) to provide information on the standard engine performance (BMEP, BSFC, exhaust emissions and combustion performance) for comparison with results from low compression ratio tests.

The specific objective of the baseline tests was to establish the values of various engine performance parameters, and in particular:

- The highest cylinder gas peak pressure occurring over the entire speed and load operating range.
- Temperatures at certain cylinder-head and liner locations. In particular, the highest metal temperature adjacent to the exhaust valve seat.
- Brake specific fuel consumption.
- Volumetric efficiency.
- Various combustion performance parameters such as ignition delay, rate of pressure rise, injection timing, and exhaust emissions.
- Temperatures at 13 locations, including intake air, exhaust gas, lubricating oil, and several cylinder head and liner metal temperatures.

3.2.2 - Experimental procedure for baseline tests

The baseline tests comprised a series of experiments at constant speed and varying brake mean effective pressure covering the entire speed and load ranges, from almost idling (1300 rev/min) to maximum speed (3000 rev/min) and from almost no load (about 0.7 bar BMEP) to full load (about 6.0 bar BMEP).

In order to reduce experimental errors, several readings were taken for most parameters measured, at each speed and load condition. These parameters, together with the number of readings taken are shown bellow:

Maximum cylinder pressure .... 10 randomly selected cycles

Injection timing ..... 10 randomly selected cycles

Start of combustion ..... 10 randomly selected cycles

Rate of pressure rise ..... 10 randomly selected cycles

Smoke in Bosch units ..... minimum of 3 samples

Each time the engine speed or load was altered, the engine was allowed to reach a stable condition for about 30 minutes, after which no change in cylinder liner and head temperatures were detected.

Start of combustion was found by differentiating once the cylinder pressure signal. The slope of the compression curve (dP/dt) normally reduces prior to the point of start of combustion, see Fig 3.5. This is normally followed by a change-over to a sharp rise in dP/dt as a result of the rise in cylinder pressure, following the ignition of the premixed fuel and air. The combustion was, therefore, taken to have started where dP/dt reached a minimum for the first time, (see Fig 3.5). This figure also shows the way in which the maximum rate of pressure rise was

obtained from the dP/dt signal.

The start of injection was taken as the crank angle at which the needle lift signal reached 5% of its maximum value (see Fig 3.5).

3.2.3 - Discussion of baseline test results

The baseline tests yielded the highest value for the cylinder peak pressure, together with the highest values of two critical metal temperatures. These are shown in Table 3.2. These values were not exceeded by more than a few percent during subsequent tests at the lower compression ratio.

Table 3.2 - Highest cylinder gas pressure and metal temperatures recorded during the baseline tests.

PARAMETERS	MEASURED VALUES	SPEED (rev/min)	BMEP (bar)
P_{max} / bar	80	1300	5.1
T_1 / °C	217	2500	4.7
T_2 / °C	181	2500	4.7

T_1 = Cylinder-head metal temperature (adjacent to the exhaust valve side)
T_2 = Cylinder-barrel metal temperature (between the valves)

The rest of this section presents and discusses, briefly, the main results from the baseline tests. For the sake of brevity, the results of the baseline tests shown in this section (Figs 3.6 and 3.8) are at a constant speed of 1300 rev/min and varying load. Corresponding results at speeds of 1700, 2160, 2500 and 3000 rev/min show similar trends, and are included in section A.3 of Appendix A.

Temperatures around the engine

The variation of combustion chamber metal temperatures, and other temperatures around the engine, at constant speed of 1300 rev/min and varying load are shown in Fig 3.6.

As one would expect, all the temperatures increase with increasing engine load. The highest metal temperature occurred at the exhaust valve side of the cylinder head. This probably was due to this position being furthest from the inlet valve and not receiving as much benefit of cooling from the fresh charge; also, the high flow rate of the exhaust gases increase the heat transfer rate to this region.

The intake air temperature, measured upstream of the inlet valve, rises by about 15-20 °C from no load to full load (at all speeds). This indicates a considerable heat transfer from the inlet manifold to the intake air.

Volumetric efficiency

The variation of volumetric efficiency with speed and load is shown on Fig 3.7. This was measured with the air supply pipe and surge tank (see Fig 3.1) connected to the engine, but with no compressed air supply; instead ambient air was admitted into the pipework, 2 m upstream of the orifice plate. The volumetric efficiency calculation was based on the atmospheric conditions.

The reduction in volumetric efficiency with load, at constant speed, is due to increase in heat transfer to the intake air from the inlet manifold and combustion chamber walls. This raises the air temperature, resulting in reduced air density and volumetric efficiency.

The tendency for the reduced volumetric efficiency with increasing

engine speed, that can be seen in Fig 3.7, is due to higher intake air temperature, and increased throttling losses as speed increases. The rise in volumetric efficiency at 3000 rev/min, against the trend, might have been due to air-inertia effects and wave action in the inlet manifold, creating a higher inlet pressure at this speed.

When the air supply to the engine was pressurised (for turbocharging simulations at low compression ratio), the calculation of the volumetric efficiency was based on the air pressure and temperature just downstream of the air heater (see Fig 3.1). Results at low compression ratio are shown in chapter 4.

Brake specific fuel and air consumption

Fig 3.8 shows the effect of engine load on brake specific fuel consumption (BSFC) and brake specific air consumption (BSAC) at 1300 rev/min. BSFC decreased initially, with increasing load, since the mechanical efficiency of the engine increased rapidly. However, at high loads the mechanical efficiency increases at a slower rate whilst the cycle thermodynamic efficiency continues to decline; as a result, the BSFC begins to rise at high loads.

The measured results for BSFC at around 80-90% of full load, is about 0.304 kg/kWh at 1300 rev/min (and 0.330 kg/kWh at 3000 rev/min) which is about 10 % higher than the manufacturer's specified value.

Smoke

Smoke, measured in Bosch units, increased with increasing load at constant speed, see Fig 3.8 (also smoke increased with increasing speed).

Apart from the lower air fuel ratio (and reduced oxygen availability at higher loads), smoke might also have risen because dynamic injection timing tended to retard somewhat at higher loads. The combination of longer injection period and late timing at higher loads, may have resulted in later fuel burning and high smoke emissions.

Dynamic injection timing

The static injection timing was set to the manufacturer's specification, 26 °CA BTDC. The dynamic injection timing was measured using both the needle lift signal, NLS, and fuel line pressure signal, FLP. These varied due to dynamic effects, as shown in Table 3.3.

TABLE 3.3 - Variations in dynamic injection timing with load, measured from the needle lift signal NLS, and the fuel line pressure signal FLP.

Speed rev/min	Injection timing °CA BTDC			
	NO LOAD		FULL LOAD	
	NLS	FLP	NLS	FLP
1300	18.6	27.6	14.8	27.2
1700	18.4	28.1	14.0	26.7
2160	18.5	27.3	15.6	26.3
2500	17.6	----	17.6	----
3000	15.6	28.4	14.3	25.5

There was no mechanical system for the automatic variation of injection timing according to load and speed. The variation shown in

Table 3.3, was a result of varying fuel leakages past the pump plunger and injector needle, the compressibility of the fuel (and any dissolved gases), and the elasticity of the injection system components. These correspond to a crank angle of 8 to 12° at no load and full load respectively.

Ignition delay

At constant engine speed the ignition delay decreased with increasing load, see Figs 3.8 and 3.9. This was most likely due to higher trapped air temperature at higher loads, as a result of higher heat transfer rates from the inlet manifold, inlet valve, and cylinder walls.

Ignition delay periods (measured in milliseconds) shortened with increasing speed at a constant load, see Fig 3.9. Similarly, this was likely to have been due to hotter trapped air, and also due to greater trapped air activity during combustion at higher speeds.

Peak cylinder pressure

At constant speed, the cylinder peak pressure, P_{max}, increases with increasing load, see Fig 3.8. This is thought to be due to more fuel being burned at higher loads, and slight advance of the start of combustion, as well as increased rate of pressure rise at higher engine loads. Also, P_{max} was observed to be higher at lower engine speeds.

3.3 - STEADY FLOW RIG

As a part of the project described in this thesis, a computer model was developed which predicted, at different compression ratios, the swirl and squish of the trapped air as the piston approached TDC. Part of the input information required by the model was the swirl imparted to the induced air at inlet valve closure (IVC). A steady flow rig was used in order to obtain this swirl at IVC.

The steady flow rig consisted of the Lister cylinder head, including the inlet manifold and valve assemblies. This was attached on to an open ended barrel which had the same internal diameter as the cylinder barrel of the Lister engine, and a length of approximately two times the bore, see Fig 3.10. The inlet valve could be held open, at different positions, using an adapted bolt. The valve opening was measured using a dial gauge with a resolution of 0.025 mm (compared with valve openings of 0 to 10 mm). Air, from the laboratory compressed-air supply, was supplied at a steady flow rate to the cylinder head.

An orifice plate installed in the air supply line (according to BS1042) was used to measure the air flow rate. This was the same orifice plate used to measure the air flow rate during the engine tests described in this Chapter and in Chapter 4. The air mass flow rate was controlled using a pressure regulator valve (see Fig 3.1) and a gate valve (for finer adjustment).

The rig was instrumented to measure the pressure drop across the inlet valve, using an inclined water manometer. The local air velocities at different locations within the barrel were measured using a single hot-wire anemometer. The anemometer could be traversed across any diameter on any horizontal plane within the vertical barrel, by means of

an axial/cross slide, mounted on a rotary base. The anemometer was calibrated in a wind tunnel so that the voltage output from the anemometer was proportional to the air velocity. The measurements of the local air velocities within the barrel, using the hot wire anemometer, were carried out by Bond (1988).

The steady flow rig was used to determine the following parameters at a number of mass flow rates and inlet valve lifts.

i - Inlet valve discharge coefficient.

ii - Air swirl within the barrel; one bore diameter below the cylinder head face.

iii - Local air velocity components, in the tangential and and axial directions, at a number of radii.

iv - Air moment of momentum rate imparted by the inlet-manifold-and-valve assembly.

Further details of the rig and the instrumentation can be found in Bond (1988). The method of calculation of the above parameters is described in Chapter 5.

3.4 - INJECTOR NOZZLE TESTS

With VCR systems which vary the clearance volume, the position of fuel-spray impingement on the piston crown would vary with varying compression ratio. This is a particularly important aspect of VCR operation with bowl-in-piston combustion chambers. With this type of chamber, the spray should be directed towards the rim of the bowl; as discussed in Chapter 2, this is a region where air activity is highest. The fact that spray impingement occurred in the case of the Lister engine was confirmed from observations of carbon deposits on the piston crown, see Fig 3.11.

A simple experiment was conducted in order to find out the way in which the position of the fuel spray impingement would change when the compression ratio of the Lister engine was lowered from the standard 17.4:1 to 12.9:1.

The injector was connected to a manually-operated Hartridge injector-testing machine. Photographs of the fuel sprays were taken, and an average value of the cone angle was found by measuring the angle from the photographs. The average cone angle when injecting test liquid into air at atmospheric conditions was found to be 16.5° for the standard-engine three-hole nozzle; and 18.3° for a four-hole nozzle used in tests described in Chapter 4. Also the position of the axis of each spray cone (with respect to injector-body axis) was determined during these tests.

From this information the point of fuel spray impingement at 15° CA BTDC was determined for the two nozzles at different compression ratios.

The tests on the Hartridge injector-tester were conducted at atmospheric conditions. At the elevated air pressure and temperature, the fuel spray cone angle would be different.

Several researchers have studied experimentally the effect of pressure and temperature on fuel spray geometry (see section 2.6.1, Chapter 2). There is general agreement that the relevant parameter is the gas density into which the fuel is injected, (Youl et al, 1984, Varde et al, 1984, Reitz and Bracco, 1979). Typical results are those of Varde et al, which shows that the cone angle increases rapidly as the gas density is raised. The rate of increase of the spray cone angle reduces as the gas density reaches values of 10 to 15 kg/m^3. Varde et al (1984) showed that the spray-cone angle and the gas density could be correlated well by the following relationship:

$$\frac{\tan\theta_1}{\tan\theta_2} = \left[\frac{\rho_1}{\rho_2}\right]^{0.33} \quad \ldots\ldots 3.2$$

Thus, using Varde's results, it was possible to correct the results of the injector tests at atmospheric conditions. The air density at onset of combustion in the Lister engine was calculated from the measured trapped air mass, and the volume of the cylinder above the piston at onset of injection.

Fig 3.12 shows the plan view of the fuel spray centre-line for both the three and the four-hole nozzles. Fig 3.13 shows the cross sections of the piston crown and the position of the fuel sprays at two compression ratios. The spray cone angle shown in Fig 3.13 is an average value calculated at an air density of about 11.0 and 12.9 kg/m^3 for the naturally aspirated and turbocharged conditions respectively.

Looking at Figs 3.12 and 3.13, it can be concluded that the change in the compression ratio from 17.4:1 to 12.9:1 is not likely to effect fuel impingement significantly.

Chapter 4: Experimental Results at Low Compression Ratio

4.1 - OUTLINE OF TESTS

Section 3.2, presented results from a series of baseline tests with the engine in its standard form. Their aim was: (a) to check correct operation of the experimental system and provide experience in its use, (b) to establish the operation limits of the engine, in terms of maximum cylinder gas pressure and maximum metal temperatures around the combustion chamber, and (c) to provide information on the standard engine performance (BSFC, exhaust emissions and combustion performance) for comparison with results from the low compression ratio tests.

The results presented in this chapter were obtained at a lower compression ratio of 12.9:1 (compared with 17.4:1 for the engine in its standard form). Note that this low compression ratio was assumed to be the lower limit of the VCR system for the Lister engine. Therefore, the broad aim of the tests at this low compression ratio were:

1 - To investigate the effect on engine performance (in particular on combustion performance) of the increase in clearance volume.

2 - To investigate ways in which detrimental effects on engine performance, specially exhaust emissions, could be ameliorated.

3 - To quantify the maximum benefits, in terms of increase in BMEP and possible reduction in BSFC, that would arise from lowering the compression ratio and increasing the boost pressure expected with VCR system operation.

In order to simulate VCR operation, throughout the tests described in this chapter, the peak cylinder pressure was maintained constant at 80 bar. This was the maximum value measured, over the entire standard engine operating range, during the baseline tests (see section 3.2).

Also, a number of critical metal temperatures around the combustion chamber were monitored (for example the metal temperature adjacent to the exhaust valve) and were not allowed to rise significantly above the maximum values recorded during the baseline tests.

Table 4.1 shows a test matrix, describing all the tests which are discussed in this chapter.

TABLE 4.1 - Test matrix.

TEST NUMBER	ENGINE SPEED (rev/min)	NOZZLE HOLES	PLUNGER DIAMETER (mm)	AIR FUEL RATIO	STATIC INJ. TIMING (^{o}CA BTDC)
1	1300	3	7.5	25:1	20
2	1300	3	7.5	25:1	25
3	1300	3	7.5	25:1	30
4	1300	3	7.5	20:1	25
5	1300	3	7.5	30:1	25
6	1300	3	8.5	25:1	20
7	1300	3	8.5	25:1	25
8	1300	3	8.5	25:1	30
9 IC	1300	3	7.5	25:1	25
10	1300	4	7.5	35:1	30
11	1300	4	7.5	25:1	30
12	1700	3	8.5	25:1	20
13	1700	3	8.5	25:1	25
14	1700	3	8.5	25:1	30
15	1700	3	7.5	20:1	25
16	1700	3	7.5	30:1	25
17 IC	1700	3	7.5	25:1	25
18	1700	4	7.5	25:1	38
19	1700	4	7.5	25:1	30
20	1700	4	7.5	25:1	25
21	1700	4	7.5	30:1	30
22	1700	4	7.5	35:1	30
23	2100	4	7.5	30:1	30
24	2100	4	7.5	35:1	30
25	2100	4	7.5	40:1	30

IC - Simulated Intercooling

Plunger diameter - diameter of the fuel pump plunger

For each test condition, the engine was controlled so as to achieve a peak cylinder pressure of 80 bar at the desired air fuel ratio and engine speed. This meant that the fuel and air flow rates to the engine had to be adjusted so as to achieve this operating condition. As it can be seen from Table 4.1, most of the tests were carried out at an air fuel ratio of 25:1 in order to investigate the engine performance near full-load conditions.

As it will be appreciated, each test proved to be time consuming; in order to achieve a peak pressure of 80 bar, at a given air fuel ratio and engine speed, four interacting operating variables had to be adjusted (fuel flow rate, air inlet temperature, exhaust back pressure, and the boost pressure). For example, if a slight adjustment to the air fuel ratio was required, this necessitated adjustments to the boost pressure and fuelling rate; this had knock-on effects on the air inlet temperature, exhaust back pressure, engine speed, and peak cylinder pressure. Since each of these variables had to be controlled individually with no automatic feedback control system, on average it took about two hours for each test condition to be investigated.

In order to simulate turbocharged operations, for each test, the air supply to the engine was pressurised and heated (see section 3.1.2); the pressure in the exhaust system was also adjusted using a gate valve (see Fig 3.1). The appropriate level of inlet air temperature and exhaust back pressure were calculated as follows: (a) air inlet temperature, from the relation for isentropic change of state and the isentropic efficiency of the compressor,

$$T_2 = \frac{T_1}{\eta_c}\left\{\left[\frac{P_2}{P_1}\right]^{\frac{(\gamma_a-1)}{\gamma_a}} - 1 + \eta_c\right\} \quad \ldots\ 4.1$$

where P_1 and T_1 are the atmospheric pressure and temperature, η_c is the compressor isentropic efficiency (assumed 74 %), and P_2 is the selected boost pressure; (b) the exhaust back-pressure, P_3 was calculated from the following expression:

$$P_3 = P_1\left\{1 - \frac{W_t}{(\dot{m}_a + \dot{m}_f)\, c_{pg}\, \eta_t\, T_3}\right\}^{\frac{\gamma_g}{(1-\gamma_g)}} \quad \ldots\ 4.2$$

where

$$W_t = \frac{\dot{m}_a\, c_{pa}\, (T_2 - T_1)}{\eta_m} \quad \ldots\ 4.3$$

and c_{pa} and c_{pg} are the specific heat capacities of air and the exhaust gases respectively. Equation 4.3 expresses the work balance of the compressor-turbine combination. $\dot{m}_a$ and $\dot{m}_f$ are the measured air and fuel mass flow rates to the engine, and T_3 is the measured exhaust

temperature. η_m is the mechanical efficiency of the turbocharger, and η_t is the isentropic efficiency of the turbine (assumed as 96% and 76% respectively). A microcomputer program was used to calculate the appropriate values of air inlet temperature and exhaust back pressure while the tests were underway.

For each test, the metal temperature near the exhaust valve was monitored, so as to ensure that it did not significantly exceed the maximum value obtained during the baseline tests.

The following sections discuss the outcome of the tests carried out at the low compression ratio.

4.2 - EFFECT OF INJECTION TIMING ON ENGINE PERFORMANCE

4.2.1 - Relation between ignition delay and maximum rate of pressure rise

Fig 4.1a shows the relation between the ignition delay and the rate of pressure rise in the case of the three-hole nozzle and various engine operating conditions. Fig 4.1b shows this relation in the case of the four-hole nozzle.

Although the trend is more pronounced in the case of the three-hole nozzle, both figures show that as the ignition delay increased, the rate of pressure rise became greater. This is believed to be due to the greater amount of prepared mixture that burned during the premixed combustion phase.

4.2.2 - Effect of injection timing on ignition delay and maximum rate of pressure rise

Fig 4.2 shows the effect of injection timing on the ignition delay, for a constant air fuel ratio of 25:1 and various engine operating conditions. There is a clear trend of rising ignition delay as the injection timing was advanced. This was , firstly, due to the fact that as timing was advanced, injection took place into less compressed and less turbulent air; secondly, as will be seen in a later section, the inlet boost pressure (and air temperature) were observed to decrease as timing was advanced.

One major effect of this increase in delay, when timing was advanced, was a rise in the maximum rate of pressure rise, as seen in Fig 4.3.

4.2.3 - Effect of injection timing on boost pressure

It has already been shown that advancing the injection timing caused an increase in the maximum rate of pressure rise. The effect on engine operation of this increase in rate of pressure rise, was to increase the maximum cylinder pressure, P_{max}. However, owing to the constant-P_{max} mode of operation adopted for the tests, this tendency for the P_{max} to rise had to be counteracted with a reduction in boost pressure (at constant air fuel ratio) and, therefore, a reduction in the trapped amount of air fuel mixture. This is shown in Fig 4.4, where it can be seen that the boost pressure decreased when the timing was advanced (at constant air fuel ratio of 30:1 and constant P_{max} of 80 bar).

4.2.4 - Effect of injection timing on BMEP

Fig 4.5 shows that at a constant air fuel ratio of 25:1, the BMEP decreased as the injection timing was advanced. This decline could be explained as follows:

(a) - As injection timing was advanced the boost pressure was lowered (as explained in section 4.2.3) and, therefore, the air mass trapped within the cylinder was reduced. To maintain a constant air fuel ratio of 25:1, the fuel supplied to the engine had to be reduced which inturn had a knock-on effect on BMEP.

(b) - As injection timing was advanced, the maximum rate of pressure rise increased (as explained in section 4.2.2), therefore the level of the cylinder gas pressure during compression increased. As a consequence, the negative work done during the compression increased, which resulted in a reduction in BMEP. The effect of maximum rate of

pressure rise on BMEP is shown explicitly in Figs 4.6a and 4.6b.

4.2.5 - Effect of injection timing on BSFC

Fig 4.7 shows the effect of injection timing on BSFC at the air fuel ratio of 25:1 and various engine operating conditions. There was a tendency for BSFC to decrease as the timing was advanced. However, further advancing of the injection timing increased the BSFC. It would appear that the timing-for-minimum-BSFC was in the region of 21 to 25 ^{0}CA BTDC. However, this range did not give the best BMEP or smoke results. Obviously, the choice of best injection timing will have to be made by considering BSFC, BMEP and smoke emission together. In addition, other parameters such as NO_x and HC emissions would have to be taken into account during a timing-optimisation exercise. The trade-offs between BSFC, BMEP and smoke are considered in a later section.

4.2.6 - Effect of injection timing on smoke emission

As discussed in section 2.2, injection timing can have a considerable effect on engine performance and smoke emission. Fig 4.8 shows that as the injection timing was advanced, the smoke level declined. This decline was accompanied by a reduction in exhaust gas temperature, indicating that combustion ended earlier with advanced timings (see also Fig 4.9). Smoke or soot particles are formed and subsequently burned throughout the combustion process. However, the unsaturated hydrocarbons, including polycyclic hydrocarbon particles, that are formed late in the combustion process fail to burn due to unfavourable conditions towards the end of the combustion process (due to low gas pressure and temperature). These particles form the nuclei

for the unburned carbon and smaller unsaturated hydrocarbons to coalesce into larger soot particles. Thus, the lower smoke levels at advanced timings could have been due to smaller amount of fuel being present late into the expansion stroke.

4.2.7 - Tradeoffs between BMEP, BSFC, and smoke with varying injection timing at constant air fuel ratio

Fig 4.10 shows the tradeoff between BSFC, BMEP and smoke, with varying injection timing at constant air fuel ratio and simulated VCR operating conditions. The figure shows that advancing injection timing was effective in reducing smoke emissions, but at the expense of reduced BMEP due to a reduction in the quantity of fuel injected (see section 4.2.4). However, it is interesting to note that BSFC reduced with reducing smoke (as the timing was advanced), despite a reduction in BMEP and a consequent reduction in mechanical efficiency. This improvement in BSFC, with advancing timing, was probably due to improvements in cycle and combustion efficiencies.

4.3 - EFFECT OF INJECTION RATE ON ENGINE PERFORMANCE

Two fuel pumps were used for these tests. The first had a 7.5 mm diameter plunger fitted by the manufacturer as standard to the engine; the second had an 8.5 mm plunger which gave a theoretical increase of 28.5% in the injection rate.

4.3.1 - Effect of injection rate on the fuel spray characteristics

For a given injection system (constant total nozzle hole flow area), an increase in the injection rate would tend to increase the pressure difference across the nozzle holes, and improve the fuel atomisation and increase the spray penetration. A simple calculation, using the orifice equation for incompressible flow with C_d=0.7, suggests that the pressure drop across the nozzle holes, δP increased when the 7.5 mm plunger was replaced by the 8.5 mm one. The fuel volume flow rate was estimated from measurements of the fuel volume injected per cycle, and the unseated period of the injector needle. The results are summarised in Table 4.2.

TABLE 4.2 - Estimated variation in pressure drop across the injector nozzle with increasing plunger diameter.

Engine Speed rev/min	Number of nozzle holes	Nozzle hole diameter	Increase in δP bar	%
1300	3	0.25mm	33.3	48.1
1700	3	0.25mm	33.6	32.7
1700	4	0.28mm	21.9	22.2
2100	4	0.28mm	-11.7	-11.5

These increases in pressure drop across the nozzle holes were expected to yield improved atomisation, and to have increased spray penetration.

4.3.2 - Effect of injection rate on ignition delay

Fig 4.11a shows that the higher injection rate increased the ignition delay in the case of the three-hole injector; but decreased it in the case of the four-hole injector. The following discussion could be advanced in an attempt to explain these results. With the three hole injector, the boost pressure and, as a result, the compressed air pressure during the delay period (measured from the pressure signal) decreased by 12% at 1700 rev/min when the 7.5 mm pump was replaced by the 8.5 mm pump (see Fig 4.11b and discussion on rate of pressure rise in section 2.3.3). In addition, the air temperature during the delay period was reduced by 26K (calculated from the test data using a polytropic index of 1.3). Considering the four-hole nozzle now, the effect of the 8.5 mm pump was the reverse, that is, a reduction in the delay period. This was because both the compressed air pressure and temperature increased when the 7.5 mm pump plunger was replaced with the 8.5 mm one. Also the four-hole nozzle provided a better fuel distribution around the combustion chamber. There is ample evidence in the literature which shows that the delay period shortened when the compressed air temperature and pressure increased, see for example Igura et al (1975).

4.3.3 - Effect of injection rate on the maximum rate of pressure rise, boost pressure, and BMEP

Fig 4.11c shows that when the standard 7.5 mm pump was replaced by

the 8.5 mm pump, the maximum rate of pressure rise increased with the three-hole nozzle, but decreased in the case of the four-hole nozzle. This could be explained by the changes in the ignition delay; as has been shown previously in Figs 4.1a and 4.1b, when the ignition delay increased the rate of pressure rise also increased.

In the case of the three hole nozzle, a consequence of the increase in delay with the 8.5 mm pump is the drop in boost pressure that was necessary in order to keep P_{max} constant at 80 bar (see Fig 4.11b). In turn, the reduction in boost pressure and, therefore, trapped amount of air fuel mixture (at constant air fuel ratio) caused the reduction in BMEP seen in Fig 4.12a.

In contrast, with the four-hole nozzle, the 8.5 mm pump plunger reduced the ignition delay and, as a consequence, the rate of pressure rise decreased, allowing the boost and BMEP to rise above their values with 7.5 mm plunger pump.

4.3.4 - Effect of injection rate on BSFC and smoke emission

When the 7.5 mm pump was replaced by the 8.5 mm pump, there was a tendency for BSFC to worsen in the case of the three-hole nozzle, and to improve in the case of the four-hole nozzle (see Fig 4.12b). Almost certainly, the reason for the trends was the decline in BMEP in the case of the three-hole nozzle, and the increase in BMEP in the case of the four-hole nozzle. Thus, the changes in BSFC mainly reflected the changes in the mechanical efficiency of the engine.

Fig 4.12c shows that with both the three and four hole nozzles, the smoke emission was lower when the injection rate increased. One of the reasons for this reduction in smoke emission was, probably, better fuel

atomisation and greater fuel spray penetration with the 8.5 mm plunger. Also in the case of the three-hole nozzle, where combustion was very poor, the reduction in fuel injected with the 8.5 mm plunger pump, (due to lower boost pressure and lower amount of trapped air fuel mixture, see section 4.1.3) reduced the amount of fuel remaining unburned at the end of combustion.

4.3.5 - Tradeoffs between BSFC, BMEP and smoke emissions with higher injection rate

Fig 4.13 shows the tradeoffs between BSFC, BMEP, and smoke emission when the injection rate was increased. Both with the three and the four-hole nozzles the smoke decreased when the injection rate was raised. However, with the three-hole nozzle this was at the expense of lower BMEP and worse BSFC, whilst the reverse effect was obtained with the four-hole nozzle. With the four-hole nozzle there was an overall improvement in all three aspects, BSFC, BMEP and smoke emissions as the injection rate was increased.

Possible underlying reasons for the different behaviour of the two nozzles have been discussed above.

4.4 - EFFECT OF AIR FUEL RATIO ON ENGINE PERFORMANCE

Soon after commencing the tests at the low compression ratio, it became evident that air fuel ratios of around 25:1 (normally associated with full load diesel engine operation) produced unacceptably high smoke emissions due to poor fuel distribution and mixing. In order to reduce smoke emissions, it was decided to carry out tests at weaker air fuel ratios, in the range of 30:1 to 40:1.

4.4.1 - Effect of air fuel ratio on BMEP, BSFC and smoke

As one would expect, Fig 4.14a shows that as the air fuel ratio was increased, the bmep decreased. The reduction in bmep was due to the reduced amount of injected fuel per cycle. Fig 4.14b shows that the bsfc improved markedly, despite the fall in BMEP and, consequently, a reduction in mechanical efficiency. This reduction in BSFC with weaker mixtures is in agreement with diesel-cycle analysis, Heywood (1988). As the mixture was weakened, there must also have been an improvement in combustion efficiency. This belief is supported by the marked reduction in smoke emission, as Fig 4.15a shows. Fig 4.15b shows that as the fuel was reduced, in order to weaken the mixture, the boost pressure tended to rise in order to maintain a constant P_{max} of 80 bar.

Fig 4.15a shows that with the four-hole nozzle and weak air fuel ratio of about 40:1, acceptable smoke emission levels of around 3.6 Bosch units were obtained. With this weak air fuel ratio, the BMEP was just over 8.0 bar, which was 40-50% higher than the full load BMEP of the standard naturally aspirated engine (at 20:1 air fuel ratio and P_{max} of 80 bar). Also, the BSFC at 45:1 was about 0.25 kg/kWh; this was about 20% lower than the value at full load with the standard naturally

aspirated engine.

4.4.2 - Tradeoffs between BSFC, BMEP and smoke emissions with varying air fuel ratio at constant dynamic injection timing

Fig 4.16 shows that the weakening of the mixture reduced the smoke substantially and, also, had a significant effect on BSFC. The effect on BMEP was relatively small. This suggests that improvements in cycle and combustion efficiency arrested the decline in BMEP due to reduced fuel injected per cycle, and reduced mechanical efficiency.

It is interesting to consider briefly a comparison between Fig 4.16 and Fig 4.10. Fig 4.10 shows the tradeoffs with varying injection timing, whilst Fig 4.16 shows these tradeoffs with varying air fuel ratio. In both cases, substantial improvements in BSFC and smoke were obtained with advanced timing and weaker mixtures. But, as shown on Fig 4.10, advanced injection timing reduces BMEP because of the substantial effect of the increased negative work (due to higher levels of gas pressure during compression) and reduced positive work (as less fuel was injected per stroke) on BMEP when timing was advanced.

4.5 - ATTEMPTS TO ELIMINATE AFTER INJECTIONS

Due to substantially more fuel being required at the lower compression ratio, the standard injection system with the three-hole nozzle was operating beyond its design range. As a consequence, when the air fuel ratio of 25:1 was approached, after-injections set in. Attempts to eliminate these included:

i - Changing the length of the high pressure fuel line, first to approximately 1.5, and then to 2.5 times the standard length.

ii - Increasing the opening pressure of the injector from the standard value of 180 bar to 233 bar.

iii - Increasing the injector needle lift by 20 percent.

None of these measures by itself, or in combination, proved to be entirely successful.

No after-injections were observed at air fuel ratios weaker than 30:1. Also, no after-injections were observed with the four-hole nozzle at any of the conditions tested.

4.6 - EFFECT OF INTERCOOLING ON ENGINE PERFORMANCE UNDER VCR OPERATING CONDITIONS

A limited number of tests were carried out at the low compression ratio, in order to simulate the effects of placing an air cooler between the air compressor and the engine. The simulation was carried out by lowering the temperature of the compressed air entering the engine. This was achieved by reducing the heat dissipated by the electric inlet-air heater. Results are shown in Fig 4.17. With intercooling, BMEP rose by a modest amount (about 7 per cent) at both speeds, as a result of higher trapped air density (5.2 per cent higher at 1300 rev/min and 6.2 per cent at 1700 rev/min). However, the ignition delay lengthened at both

speeds due to lower compression temperature. At 1300 rev/min there was a 4.5 per cent improvement in BSFC, whilst at 1700 rev/min there was a 3 per cent deterioration in BSFC. At both speeds smoke emission worsened by almost one Bosch unit.

The overall conclusion appears to be that any benefits from intercooling would be modest. There are two main reasons for this. Firstly, due to poor air fuel mixing, the extra fuel quantity per cycle that is made possible by the greater air density cannot be burned efficiently. Secondly, intercooling tends to increase ignition delay and rate of pressure rise, thus forcing a lower boost pressure under constant P_{max} operation (this was illustrated in Fig 4.17). This, in turn, tends to moderate the increase in density gained with intercooling and lower air inlet temperature.

4.7 - METAL TEMPERATURE AROUND THE COMBUSTION CHAMBER

Fig 4.18 shows the temperatures, measured at various operating conditions, at the low compression ratio. This was recorded by means of a thermocouple in the cylinder head (location 2 and 5 in Fig 3.3) and in the exhaust manifold.

As would be expected, all temperatures rose as the BMEP increased. At the locations shown, the highest metal temperature at the low compression ratio exceeded the maximum recorded with the standard engine at full load, by about 30°C. However, at the low compression ratio, the BMEP was much higher than the full load BMEP of the standard engine.

Intercooling was effective in reducing the metal and exhaust temperatures to about the same levels as those for the standard engine, despite the substantial increase in BMEP compared to the BMEP of the

standard naturally aspirated engine at full load.

4.8 - NOISE

Russel and Haworth (1985) found that the level of the noise from DI diesel engines was related to the maximum rate of pressure rise. An examination of the results reported here for the lower compression ratio, shows high rates of pressure rise (higher than those for the standard engine at full load). This suggests that the engine may have been more noisy at the lower compression ratio, and this agrees with the subjective impression of the author formed by listening to the engine during the tests. In general, the higher maximum rates of pressure rise recorded at the lower compression ratio, were associated with longer ignition delay periods and more advanced timings.

4.9 - OXIDES OF NITROGEN

Using results obtained form several DI diesel engines Russel and Haworth (1985) found a good correlation between the maximum cylinder gas pressure and nitric oxide emissions. Such a correlation is not unexpected, because the level of these emissions is sensitive to the maximum cycle temperature, which generally rises as the peak cylinder pressure rises.

NO_x measurements were made during the tests with the four-hole nozzle; these are shown in Table 4.3. These results show that despite wide changes in injection timing, inlet air temperature (with intercooling), speed, and air fuel ratio, the NO_x level stayed within the range of 620 to 780 ppm. It appears that these results tend to support Russel and Haworth's conclusion that the main influence on NO_x emission was the peak cylinder pressure.

Table 4.3 - The effect on NO_x emissions of changes in engine operating conditions with the 8.5 mm pump plunger at constant maximum cylinder gas pressure of 80 bar

Engine speed (rev/min)	1700	1700	1700	1700	2100	2100
Air fuel ratio	35:1	40:1	40:1	40:1	40:1	40:1
Inj. timing (°CA BTDC)	20.3	20.9	18.4	18.3	25.6	17.0
Intercooling	NO	NO	NO	YES	NO	NO
NO_x (ppm)	710	630	605	640	720	760

Russel and Haworth's results show a NO_x level of about 750 ppm corresponding to a maximum cylinder pressure of 80 bar; this NO_x level is similar to the levels found during the tests reported here.

4.10 - OPTIMISATION OF OTHER ENGINE PARAMETERS

The level of turbulence in the combustion chamber at the low compression ratio is expected to be lower than that at the standard engine. Although the level of air squish is expected to have decreased considerably, the air swirl when the piston is approaching TDC is not expected to have been reduced much, despite the increase in the bump clearance. This argument is based on the expectation that the swirl induced by the inlet port must have increased considerably due to turbocharging (Dent and Derham, 1974). This will be discussed further in Chapter 5.

The valve overlap of the standard engine was not increased when the engine was turbocharged at the lower compression ratio. A greater valve overlap would be needed in order to keep the combustion-chamber metal temperatures within designed limits at higher BMEP levels and higher engine speeds than those achieved to date.

Both Charlton (1984) and Grundy et al (1974) found that when the compression ratio is reduced and the boost pressure is increased, the exhaust valve must open earlier for maximum thermal efficiency. Charlton suggests that this is necessary in order to provide sufficient time for the blow-down from the higher cylinder gas pressure. During the tests reported here it was observed that the cylinder pressure at exhaust-valve-opening (EVO) was considerably higher than for the standard engine at full load. It is, therefore, possible that earlier EVO might improve BSFC at the lower compression ratio.

4.11 - ENGINE PERFORMANCE AT THE STANDARD COMPRESSION RATIO WITH THE FOUR-HOLE NOZZLE AND THE HIGH INJECTION RATE PUMP

Section 4.3.1 has shown that, in comparison with the standard engine, the performance at the low compression ratio could be substantially better under VCR operation. This improved performance was obtained with the four-hole nozzle, with the high injection rate pump (8.5 mm plunger diameter), and with a relatively weak air fuel ratio.

The question arises as to whether the engine will perform satisfactorily at the standard compression ratio (without boost) with the four hole nozzle and the high rate pump. This operating condition will arise with VCR operation at mid-loads. Table 4.4 shows the engine performance under this condition.

At all speeds, BMEP and BSFC with the four hole nozzle and an air fuel ratio of 20:1, are very similar to the values for the three-hole nozzle and the standard pump (7.5 mm plunger diameter). However the exhaust emissions differed substantially; smoke levels increased with the four-hole nozzle by 1.85, 1.65 and 0.85 Bosch units at 1300, 1700 and 2160 rev/min respectively, and the NO_x concentrations decreased by about 50-60 % at all speeds.

The smoke emissions with the four-hole nozzle could be improved by operating with a weaker air fuel ratio of 25:1. The table shows that in comparison with the engine performance with the three-hole nozzle and 20:1 air fuel ratio, smoke emission is almost comparable; however, there was a reduction of about 15% in BMEP at all speeds, although BSFC was better than that of the standard engine at 20:1 air fuel ratio.

Table 4.4 - Comparison of engine parameters at 17.4:1 compression ratio with three and four-hole nozzles; the 7.5 mm pump plunger was used with the three-hole nozzle, whilst the 8.5 mm plunger was used with the four-hole nozzle.

ENGINE SPEED rev/min	1300			1700			2160		
NOZZLE HOLES	3	4	4	3	4	4	3	4	4
AIR FUEL RATIO	20:1	20:1	25:1	20:1	20:1	25:1	20:1	20:1	25:1
BMEP / bar	5.83	5.54	4.93	5.41	5.33	4.54	5.41	5.33	4.64
BSFC / kg/kWh	0.29	0.30	0.28	0.29	0.29	0.28	0.28	0.28	0.28
BSAC / kg/kWh	7.15	7.50	8.57	7.06	7.23	8.63	6.78	6.96	8.32
SMOKE / Bosch	3.45	5.30	3.85	3.15	4.80	3.75	3.75	4.60	3.40
NO_x / ppm	1440	690	620	1250	600	600	650	250	285
P_{max} / bar	71.0	66.9	62.8	68.3	64.7	63.2	65.2	62.5	62.2
P POS/°CA ATDC	3.22	3.83	4.05	5.68	3.64	3.87	4.48	4.49	3.99
IT / °CA BTDC	17.1	12.9	15.0	16.6	16.9	16.7	16.1	16.1	15.8
ID / °CA	4.09	2.66	5.51	4.15	6.30	6.13	5.80	6.10	6.14
RPR / bar/°CA	3.40	5.06	5.63	3.60	5.33	6.06	3.91	3.83	4.29
VOL. EFF. / %	92.9	90.0	90.6	84.6	85.3	82.6	79.8	80.0	85.2
SOC / °CA BTDC	13.0	10.2	9.5	12.5	10.6	10.6	10.3	10.0	9.6
EX. TEMP / °C	476	460	392	496	496	417	552	575	476
Tm / °C	216	213	177	221	213	190	228	239	196

p POS - Crank angle at which the cylinder pressure reached a maximum.
IT - Dynamic injection timing.
ID - Ignition delay.
RPR - Rate of pressure rise.
SOC - Start of combustion.
Tm - Cylinder head metal temperature adjacent to the exhaust valve

The exhaust and critical metal temperatures were all below the highest values recorded during the baseline tests for the standard engine.

Considering the engine performance with the four-hole nozzle, presented in Table 4.4, it would probably be possible to improve on it by optimising the injection timing and operating with a slight boost pressure. This could lower the smoke emission and BSFC further, without a significant penalty in the BMEP.

4.12 - A CORRELATION FOR THE PREDICTION OF IGNITION DELAY

4.12.1 - Introduction

Ignition delay is a very important parameter affecting a number of aspects of diesel engine performance. In the context of VCR operation with constant P_{max}, sections 4.1.2 and 4.1.3 have shown that the ignition delay has an added importance; through rate of pressure rise, it affects the inlet boost pressure and other aspects of the engine performance.

It would be of considerable benefit to be able to predict the ignition delay at any engine operating condition. Over the years, several semi-empirical correlations have been developed by a number of investigators, which predict ignition delay. Four of these correlations are assessed in this section; their predictions of ignition delay are compared with the ignition delay measured on the standard Lister engine (naturally aspirated with standard inlet manifold, no air supply pipe-work connected, standard compression ratio, and standard injection system).

4.12.2 - Ignition Delay Correlations

Before a significant proportion of the chemical energy of the fuel can be released through burning, certain physical and chemical processes must take place during the ignition delay period. The length of this delay period depends on the physical and chemical characteristics of the fuel, and on the temperature and pressure of the compressed air in the cylinder. Some fuels are more prone to autoignition than others, which affects the length of the ignition delay period. Fuels with long single-

bond molecular chains (e.g. paraffins), which can be broken up more easily, have better autoignition quality (higher Cetane number) and lower ignition delays. The converse is true for fuels made up of benzene ring structures (e.g. aromatics).

The four correlations selected for evaluation are all based on the Arrhenius Equation, Eq 4.4, and have been developed from tests on diesel engines.

$$\tau_{id} = A\ P^{-K} \exp\left(E_a / R_o\ T\right) \qquad \ldots\ 4.4$$

where τ_{id} is the predicted ignition delay (in milliseconds), E_a is an apparent activation energy for the fuel autoignition process, R_o is the universal gas constant, A and K are constants dependent on the fuel (and, to some extent, the injection and air-flow characteristics); P and T are the pressure and temperature of the compressed air.

Table 4.5 shows the values of these parameters appearing in correlations by Watson (1979), Wolfer (Watson,1979), Zimmerman (Watson, 1979) and Schmidt (Watson,1979). A number of other correlations for ignition delay have been published which rely on tests with single droplets, or on tests with combustion bombs, (for example, see Belardini, 1983); these are not considered here.

In order to use the ignition delay correlations the mean gas pressure during delay, P, is required. This mean pressure was taken as the arithmetic average of the pressures at the start of injection and at the start of combustion (both these pressures were measured from the recorded pressure signal).

Table 4.5 - Values of constants for Arrhenius equation determined by different investigators.

AUTHOR	A	k	E_a/R_o
Watson	3.52	1.022	2100
Wolfer	0.429	1.19	4650
Zimmerman	0.392	1.05	4650
Schmidt	0.0646	1.08	6330

The four correlations also require the mean temperature of the gas, T, during the ignition delay period. This temperature was calculated from the mean pressure, P, using an estimated value of the polytropic index of compression and the initial pressure and temperature at IVC. The way in which the polytropic index was estimated is described below.

The heat transfer between the trapped air and the surrounding combustion chamber surfaces during the compression process decides the value of the polytropic index during the compression stroke (before the start of combustion). After start of combustion, the rise in the cylinder pressure is primarily governed by the heat released from the combustion of the fuel rather than the compression of the gases due to piston movement.

Values of the polytropic index were calculated for various engine loads, at two constant speeds (1300 and 2000 rev/min). For this calculation, the cylinder gas pressure at IVC was needed. This was assumed to be equal to the inlet manifold pressure. The factors surrounding this assumption are as follows: close analysis of the pressure signal showed that the cylinder pressure reaches a constant

value between about 10°CA BBDC and IVC (50°CA ABDC). The pressure during this period can be assumed to be the closest it approaches manifold pressure; here it was assumed that the cylinder pressure at IVC is equal to the manifold pressure (i.e. atmospheric pressure).

The polytropic index, n, during the compression was calculated using the polytropic relationship:

$$\frac{P_1}{P_2} = \left[\frac{V_2}{V_1} \right]^n \qquad \ldots\ 4.5$$

$$n = \frac{\ln(P_1/P_2)}{\ln(V_2/V_1)} \qquad \ldots\ 4.6$$

where P_1 and V_1 are the pressure and volume at the start of a crank angle interval, and P_2 and V_2 are the corresponding values at the end of the interval. The first crank angle interval considered started at IVC; the size of the intervals was chosen to be between 2 and 30°CA, depending on the rate at which the polytropic index changed with crank angle. The pressure of the air in the cylinder was measured using the cylinder pressure transducer; the trapped air volume at a given crank angle was calculated from the engine geometry.

Fig 4.19 shows the value of the polytropic index at different crank angles, at two engine speeds, and various loads. The value of the index varied with crank angle in a predictable way. The value during the earlier part of the induction process, when heat was being transferred to the trapped air from the cylinder walls, was greater than the

adiabatic value for air of 1.4. The scatter in this part of the induction period could be due to analogue to digital conversion descritization and the effect of datum value error. During the middle of the compression stroke, when the trapped air temperature rose to the temperature of the surrounding surfaces, the calculated value of the index was around 1.4. During the latter part of the compression process, when the trapped air temperature rose substantially above the surrounding metal temperature and heat was being transferred from the air to the metal, the calculated value of the index fell.

The polytropic relationship was used in order to calculate the mean temperature, T, during the delay period:

$$T = T_{ivc} \left[\frac{P}{P_{ivc}} \right]^{\frac{n-1}{n}} \quad \ldots\ 4.7$$

where n is an overall value relating to the process between IVC and half-way through the delay period. This overall value was obtained for each engine speed and load from Eq 4.6 with P_1 and V_1 at IVC and P_2 and V_2 at half-way through the delay period.

Two methods were used in order to evaluate the air temperature, T_{ivc}, at IVC. The first method was to assume that T_{ivc} is equal to the air temperature measured with a thermocouple just upstream of the inlet valve. The measured air temperature increased with increasing load at a constant speed, (varying between 30 and 60°C). The calculated value of the average compression temperature, T, during the ignition delay using this method, showed an implausible trend of decreasing compression

temperature with increasing engine load. This decreasing temperature trend resulted in a prediction of increasing ignition delay with increasing load; in fact, the measured delay decreased as the load increased, as Fig 3.9 shows. Also, comparison of the predicted ignition delay period from the four correlations using this compression temperature, at best overestimated the measured value by more than 200%.

The second method of evaluating T_{ivc} involved the use of the equation of state for a perfect gas at IVC conditions:

$$P_{ivc}\, V_{ivc} = m_{ivc}\, R\, T_{ivc} \qquad \ldots\ 4.8$$

where m_{ivc} was obtained from the measured air flow rate using a Dawe corona-discharge air flow meter, Etminan (1990). It was assumed that the mass of the residual gases was negligible.

Now the calculated compression temperature using these values of T_{ivc} showed an increasing trend with increasing load at constant speed, as would be expected. The relation between this compression temperature and the measured ignition delay is shown in Fig 4.20 (note, however, that these estimated compression temperatures are felt to be higher than expected).

These latter compression temperatures were used in the correlations by Watson, Wolfer, Zimmerman and Schmidt, in order to predict the ignition delay period at various engine operating conditions. These predicted values are compared with the measured value, in Fig 4.21.

On the whole, the calculated ignition delays were lower than the measured value. This was probably due to an overestimation of the

compression temperature during the ignition delay (see above). However, the correlations predicted the trend in ignition delay correctly; Fig 4.21 shows that the predicted ignition delay increases as the measured delay increased.

The predicted results using Watson's and Zimmerman's correlations were of a better match, at both speeds, than those predicted using Wolfer's and Schmidt's correlations; predictions at 1300 rev/min being closer to measured results than those predicted at 2000 rev/min.

In conclusion, it would appear that the correlations are capable of predicting the correct trends in ignition delay. The accuracy of the prediction is, however, sensitive to the estimation of the mean air temperature during the delay period. This compression temperature is rather difficult to estimate accurately in practice. The variation in calculated ignition delay can be attributed to a number of factors such as, the method used to detect the start of combustion and therefore the length of the ignition delay period, and the type of engine and injection system used.

4.13 - SUMMARY AND CONCLUSIONS

1 - As The ignition delay increases the maximum rate of pressure rise also increases.

2 - One parameter with a significant effect on ignition delay is the injection timing; as the timing is advanced, the ignition delay increases. This is, firstly, due to the fact that as the timing is advanced, injection takes place into a less compressed (i.e. low temperature and pressure) and less turbulent air; secondly, with constant P_{max} operation, the inlet boost pressure (and therefore inlet air temperature) decreases.

3 - At the low compression ratio of 12.9:1 (compared with the standard compression ratio of 17.4:1) and simulated VCR conditions, the marked decrease in swirl and squish worsened substantially the combustion performance of the engine with the standard injection system. Replacement of the three-hole nozzle with the four-hole nozzle, and replacement of the standard pump with a higher injection rate pump (a theoretical increase of 28.5% in injection rate) brought about improvements in combustion performance. However it was still found necessary to operate at weak air fuel ratios (in the region of 35 to 40:1) in order to obtain acceptable smoke emission levels.

4 - With simulated VCR conditions at the low compression ratio a particularly good performance was obtained at 2160 rev/min. At this speed, the operating conditions were as follows: high injection rate pump, four-hole injector nozzle, and a weak air fuel ratio of 40:1. The BMEP was almost 50% higher, and the BSFC was 20% lower, than values for the full load standard naturally aspirated engine; the smoke emission was at an acceptable level of 3.6 Bosch units (slightly above the level

for the standard engine at full load, at this speed).

5 - The benefits from intercooling, when operating under VCR conditions, are likely to be modest for the following two reasons: firstly, due to poor air fuel mixing, the extra fuel quantity per cycle, that is made possible by the greater air density, cannot be burned efficiently; secondly, intercooling tends to increase ignition delay and rate of pressure rise, thus forcing lower boost pressure under constant P_{max} operation. This, in turn, tends to moderate the increase in density gained with intercooling from the lower air temperature.

6 - Some preliminary work was carried out with the aim of obtaining a correlation which could be used to predict ignition delay. Such a correlation would be useful in a cycle simulation computer program for VCR engines. Out of four published correlations, investigated using test results from the Lister engine, the ignition delay correlation, by Watson (1979), and Zimmerman (Watson, 1979), gave the best predictions of ignition delay; even so, these deviated by up to 50% from the measured values. The accuracy of the predictions of ignition delay was sensitive to the estimation of the mean air temperature during the delay period. This compression temperature is rather difficult to estimate accurately from experimental measurements. Also the differences in the methods used for detecting start of combustion, and therefore the ignition delay period, could have an effect on the accuracy of the correlations.

Chapter 5: Computer Simulation of In-Cylinder Air Flow and Fuel Spray Trajectories

5.1 - INTRODUCTORY OVERVIEW OF THE COMPUTER MODEL

The computer model can be divided into two major sections:

1 - Simulation of air motion within the engine cylinder during induction and compression.

2 - Interaction of the fuel jets with the swirling air during the injection process.

The first section of the model is based on work by Fitzgeorge and Allison (1963), and by Dent and Derham (1974). The second section is based on a more recent concept of air and fuel mixing proposed by Timoney (1985).

The air motion model first simulates the induction process; the aim being to estimate the total moment of momentum of the trapped air at the end of the induction period. The model then simulates the compression process; it calculates the instantaneous air swirl and squish velocities. The model assumes that during compression, the moment of momentum of the trapped air is conserved, save for the dissipation due to friction at the combustion chamber surfaces which is taken into account.

The interaction between the fuel jets and the swirling air is evaluated by the fuel jet model. This model first estimates the trajectory of the fuel jets. Then, the air velocity relative to the tangential component of the fuel spray tip velocity is calculated at the moment the spray tip impinges onto the walls of the piston bowl, Fig 2.23. This relative velocity in the tangential direction is known as the crosswind velocity (V_{cw}). Timoney (1985) has presented experimental evidence showing that there is a correlation between V_{cw} and engine smoke and BSFC (see section 2.6.2).

The structure of the rest of this chapter is as follows: section 5.2 describes the mathematical models. Section 5.3 describes the computer simulation programs. The validation and demonstration of the computer model is presented in section 5.4 . Section 5.5 presents an analysis of the interaction between the air and the fuel jets in the Lister engine at a lower compression ratio than the standard value. The chapter ends with conclusions in section 5.6 .

5.2 - MATHEMATICAL MODEL

In order to predict the swirl and squish velocities in the Lister engine during the compression stroke, it was necessary first to estimate the total moment of momentum of the mass trapped in the cylinder at the end of induction. The way in which the moment of momentum was estimated is described in section 5.3.2; this required the knowledge of the instantaneous air mass flow rate during induction, which is the subject of the following section.

5.2.1 - Prediction of air mass flow rate through the inlet valve during induction

The instantaneous air mass flow rate through the inlet valve was estimated from the following simultaneous equations:

$$\dot{m}_{av} = \frac{\rho_{tt} V_{tt} - \rho_t V_t}{\delta t} \qquad \ldots\ 5.1$$

$$\dot{m}_{av} = \frac{\dot{m}_{tt} + \dot{m}_t}{2} \qquad \ldots\ 5.2$$

where suffix 't' and 'tt' represent the time t, and the time t + δt after a small interval δt. ρ is the air density within the cylinder and V is the cylinder volume. $\dot{m}_{av}$ is the average air mass flow rate during interval δt.

Eq 5.1 represents the flow through the valve caused by the motion of the piston. Eq 5.2, however, is based on the compressible flow equation through an orifice, Eq 5.2a, in this case the inlet valve. It relates the mass flow rate of a compressible gas through an orifice with a pressure difference across it.

$$\dot{m}_t = C_d A_o \left\{ \frac{2 P_o^2 \gamma}{R T_o (\gamma - 1)} \left[(P_t / P_o)^{\frac{2}{\gamma}} - (P_t / P_o)^{\frac{(\gamma+1)}{\gamma}} \right] \right\}^{1/2} \quad \ldots\ldots 5.2a$$

where suffix 'o' represents the conditions in the inlet manifold, V represents the cylinder volume, and P and T stand for pressure and temperature. C_d is the valve discharge coefficient, A_o is the valve flow area (see section B.1 of appendix B), and R and γ are the specific gas constant and ratio of the specific heats of air respectively.

The following were assumed:

1 - The manifold pressure (P_o) remains constant for most of the induction period, except for a short period before inlet valve closure, IVC, when P_o is assumed to rise at a predetermined rate due to the inertia of the moving air in the manifold (see section B.2 of appendix B).

2 - Induction starts at TDC and the exhaust valve is by then closed.

3 - At TDC (induction) the cylinder pressure is equal to the manifold pressure.

4 - Throughout the induction process the temperature of the cylinder contents is constant and equal to the manifold temperature, T_o.

Eqs 5.1 and 5.2 were solved at successive crank angle steps, during induction, in order to obtain the average mass flow rate at each interval between the successive crank angle steps. To start the solution, the crank angle (and time) were incremented by a small step beyond TDC. The solution to these equations was then obtained by iteration until a sufficiently accurate estimate of mass flow rate was obtained, after which the crank angle was incremented and the process was repeated. The details of the computational scheme for the solution of Eqs 5.1 and 5.2 are given in section B.3 of appendix B.

5.2.2 - Prediction of total angular momentum at IVC

The preceding section gave a description of the way in which the average mass flow rate through the inlet valve was predicted at a given crank angle interval. The corresponding average moment of momentum rate is then estimated as follows:

The moment of momentum M of the mass admitted after the interval δt is given by:

$$M = \left[2\pi\rho \int_0^{B/2} V_a \, \omega \, r^3 \, dr \right] \delta t \qquad \ldots\ldots 5.3$$

where ω and V_a are the angular and axial velocities of the air, respectively, at radius r of the cylinder section, and B is the cylinder bore. The derivation of this equation is given in section B.4 of appendix B.

In fact the computer model relies on experimental information for the estimation of the moment of momentum rate, $(M/\delta t)$, at each crank angle interval.

Once the mass flow rate $\dot{m}_{av}$ was predicted at a given crank angle interval, this value together with the valve lift were used in order to obtain the corresponding value of the moment of momentum rate using tabulated experimental data. These experimental values of moment of momentum rate were obtained at each mass flow rate and valve lift using the rig and methods described in section 3.3. Using this rig, at a given steady mass flow rate and valve lift, the value of moment of momentum rate ($M / \delta t$) was calculated using Eq 5.3 above. This was repeated for a wide range of mass flow rate and valve lift combinations. The average moment of momentum estimated at each time interval was, therefore, the product of the moment of momentum rate and the time interval δt.

At the end of the induction process, the values of the moment of momentum at each crank angle increment were summed up (over the induction period) in order to obtain the total moment of momentum at IVC.

Since the inlet valve closes after BDC, in practice, under some running conditions a negative mass flow rate (flow from the cylinder to the inlet manifold) will arise, towards the end of the induction process. This reduces the mass trapped and the moment of momentum at IVC. The model includes a simple method of taking this into account. The moment of momentum of the trapped air at IVC, M_{ivc}, was assumed to be a fraction of the maximum moment of momentum M_{max}, prior to the start of the negative mass flow:

$$M_{ivc} = \left[\frac{m_{ivc}}{m_{max}} \right] M_{max} \qquad \ldots\ 5.4$$

where m_{max} is the maximum air mass trapped in the cylinder (just prior to the air mass flow rate becoming negative), and m_{ivc} is the predicted

trapped mass at inlet valve closure.

5.2.3 - Prediction of swirl during the compression stroke

The total moment of momentum and the mass trapped at the end of the induction process (at IVC) were estimated as explained above. These values have been used by the model in order to predict the variation in swirl during the compression process. This prediction relies on the principle of conservation of moment of momentum of the cylinder contents. In general, considering the rotation of the contents about the cylinder axis,

sum of all the torque forces acting on the fluid	=	Rate of change of moment of momentum of the cylinder content at any instant

$$\sum T_i = \frac{d}{dt}\left[I\,\omega_c \right] \qquad \ldots\ldots 5.5$$

where T_i is any external torque force applied to the cylinder contents, I is the moment of inertia of the contents, and ω_c is the angular velocity of the cylinder contents during compression. As discussed in section 2.3.1, it is assumed that during compression, the cylinder contents rotate about the cylinder axis as a solid body (forced vortex). The moment of inertia of the rotating contents is given by:

$$I = \frac{m_{ivc}}{2}\left[\frac{\frac{\pi (B/2)^4 s}{v} + (D/2)^2}{\frac{\pi (B/2)^2 s}{v} + 1} \right] \qquad \ldots\ldots 5.6$$

where s is the distance between the cylinder head and the piston crown at a given crank angle, and D is the piston bowl diameter. This is made

up of two components: the moment of inertia of the gas within the piston bowl, plus the moment of inertia of the gas above the piston crown. The details of this equation are given in section B.5 of appendix B.

Friction between the fluid and cylinder walls, cylinder head, and piston crown, resist the rotation of the fluid. It was assumed that the sum of the frictional torques at these fluid/solid interfaces was the only external force. It was also assumed, that this external force was acting to reduce the rotation of the fluid by dissipating some of the moment of momentum imparted during induction. This resisting torque was calculated at each crank angle by:

$$T = \tau A\, r \qquad \ldots\ldots 5.7$$

where τ is the shear force at the fluid solid interface, A is the area of the interface on which the shear force is acting, and r is the radius at which the shear force acts. The shear force τ was estimated using appropriate values of skin friction coefficients for the piston crown, cylinder head, and cylinder wall areas. Estimates of the values of the skin friction coefficients were made from the Blasius's equation (which is a function of Reynolds number) for a turbulent boundary layer on a flat plate. Rewriting Eq 5.7:

Total torque resisting fluid rotation

$$T = \frac{d}{dt}\left[I\, \omega_c \right] = \frac{\rho\, \omega_c^2\, \pi B^4}{16}\left[f_{cyl}\, S + f_{pc}\, \frac{B}{16} \right] \qquad \ldots\ldots 5.8$$

where f_{cyl} and f_{pc} are the Skin friction coefficients of the cylinder walls, and the cylinder head and piston crown respectively. The way in which Eq 5.8 was arrived at, and the evaluation of the skin friction

coefficients and fluid properties can all be found in section B.6 of appendix B. Substituting for T from Eq 5.8 in to Eq 5.5 and using the relations for the skin friction coefficients developed in appendix B, section B.6,

$$\frac{d}{dt}[I\ \omega_c] = I\ \frac{d\omega_c}{dt} + \omega_c\ \frac{dI}{dt} = \left[\frac{-\pi\,\rho^{0.8}\,\mu^{0.2}\,B^{3.6}}{16}\left(0.067\,s + 0.0055\,B\right)\right]\omega_c{}^{1.8} \qquad \ldots\ 5.9$$

where μ is the dynamic viscosity of air.

Eq 5.9 was solved numerically in order to compute the value of the swirl (angular velocity, ω_c) during the compression stroke as a function of crank angle θ, or time t. For the numerical solution, Eq 5.9 is rewritten as:

$$I\ \delta\omega_c + \omega_{av}\ \delta I = K\,\omega_{av}^{1.8}$$

where K is the term in brackets on the right-hand side of Eq 5.9, and ω_{av} is the average angular velocity of the air during a small time interval δt. Hence rearranging this equation in terms of $\delta\omega_c$:

$$\delta\omega_c = \frac{K\ \omega_{av}^{1.8} - \omega_{av}\ \delta I}{I} \qquad \ldots\ 5.10$$

The details of the computational scheme for the solution of this non-linear equation (Eq 5.10) for any interval between successive crank angles are given in section B.7 appendix B.

5.2.4 - Prediction of squish during the compression stroke

During the compression stroke the air is displaced across the piston crown, by the action of the piston, towards the combustion bowl. The squish velocity (air velocity in the radially inward direction) was estimated by applying the principle of conservation of mass to the cylinder contents. This resulted in the following expression, Fitzgeorge and Allison (1963), Dent and Derham (1974):

$$V_{sq} = \frac{r\,[(B/2r)^2 - 1]}{2s}\left[\frac{v}{A_c\,s + v}\right]\frac{ds}{dt} \qquad \ldots\ 5.11$$

where r is the radius at which the squish velocity is to be calculated (usually at the combustion bowl radius), v is the combustion bowl volume, and A_c is the cylinder cross sectional area.

As mentioned in section 2.3.1, Eq 5.11 does not take into account pressure gradient due to the effects of fluid friction, centripetal acceleration of the rotating cylinder contents, and the gas inertia; it also neglects leakage past the piston rings and heat transfer between the fluid and the combustion chamber walls (the effects on V_{sq} of some of these assumptions were discussed in section 2.3.1).

5.2.5 - Prediction of crosswind velocity

The crosswind velocity (V_{cw}) was defined in section 2.6.2, Fig 2.23. In the same section, Timoney's results were also discussed which demonstrated correlations between crosswind velocity and bsfc and smoke. In order to calculate the crosswind velocity, the radial and tangential components of the fuel spray tip were first estimated. This estimation

was done at the moment that the spray tip impinged on the walls of the piston bowl (bowl rim). Also, the tangential velocity of the swirling air at the bowl rim was estimated.

The computer model which predicts V_{cw} assumes that the position of the injector nozzle, the axis about which the swirling air rotates, and the axis of the combustion bowl, coincide with the axis of the cylinder. The actual geometry of the piston and the cylinder head are shown in Figs 3.3 and 3.12.

Spray tip radial velocity

There are numerous correlations which predict the radial position of the fuel spray tip (penetration) as a function of time when the spray is injected into a quiescent atmosphere of air. From these correlations, the radial velocity can be obtained by differentiation with respect to time of the radial penetration distance.

Several methods have been used to obtain these correlations. Many, (Lyn and Valdmanis (1962), Scott (1969), Heap et al (1975)) simply fit expressions to experimental data. The independent parameters in these expressions are the variables which have an effect on the penetration distance. Some investigators have grouped these parameters into dimensionless groups, and then used them in appropriate expressions fitted to experimental data. Some investigators have based their expressions on turbulent gas jet theory, Adler and Lyn (1970), Abramovich (1963), Chiu et al (1976).

The spray tip penetration after a given time interval following injection, depends partly on the momentum with which the fuel emerges from the nozzle. It also depends on the nature of the spray, as well as

on the trapped air characteristics. The parameters which can be used to represent these effects are: the pressure drop across the nozzle, the nozzle orifice diameter and length, the physical properties of the fuel (density, viscosity, surface tension), the trapped air properties (density, viscosity, temperature), and the air swirl.

Published correlations included only some of these parameters; usually, they include the pressure drop across the nozzle, nozzle hole geometry, and the air density.

A widely used correlation for predicting spray tip penetration was developed by Chiu et al (1976) of the Cummins Engine Company. This was used in order to predict the spray tip penetration and radial velocity in the case of the Lister engine.

In Chiu's correlations, the spray tip penetration (without swirl), X_t, is expressed as a function of time t (t = 0 at the start of injection):

$$X_t = F\, t^{0.6} \qquad \ldots. 5.12$$

where F is an empirical factor which accounts for the characteristics of the spray and the surrounding compressed air. The most important parameter of the spray is the droplet size distribution and the initial injection velocity. Both of these are a function of the pressure difference across the nozzle at injection, and the nozzle hole diameter, Heywood (1988). Also, the most important characteristic of the air is the density, since this affects the retarding drag on the spray (Heywood). All these variables appear in the following expression which is used for the calculation of F.

$$F = 140 \frac{\left[\frac{d\,\rho_a}{\rho_{atm}}\right]^{0.5} \left[\frac{\rho_f}{\rho_d}\right]^{0.4} \delta P^{0.25}}{\left[1 + \frac{\rho_a}{\rho_{atm}}\right]^{0.85}} \quad \ldots\ldots 5.13$$

where d is the nozzle hole diameter, ρ_a and ρ_f are the densities of the compressed air in the cylinder and the fuel in use, normalised by the density of atmospheric air ρ_{atm} and the density of the standard diesel fuel ρ_d, respectively. δP is the mean pressure drop across the nozzle holes. This was estimated from the average volume flow rate during injection and the total effective flow area of the injector nozzle holes, using the incompressible form of the equation for the flow through an orifice. This is given by:

$$\delta P = \frac{\rho_f}{2} \left[\frac{360\, q\, N}{\theta_i} \frac{4}{\pi\, n\, d^2\, C_d}\right]^2 \quad \ldots\ldots 5.14$$

where q is the volume of fuel injected per engine cycle (measured during the tests on the Lister engine), N is the engine speed, θ_i is the injection period (measured), n is the number of nozzle holes and C_d is the discharge coefficient for the nozzle holes (taken as 0.7).

In the presence of swirl, the spray tip will be deflected from its radial path. As a result, the penetration in the radial direction (after a given time following injection) would be reduced in comparison with that in a stagnant atmosphere. The fractional reduction in radial penetration was obtained by Chiu et al (1976) from experimental tests and is given by the following expression:

$$\frac{X_t - X_{tw}}{X_t} = 0.35 \left[\frac{X_{tw}\, Q_a}{\mathrm{d}\, Q_j} \right]^{0.44} \qquad \ldots\ 5.15$$

where X_{tw} is the radial penetration of the spray tip in the presence of swirl, Q_a is the rate of change of the momentum flux of the swirling air at the tip of the spray, and Q_j is the rate of change of the mean momentum flux of the fuel jet at the nozzle orifice. A physical interpretation of Eq 5.15 can be found in section B.8 of appendix B. They are calculated from:

$$Q_a = \rho_a\, X_{tw}^2\, \omega^2 \qquad \ldots\ 5.16$$

(note, X_{tw} is also the radius from the centre of the cylinder at which the spray tip is located at time t), and

$$Q_j = \rho_f\, V_{inj}^2 = 2\,(\delta P \times 10^5) \qquad \ldots\ 5.17$$

where V_{inj} is the mean fuel injection velocity at the nozzle orifice.

Eq 5.15 was solved numerically and the spray tip penetration in the presence of swirl was calculated at successive crank angles. For the numerical solution, Eq 5.15 was rearranged as follows:

$$(X_{tw})_i = X_t \left\{ 1 - 0.35 \left[\frac{(X_{tw})_{i-1}\, (Q_a)_{i-1}}{d\, Q_j} \right]^{0.44} \right\} \qquad \ldots\ 5.18$$

The details of the computational scheme for the solution of this equation are shown in section B.9 of appendix B.

Eq 5.15 for the spray tip penetration can be differentiated to obtain an estimate of the radial component of the spray tip velocity. Thus differentiating X_{tw} in Eq 5.15 with respect to time,

$$\frac{dX_{tw}}{dt} = \frac{0.6\,F\,(1 - E\,X_{tw}^{1.32})\,t^{-0.4}}{1 + 1.32\,E\,F\,X_{tw}^{0.32}\,t^{0.60}} \qquad \ldots\ldots 5.19$$

where E denotes:

$$E = \frac{0.35\,\rho_a^{0.44}\,\omega^{0.88}}{(2\,d\,\delta P \times 10^5)^{0.44}}$$

The radial component of the velocity from Eq 5.19 is obtained after a value of X_{tw} has been evaluated from Eq 5.15.

Spray tip tangential velocity

Before the tangential component of the spray tip velocity is calculated, the deflection, S, of the spray, caused by the swirling air, in the tangential direction is first estimated from:

$$\frac{S}{d} = \frac{Q_a}{Q_j}\left[\frac{X_{tw}}{d}\right]^{2.217} \qquad \ldots\ldots 5.20$$

The tangential component of the spray tip velocity can be estimated by differentiating S with respect to time:

$$\frac{dS}{dt} = \left[\frac{dX_{tw}}{dt} \right] \left[\frac{2.1085\, \rho_a\, \omega^2}{(\delta P \times 10^5)\, d^{1.217}} \right] X_{tw}^{3.217} \qquad \ldots\ 5.21$$

where $\frac{dX_{tw}}{dt}$ is the radial component of the spray tip velocity given by Eq. 5.19.

Spray impingement and crosswind velocities

The velocity V_i with which the spray impinges on the piston bowl sides, and the crosswind velocity at impingement V_{cw}, are calculated from:

$$V_i = \left\{ \left[\frac{dX_{tw}}{dt} \right]^2 + \left[\frac{dS}{dt} \right]^2 \right\}^{1/2} \qquad \ldots\ 5.22$$

and,

$$V_{cw} = (B\ /\ 2)\, \omega - \frac{dS}{dt} \qquad \ldots\ 5.23$$

5.3 - DESCRIPTION OF THE COMPUTER SIMULATION PROGRAM

A computer simulation program has been developed which is based on the mathematical models presented in section 5.2. This simulation program comprises four main parts, each one being a self contained program. The first program works out the instantaneous air mass flow rate during induction and the total mass trapped at inlet valve closure. The second program estimates the total moment of momentum at inlet valve closure. The third program estimates the instantaneous squish and swirl velocities during the compression stroke, and the fourth program calculates the crosswind velocity during the injection process. These programs were written in BASIC and ran on various IBM and IBM compatible machines (such as IBM XT(286), Opus III and Opus V). On the Opus V the total running time for the four programs was around 15 minutes when the crank angle increment for the first three programs was 2° CA and 0.1° CA for the last program. A listing of all four programs can be found in section B.10 of appendix B.

5.3.1 - Simulation of the induction process - Program ITERAM

This program uses information stored in three data files. The first file contains information on the engine geometry, the second contains the values of the discharge coefficient at different valve lifts (obtained from steady flow tests), and the third contains the inlet valve cam profile data (that is, valve lift at different crank angles) . Further information (engine speed, inlet manifold conditions, and crank angle interval) are input by the operator.

The program starts from TDC induction, and the crank angle is incremented by the specified value. The instantaneous air mass flow rate

and the trapped mass during successive crank angle intervals are estimated using the model in section 5.2.1. The estimated air mass flow rate, and the corresponding crank angle are stored in an external file "FILEF". The program ends when the crank angle at which the inlet valve closes is reached. When this happens, the total trapped mass and other information (mostly input by the user) are stored in a file "TRANSFER" which forms an input to the second program. A flow diagram of the first program is shown in section B.11 of appendix B.

5.3.2 - Estimation of the total moment of momentum at IVC - Program SUMMOM

This program uses information stored in three data files. The first file, "FILED", contains the data on the moment of momentum rate, at a number of valve lift and mass flow rate combinations. Data stored in file "FILED" were obtained experimentally from steady flow tests. The other two files "FILEF" and "TRANSFER" were created by the program "ITERAM".

This program also starts from TDC induction, and the crank angle is incremented by the same interval as the first program. At each crank angle, the mass flow rate and the corresponding inlet valve lift (estimated by the program "ITERAM") are read from "FILEF". The program then estimates the moment of momentum rate at each crank angle. This is estimated from data obtained from the steady flow rig tests stored in file "FILED". The moment of momentum at each crank angle interval is obtained from the product of the estimated moment of momentum rate and the time interval, Δt, corresponding to crank angle increment. The total moment of momentum at inlet valve closure is obtained by summing

up, over the induction period, the incremental moment of momenta at successive crank angle intervals. This value is added to the data stored in file "TRANSFER", which is also used by the third program. A flow chart of this program is shown in section B.11 of appendix B.

5.3.3 - Estimation of the swirl and squish velocities during compression stroke - Program COMPRESS

This program uses data transferred from the program "SUMMOM" via file "TRANSFER". The program estimates the instantaneous air swirl and squish velocities during the compression stroke, from inlet valve closure to 10° CA after TDC, using the model described in section 5.2.3. The crank angle and the instantaneous swirl and squish velocities are stored in file "CWCOMP". A printout of these data can also be obtained if required. A flow chart of this program is shown in section B.11 of appendix B.

5.3.4 - Estimation of crosswind velocity at impingement - Program CWVEL

This program uses the data on swirl velocity stored in file "CWCOMP" and additional data input by the user (injection timing and period, quantity of fuel injected, nozzle geometry, ignition delay and crank angle increment). The program uses the models of section 5.2.4 in order to estimate the crosswind velocity at the tip of the spray, at the instant the spray impinges on the walls of the piston bowl. It also estimates the fuel spray tip trajectory. The program starts at the start of injection and the crank angle is incremented by the value specified by the user. The program ends when the fuel impinges on the piston

walls, or when combustion begins (whichever occurs first). The crank angle at which combustion begins is entered by the user. This crank angle was obtained experimentally during the tests on the Lister engine described in chapter four. A flow chart of this program is shown section B.11 of appendix B.

5.4 - DEMONSTRATION AND VALIDATION OF THE COMPUTER MODEL

5.4.1 - Prediction of instantaneous mass flow rate during induction and total mass trapped at IVC - Program ITERAM

In order to obtain an assessment of the accuracy of the induction model (ITERAM), the mass trapped at the end of the induction period was predicted at different running conditions for the Lister engine, and were compared with measured values. Fig 5.1 shows that a good correlation exists between measured and predicted trapped mass. A statistical analysis on these data produced the following results:

number of data points	13
average value of the error: ((predicted - measured) / measured) x 100% ...	+0.326 %
Standard deviation of the error	5.775 %

5.4.2 - Prediction of moment of momentum at IVC - Program SUMMOM

A quantitative validation of the total moment of momentum at IVC was not possible due to lack of experimental data. The following is a qualitative assessment of the predicted values of the total moment of momentum at IVC.

Fig 5.2 shows the effect of the predicted trapped mass (m_{ivc}) on the total moment of momentum of the air at inlet valve closure. The figure shows: (a) at a constant engine speed, an increase in m_{ivc} (due to a rise in the boost pressure) increases the total moment of momentum at IVC; (b) at a given predicted m_{ivc}, the total moment of momentum at IVC increases with increasing engine speed.

In both cases, the total moment of momentum increases due to a rise

in the instantaneous air mass flow rate, either due to a rise in the boost pressure, or due to higher engine speed. Results from steady flow rig tests have shown that a higher instantaneous air mass flow rate increases the instantaneous moment of momentum rate at a given valve lift, Bond (1988). Hence, in an operating engine, at a given crank angle, higher boost pressure or engine speed would increase the instantaneous air mass flow rate and, therefore, the moment of momentum rate. Thus, the total moment of momentum over the whole of the induction period would be greater. This higher total moment of momentum at the end of the induction process with increasing air mass flow rate was predicted by the model.

5.4.3 - Prediction of swirl and squish during compression stroke - Program COMPRESS

Figs 5.3a and 5.4a show, respectively, the development of the predicted values of swirl and squish, within the Lister engine, during the compression process. Again, as in the case of the moment of momentum, (sec. 5.4.2), no quantitative validation for the compression model was possible due to lack of experiment data for the Lister engine. However, experimental data during the compression process were obtained by Dent and Derham (1974) using hot-wire anemometers, on a similar type of engine (bowl-in-piston combustion chamber). Their data, Fig 5.3b, shows measured swirl values of almost twice as high as those predicted for the Lister engine by the computer model presented here. This could be due to the engine used by Dent and Derham having a greater cylinder bore and swept volume than the Lister engine. As explained in appendix B (section B.12), the greater cylinder bore and greater air mass flow rate

during induction (due to the larger swept volume) resulted in a greater total moment of momentum at IVC. However, the mass and the inertia of the trapped air will increase with increasing bore and swept volume and, consequently, there may not be a net effect in the swirl speed during the compression process.

It is more likely that this differences between the swirl speed for the Lister engine and the engine used by Dent and Derham arose from differences in the inlet port design and geometry.

Experimental results of squish produced by Dent and Derham, Fig 5.4b, are of the same order of magnitude and are roughly, 20% greater than those predicted by this model for the Lister engine. At a given engine speed, squish is dependent on piston speed and on the changes in the geometry of the combustion chamber whilst the piston compresses the contents of the cylinder. The difference in the squish levels predicted for the Lister engine and the experimental values obtained by Dent and Derham at a given engine speed and crank angle, probably arises from differences in engine compression ratio, stroke, and cylinder bore (17.4:1, 8.23 cm, 8.57 cm respectively for the Lister engine and 16:1, 10.48 cm, 10.16 cm respectively for the Dent and Derham engine). The lower compression ratio of the Dent and Derham engine would tend to reduce squish at a given engine speed and crank angle, whilst the greater stroke would tend to increase piston speed and the squish velocity at a given engine speed and crank angle (Eq 5.11).

Fig 5.3a also shows the way in which swirl is affected by the compression ratio, the engine speed and the inlet manifold conditions in the case of the Lister engine. As shown on Fig 5.3a, increasing the compression ratio increases the maximum swirl reached at the end of the

compression stroke. The increase in maximum swirl was due to the fact that when the compression ratio was increased, more of the air that would have remained in the bump clearance was displaced into the piston bowl, and hence to a smaller moment of inertia.

It can be seen from Fig 5.3a that at higher **engine speeds** the maximum swirl is greater because the moment of momentum at IVC is greater for a given compression ratio and air inlet conditions (see section 5.4.2, Fig 5.2).

It can also be seen that at a given engine speed and compression ratio higher **air mass flow rates** (due to higher boost pressures) result in higher swirl rates at the end of the compression stroke (see section 5.4.2, Fig 5.2). An important result arising from Fig 5.3a was that a reduction in swirl due to lower compression ratio was restored by higher boost pressures. This is a very significant observation as far as VCR engine operation is concerned.

Fig 5.4a shows that only the compression ratio and engine speed effect the squish velocity. Higher **compression ratios** increased the squish velocity at a given engine speed. This was due to the fact, that at higher compression ratios the bumping clearance was smaller and, therefore, more of the cylinder contents were displaced into the piston bowl towards the end of the compression stroke. Since this greater air transfer must take place during the same time interval (at a constant engine speed), the velocity at which the air is displaced (i.e. the squish velocity) will be greater.

The squish velocity increased with increasing **engine speed**. This was, simply, a result of a higher piston speed and greater rate at which the piston displaced the air from the bump clearance volume into

the piston bowl (Eq 5.11).

As explained before, squish depends on the rate of displacement of a volume of air from the bump clearance into the combustion bowl (i.e. the rate of change of cylinder volume during compression). This explains why the greater mass trapped, due to the boost pressure, did not affect the squish velocity at a given compression ratio and engine speed, Fig 5.4a. This was also reflected by the absence of the term for density in Eq 5.11 .

Another notable feature of the Fig 5.4a is the crank angle at which the maximum squish velocity occurred. This crank angle was retarded by about 8° when the compression ratio was increased from 13:1 to 17:1.

It will be recalled from Chapter 2 that an engine equipped with a VCR piston running under high load conditions will operate at lower compression ratios and, therefore, with higher boost pressures than a normal fixed high compression ratio engine. This section leads to the conclusion that when the VCR piston is in operation, the effect of change in combustion volume geometry on the squish motion will be greater than its effect on the swirl motion. This is because, the boost pressure associated with VCR piston operation would tend to offset the effect on swirl of the lower compression ratio. No such compensation would occur in the case of squish. This is because a lower compression ratio reduces the squish, and a higher boost pressure has no effect on squish velocity.

5.4.4 - Prediction of crosswind velocity and spray tip trajectory - Program CWVEL

Fig 5.5 shows the predicted trajectory and the values of the

components of velocity at impingement. The predicted values of the crosswind velocity are of similar order of magnitude as those presented by Timoney. There are , however, differences in the values of V_{cw} due to the difference in the fuel injection system and engine geometry between the Lister engine and the engine used by Timoney. There is no readily available experimental data which can be used to assess the accuracy of the crosswind velocity predicted by the model. For this reason, only the trends in V_{cw} shown in the figures are discussed and assessed in the rest of this section. For a given piston bowl diameter, there are a number of factors which effect the crosswind velocity at impingement on the walls of the piston bowl. These factors are:

1 - The mean initial spray tip velocity.

2 - The drag force on the fuel droplets.

3 - The inertia of the fuel spray tip.

Consider, first, the spray tip initial velocity; this is a function of the mean pressure drop across the nozzle hole δP. As δP increases, the initial velocity with which the spray tip is injected increases. δP is a function of the overall nozzle area. A small overall nozzle area will result in a greater mean pressure drop across the nozzle δP, and a greater initial spray tip velocity. In practice the total nozzle area could be varied by either changing the number of nozzle holes or the diameter of each hole.

Consider, next, the drag force on the spray tip. For a given set of in-cylinder air conditions (air density and swirl), the drag force is dependent on the profile area of the spray tip droplets. Also, it is dependent on the Reynolds number (based on the droplet diameter). Thus,

for a given in-cylinder air conditions, the drag force on the spray tip will depend on the droplet diameter. Data presented by Heywood (1988) show that the mean fuel droplet diameter is reduced by:

1 - Increasing the pressure drop across the nozzle hole, δP.

2 - Reducing the nozzle hole diameter for a given δP.

3 - Reducing the number of nozzle holes (of a given diameter) since δP increases.

Finally, consider the spray tip inertia. The inertia increases as the droplet mass and, therefore, diameter increases.

In conclusion, the injection system parameters of interest are:

1 - The nozzle hole diameter.

2 - The number of nozzle holes.

3 - The pressure drop across the nozzle hole.

In practice, for a given number and diameter of the nozzle holes, the pressure drop across the nozzle holes is controlled by the injection rate.

Some results obtained from the computer model are shown in Fig 5.6. This figure illustrates the effect of these injection system design parameters on the crosswind velocity. Effects of the above parameters on V_{cw} are discussed in the following section.

5.5 - INJECTION SYSTEM OPTIMISATION FOR HIGH CROSSWIND VELOCITY

In VCR engine application several injection system parameters can be varied in order to ameliorate the effect of low compression ratio on fuel air mixing at high loads. There follows here a discussion on how each of the following parameters can effect the crosswind velocity.

1 - Nozzle hole diameter.

2 - Number of nozzle holes.

3 - Injection rate (or δP).

The above three parameters can be varied in order to maximise V_{cw}. However, the best combination of these three parameters is not so obvious. For this reason, the crosswind velocity model was used to demonstrate the effect of these three parameters on V_{cw}. Fig 5.6 shows the variation of V_{cw} as the diameter of the nozzle holes was varied. Consider the following:

1 - For a given number and diameter of nozzle holes, increasing the injection rate increases the crosswind velocity, V_{cw}. As discussed above, the higher pressure drop across the nozzle holes (produced by the higher injection rate) increases the initial spray tip velocity and reduces the residence time in the swirling air field. It also reduces the drag force on the droplets and their inertia (due to lower droplet diameter). The net effect is an increase in crosswind velocity.

2 - For a given injection rate and number of nozzle holes, increasing hole diameter reduces V_{cw}. Increasing hole diameter reduces the initial spray tip velocity and increases droplet diameter. Further more, the greater hole size reduces the pressure drop across the nozzle which also has the effect of increasing droplet diameter. The net effect

is larger droplets travelling slower, and a lower crosswind velocity.

3 - For a given injection rate and nozzle hole diameter, increasing the number of holes decreases the pressure drop across the injector nozzle holes and, as a consequence, decreases the initial spray tip velocity and increases the droplet diameter. The net effect is as in the case of (2) above, larger droplets travelling slower, and a lower crosswind velocity.

However, the number and diameter of the nozzle holes does not only affect the magnitude of the crosswind velocity, it also affects the fuel distribution within the combustion chamber, which may prove to be a factor as important as the crosswind velocity.

Summarising: reducing the nozzle hole diameter or increasing the injection rate increases the crosswind velocity. Increasing the number of holes reduces the crosswind velocity, but improves the fuel distribution in the combustion chamber.

It may be concluded that in VCR applications it may be best to adopt an injection system with a large number of holes (say 4 or 5) and restore the fall in V_{cw} by reducing the nozzle hole diameter and, possibly by increasing the injection rate further. However, one of several problems that might arise with higher injection rate is an increase in the amount of fuel injected during the ignition delay period. This increases the amount of premixed fuel at the start of ignition and, as a consequence, the peak cylinder pressure would tend to increase. In VCR engine operation, at mid load, the compression ratio will automatically decrease in order to compensate for this. However, at high engine load, when the compression ratio has reached its lowest limit, no more compensation through the compression ratio is possible.

Thus, at high loads, the tendency for higher peak pressure due to higher injection rates, would have to be compensated for by a reduction in boost pressure or less advanced injection timing. There will be, as a result, a penalty in terms of some reduction in full load power, and a possible increase in smoke concentration respectively.

5.6 - DISCUSSION OF EXPERIMENTAL RESULTS AND COMPUTER DATA

The computer model was used in order to estimate the crosswind velocity relating to a number of the experimental tests carried out on the Lister engine. This section is an attempt to investigate whether a good engine performance (low smoke emissions and BSFC) are consistent with high V_{cw}.

The comparison between the magnitude of the V_{cw} and relative engine performance parameters was made for five groups of tests: two at 1300 revs/min and three at 1700 revs/min. Care was taken to exclude the effect of dynamic injection timing and air fuel ratio by keeping these two variables approximately constant. This was necessary since these two parameters have an overwhelming effect on engine performance in addition to whatever effect that V_{cw} might have. Engine running conditions were in accordance with VCR operation, that is a fixed peak cylinder pressure.

In Fig 5.7 the only change in test running conditions was the increase in the number and size of the nozzle holes. The engine performance was improved which was consistent with an increase in V_{cw}. However, it is not possible to separate the contribution of higher V_{cw} to the improvement in performance from that of better fuel distribution brought about by the increase in number of sprays from three to four.

In Fig 5.8 the only change in the test running conditions was the increase in pump size from the standard pump of 7.5 mm plunger diameter to 8.5 mm. This resulted in an increase of about 28 % in injection rate. The V_{cw} increased substantially. It can be argued that in this case the combustion performance improved, that is, smoke emission was lower, although the overall engine efficiency decreased. The reduction in

efficiency was due to a fall in the BMEP which reduced the mechanical and overall efficiency of the engine, (see section 4.2.4).

The conditions in Fig 5.9 are the same as those of Fig 5.8, except for the higher engine speed of 1700 revs/min. It is interesting to note that the same trends as those at 1300 revs/min are evident and that similar conclusions can be drawn.

In Fig 5.10, results for the following two test conditions were compared: (a) nozzle with 3 * 0.25 mm diameter holes and high injection rate pump; (b) nozzle with 4 * 0.28 mm diameter holes and standard pump. The figure suggests that the combustion performance has worsened, in the case of the three hole nozzle, consistent with a substantially lower V_{cw}, but overall engine efficiency has improved. The increase in overall engine efficiency was almost certainly due to an increase in mechanical efficiency resulting from a 30% rise in BMEP. The reduction in combustion performance can not be readily attributed to a reduction in V_{cw} since several other parameters which can have an effect on combustion were also changed (number of nozzle holes and injection rate).

In Fig 5.11 the only change in test conditions was the increase in pump size. Note that results in this figure are at 35:1 air fuel ratio compared with 25:1 in all the previous results. Unfortunately it was not possible to judge the effect of V_{cw} in the case of this group of tests since the difference in the test conditions were such that no significant change in V_{cw} resulted.

5.7 CONCLUSION

The computer model which predicts the magnitude of swirl and squish during fuel injection can be combined with the computer model which predicts spray trajectories to give useful insights into the fuel distribution within the cylinder. Also, useful information on the interaction between the fuel spray and air was obtained, such as the magnitude of the crosswind and impingement velocities when the spray impinges on the piston bowl walls.

Due to the limited number of data available, it was not possible to draw a concrete conclusion as to the contribution which high crosswind velocity might have had on engine performance; however some tentative trends were identified which showed that in some tests high crosswind velocity coincided with better engine performance. Further tests designed to ascertain the effect of crosswind velocity on combustion performance could be worthwhile.

Chapter 6: Conclusions and Recommendations for Future Work

Conclusions on detailed aspects of this study have been included in Chapters 2,4, and 5. Major conclusions of a more general nature are given below, and these are followed by recommendations for future work.

6.1 - CONCLUSIONS

Performance improvements

1 - With simulated VCR operation, at a low compression ratio of 12.9:1, substantial improvements in BMEP and BSFC were obtained. These were achieved without the maximum cylinder gas pressure or engine temperatures exceeding the highest levels for the standard naturally-aspirated engine. For example, at 2160 rev/min the BMEP was almost 50% higher, and the BSFC was 20% lower than the values at full-load for the standard naturally-aspirated engine; the smoke emission was at an acceptable level of 3.6 Bosch units.

Measures to ameliorate problems with combustion

2 - At the lower compression ratio, the reduction in the swirl and squish levels during compression (and as a result the reduction in the level of air turbulence), had a substantial detrimental effect on the combustion process. This was manifested by marked increase in smoke emissions.

3 - Certain modifications to the injection system proved successful in ameliorating problems with combustion. These included, replacement of the standard-engine three-hole injector nozzle (3 x 0.25mm diameter holes) by a four-hole nozzle (4 x 0.28mm), an increase in injection rate of about 28%, and advancing the injection timing from around 15°CA BTDC to around 21°CA BTDC.

4 - In addition, operation with weaker air fuel ratios, in the range of 30 to 40:1 (compared with 20:1 at full load for the standard naturally-aspirated engine), proved successful in improving engine performance.

Use of intercooling

5 - The benefits from intercooling, when operating under VCR conditions, are likely to be modest for the following two reasons: firstly, due to poor air fuel mixing, the extra fuel quantity per cycle, that was made possible by the greater air density, could not be burned efficiently; secondly, intercooling tended to increase ignition delay and rate of pressure rise, thus forcing lower boost pressure under constant P_{max} operation. This, in turn, tended to moderate the increase in density gained with intercooling from the lower air temperature.

6 - Use of intercooling did not reduce appreciably the NO_x level in the exhaust gases. In fact, the NO_x level was found to be insensitive to engine operating conditions, as long as the peak cylinder pressure was maintained constant. A similar conclusion was reached by Russel and Haworth (1985).

Use of computer models for optimisation of engine performance with VCR

7 - Computer models were developed which predicted the magnitude of swirl and squish during fuel injection. These were combined with a computer model which predicted the fuel spray trajectories. Together, these models produced useful insights into the fuel distribution within the cylinder. They also proved useful in revealing the interaction between the fuel spray and the swirling air at the low compression ratio. It became possible to quantify this interaction in terms of two parameters: the crosswind and the impingement velocities of

the fuel spray when it impinges on the piston-bowl walls.

The insights gained from the use of the computer models proved useful when interpreting the experimental results obtained from the Lister engine.

8 - Tentative trends were identified which showed that high crosswind velocity coincided with better engine performance in terms of lower smoke emission and lower BSFC. Further tests to ascertain the effect of crosswind velocity on combustion performance would be worthwhile.

9 - The computer simulation of the induction and compression processes was used in order to predict the swirl and squish velocities as the piston approached TDC. This was done for both the standard naturally-aspirated engine, as well as for the engine under simulated turbocharged conditions at the lower compression ratio. The computer models showed that at the low compression ratio the squish levels fell to about one-fifth of their level for the standard engine (at a given engine speed, and irrespective of air inlet conditions). However, at the low compression ratio, there was almost no loss of swirl (as the piston approached TDC). This was because, at a given engine speed, the swirl imparted during induction increased at the low compression ratio, as a result of boosting the air supply to the engine.

10 - Using test results from the Lister engine, preliminary work was carried out with the aim of assessing the accuracy of four published correlations for predicting ignition delay. These correlations would be useful in a cycle simulation computer program for VCR engines. The best prediction of ignition delay deviated by up to 50% from the measured values. The accuracy of the predictions was found to be sensitive to the estimation of the mean air temperature during the ignition delay period.

6.2 - FUTURE WORK

1 - Alterations to the combustion chamber geometry could be investigated. The aim of these being to increase turbulence during combustion at the rim of the piston bowl. The literature survey of Chapter 2 has shown that high turbulence in this region correlates well with smoke emission, over a wide range of engine operating conditions.

2 - It would be worthwhile to investigate further whether the values of the crosswind and spray impingement velocities are useful criteria for combustion chamber design.

3 - Due to constraints with availability of injection system components, only a limited number of modifications to the standard-engine system could be investigated experimentally. These could be extended to include: a greater number of nozzle holes, greater injection pressure, and greater injection rate than the levels adopted in this investigation.

4 - Since the diesel combustion process depends greatly on the detailed air activity during combustion, it would be useful to use a computational fluid dynamics (CFD) model to predict turbulence, as well as swirl and squish during combustion. Because much of the detailed air activity depends on the interaction between the fuel spray and the surrounding air, such a model should, if possible, include this interaction process.

Appendix A

A.1 - ORIFICE PLATE CALIBRATION

The air mass flow rate, supplied to the engine, was measured using a 21.6 mm (0.85") orifice plate, Fig A.1, constructed and installed upstream of the surge tank (see Fig 3.1), according to British Standard BS1042. The orifice plate was calibrated using both a positive displacement volumetric meter manufactured by Romet, and a Lucas-Dawe corona discharge instantaneous air mass flow meter. The Dawe meter was calibrated by the manufacturer on rigs approved by the National Physical Laboratory.

The air mass flow rate measured by the orifice plate was estimated using the computer program **"MASSFLOW"** based on the calculation procedure given in the British Standard BS1042.

For steady flow calibration, the Romet positive displacement meter was connected downstream of the orifice plate and the surge tank. Air was supplied, from the laboratory compressed air supply line, through the orifice plate, to the positive displacement meter. The air mass flow rate was varied using the pressure regulator valve upstream of the orifice plate. The orifice plate underestimated the air flow rate by 3% over an air mass flow rate range of 0 - 15 g/s.

With the rig set up as shown in Fig 3.1, the pressure regulator valve was removed and the Dawe instantaneous air mass flow meter was connected upstream of the orifice plate. The orifice plate was calibrated, under engine running conditions (naturally aspirated), over a range of air mass flow rates. The air mass flow rate was varied by varying the engine speed. Fig A.2 shows the percentage error of the orifice plate compared to the Dawe meter data. To facilitate processing of future test results, a polynomial curve was fitted to the data of Fig

A.2. The equation of this curve was found using the main-frame computer NAG subroutine E02ADF. The equation of the fitted polynomial is as follows:

$$E_o = 0.0470\,M_o^3 - 1.5138M_o^2 + 15.5012M_o - 53.8695$$

Where: $$E_o = \left[\frac{M_o - M_d}{M_o}\right] \times 100$$

and M_d and M_o are the air mass flow rates measured using the Dawe meter and the orifice plate respectively.

Both calibrations were then incorporated in the BBC microcomputer program.

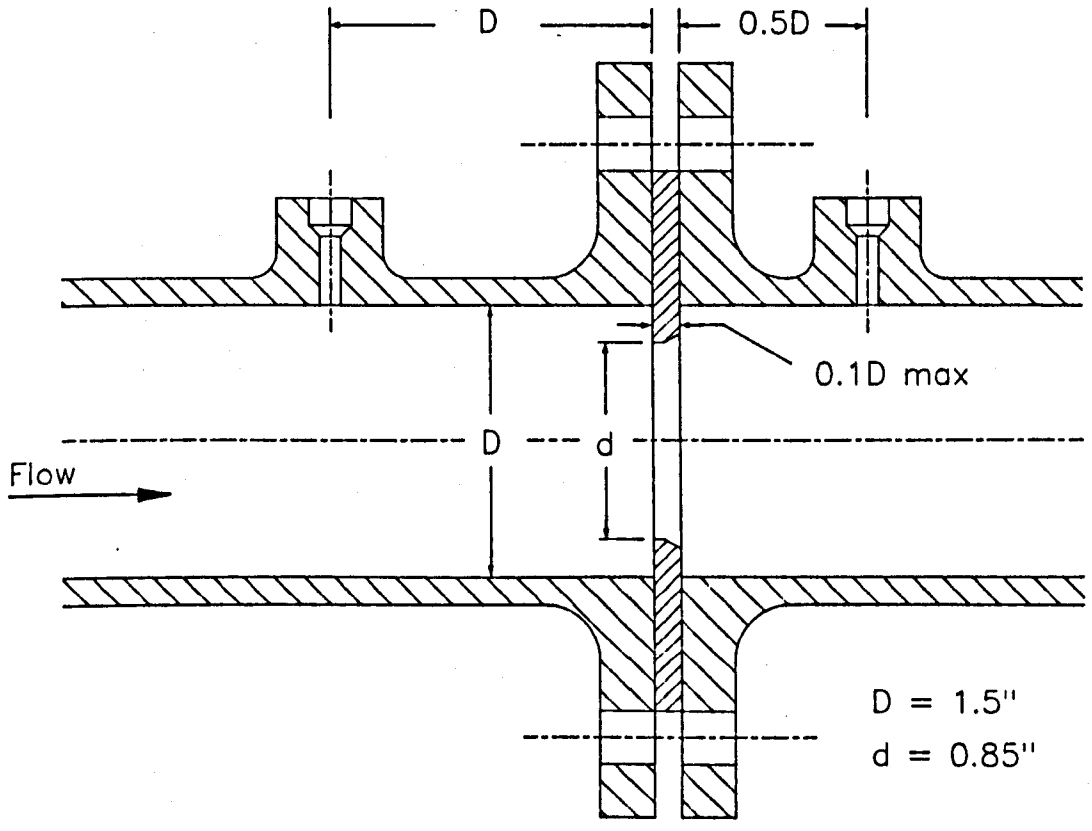

FIGURE A.1
Cross-sectional view of the orifice plate with D and D/2 tappings.

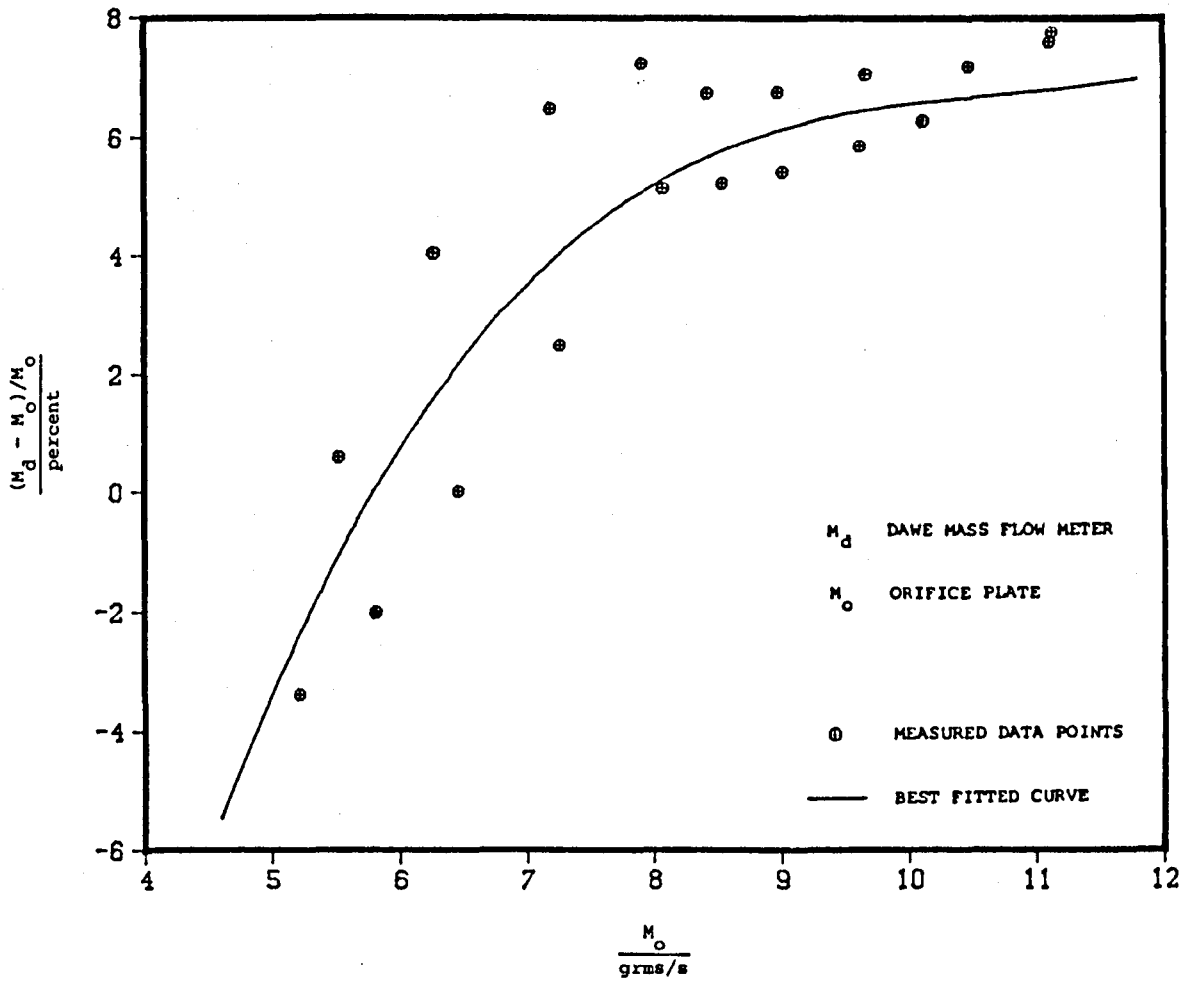

FIGURE A.2
Variation of the percentage error of the mass flow rate measured using the orifice plate compared with values obtained from the Dawe instrument, (calibrated under engine running conditions).

The following is a listing of the program MASSFLOW.

```
1000 REM PROGRAM "MASSFLOW"
1010 @%=&00020300
1020 DIM X(30),Y(30),Q(50),H(50): CLS: ROUND=1
1030 REM SCREEN
1040 PRINT TAB(43,0) "_____"
1050 PRINT TAB(43,7) "_____"
1060 PRINT TAB(43,9) "_____"
1070 PRINT TAB(43,12) "_____"
1080 PRINT TAB(1,0) "_____"
1090 PRINT TAB(2,8) "----------"
1100 PRINT TAB(1,13) "_____"
1110 PRINT TAB(1,15) "_____"
1120 PRINT TAB(1,23) "_____"
1130 PRINT TAB(2,19) "----------"
1140 PRINT TAB(44,19) "----------"
1150 PRINT TAB(43,14) "_____"
1160 PRINT TAB(43,23) "_____"
1170 FOR I=1 TO 13 : PRINT TAB(0,0+I) "¦" : PRINT TAB(40,0+I) "¦" : NEXT I
1180 FOR I=1 TO 7 : PRINT TAB(42,0+I) "¦" : PRINT TAB(78,0+I) "¦" : NEXT I
1190 FOR I=1 TO 3 : PRINT TAB(42,9+I) "¦" : PRINT TAB(78,9+I) "¦" : NEXT I
1200 FOR I=1 TO 8 : PRINT TAB(0,15+I) "¦" : PRINT TAB(40,15+I) "¦" : NEXT I
1210 FOR I=1 TO 9 : PRINT TAB(42,14+I) "¦" : PRINT TAB(78,14+I) "¦" :NEXT I
1220 PRINT TAB(45,2) "1 - INPUT BAROMETRIC PRESSURE"
1230 PRINT TAB(45,3) "2 - A/F FROM ORIFICE PLATE"
1240 PRINT TAB(45,4) "3 - A/F FROM COMBUSTION PRODUCTS"
1250 PRINT TAB(45,5) "4 - TURBOCHARGING SIMULATION"
1260 PRINT TAB(45,11) "BARO. PRESS.    /mmHg"
1270 PRINT TAB(2,2) "ORIF. PRESS. DIFF.   /in "
1280 PRINT TAB(2,3) "ORIF. UPST. PRESS. /mmHg "
1290 PRINT TAB(2,4) "ORIF. UPST. TEMP.    /oC "
1300 PRINT TAB(2,5) "FUEL FLOW TIME        /s "
1310 PRINT TAB(2,6) "FUEL TEMPERATURE     /oC "
1320 PRINT TAB(2,7) "MOISTURE CONTENT  /kg/kg "
1330 PRINT TAB(2,10) "AIR MASS FLOW RATE / g/s"
1340 PRINT TAB(2,11) "A/F (ORIFICE PLATE)"
1350 PRINT TAB(2,12) "EXHAUST TEMPERATURE /oC"
1360 PRINT TAB(2,17) "PERCENT CO2 " : PRINT TAB(2,18) "PERCENT O2 "
1370 PRINT TAB(2,21) "A/F (COMBUSTION PRODUCTS) "
1380 PRINT TAB(2,22) "PERCENT CO "
1390 PRINT TAB(45,16) "ORIF. UPST. TEMP. /oC"
1400 PRINT TAB(45,17) "EXHAUST TEMP.     /oC"
1410 PRINT TAB(45,18) "BOOST PRESSURE  /mmHg"
1420 PRINT TAB(45,21) "AIR INLET TEMP.   /oC"
1430 PRINT TAB(45,22) "EX. BACK PRESS.  /psi"
1440 REM INPUT OPTION
1450 PRINT TAB(45,6) "      " : INPUT TAB(45,6) ZZ
1460 IF ZZ=1 GOTO 1510
1470 IF ZZ=2 GOTO 1540
1480 IF ZZ=3 GOTO 2160
1490 IF ZZ=4 GOTO 2230 : ELSE GOTO 1450
1500 REM MASS FLOW AND AIR FUEL RATIO CALCULATIONS
1510 PRINT TAB(70,11) "      " : INPUT TAB(70,11) PB : REM BAROMETRIC PRESSURE
1520 GOTO 1450
1530 REM INPUT DATA REQUIRED
1540 FOR I=1 TO 6 : PRINT TAB(30,1+I) "        " :NEXT I : REM SCREEN
1550 INPUT TAB(31,2) PH : INPUT TAB(31,3) P : INPUT TAB(31,4) T
1560 INPUT TAB(31,5) SEC : INPUT TAB(31,6) TFUEL : INPUT TAB(31,7) MC
1570 REM CONVERT UNITS
1580 CC=20.315-(0.016597*TFUEL) : P1=P : P=P+PB : P=P/51.715
1590 D1=0.8505 : D2=1.5000 :S=1.0 : EP=1.0 : ZR=1.0 :ZD=1.0
1600 PH=PH*0.784*COS(RAD(48.5)) : APH=PH*25.4/13.6
1610 TF=(1.8*T)+32 : TR=TF+459.67
1620 DR=D1/D2 : M=DR^2
```

```
1640 IF ROUND<>1 GOTO 1660
1650 FOR I=1 TO 32 : READ ALF : READ PARP :Q(I)=ALF : H(I)=PARP : NEXT I
1660 PV=(P*MC)/(MC+0.622)
1670 GOTO 1830
1680 REM INTERPOLATE BETWEEN DATA POINTS
1690 FOR I=1 TO 32
1700 IF TF>=Q(I) AND TF<=Q(I+1) GOTO 1720
1710 GOTO 1740
1720 PVS=((TF-Q(I))*(H(I+1)-H(I)))+H(I)
1730 PV=PVS*FI
1740 NEXT I
1750 DATA 56,0.222,57,0.230,58,0.239,59,0.247
1760 DATA 60,0.256,61,0.266,62,0.275,63,0.285
1770 DATA 64,0.295,65,0.306,66,0.316,67,0.328
1780 DATA 68,0.339,69,0.351,70,0.363,71,0.376
1790 DATA 72,0.389,73,0.402,74,0.416,75,0.430
1800 DATA 76,0.444,77,0.459,78,0.475,79,0.491
1810 DATA 80,0.507,81,0.524,82,0.541,83,0.559
1820 DATA 84,0.578,85,0.597,86,0.617,87,0.637
1830 K=1.0 : C=0.6082
1840 REM READ DATA ONLY ONCE (WHEN ROUND-1) FROM DATA FILE
1850 IF ROUND<>1 GOTO1900
1860 FOR I=44 TO 49 : READ TEMP : READ MUM : Q(I)=TEMP : H(I)=MUM  : NEXT I
1870 DATA 0,1.722E-4,20,1.818E-4,40,1.910E-4,60,2.000E-4
1880 DATA 80,2.082E-4,100,2.180E-4
1890 REM INTERPOLATE BETWEEN DATA POINTS
1900 FOR I=44 TO 49
1910 IF T>=Q(I) AND T<Q(I+1) GOTO 1930
1920 GOTO 1940
1930 MU=(((T-Q(I))/20)*(H(I+1)-H(I)))+H(I)
1940 NEXT I
1950 REM MASS FLOW RATE AND AIR FUEL RATIO CALCULATIONS
1960 GOSUB 2100
1970 GAMA=1.4 : XX=(PH/P)/0.7746 : EP=(-0.00888*XX)+1 : ZD=1.007
1980 REM                REYNOLDS No. CORRECTION FACTOR
1990 X(1)=1.0177 : X(2)=1.0128 : X(3)=1.0085
2000 IF RD>=20000 AND RD<=50000 : ZR=(((X(1)-X(2))/30000)*(50000-RD))+X(2)
2010 IF RD>=50000 AND RD<=100000 : ZR=(((X(2)-X(3))/50000)*(100000-RD))+X(3)
2020 GOSUB 2100
2030 @%=&00020300
2040 WF=(CC*0.8364)/SEC : PRINT TAB(31,10) W2 : AF=W2/WF : PRINT TAB(31,11) AF
2050 REM INPUT EXHAUST GAS TEMPERATURE FOT TURBOCHARGING SIMULATION
2060 PRINT TAB(31,12) "        " : INPUT TAB(31,12) T3
2070 ROUND=ROUND+1
2080 GOTO 2270
2090 REM SUBROUTINE FOR AIR MASS FLOE RATE AND AIR FUEL RATIO CALCULATIONS
2100 DEN=2.7*(((S*(P-PV)/(K*TR))+((0.62*PV)/TR))) : Z=ZD*ZR
2110 E=1/((1-M^2))^0.5 : REM VELOCITY OF APPROACH FACTOR
2120 W=359.2*C*Z*E*EP*(D1^2)*((PH*DEN)^0.5)
2130 W2=0.126*W
2140 RD=W/(15.8*MU*D1): REM REYNOLDS No. AT ABOVE RATE OF FLOW
2150 RETURN
2160 FOR I=1 TO 2 : PRINT TAB(31,16+I) "          " : NEXT I : REM SCREEN
2170 REM AIR FUEL RATIO CALCULATIONS FROM EX. GAS ANALYSIS RESULTS
2180 INPUT TAB(31,17) A : INPUT TAB(31,18) B : A=A/100 : B=B/100
2190 AF=(9.883*((A/2)+B)+9.7683*(1-B))/((1-B)+3.76*((A/2)+B))
2200 M=AF*0.21/28.96 : N1=(A*(3.76*M+0.0717)/(1-B))
2210 N3=0.0717-N1 : N5=B*N1/A : N6=3.76*M : C=N3/(N1+N3+N5+N6) : CO=C*100
2220 PRINT TAB(31,21) AF : PRINT TAB(31,22) CO : GOTO 1450
2230 FOR I=1 TO 3 : PRINT TAB(70,15+I) "          " :NEXT I
2240 INPUT TAB(70,16) AT01 : INPUT TAB(70,17) AT3 : INPUT TAB(70,18) AP
2250 GOTO 2290
2260 REM CALCULATIONS FOR THE TUBOCHARGING SIMULATIONS
2270 AT01=T : AT3=T3 : AP=P1-APH
2280 PRINT TAB(70,16) AT01 : PRINT TAB(70,17) AT3 : PRINT TAB(70,18) AP
2290 CP12=1.005 :CP34=1.15 :PEC=0.77 :PET=0.78 :AME=0.96 :G12=1.4 :G34=1.33
2300 AT01=AT01+273 :AT3=AT3+273 :G12=(G12-1)/(G12*PEC) :G34=G34/((G34-1)*PET)
2310 APR=(AP+PB)/PB :A=(CP12*AT01)/(CP34*AT3*AME) :B=(1-A*((APR^G12)-1))^G34
2320 AR=1/B :AEP=AR*1.1 :AT2=(AT01*(APR^G12))-273
2330 FOR I=1 TO 2 : PRINT TAB(70,20+I) "          " :NEXT I
2340 PRINT TAB(70,21)AT2 : PRINT TAB(70,22) AEP
2350 GOTO 1450
```

A.2 - Cylinder pressure transducer calibration

The cylinder gas pressure was measured using an AVL water-cooled piezoelectric pressure transducer (type 8QP500C) and a Kistler S/N747 model 566 charge amplifier.

The pressure transducer together with the amplifier were calibrated, under steady state conditions, using a dead-weight tester and a digital voltmeter. It was essential that all the connecting plugs and sockets were kept clean so as to prevent leakage of charge due to dampness or dirt.

The calibration was carried out both with increasing and decreasing pressure. Fig A.3 shows the transducer calibration curve. The slope of the curve in Fig A.3 is the pressure transducer calibration factor measured to be 10.11 bar/V. It is assumed that the rate of change of the transducer output signal with pressure (i.e. the calibration factor) will remain constant at all working temperatures. However, it is important to note that since the transducer output is affected by its working temperature, the y-axis intersection of the calibration curve can not be relied upon. Therefore, only a change in the cylinder pressure can be estimated accurately from the transducer signal. For this reason it is necessary to chose a datum position on the signal for which an absolute pressure can be attributed. The datum position chosen for this project was bottom-dead-centre (BDC) during the induction stroke where the cylinder pressure was assumed to be equal to the manifold pressure.

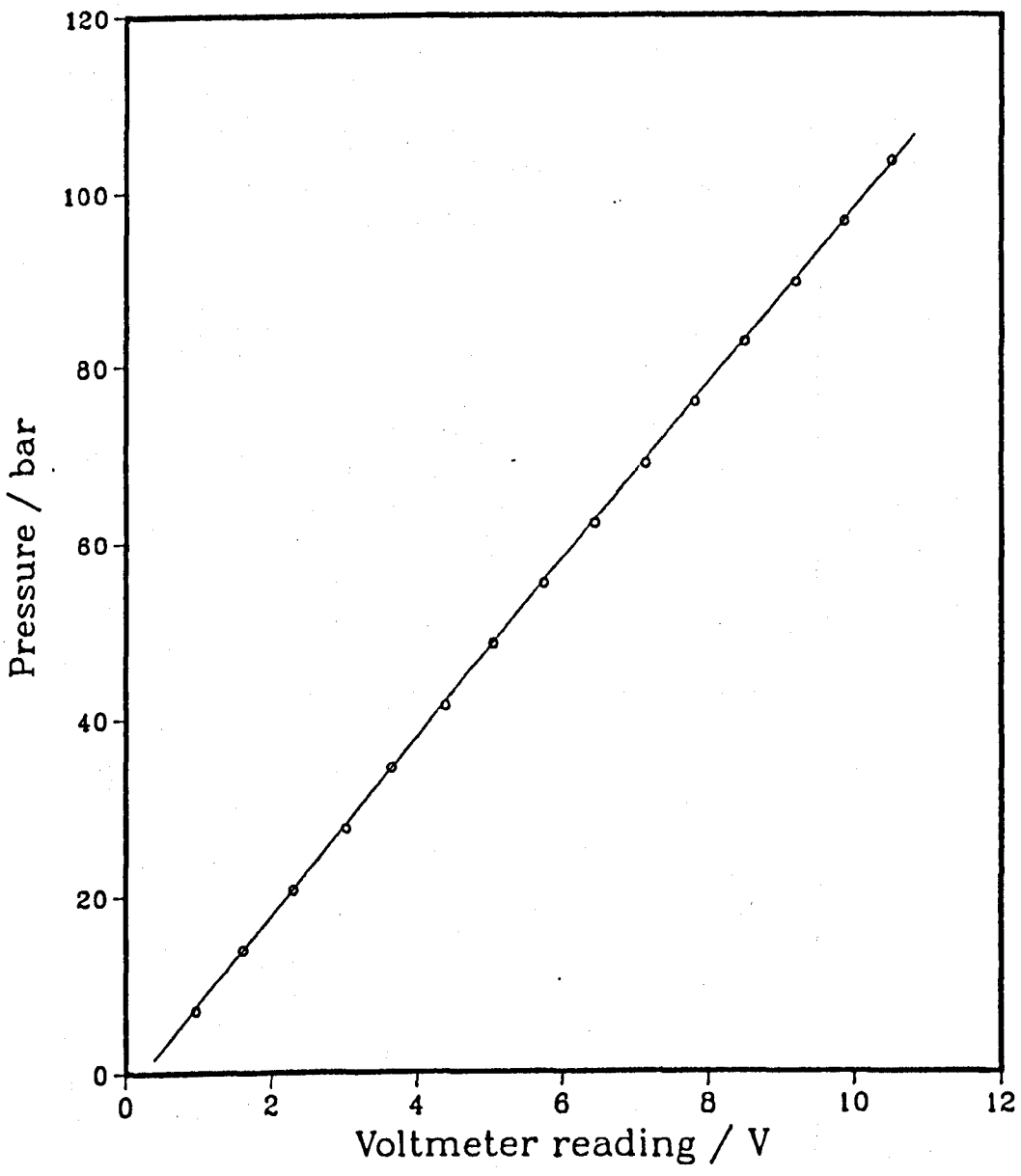

FIGURE A.3
Cylinder pressure transducer calibration curve, (Kistler S/N747, model 566). Transducer calibration factor = 10.11 bar/V.

A.3 - Plots of baseline test data

The following are the plots of the baseline test data at constant speeds of 1700, 2160, 2460 and 3000 rev/min and varying load. The discussion of these results is included in section 3.2.3 of Chapter 3.

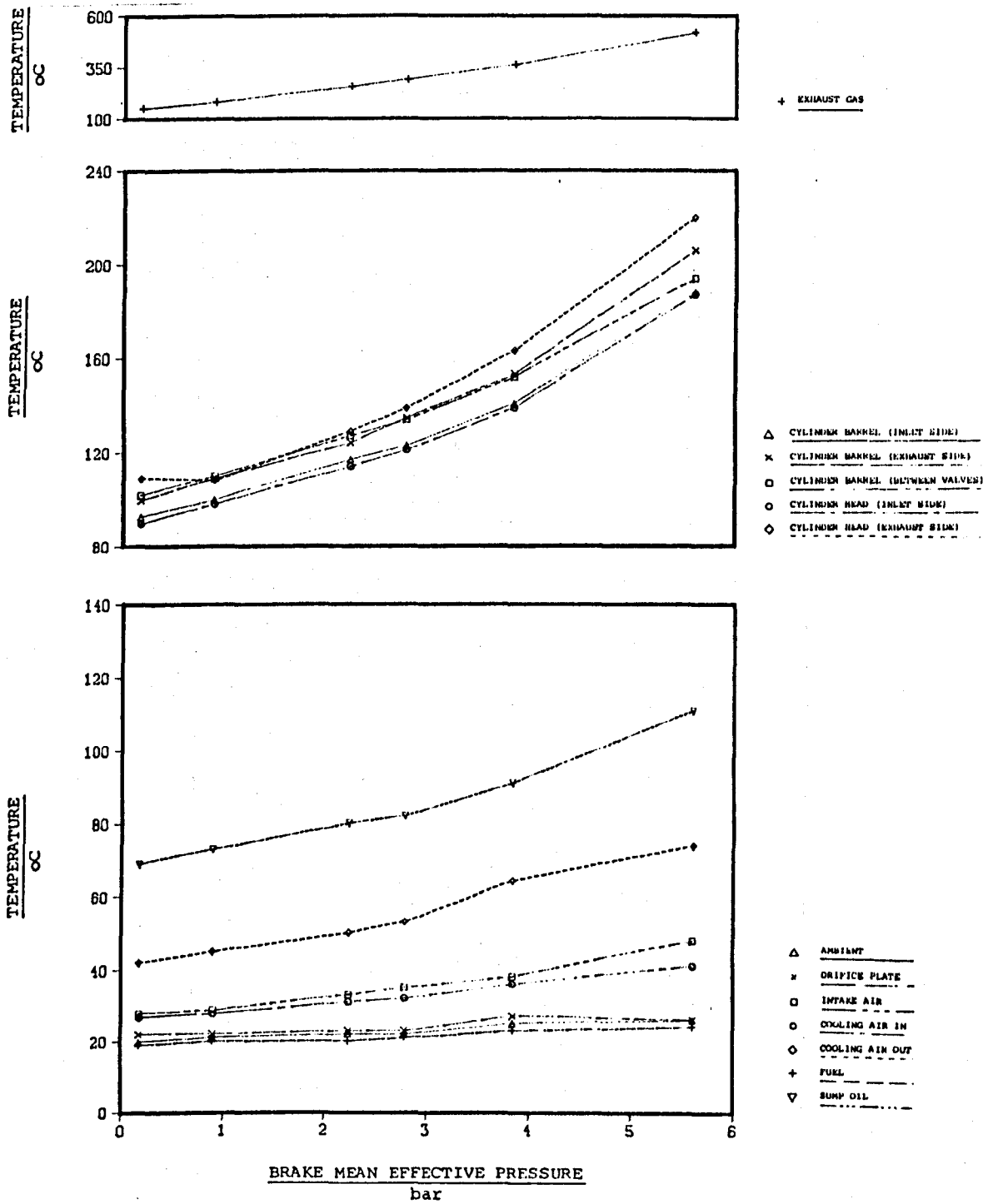

FIGURE A.4
Variation of temperature at a number of locations with brake mean effective pressure at constant speed of 1700 rev/min.

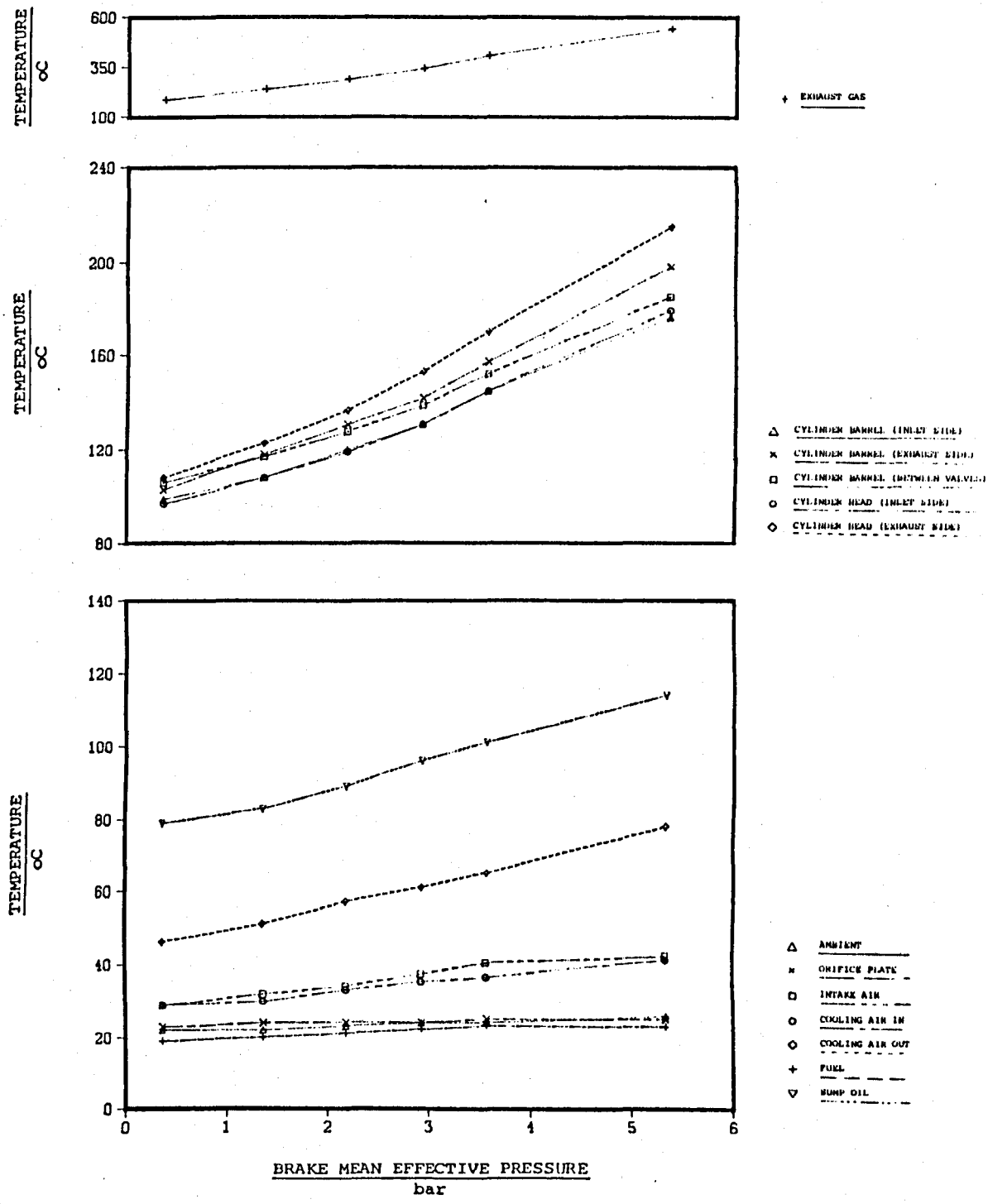

FIGURE A.5
Variation of temperature at a number of locations with brake mean effective pressure at constant speed of 2160 rev/min.

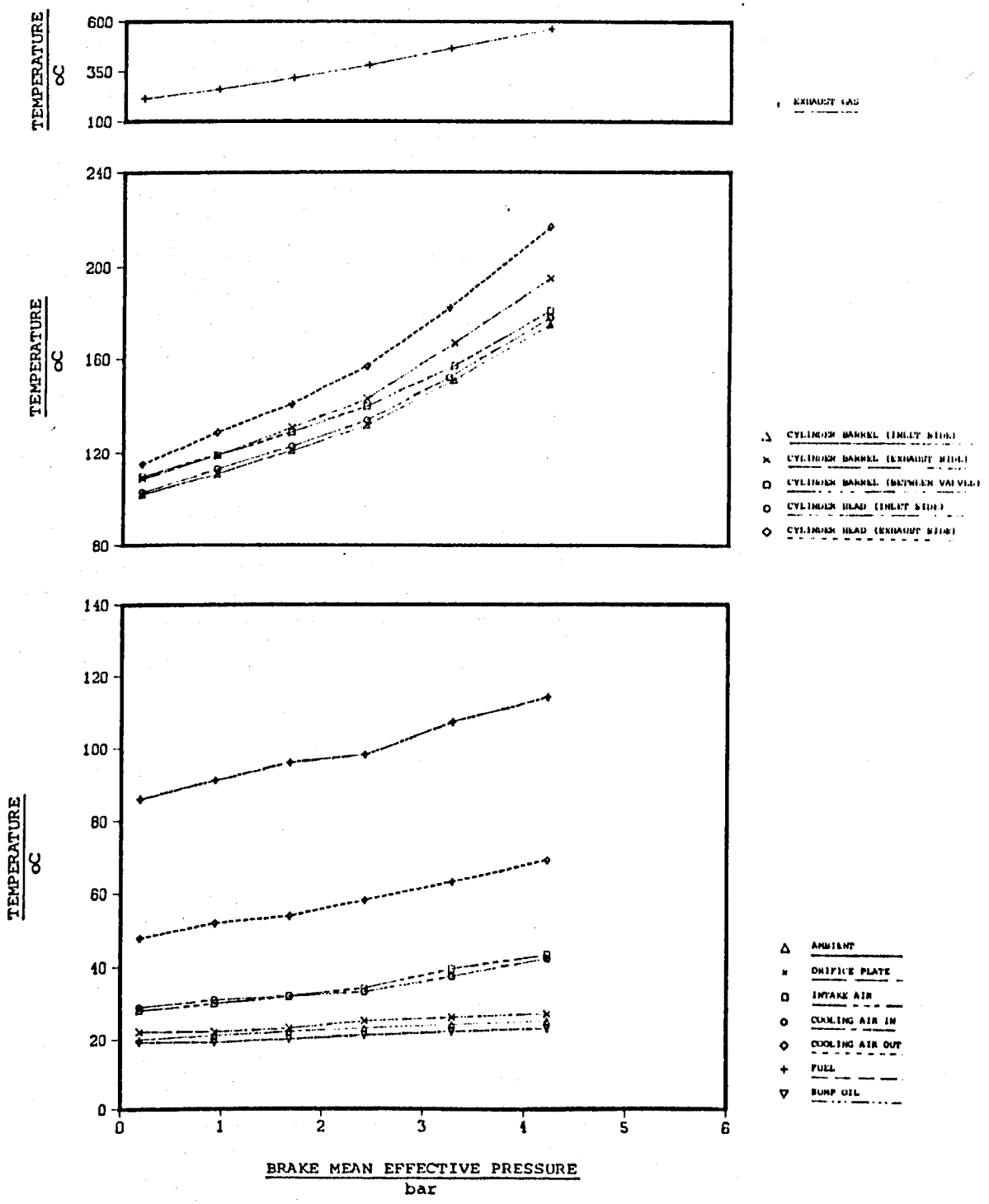

FIGURE A.6
Variation of temperature at a number of locations with brake mean effective pressure at constant speed of 2460 rev/min.

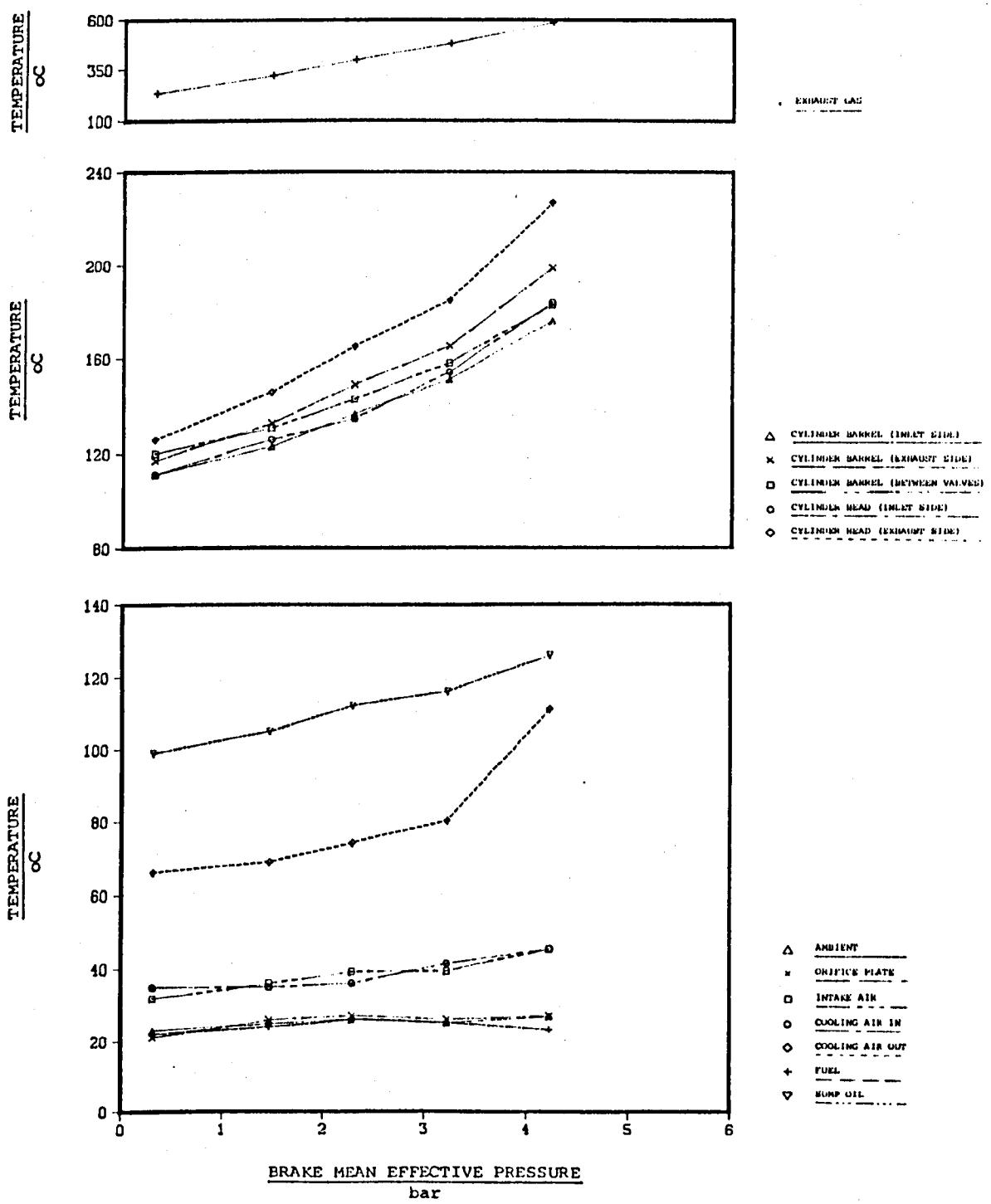

FIGURE A.7
Variation of temperature at a number of locations with brake mean effective pressure at constant speed of 3000 rev/min.

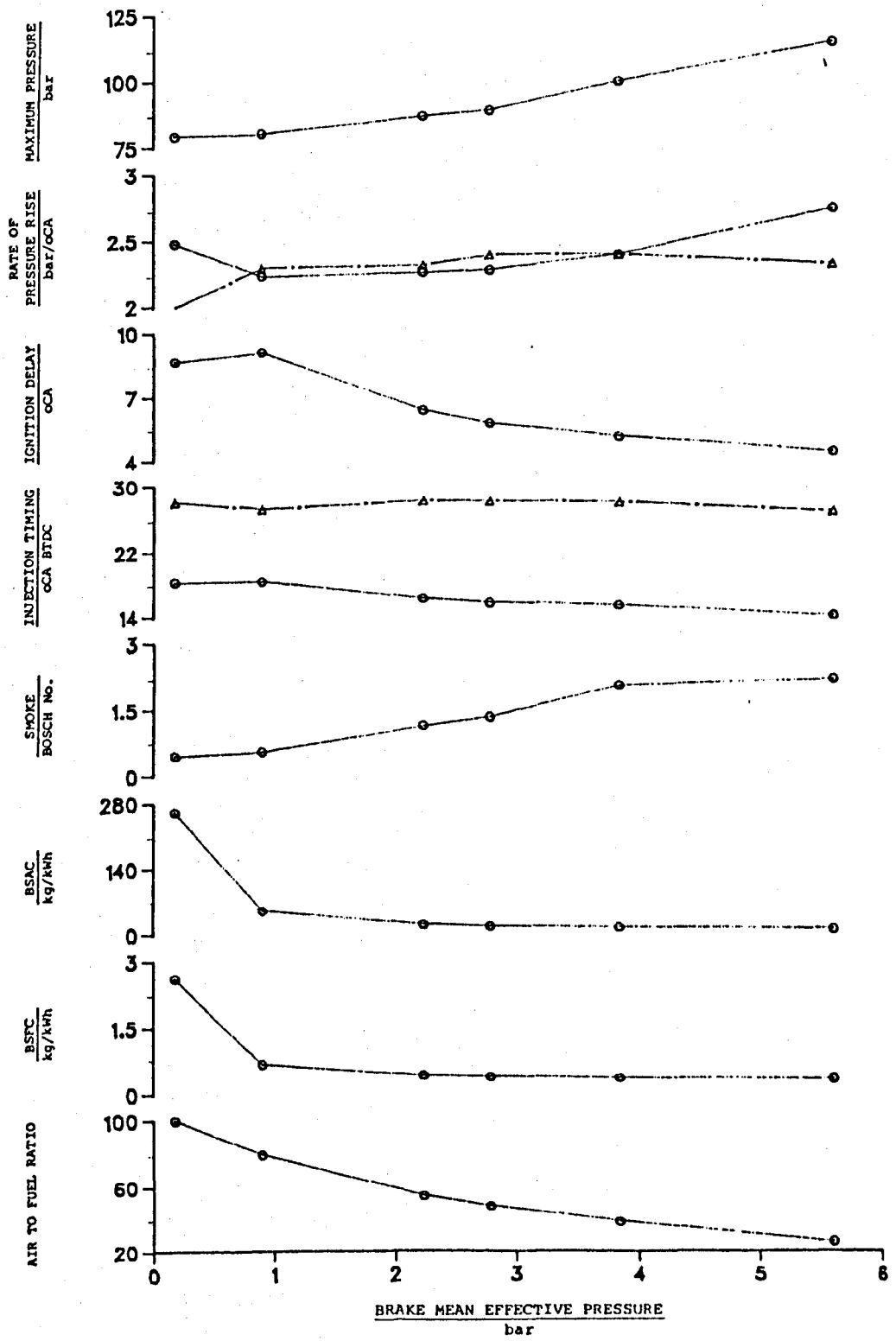

FIGURE A.8
Typical results at 1700 rev/min obtained from the baseline tests.

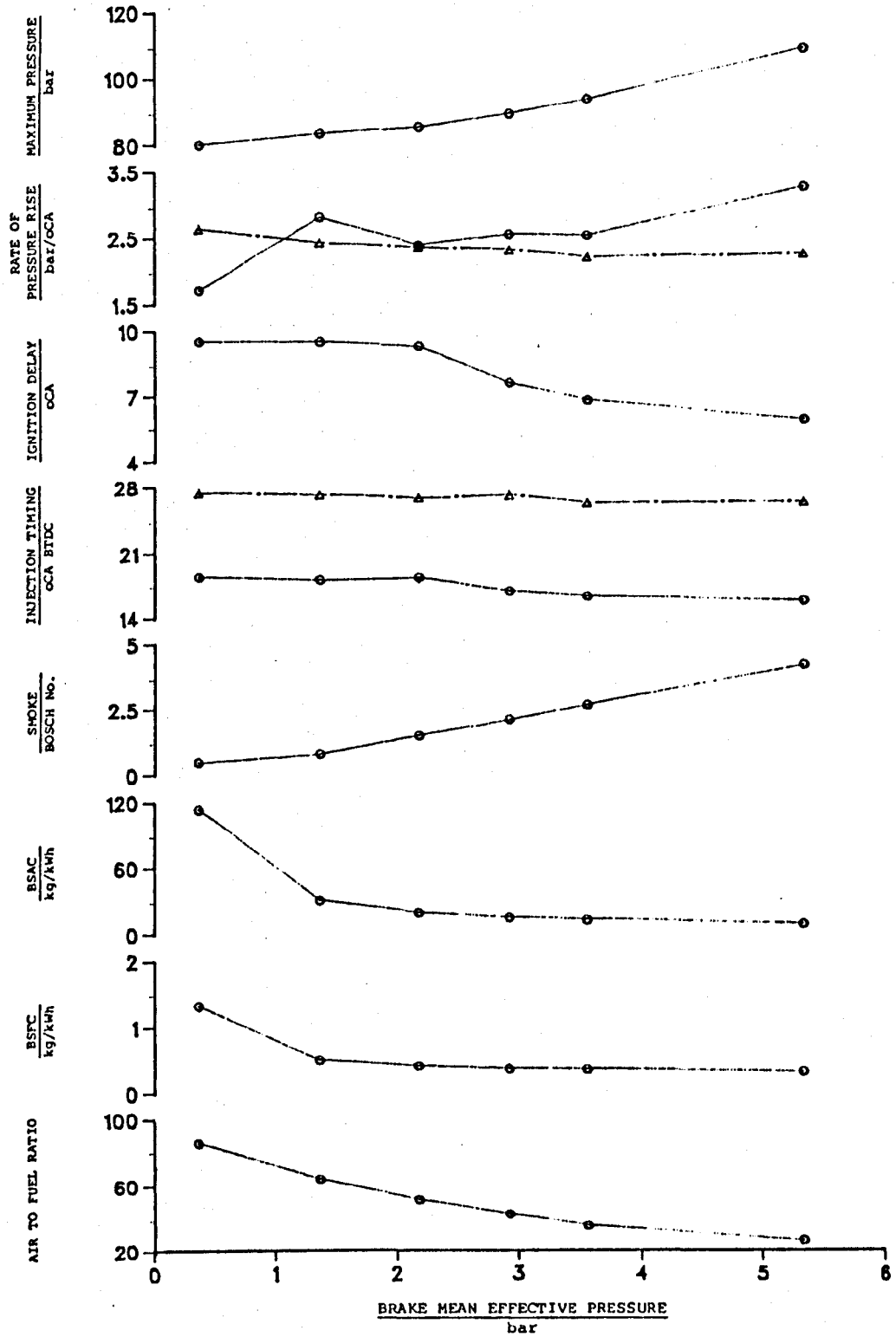

FIGURE A.9
Typical results at 2160 rev/min obtained from the baseline tests.

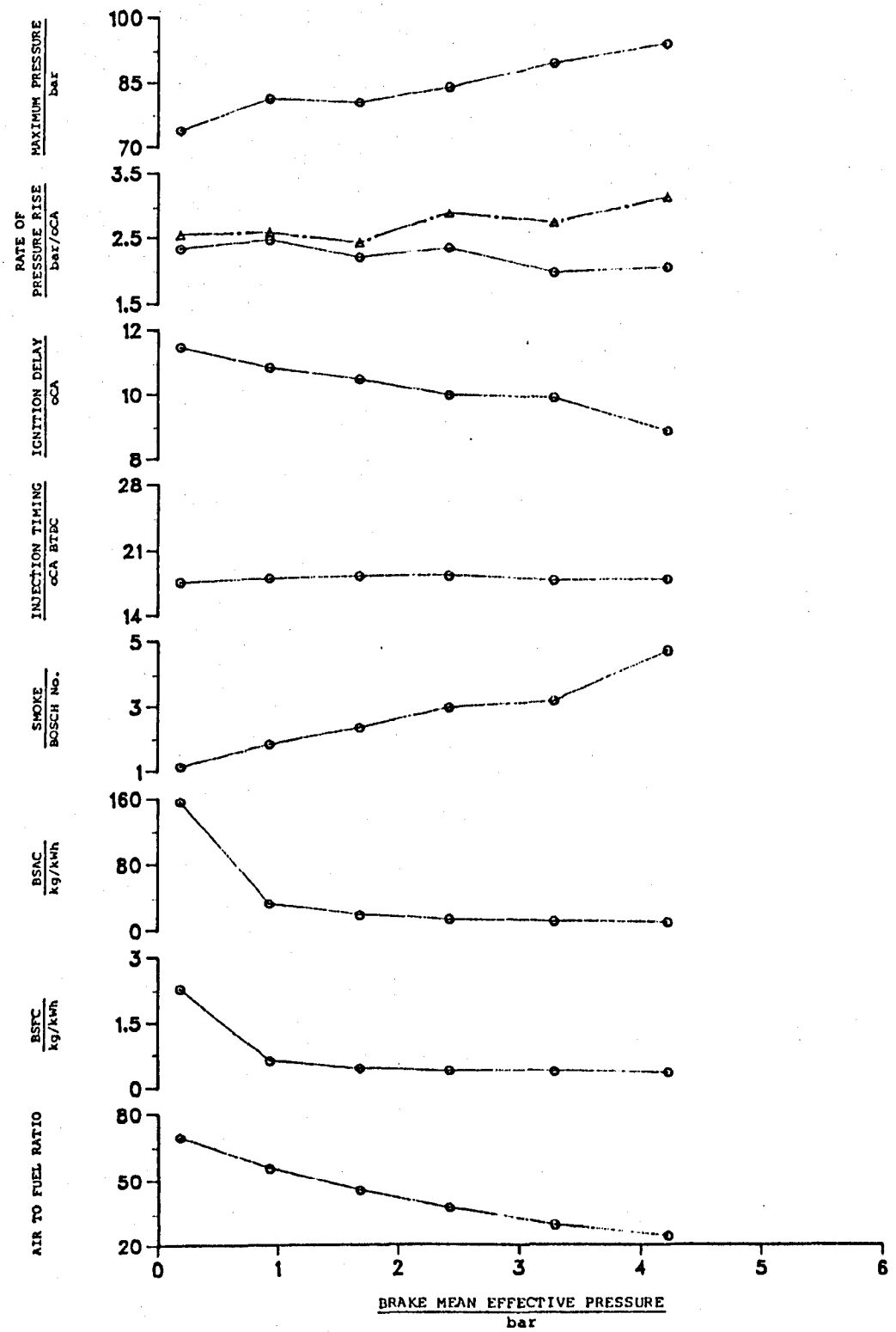

FIGURE A.10
Typical results at 2460 rev/min obtained from the baseline tests.

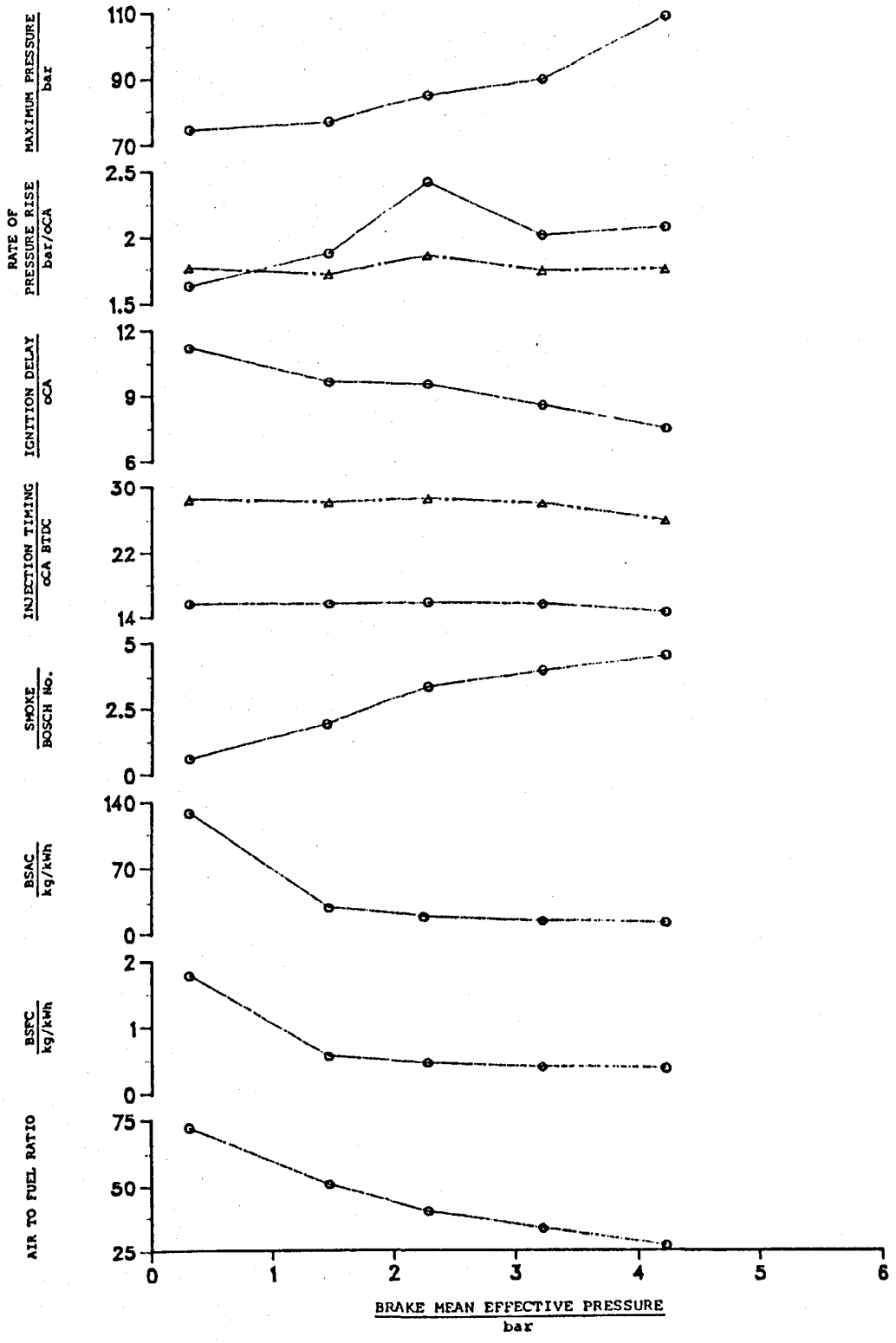

FIGURE A.11
Typical results at 3000 rev/min obtained from the baseline tests.

Appendix B

B.1 - Calculation of the inlet valve flow area

The inlet valve flow area A_o is given by:

$$A_o = \pi l \left[\frac{D_a + D_b}{2} \right] \quad \text{.... B.1}$$

where l is the valve lift, and D_a and D_b are the upper and lower diameters of the inlet valve seat, Fig B.1.

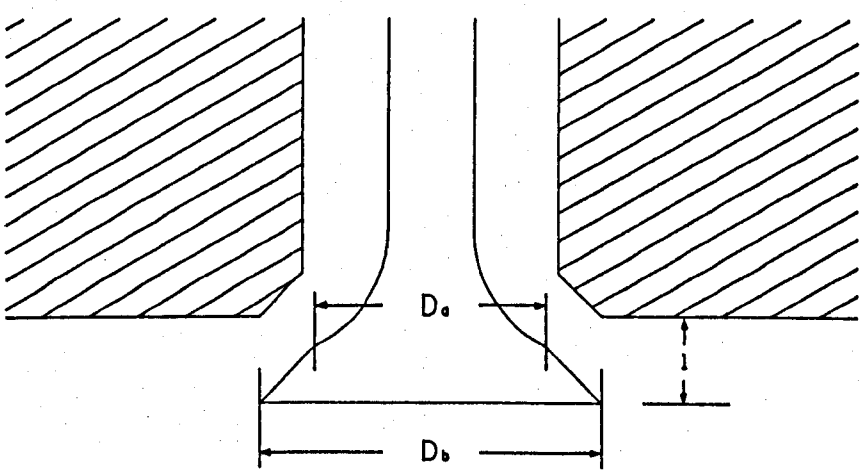

FIGURE B.1
Diagram showing the inlet valve and the way in which the valve flow area was calculated.

B.2 - Change in manifold pressure towards the end of the induction period

In the Lister engine the inlet valve closes at 230°CA ATDC. By examining the inlet manifold pressure recordings for this engine, it was found that the inlet manifold pressure remained at more or less a constant level until about 130°CA ATDC, where it began to rise reaching a peak at about 200°CA ATDC. From this examination of the manifold pressure traces, it was decided to represent this air inertia effect as shown on Fig B.2.

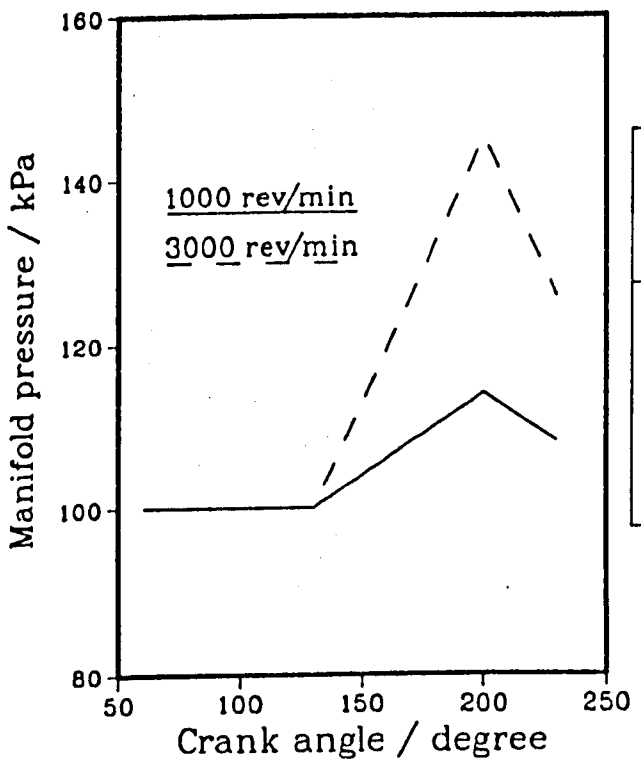

Engine speed rev/min	Rate of change of pressure with crank angle Pa/oCA
1000	200
1300	357
1700	471
2160	557
2500	610
3000	654

FIGURE B.2
Inlet manifold pressure variation with crank angle during induction for the Lister engine.

B.3 - Computational scheme for the solution of Equation 5.1 and 5.2

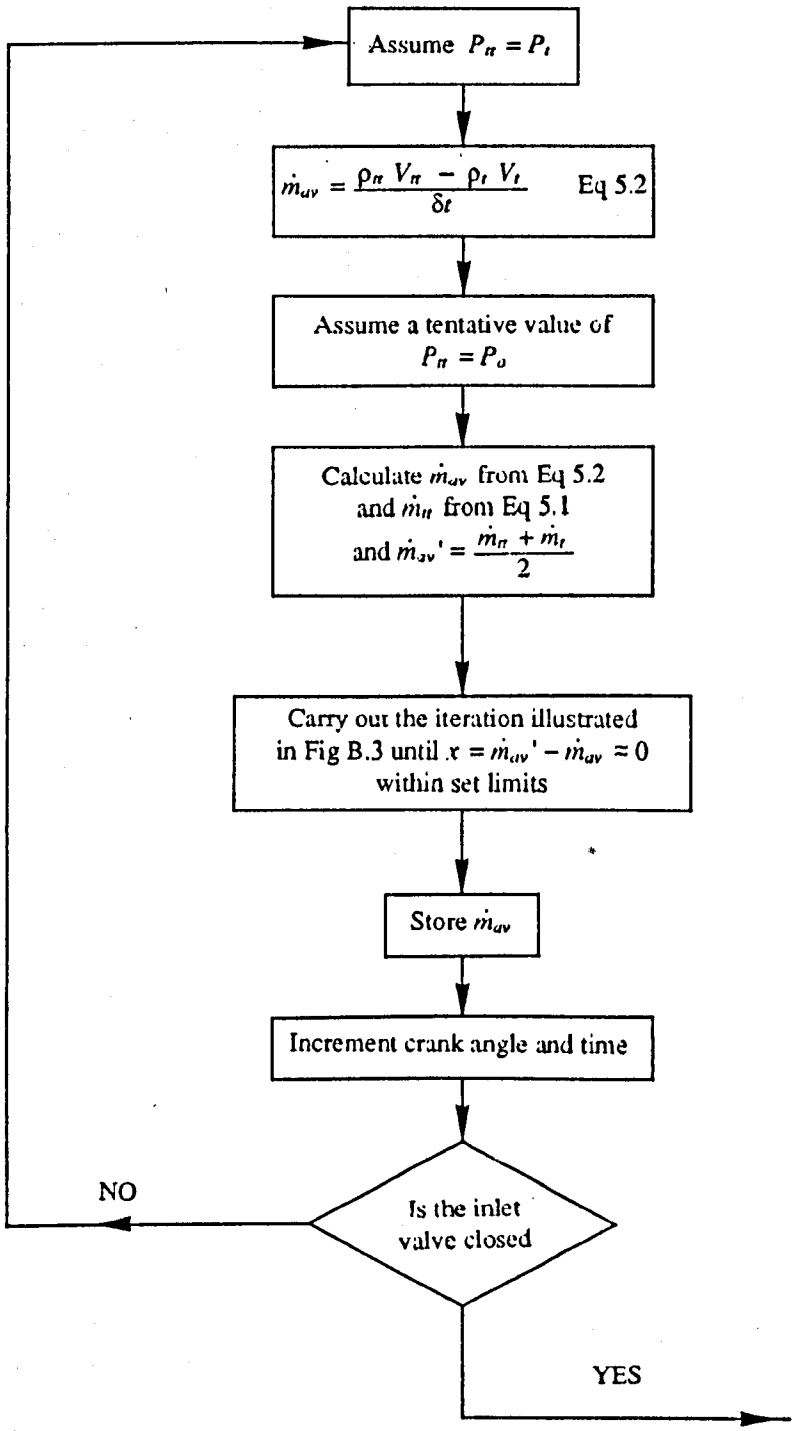

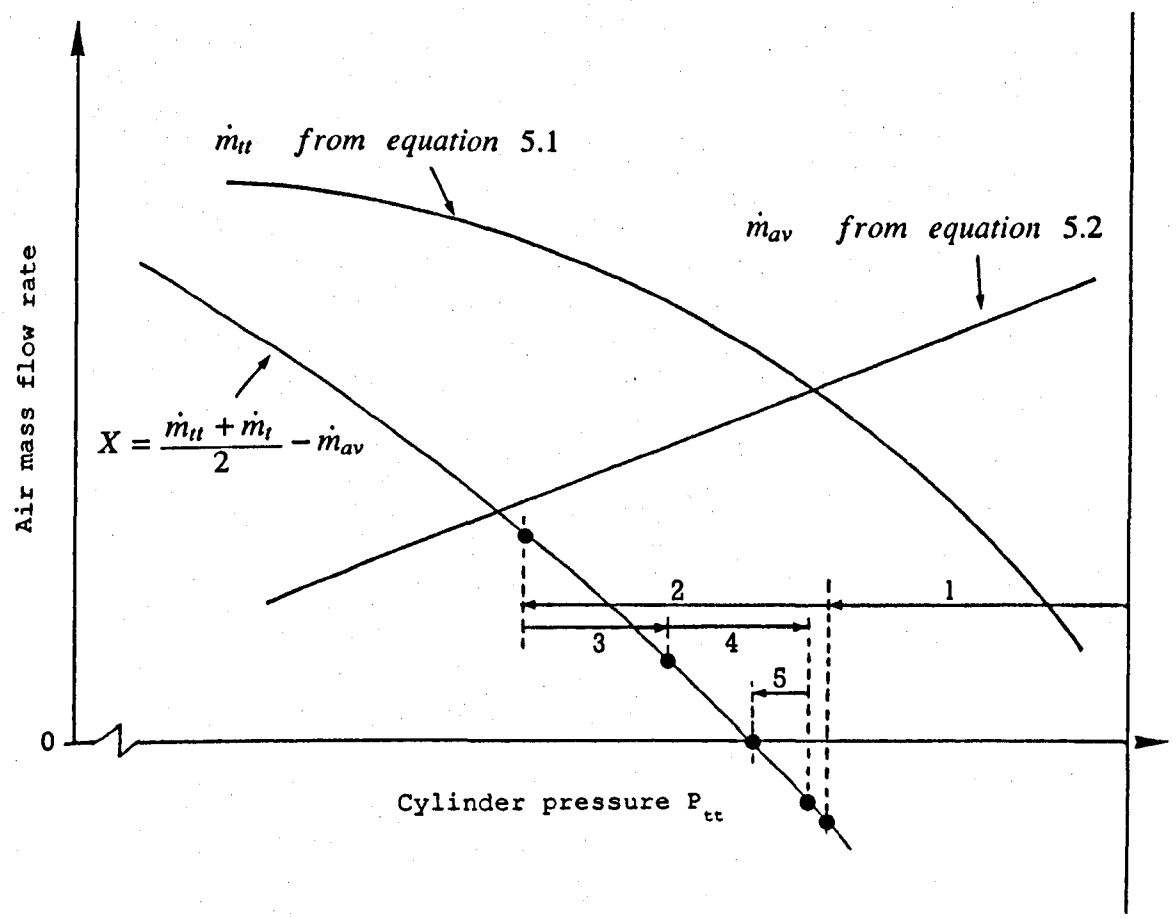

Inlet manifold pressure P_o. Also, initial tentative value of $P_{tt} = P_o$.

Solution starts with $P_{tt} = P_o$.
P_{tt} is reduced by constant δP in steps 1 and 2 until X is positive; then δP step was reduced to less than half its value and continuously added to P_{tt} in successive steps 3 and 4 until X is negative again, and so on until X = 0

FIGURE B.3
Graphical representation of the steps involved in solving equations 5.1 and 5.2 at a given crank angle.

B.4 - Derivation of equation for the moment of momentum rate

In order to obtain the moment of momentum rate for an elemental disc of air within the cylinder, consider the moment of momentum, M, of the ring shown below:

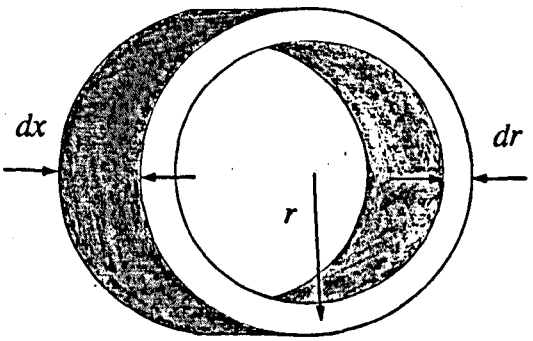

$$M = m\, r^2\, \omega \qquad \text{.... B.2}$$

where ω is the angular velocity at radius r, and m is the mass of the ring which can be expressed as:

$$m = 2\,\pi\, r\, dr\, dx\, \rho \qquad \text{.... B.3}$$

For a disc of thickness dx, density ρ and overall radius B/2, substituting Eq B.3 into Eq B.2, and integrating:

$$M = 2\,\pi\,\rho \int_0^{B/2} \omega\, dx\, r^3\, dr \qquad \text{.... B.4}$$

In the case of air swirling in the cylinder of an IC engine during induction when the air is being admitted at an average rate, $\dot{m}_{av}$, over an interval δt,

$$dx = V_a \, \delta t \qquad \text{.... B.5}$$

where V_a is the axial velocity at radius r. Hence, moment of momentum rate of the average mass admitted over interval δt can be expressed as,

$$\frac{M}{\delta t} = 2\pi\rho \int_0^{B/2} V_a \, \omega r^3 \, dr \qquad \text{.... B.6}$$

Bond (1988) measured, experimentally, the values of V_a and ω at a number of radii, using the steady flow rig. These results were used to calculate the moment of momentum rate, using the above integral (Eq B.6), at a number of valve lift and air mass flow rate combinations. These data were used to produce a table, for the Lister engine, which contained the mass flow rate and the moment of momentum rate for each valve opening.

The computer model that predicts the total moment of momentum during induction, does this by first predicting the mass flow rate during a time (or crank angle) interval δt. Also, the valve opening is known at that given time interval. A corresponding value of the average moment of momentum rate is then read from the above mentioned table (FILED in the computer program) for the given time interval δt. The moment of momentum over this time interval is calculated from the product of the average moment of momentum rate and the interval δt. During induction, these moments of momenta for individual time (or crank angle) intervals are summed up in order to arrive at the total moment of momentum of the trapped air at IVC.

B.5 - Derivation of equation for moment of inertia of the cylinder contents

The moment of inertia of a circular disk is given by:

$$I = \frac{m\,r^2}{2} \qquad \text{.... B.7}$$

where m is the mass and r is the radius of the disk.

Assuming that the axis of the piston bowl coincides with the axis of the cylinder, and that the total mass of the air trapped in the cylinder is represented by m, the moment of inertia of the cylinder contents can be expressed as:

$$I = \left[\frac{m_{ivc}}{2}\right]\left[\frac{v}{v + \pi (B/2)^2 s}\right](D/2)^2 + \left[\frac{m_{ivc}}{2}\right]\left[\frac{\pi (B/2)^2 s}{v + \pi (B/2)^2 s}\right](B/2)^2 \qquad \text{.... B.8}$$

fraction of the total mass in combustion bowl

fraction of the total mass above piston crown

where s is the distance between the piston crown and the cylinder head at a given crank angle, and v and D are the volume and the diameter of the combustion bowl respectively. Rearranging the above equation:

$$I = \frac{m_{ivc}}{2}\left[\frac{\frac{\pi (B/2)^4 s}{v} + (D/2)^2}{\frac{\pi (B/2)^2 s}{v} + 1}\right] \qquad \text{.... B.9}$$

B.6 - Breakdown of the frictional torque forces and evaluation of the skin friction coefficients

The frictional torque acting on the fluid due to the shear forces at the fluid-solid interface is given by:

$$T = \tau A\, r \qquad \text{.... B.10}$$

where τ is the shear force at the fluid-solid interface, A is the area at which the force is acting on and r is the radius.

The fluid-solid interface can be divided into two sections:

1 - Cylinder walls, for which:

$$A = \pi B\, s \qquad r = \frac{B}{2}$$

$$\tau = f_{cyl}\, \frac{\rho\, \omega_\ell^2\, B^2}{8}$$

where B is the cylinder bore, s is the distance between the cylinder head and the piston crown at a given crank angle (calculated from the standard equation, Taylor, 1968), ρ is the air density (calculated from the trapped mass and the volume at a given crank angle), ω_ℓ is the angular velocity of the cylinder contents, and f_{cyl} is the frictional coefficient for the cylinder walls. Substituting the above in Eq B.10, the frictional torque at the cylinder walls is,

$$T_{cyl} = f_{cyl}\, \frac{\rho\, \omega_\ell^2\, \pi\, B^4\, s}{16}$$

2 - Cylinder head and piston crown, together, for which:

$$A = 2\pi (B/2)^2 \qquad r = \frac{B}{4}$$

$$\tau = f_{pc} \frac{\rho \omega_c^2 B^2}{32}$$

where f_{pc} is the frictional coefficient for the cylinder head and the piston crown. Substituting the above in Eq B.10 gives the combined frictional torque for the cylinder head and piston crown:

$$T_{pc} = f_{pc} \frac{\rho \omega_c^2 \pi B^5}{256}$$

Therefore the total torque resisting the fluid rotation can be expressed as:

$$T = T_{cyl} + T_{pc} \qquad \text{.... B.11}$$

The skin friction coefficients f_{cyl} and f_{pc} were evaluated from the Blasius theory for turbulent boundary layers on a flat plate, Bird et al (1960):

$$f = 0.037 \lambda \, Re^{-1/5} \qquad \text{.... B.12}$$

where λ is an empirical constant of about 2, to allow for the deviation from the flat plate theory and Re is the Reynolds number expressed as:

$$\mathrm{Re} = \frac{L\,V\,\rho}{\mu}$$

where L is the characteristic length, which is taken as the circumference of the cylinder in the case of the cylinder wall, and half the cylinder circumference for the cylinder head and piston crown. V is the fluid velocity; owing to the assumption of solid body rotation , V varies linearly with radius. μ is the absolute viscosity of the cylinder air. A constant value of μ for air at 500K was used. The value of μ is not of critical importance to the accuracy with which the friction coefficients are estimated, since, as seen from Eq B.12, μ is raised to a power of 1/5. Hence:

$$\mathrm{Re}_{cyl} = \frac{\pi B^2 \omega_c \rho}{2\mu} \qquad \mathrm{Re}_{pc} = \frac{\pi B^2 \omega_c \rho}{8\mu}$$

Substituting these into Eq B.12:

$$f_{cyl} = 0.067 \left[\frac{B^2 \omega_c \rho}{\mu} \right]^{-1/5} \qquad f_{pc} = 0.089 \left[\frac{B^2 \omega_c \rho}{\mu} \right]^{-1/5}$$

and substituting the above expressions in Eq B.11:

$$T_i = \frac{d}{dt}[I\,\omega_c] = \left[\frac{-\pi \rho^{0.8} \mu^{0.2} B^{3.6}}{16} \left(0.067\,s + 0.0055\,B \right) \right] \omega_c^{1.8}$$

B.7 - Computational scheme for the solution of equation 5.10

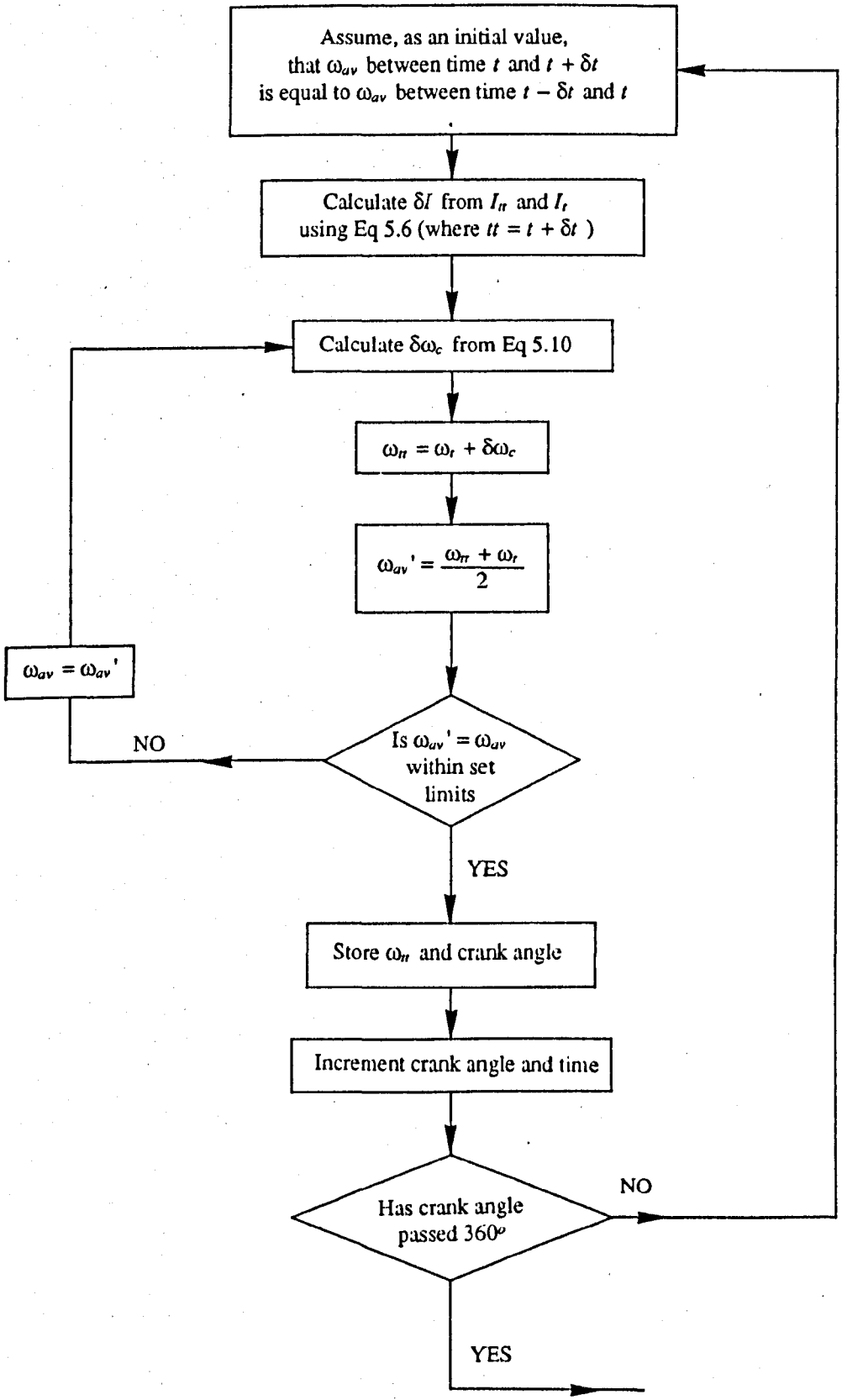

B.8 - Interpretation of Equation 5.15 for the spray tip penetration

$$\frac{X_t - X_{tw}}{X_t} = 0.35 \left[\frac{X_{tw}\, Q_a}{\mathrm{d}\, Q_j} \right]^{0.44} \qquad \ldots\ldots 5.15$$

The extend to which the spray tip would be deflected away from a purely radial path, in the tangential direction, will depend on the magnitude of the drag force applied on the spray tip by the swirling air. This drag force is given by:

$$F = \frac{\rho V^2 A\, C_d}{2}$$

$$F = \frac{\rho_a X_{tw}^2 \omega^2 A\, C_d}{2}$$

where V is the tangential velocity of the swirling air at the spray tip, ω is the angular velocity of the swirling air, A is the profile area of the spray tip and C_D is the drag coefficient (C_D depends on the Reynolds number and geometry of the spray tip). Hence,

$$F = \frac{Q_a A\, C_d}{2}$$

and

$$Q_a = \frac{2F}{C_d A}$$

In Eq 5.15, Q_a is normalised by the corresponding value at the nozzle orifice, Q_j, where

$$Q_j = \rho_f V_{inj}^2 = 2 (\Delta P \times 10^5)$$

where ρ_f is the fuel density and V_{inj} is the mean injection velocity at the nozzle orifice (calculated from measurements of fuel injected per cycle, the injection period, the nozzle geometry and an appropriate value of discharge coefficient, taken as 0.7). The value of Q_j is constant for a given engine running conditions. The value of $(A\ C_D)/2$ will depend on the spray geometry and flow conditions at the spray tip. In order to account for this effect of spray tip geometry on, AC_D (and Q_a), the nozzle hole diameter, d, is included in equation 5.15. The hole diameter has a great effect on the spray angle and, therefore, on the profile area, A, of the spray tip. The power of 0.44 and the constant 0.35 in the right hand side of the Eq 5.15 are empirical factors obtained, by Chiu et al (1976), from tests with a number of different injector nozzles.

B.9 - Computational scheme for the solution of Equation 5.18

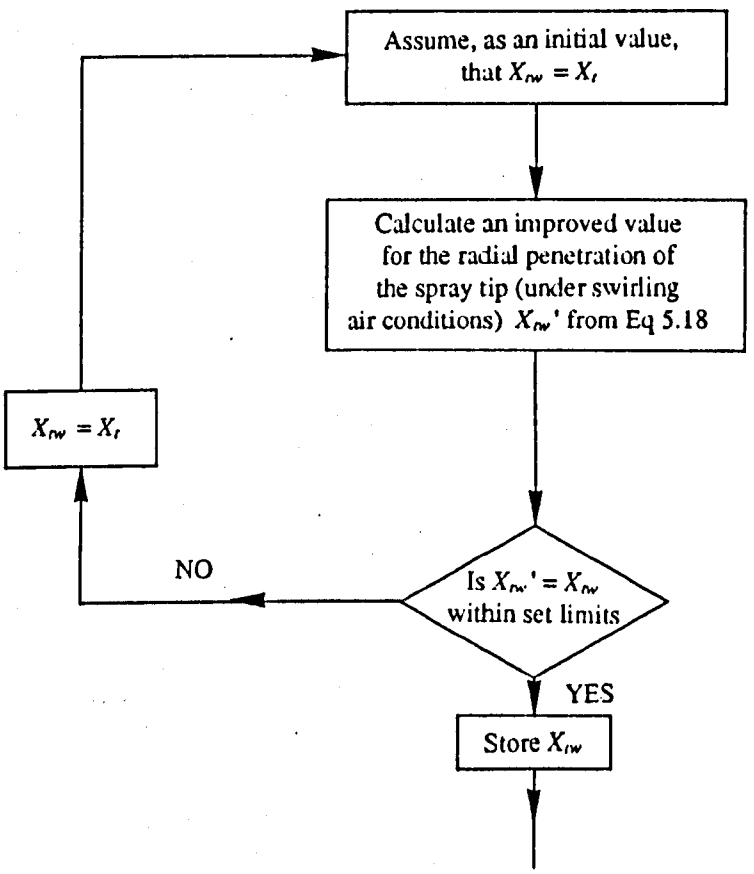

B.10 - Listing of the programs ITERAM, SUMMOM, COMPRESS, and CWVEL

```
1000 REM **  PROGRAM ITERAM  **  14/3/88 J.BOND  **  13/4/89 R.A.BALIAN **
1010 CLS : REM ====  SCREEN  ==========
1020 GOSUB 2880
1030 REM =====  INPUT DIS. COEF. DATA  ==========
1040 GOSUB 2040
1050 REM =====  INPUT VALVE LIFT DATA  ==========
1060 GOSUB 2190
1070 REM =====  INPUT ENGINE SPEC  ==========
1080 GOSUB 2340
1090 REM =====  INPUT AMBIENT COND.  ==========
1100 GOSUB 2390
1110 REM ====  INPUT ENGINE SPEED AND INCREMENT  ==========
1120 GOSUB 2450
1130 REM ====  INPUT RADIAL POS.  ==========
1140 GOSUB 2620
1150 REM ====  SET INITIAL COND.  ==========
1160 GOSUB 2770
1170 REM LPRINT "   TIT       VLT       MTT       MT        M         Q"
1180 REM LPRINT DISC$
1190 REM ====  CREATE FILE F  VALVE LIFT MASS FLOW  ==========
1200 OPEN "O",1,"FILEF"
1210 LOCATE 21,5 : PRINT "CREATING FILE F       "
1220 LOCATE 22,30: PRINT "ITERATION IN PROGRESS"
1230 TITO=INC*.01745
1240 FOR TIT = INC TO VCLOSE STEP INC
1250 TITRAD=TIT*.01745       :REM CRANC ANGLE IN RADIANS
1260 REM ====  CALC. VOLUME AT t+dt  ==========
1270 GOSUB 2510
1280 REM ====  ADJUST MANIFOLD PRESSURE  ==========
1290 IF TIT>200 THEN GOTO 1370
1300 IF TIT>130 AND RPM=1000 THEN P=P+(.002*INC*PMAN)
1310 IF TIT>130 AND RPM=1300 THEN P=P+(.00357*INC*PMAN)
1320 IF TIT>130 AND RPM=1700 THEN P=P+(.00471*INC*PMAN)
1330 IF TIT>130 AND RPM=2160 THEN P=P+(.00557*INC*PMAN)
1340 IF TIT>130 AND RPM=2600 THEN P=P+(.0061*INC*PMAN)
1350 IF TIT>130 AND RPM=3000 THEN P=P+(.00645*INC*PMAN)
1360 IF TIT>200 AND RPM=1000 THEN P=P-(.002*INC*PMAN)
1370 IF TIT>200 AND RPM=1300 THEN P=P-(.00357*INC*PMAN)
1380 IF TIT>200 AND RPM=1700 THEN P=P-(.00471*INC*PMAN)
1390 IF TIT>200 AND RPM=2160 THEN P=P-(.00557*INC*PMAN)
1400 IF TIT>200 AND RPM=2600 THEN P=P-(.0061*INC*PMAN)
1410 IF TIT>200 AND RPM=3000 THEN P=P-(.00645*INC*PMAN)
1420 REM ====  CALC. VALVE SKIRT AREA  ==========
1430 GOSUB 2550
1440 REM ====  CALCULATE CD  ==========
1450 GOSUB 2710
1460 ZZ = ZZ + 1                                  :REM zz is the subtraction counter to

1470 Y =250                                        :REM arbitary pressure step Y n/m^2
1480 PTT = P-(ZZ*Y)                                :REM get ptt too small to start with

1490 ROTT = PTT/(287*T)
1500 X = (((CDT*SKA*P*((1/(287*T))^.5)*(7*(((PTT/P)^1.4286) - ((PTT/P)^1.7143)))^
.5)+MT)/2) -(((ROTT*VTT)-(ROT*VT))*W/TITO)
```

```
1510 IF X > 0 THEN GOTO 1530                    :REM ptt too small.Z has been found
1520 GOTO 1460                                  :REM ptt too big.Try another z
1530 Z = ZZ
1540 PTT = P -(Z*Y)                             :REM small.Now start closing in.
1550 ROTT = PTT/(287*T)
1560 IF PTT>.99*P THEN GOTO 1700
1570 X = (((CDT*SKA*P*((1/(287*T))^.5)*(7*(((PTT/P)^1.4286)- ((PTT/P)^1.7143)))^
.5)+MT)/2) -(((ROTT*VTT)-(ROT*VT))*W/TITO)
1580 IF X > 0 THEN Y = (Y/2)                    :REM Keep adding or subtracting
1590 IF X > 0 THEN Z = (2*Z)-1                  :REM half the previous step length
1600 IF X < 0 THEN Y = (Y/2)                    :REM until we close in on ptt that
1610 IF X < 0 THEN Z = (2*Z)+1                  :REM makes x = 0
1620 LOCATE 18,55 : PRINT X : LOCATE 19,55 : PRINT Z
1630 IF Z>1E+30 THEN GOTO 1870
1640 IF INT(X*(10^4)) = 0 THEN GOTO 1700    :REM Is x aproximately zero?
1650 REM Equation in line 620 becomes meaningless when the cylinder presure
1660 REM aproaches the manifold pressure towards the end of the comp. stroke.
1670 REM The programme is complete when this occurs. ie there is no reverse
1680 REM gas flow through the valve.
1690 GOTO 1540
1700 IF TIT=INC THEN ROT=ROTT
1710 M = ((ROTT*VTT)-(ROT*VT))*W/TITO          :REM Average mass flow
1720 MTT = MT + ((M-MT)*2)                      :REM mass flow at t + delta t
1730 Q = Q+(M*TITO/W)                          :REM CALC. TOTAL MASS TRAPPED
1740 REM IF TIT>200 THEN LPRINT USING "£££.££££";TIT,VLT,MTT,MT,M,Q*1000
1750 LOCATE 8,55  : PRINT TIT: LOCATE 9,55  : PRINT VTT*1000000!
1760 LOCATE 11,55 : PRINT PT : LOCATE 13,55 : PRINT CDT
1770 LOCATE 14,55 : PRINT M*1000  : LOCATE 15,55 : PRINT Q*1000
1780 LOCATE 12,55 : PRINT VLT*1000: LOCATE 10,55 : PRINT P
1790 PT = PTT : VT = VTT : ROT = ROTT : MT = MTT :ZZ = 0
1800 WRITE £1,VLT,M,Q
1810 REM ====  CALC. VOLUMETRIC EFF.  ========================================
1820 MO=STR*AREA*(PMAN/(287*T))
1830 VOLEFF=(Q/MO)*100
1840 LOCATE 16,55 : PRINT VOLEFF
1850 NEXT TIT
1860 WRITE £1,9999
1870 CLOSE
1880 LOCATE 21,5 : PRINT "FILE F CLOSED                    "
1890 REM ====  CREATE FILE TRANSFER  ========================================
1900 OPEN "O",1,"TRANSFER"
1910 WRITE £1,DISC$
1920 WRITE £1,RSQ(1),RSQ(2),RSQ(3),RSQ(4),RSQ(5)
1930 WRITE £1,RSQ(6),RSQ(7),RSQ(8),RSQ(9),RSQ(10)
1940 WRITE £1,VCLOSE,Q,PTT,ROTT,RPM,INC,TIT,VOLEFF,PAMB,PBOOST
1950 CLOSE
1960 LOCATE 21,40 : PRINT "FILE TRANSFER CREATED"
1970 LOCATE 22,5 : PRINT "                                                    "
1980 REM LOCATE 22,5 : INPUT "PRESS ANY KEY TO CHAIN SUMMOM PROGRAMME",DUMM
1990 CHAIN "SUMMOM.BAS",ALL
2000 REM ************************************************************************
```

```
2010 REM ********************  SUBROUTINES  ********************************
2020 REM ***************************************************************
2030 REM ====  DISCHARGE COEF.  ==========================================
2040 OPEN "I",1,"FILEA"
2050 LOCATE 21,5 : PRINT "READING FILE A        "
2060 NA = 0
2070 WHILE DUMA <> 9999
2080 INPUT £1,DUMA : NA = NA + 1
2090 WEND
2100 CLOSE
2110 DIM CD(NA/2),VR(NA/2)
2120 OPEN "I",2,"FILEA"
2130 FOR J = 1 TO NA/2
2140 INPUT £2,VR(J),CD(J)
2150 NEXT J
2160 CLOSE
2170 RETURN
2180 REM ====  VALVE LIFT  ===============================================
2190 NB = 0
2200 OPEN "I",1,"fileB"
2210 LOCATE 21,5 : PRINT "READING FILE B        "
2220 WHILE DUMB <> 9999
2230 INPUT £1,DUMB : NB = NB + 1
2240 WEND
2250 CLOSE
2260 DIM VL(NB/2),CA(NB/2)
2270 OPEN "I",2,"fileB"
2280 FOR J = 1 TO NB/2
2290 INPUT £2,CA(J),VL(J)
2300 NEXT J
2310 CLOSE
2320 RETURN
2330 REM ====  ENG. SPEC.  ==============================================
2340 OPEN "I",1,"FILEC"
2350 LOCATE 21,5 : PRINT "READING FILE C        "
2360 INPUT £1,CRL,STR,AREA,VD,CIR,VC,B,D,H
2370 CLOSE
2380 RETURN
2390 REM ====  AMBIENT CONDITIONS  ======================================
2400 LOCATE 5,67 : INPUT " ",PAMB : PAMB=(PAMB/750)*10^5
2410 LOCATE 6,67 : INPUT " ",PBOOST : P=(PBOOST*10^5)+PAMB
2420 LOCATE 7,67 : INPUT " ",T : T=T+273
2430 RO=P/(287*T)
2440 RETURN
2450 REM ====  ENGINE SPEED AND INCREMENT  ==============================
2460 LOCATE 5,28 : INPUT " ",RPM
2470 IF RPM <= 0 THEN GOTO 2460
2480 LOCATE 6,28 : INPUT " ",INC
2490 W = RPM*.10472
2500 RETURN
```

```
2510 REM ====  CYL. VOLUME  ================================================
2520 R = STR/2 : NN = CRL/R : CR = (VC+(STR*AREA))/VC
2530 VTT = AREA*R*(1+NN-(NN^2-(SIN(TITRAD))^2)^.5-COS(TITRAD)+(2/(CR-1)))
2540 RETURN
2550 REM ====  VALVE SKIRT AREA  ==========================================
2560 FOR I = 1 TO NB+100
2570 IF TIT>CA(I) AND TIT<=CA(I+1) THEN GOTO 2590
2580 NEXT I
2590 VLT = VL(I+1)-((VL(I+1)-VL(I))*((CA(I+1)-TIT)/10))
2600 VLT = VLT/1000 : SKA = VLT*CIR
2610 RETURN
2620 REM ====  RADII  =====================================================
2630 RSQ(1)=4 : RSQ(2)=8 : RSQ(3)=12 : RSQ(4)=16 : RSQ(5)=21.5
2640 RSQ(6)=24 : RSQ(7)=28 : RSQ(8)=32.05 : RSQ(9)=36 : RSQ(10)=40
2650 REM Convert the radiuses to metres
2660 RSQ(1)=RSQ(1)/1000 : RSQ(2)=RSQ(2)/1000 : RSQ(3)=RSQ(3)/1000
2670 RSQ(4)=RSQ(4)/1000 : RSQ(5)=RSQ(5)/1000 : RSQ(6)=RSQ(6)/1000
2680 RSQ(7)=RSQ(7)/1000 : RSQ(8)=RSQ(8)/1000 : RSQ(9)=RSQ(9)/1000
2690 RSQ(10)=RSQ(10)/1000
2700 RETURN
2710 REM ====  CD CALC.  ==================================================
2720 FOR I = 1 TO NA+100
2730 IF (VLT/VD)>=VR(I) AND (VLT/VD)<VR(I+1) THEN GOTO 2750
2740 NEXT I
2750 CDT=CD(I)+((CD(I+1)-CD(I))*(((VLT/VD)-VR(I))/(VR(I+1)-VR(I))))
2760 RETURN
2770 REM ====  INITIAL COND.  =============================================
2780 MT = 0                  : REM INITIAL FLOW RATE AT TDC IS ZERO
2790 ZZ=0                    : REM SET PRESSURE COUNTER
2800 PT = P : ROT = RO       : REM INITIAL CONDITIONS ARE MANIFOLD COND.
2810 Q = 0                   : REM NO MASS TRAPPED IN CYLINDER AT TDC
2820 VT = VC                 : REM INITIAL CYLINDER VOLUME AT TDC
2830 PMAN=P
2840 VCLOSE=230              : REM INLET VALVE CLOSURE
2850 RETURN
2860 REM ====  SCREEN  ====================================================
2870 LOCATE 1,1
2880 PRINT "*********************************************************************
*******"
2890 LOCATE 3,1
2900 PRINT "*********************************************************************
*******"
2910 LOCATE 2,5
2920 PRINT"I          T          E          R          A          T          E"
2930 LOCATE 5,1 : PRINT "ENGINE SPEED   / revs/min  "
2940 LOCATE 5,38: PRINT "ATMOSPHERIC PRESSURE   /mmHg"
2950 LOCATE 6,1 : PRINT "C.A. INCREMENT / oCA       "
2960 LOCATE 6,38: PRINT "BOOST PRESSURE         / bar"
2970 LOCATE 7,38: PRINT "MANIFOLD AIR TEMP.     /oC"
2980 LOCATE 8,1 : PRINT "CRANK ANGLE            / o"
2990 LOCATE 9,1 : PRINT "CYLINDER VOLUME        / cm3"
3000 LOCATE 10,1: PRINT "MANIFOLD PRESSURE     / N/m2"
```

```
3000 LOCATE 10,1: PRINT "MANIFOLD PRESSURE     / N/m2"
3010 LOCATE 11,1: PRINT "CYLINDER PRESSURE      / N/m2"
3020 LOCATE 12,1: PRINT "VALVE LIFT             / mm"
3030 LOCATE 13,1: PRINT "DISCHARGE COEFFICIENT"
3040 LOCATE 14,1: PRINT "AVERAGE MASS FLOW RATE / g/s"
3050 LOCATE 15,1: PRINT "TOTAL MASS TRAPPED     / g"
3060 LOCATE 16,1: PRINT "VOLUMETRIC EFFICIENCY  / %"
3070 LOCATE 18,1: PRINT "MASS FLOW RATE ERROR   / kg"
3080 LOCATE 19,1: PRINT "PRESSURE CORR. FACTOR"
3090 LOCATE 22,5: PRINT "PLEASE WAIT                "
3100 LOCATE 20,1 : PRINT "==========================================================
====================="
3110 LOCATE 23,1 : PRINT "==========================================================
====================="
3120 LOCATE 21,1 : PRINT "|" : LOCATE 21,75 : PRINT "|"
3130 LOCATE 22,1 : PRINT "|" : LOCATE 22,75 : PRINT "|"
3140 LOCATE 22,5 : INPUT "DATA IDENTIFICATION NAME   ",DISC$
3150 LOCATE 22,5 : PRINT "                                                    "
3160 RETURN
```

```
1000 REM **  COMPRESS  **  5/3/88 J. BOND  **  16/4/89 R.A.BALIAN **
1010 REM LPRINT
1020 REM LPRINT "CRANK ANGLE     SWIRL    SWIRL RATIO   SQUISH AT BOWL RAD."
1030 REM ====  SCREEN  ==========================================================
1040 GOSUB 2130
1050 REM ====  CONSTANTS  =======================================================
1060 GOSUB 1980
1070 REM ====  INPUT TRANSFER FILE  ============================================
1080 GOSUB 1740
1090 REM ====  INPUT FILEC  ====================================================
1100 GOSUB 1910
1110 REM ====  CYL. VOL., CLEARANCE HIGHT, PISTON SPEED  AT IVO  ===============
1120 TIT = VCLOSE : TITA = TIT * .01745 : GOSUB 2000
1130 REM ====  MOMENT OF INERTIA AT IVO ========================================
1140 GOSUB 2080
1150 REM ====  SWIRL AT IVO  ===================================================
1160 WTT = TOTMOM/ITT
1170 LOCATE 7,30 : PRINT TIT : LOCATE 9,23 : PRINT USING "£££££.££";WTT*9.5493
1180 LOCATE 10,22: PRINT USING "£££.£££";WTT/W
1190 LOCATE 5,69 : PRINT USING "££.£££";CR
1200 REM === OPEN FILE CWCOMP FOR DATA TO BE TRANSFERED TO CR. WIND  ============
1210 OPEN "O",£1,"CWCOMP"
1220 LOCATE 21,5 : PRINT "CREATING FILE CWCOMP       "
1230 REM ***************************************************************************
1240 REM ************ INITIAL CONDITIONS SET - START COMPRESSION ***************
1250 REM ***************************************************************************
1260 REM ====  REPEAT PROCEDURE UNTIL TDC IS REACHED  ==========================
1270 TIT = TIT + INC : TITA = TIT * .01745
1280 IF TIT > 360 THEN GOTO 1650
1290 REM ====  SET CONDITIONS AT TIMT T  ========================================
1300 WT=WTT : IT=ITT : CLHO=CLH
1310 REM ====  SET CONDITIONS AT TIME TT  =======================================
1320 REM ====  CYL. VOL., CLEARANCE HIGHT AT TIME TT  ===========================
1330 GOSUB 2000
1340 REM ====  MOMENT OF INERTIA AT TIME TT  ====================================
1350 GOSUB 2080
1360 IM = (ITT+IT)/2
1370 REM ====  RATE OF CHANGE OF MOMENT OF INERTIA AT TIME TT  ==================
1380 IDOT = (ITT-IT)/(TITO/W)
1390 REM ====  DENSITY AT TIME TT  =============================================
1400 ROTT = Q/VCYL
1410 REM ====  SWIRL AT TIME TT  ===============================================
1420 WM=10
1430 KCON = (PI/16)*(ROTT^.8)*(MUTT^.2)*(B^3.6)*((.067*CLH)+(.0055*B))
1440 DELW = ((TITO/W)/IM)*((KCON*(WM^1.8))-(WM*IDOT))
1450 WTT = WT + DELW : WW = (WTT+WT)/2
1460 IF WM=WW THEN GOTO 1480 ELSE WM=WW
1470 GOTO 1440
1480 REM ====  SQUISH AT EACH GIVEN RADIUS RSQ  ================================
1490 FOR Z = 1 TO 10
1500 VSQ(Z) =(((B^2)/4)-((RSQ(Z))^2))*VOL*SDOT / ((2*RSQ(Z))*(((AREA*CLH)+VOL)*C
LH))
```

```
1510 VSW(Z) = RSQ(Z)*WTT
1520 NEXT Z
1530 REM ====  PRINT RESULTS  ============================================
1540 SWIRL=WTT*9.549296  : REM ====  CONVERT TO revs/min  ================
1550 LOCATE 7,30 : PRINT TIT : LOCATE 9,23 : PRINT USING "£££££.££";SWIRL
1560 LOCATE 10,22 : PRINT USING "£££.£££";SWIRL/RPM
1570 LOCATE 11,23 : PRINT ITT
1580 LOCATE 12,24 : PRINT USING "££.£££";CLH*1000
1590 LOCATE 13,22 : PRINT USING "£££.£££";SDOT
1600 FOR G=1 TO 10 : LOCATE 9+G,55 : PRINT USING"££££.££";VSQ(G)
1610 LOCATE 9+G,67 : PRINT USING"£££.££";VSW(G) : NEXT G
1620 REM LPRINT TIT,SWIRL,SWIRL/RPM,VSQ(5)
1630 IF TIT>=320 THEN WRITE £1,TIT,WTT,VSQ(5)
1640 GOTO 1260
1650 LOCATE 21,5 : PRINT "FILE CWCOMP CLOSED       "
1660 WRITE £1,9999
1670 CLOSE
1680 END
1690 LOCATE 22,5 : INPUT "PRESS ANY KEY TO CHAIN CWVEL PROGRAM",DUMM
1700 CHAIN "CWVEL.BAS",ALL
1710 REM ************************************************************
1720 REM **************  SUBROUTINES  ***********************************
1730 REM ************************************************************
1740 REM ====  TRANSFER FILE  ===========================================
1750 OPEN "I",1,"TRANSFER".
1760 LOCATE 21,5 : PRINT "READING FILE TRANSFER"
1770 DIM RSQ(10),VSQ(10),VSW(10)
1780 INPUT £1,DISC$
1790 INPUT £1,RSQ(1),RSQ(2),RSQ(3),RSQ(4),RSQ(5)
1800 INPUT £1,RSQ(6),RSQ(7),RSQ(8),RSQ(9),RSQ(10)
1810 INPUT £1,VCLOSE,Q,PTT,ROTT,RPM,INC,TI,VOLEFF,PAMB,PBOOST,TOTMOM
1820 CLOSE
1830 FOR I=1 TO 10 : LOCATE 9+I,43 : PRINT USING"££.£";RSQ(I)*1000 : NEXT I
1840 TITO = INC * .01745 : W = RPM * .10472 : LOCATE 5,30 : PRINT RPM
1850 LOCATE 6,30 : PRINT INC : LOCATE 6,69 : PRINT USING "£.£££";Q*1000
1860 REM LOCATE 22,5 : INPUT "WOULD YOU LIKE TO CHANGE THE INCREMENT:  ",ANS$
1870 REM IF ANS$="Y" OR ANS$="y" THEN LOCATE 6,30 : INPUT" ",INC
1880 LOCATE 22,5 : PRINT "PLEASE WAIT                                  "
1890 TITO=INC*.01745
1900 RETURN
1910 REM ====  ENGINE SPEC  ==============================================
1920 OPEN "I",1,"fileC"
1930 LOCATE 21,5 : PRINT "READING FILE C          "
1940 INPUT £1,CRL,STR,AREA,VD,CIR,VC,B,D,H,VOL,VOLX
1950 CLOSE
1960 RETURN
1970 REM ====  INITIAL CONDITIONS  ======================================
1980 GAMA=1.4 : MUTT=2*10^-5 : PI=3.1415926£ : CLHO=1
1990 RETURN
2000 REM ====  CYLINDER VOLUME AT CRANK ANGLE TITA  ======================
```

```
2010 R=STR/2 : NN=CRL/R : CR=(VC+(STR*AREA))/VC
2020 VCYL=AREA*R*(1+NN-(NN^2-(SIN(TITA))^2)^.5-COS(TITA)+(2/(CR-1)))
2030 REM ====  CYLINDER CLEARANCE HIGHT AT CRANK ANGLE TITA  ===============
2040 CLH=(VCYL-VOLX)/AREA
2050 REM ====  PISTONE SPEED AT CRANK ANGLE TITA  ============================
2060 SDOT = (CLHO-CLH)/(TITO/W)
2070 RETURN
2080 REM ====  MOMENT OF INERTIA  ITT  ======================================
2090 ITTA = ((PI/16)*(B^4)*CLH/VC) + ((D^2)/4)
2100 ITTB = (((PI/4)*(B^2)*CLH/VC) + 1)
2110 ITT = (Q/2)*ITTA/ITTB
2120 RETURN
2130 CLS : REM ====  screen  ======================================================
2140 LOCATE 1,1 : PRINT "*************************************************************
************************"
2150 LOCATE 3,1 : PRINT "*************************************************************
************************"
2160 LOCATE 2,4 : PRINT "C          O          M          P          R          E
     S          S"
2170 LOCATE 20,1 : PRINT "=============================================================
========================"
2180 LOCATE 23,1 : PRINT "=============================================================
========================"
2190 LOCATE 21,1 : PRINT "|" : LOCATE 21,78 : PRINT "|"
2200 LOCATE 22,1 : PRINT "|" : LOCATE 22,78 : PRINT "|"
2210 LOCATE 22,5 : PRINT "PLEASE WAIT"
2220 LOCATE 5,1 : PRINT "ENGINE SPEED     / revs/min"
2230 LOCATE 6,1 : PRINT "C.A. INCREMENT   / oCA"
2240 LOCATE 5,43: PRINT "COMPRESSION RATIO"
2250 LOCATE 6,43: PRINT "TOTAL MASS TRAPPED  / g"
2260 LOCATE 7,1 : PRINT "CRANK ANGLE      / oCA"
2270 LOCATE 9,1 : PRINT "SWIRL / revs/min"
2280 LOCATE 10,1: PRINT "SWIRL RATIO"
2290 LOCATE 11,1: PRINT "MOM. OF INERTIA"
2300 LOCATE 12,1: PRINT "CLEARANCE HIGHT / mm"
2310 LOCATE 13,1: PRINT "PISTON SPEED / m/s"
2320 LOCATE 9,38: PRINT "| RADIUS / mm | SQUISH m/s | Vt / m/s |"
2330 FOR I=1 TO 10 : LOCATE 9+I,38
2340 PRINT "|              |              |           |" : NEXT I
2350 RETURN
```

```
1000 REM **  PROGRAM SUMMOM  **  4/3/88 J.BOND  **  13/4/89 R.A.BALIAN **
1010 REM LPRINT
1020 REM LPRINT "    TIT        VLT      MTT       Q        MOM      TOTMOM"
1030 REM ====  INITIAL COND. ================================================
1040 GOSUB 2520
1050 REM ====  INITIAL CONDITIONS  ==========================================
1060 GOSUB 2200
1070 REM ====  READ FILED INTO ARRAY ARD(N)  ================================
1080 GOSUB 2240
1090 REM ==== READ TRANSFER FILE  ============================================
1100 GOSUB 2400
1110 REM ====  OPEN FILEF FOR VALVE LIFT AND MASS FLOW RATE DATA  ============
1120 OPEN "I",1,"FILEF"
1130 LOCATE 21,5 : PRINT "FILE F OPENED"
1140 LOCATE 22,30 : PRINT "CALCULATION IN PROGRESS"
1150 TITO=INC*.01745
1160 REM ==== SELECT NEXT VALVE LIFT AND MASS FLOW RATE  ======================
1170 INPUT £1,VL
1180 IF VL = 9999 THEN GOTO 2050    : REM END OF FILEF  ======================
1190 TIT = TIT + INC
1200 INPUT £1,M,Q
1210 IF M<0 THEN GOTO 2000     : REM NEGATIVE MASS FLOW  ====================
1220 LOCATE 16,30 : PRINT USING "£££££.££";VL*1000,M*1000
1230 REM ====  SET EXTREAME VALUES AT POINTS  AA  BB  CC  DD  ================
1240 AAVL = 1000 : AAM = 1000 : AAMOM = 0
1250 BBVL = 1000 : BBM = 0    : BBMOM = 0
1260 CCVL = 0    : CCM = 0    : CCMOM = 0
1270 DDVL = 0    : DDM = 1000 : DDMOM = 0
1280 REM ====  SEARCH FOR POINTS  AA  BB  CC  DD  ============================
1290 FOR N = 1 TO NN-4 STEP 3 : REM reset marker
1300 REM
1310 REM       DDVL<VL  DDM>M                                    AAVL>VL  DDM>M
1320 REM                                  VL    M
1330 REM       CCVL<VL  CCM<M                                    BBVL>VL  BBM<M
1340 REM
1350 REM ====  TO FIND AA  ==================================================
1360 WHILE ARD(N)>=VL AND ARD(N+1)>=M AND ARD(N)<AAVL
1370 AAVL = ARD(N) : AAM = ARD(N+1) : AAMOM = ARD(N+2)
1380 WEND
1390 WHILE ARD(N)>=VL AND ARD(N+1)>=M AND ARD(N)=AAVL AND ARD(N+1)<AAM
1400 AAVL = ARD(N) : AAM = ARD(N+1) : AAMOM = ARD(N+2)
1410 WEND
1420 REM ====  TO FIND DD  ==================================================
1430 WHILE ARD(N)<=VL AND ARD(N+1)>=M AND ARD(N)>DDVL
1440 DDVL = ARD(N) : DDM = ARD(N+1) : DDMOM = ARD(N+2)
1450 WEND
1460 WHILE ARD(N)<=VL AND ARD(N+1)>=M AND ARD(N)=DDVL AND ARD(N+1)<DDM
1470 DDVL = ARD(N) : DDM = ARD(N+1) : DDMOM = ARD(N+2)
1480 WEND
1490 IF DDM=1000 THEN DDM=AAM
1500 REM ====  TO FIND BB  ==================================================
```

```
1510 WHILE ARD(N)>=VL AND ARD(N+1)<=M AND ARD(N)<BBVL
1520 BBVL = ARD(N) : BBM = ARD(N+1) : BBMOM = ARD(N+2)
1530 WEND
1540 WHILE ARD(N)>=VL AND ARD(N+1)<=M AND ARD(N)=BBVL AND ARD(N+1)>BBM
1550 BBVL = ARD(N) : BBM = ARD(N+1) : BBMOM = ARD(N+2)
1560 WEND
1570 REM ====  TO FIND CC  ==========================================
1580 WHILE ARD(N)<=VL AND ARD(N+1)<=M AND ARD(N)>CCVL
1590 CCVL = ARD(N) : CCM = ARD(N+1) : CCMOM = ARD(N+2)
1600 WEND
1610 WHILE ARD(N)<=VL AND ARD(N+1)<=M AND ARD(N)=CCVL AND ARD(N+1)>CCM
1620 CCVL = ARD(N) : CCM = ARD(N+1) : CCMOM = ARD(N+2)
1630 WEND
1640 REM ====  DISPLAY  ============================================
1650 IF AVLO=1000 OR AMO=1000 OR DMO=1000 GOTO 1660 ELSE GOTO 1670
1660 LOCATE 13,10 : PRINT "
     "
1670 IF BVLO=1000 GOTO 1680 ELSE GOTO 1690
1680 LOCATE 19,10 : PRINT "
     "
1690 LOCATE 13,9 : PRINT USING "£££££.££";DDVL*1000,DDM*1000
1700 LOCATE 13,49: PRINT USING "£££££.££";AAVL*1000,AAM*1000
1710 LOCATE 19,9 : PRINT USING "£££££.££";CCVL*1000,CCM*1000
1720 LOCATE 19,49: PRINT USING "£££££.££";BBVL*1000,BBM*1000
1730 AVLO=AAVL : AMO=AAM : DMO=DDM : BVLO=BBVL
1740 NEXT N
1750 REM ====  TEST DATA IF EXTENDED FAR ENOUGH  ====================
1760 IF AAVL = 1000 OR BBVL=1000 THEN LOCATE 21,5 ELSE GOTO 1800
1770 PRINT "DATA IN FILE D DOES NOT EXTEND FAR ENOUGH                "
1780 LOCATE 22,5 : PRINT "END OF PROGRAMME  ***  CHANGE FILE D OR F"
1790 END
1800 REM ====  INTERPOLATE IN 3D TO FIND MOMENTUM FLUX AT GIVEN POINT  =====
1810 REM calculate xx = x/l (see diagram)
1820 XX = (VL-CCVL)/(BBVL-CCVL)
1830 REM calculate mass at ee -- mee
1840 MEE = (XX*(BBM-CCM))+CCM
1850 REM calculate momentum flux at gg --wgg
1860 WGG = (XX*(BBMOM-CCMOM))+CCMOM
1870 REM calculate yy = y/m (see diagram)
1880 YY = (VL-DDVL)/(AAVL-DDVL)
1890 REM calculate mass at ff -- mff
1900 MFF = (YY*(AAM-DDM))+DDM
1910 REM calculate momentum at h -- whh
1920 WHH = (YY*(AAMOM-DDMOM))+DDMOM
1930 REM calculate zz = z/m
1940 ZZ = (M-MEE)/(MFF-MEE)
1950 REM calculate the momentum flux required
1960 MOM = (ZZ*(WHH-WGG))+WGG
1970 REM now evaluate the integral G d (theta)equation9
1980 QOLD=Q
1990 TOTMOM = TOTMOM + (MOM*TITO/W)  : GOTO 2010
2000 TOTMOM = TOTMOM * (Q/QOLD) : QOLD=Q
```

```
2010 REM IF TIT>200 THEN LPRINT USING"£££.££££";TIT,VL,M,Q*1000,MOM,TOTMOM*1000
2020 LOCATE 7,45 : PRINT TIT    : LOCATE 8,45 : PRINT MOM
2030 LOCATE 9,45 : PRINT TOTMOM
2040 GOTO 1160                  : REM next set point
2050 CLOSE
2060 LOCATE 21,5 : PRINT "FILE F CLOSED"
2070 REM ====  RECREATE FILE TRANSFER WITH THE ADDITIONAL DATA  ================
2080 OPEN "O",1,"TRANSFER"
2090 WRITE £1,DISC$
2100 WRITE £1,RSQ(1),RSQ(2),RSQ(3),RSQ(4),RSQ(5)
2110 WRITE £1,RSQ(6),RSQ(7),RSQ(8),RSQ(9),RSQ(10)
2120 WRITE £1,VCLOSE,Q,PTT,ROTT,RPM,INC,TIT,VOLEFF,PAMB,PBOOST,TOTMOM
2130 LOCATE 21,40: PRINT "FILE TRANSFER RECREATED"
2140 LOCATE 22,5 : PRINT "
     "
2150 REM LOCATE 22,5 : INPUT "PRESS ANY KEY TO CHAIN COMPRESS PROGRAMME",DUMM
2160 CLOSE: CHAIN "COMPRESS.BAS",ALL
2170 REM ************************************************************************
2180 REM **************  SUBROUTINES  ***************************************
2190 REM ************************************************************************
2200 REM ====  INITIAL VALUES  ========================================
2210 AMO=0 : DMO=0 : AVLO=0 : BVLO=0
2220 TINC=0 : RPM=0
2230 RETURN
2240 REM =====  STORE FILED IN ARRAY ARD(N)  ============================
2250 LOCATE 21,5 : PRINT "READING FILE D"
2260 OPEN "I",1,"FILED"
2270 WHILE DFILE <>9999
2280 INPUT £1, DFILE
2290 N = N + 1
2300 WEND
2310 CLOSE
2320 DIM ARD(N)
2330 OPEN "I",1,"FILED"
2340 FOR NN = 1 TO N
2350 INPUT £1,ARD(NN)
2360 NEXT NN
2370 CLOSE
2380 LOCATE 21,5 : PRINT "                                    "
2390 RETURN
2400 REM =====  READ TRANSFER  ==========================================
2410 LOCATE 21,5 : PRINT "READING FILE TRANSFER"
2420 OPEN "I",2,"TRANSFER"
2430 INPUT £2,DISC$
2440 INPUT £2,RSQ(1),RSQ(2),RSQ(3),RSQ(4),RSQ(5),RSQ(6),RSQ(7)
2450 INPUT £2,RSQ(8),RSQ(9),RSQ(10)
2460 INPUT £2,VCLOSE,Q,PTT,ROTT,RPM,INC,TI,VOLEFF,PAMB,PBOOST
2470 CLOSE
2480 LOCATE 5,45 : PRINT RPM : LOCATE 6,45 : PRINT INC
2490 W=RPM*.10472 : TITO=INC*.01745 : TIT=0
2500 LOCATE 21,5 : PRINT "                                    "
```

```
2510 RETURN
2520 REM *********  SCREEN  ************************************************
2530 CLS
2540 LOCATE 1,1
2550 PRINT "*****************************************************************************
*******"
2560 LOCATE 3,1
2570 PRINT "*****************************************************************************
*******"
2580 LOCATE 2,5
2590 PRINT"S   U   M        M   O   M   E   N   T   U   M        F   L   U   X"
2600 LOCATE 5,1 : PRINT " ENGINE SPEED              / revs/min"
2610 LOCATE 6,1 : PRINT " C.A. INCREMENT            / oCA"
2620 LOCATE 7,1 : PRINT " CRANK ANGLE               / oCA"
2630 LOCATE 8,1 : PRINT " ANGULAR MOMENTUM FLUX     / kgm2/s2"
2640 LOCATE 9,1 : PRINT " TOTAL ANGULAR MOMENTUM    / kgm2/s"
2650 LOCATE 12,13 : PRINT "VL & MF AT DD": LOCATE 12,53 : PRINT "VL & MF AT AA"
2660 LOCATE 18,13 : PRINT "VL & MF AT CC": LOCATE 18,53 : PRINT "VL & MF AT BB"
2670 LOCATE 15,34 : PRINT "VL & MF ACT."
2680 LOCATE 20,1 : PRINT "=================================================
====================="
2690 LOCATE 23,1 : PRINT "=================================================
====================="
2700 LOCATE 21,1 : PRINT "|" : LOCATE 21,75 : PRINT "|"
2710 LOCATE 22,1 : PRINT "|" : LOCATE 22,75 : PRINT "|"
2720 LOCATE 22,5 : PRINT "PLEASE WAIT"
2730 RETURN
```

```
1000 REM ****  CWVEL  ****  22/4/89 R.A.BALIAN  ****************************
1010 REM ====  SCREEN  ==========================================================
1020 GOSUB 2030
1030 REM ====  INPUT FILE TRANSFER  ============================================
1040 GOSUB 1720
1050 REM ====  INPUT FILE C  ===================================================
1060 GOSUB 1800
1070 REM ====  INPUT FILE CWCOMP  ==============================================
1080 GOSUB 1860
1090 REM ====  PRINT ORIGINAL DATA ON SCREEN  ==================================
1100 LOCATE 5,30 : PRINT RPM : LOCATE 6,69 : PRINT USING "£.££££";Q*1000
1110 CR=(VC+(STR*AREA))/VC : LOCATE 5,68 : PRINT CR
1120 REM ====  INPUT DATA FROM SCREEN  =========================================
1130 GOSUB 2250
1140 REM ====  INITIAL CONDITIONS AND CONSTANTS  ================================
1150 PI=3.1415926£ :TITO=INC*.01745 :XTWDOT=0 :STDOT=0 :ZI=0
1160 RPS=RPM/60 : W=RPM*.10472 : CDH=.7 : DIM BOB(10)
1170 REM ====  FUEL DENSITY  ===================================================
1180 ROF = 844 * (1-((.000817)*TF))
1190 REM ====  PRESSURE DROPE ACCROSS NOZZLE HOLES  ============================
1200 AMO = ((1440*VOLF*RPS)/(INPER*PI*NH*CDH*DH^2))^2
1210 DELP = (ROF*AMO)/200000! : REM ====  CONVERT TO BAR  ======================
1220 FOR TIT=(SOI+INC) TO SOC STEP INC
1230 TITA=TIT*.01745
1240 REM ====  AIR DENSITY IN CYLINDER  ========================================
1250 R=STR/2 : NN=CRL/R : CR=(VC+(STR*AREA))/VC
1260 VCYL = AREA*R*(1+NN-(NN^2-(SIN(TITA))^2)^.5-COS(TITA)+(2/(CR-1)))
1270 ROAIR = Q/VCYL
1280 REM ====  AMBIENT AIR DENSITY  ============================================
1290 TAMB = 20 + 273 : ROAMB = PAMB / (287 * TAMB)
1300 REM ====  SPRAY TIP PENETRATION WITHOUT SWIRL  ============================
1310 BMO = 140*((DH*ROAIR)/ROAMB)^.5*DELP^.25
1320 CMO = (1+(ROAIR/ROAMB))^.85
1330 FCON = BMO/CMO
1340 TIME = ((TIT-SOI)*.01745)/W
1350 XT = FCON * TIME^.6
1360 REM ====  SWIRL AND SQUISH AT GIVEN CRANK ANGLE  ==========================
1370 FOR I = 1 TO ZIZ
1380 IF TIT>CA(I) AND TIT<=CA(I+1) THEN GOTO 1390 ELSE GOTO 1420
1390 RATIO=(TIT-CA(I))/(CA(I+1)-CA(I))
1400 WT=WTT(I)+(RATIO*(WTT(I+1)-WTT(I)))
1410 SQU=VSQ(I)+(RATIO*(VSQ(I+1)-VSQ(I))) : GOTO 1430
1420 NEXT I
1430 REM ====  SPRAY TIP PENETRATION WITH SWIRL  ===============================
1440 XXTW=XT
1450 QJ = 2*(DELP*10^5)
1460 QA = ROAIR*(XXTW^2)*(WT^2)
1470 DMO = ((XXTW*QA)/(DH*QJ))^.44
1480 XTW = XT * (1-.35*DMO)
1490 IF XTW>=.99*XXTW AND XTW<1.1*XXTW THEN GOTO 1510 ELSE GOTO 1500
1500 XXTW=XTW : GOTO 1460
1510 IF XTW>.99*(D/2) THEN FINAL=1
1520 REM ====  RADIAL COMP. OF SPRAY TIP VELOCITY  =============================
```

```
1530 EMO=(.35*ROAIR^.44*WT^.88)/(2^.44*DH^.44*(DELP*10^5)^.44)
1540 XTWDOT=(.6*FCON*(1-EMO*XTW^1.32)*TIME^-.4)/(1+1.32*EMO*FCON*XTW^.32*T^.6)
1550 REM ====  TANGENTIAL DEFLECTION OF SPRAY TIP  ==========================
1560 ST = DH*((QA/QJ)*(XTW/DH)^2.217)
1570 REM ====  TANGENTIAL COMP. OF SPRAY TIP VELOCITY  ======================
1580 STDOT=((2.1085*ROAIR*WT^2*XTW^3.217)/((DELP*10^5)*DH^1.217))*XTWDOT
1590 REM ====  TANGENTIAL VELOCITY OF SWIRLING AIR  =========================
1600 VA = WT*XTW
1610 REM ====  CROSS WIND VELOCITY AT THE TIP OF THE FUEL JET  =============
1620 VCW=ABS(STDOT-VA)
1630 IF FINAL=1 THEN GOTO 1640 ELSE GOTO 1650
1640 VIMP=((XTWDOT^2)+(STDOT^2))^.5 : SQIMP=SQU : GOTO 1680
1650 REM ====  PRINT RESULTS  ==============================================
1660 GOSUB 2460
1670 NEXT TIT
1680 LOCATE 18,50: PRINT VIMP
1690 LOCATE 21,5 : PRINT "END OF PROGRAM                                    "
1700 LOCATE 22,5 : INPUT "WOULD YOU REQUIRE A PRINT OUT OF RESULTS  ",DUM$
1710 IF DUM$="Y" OR DUM$="y" THEN GOTO 2570 ELSE END
1720 REM ====  FILE TRANSFER  ==============================================
1730 OPEN "I",£1,"TRANSFER"
1740 LOCATE 21,5 : PRINT "READING FILE TRANSFER"
1750 INPUT £1,DISC$
1760 FOR I=1 TO 10 : INPUT £1,DUM : NEXT I
1770 INPUT £1,VCLOSE,Q,PTT,ROTT,RPM,INC,TI,VOLEFF,PAMB,PBOOST,TOTMOM
1780 CLOSE
1790 RETURN
1800 REM ====  FILE C  ====================================================
1810 OPEN "I",£1,"FILEC"
1820 LOCATE 21,5 : PRINT "READING FILE C          "
1830 INPUT £1,CRL,STR,AREA,VD,CIR,VC,B,D,H,VOL,VOLX
1840 CLOSE
1850 RETURN
1860 REM ====  FILE CWCOMP  ===============================================
1870 OPEN "I",£1,"CWCOMP"
1880 LOCATE 21,5 : PRINT "READING FILE CWCOMP     "
1890 INPUT £1,DUM
1900 IF DUM=9999 THEN GOTO 1920
1910 ZI=ZI+1 : GOTO 1890
1920 CLOSE
1930 ZIZ=(ZI+1)/3
1940 DIM CA(ZIZ),WTT(ZIZ),VSQ(ZIZ)
1950 OPEN "I",£1,"CWCOMP"
1960 FOR I=1 TO ZIZ
1970 INPUT £1,CA(I),WTT(I),VSQ(I)
1980 IF CA(I)=360 THEN GOTO 1990 ELSE GOTO 2000
1990 SWTDC=WTT(I)*9.549296 : SQTDC=VSQ(I)
2000 NEXT I
2010 CLOSE
2020 RETURN
2030 CLS : REM ====  screen  ================================================
2040 LOCATE 1,1 : PRINT "*****************************************************
*************************"
```

```
2050 LOCATE 3,1 : PRINT "**********************************************************
**********************"
2060 LOCATE 2,4 : PRINT "C       R       O       S       S               W
I       N       D"
2070 LOCATE 20,1 : PRINT "==========================================================
========================"
2080 LOCATE 23,1 : PRINT "==========================================================
========================"
2090 LOCATE 21,1 : PRINT "|" : LOCATE 21,78 : PRINT "|"
2100 LOCATE 22,1 : PRINT "|" : LOCATE 22,78 : PRINT "|"
2110 LOCATE 5,1  : PRINT "ENGINE SPEED     / revs/min"
2120 LOCATE 6,1  : PRINT "C.A. INCREMENT   / oCA"
2130 LOCATE 5,43 : PRINT "COMPRESSION RATIO"
2140 LOCATE 6,43 : PRINT "TOTAL MASS TRAPPED  / g"
2150 LOCATE 7,1  : PRINT "CRANK ANGLE      / oCA"
2160 LOCATE 10,1 : PRINT "VOLUME OF FUEL PER INJECTION  / mm3"
2170 LOCATE 11,1 : PRINT "FUEL TEMPERATURE              / oC"
2180 LOCATE 12,1 : PRINT "MEASURED INJECTION PERIOD     / oCA"
2190 LOCATE 13,1 : PRINT "NUMBER OF NOZZLE HOLES"
2200 LOCATE 14,1 : PRINT "NOZZLE HOLE DIAMETER          / mm"
2210 LOCATE 15,1 : PRINT "START OF INJECTION            / oCA"
2220 LOCATE 16,1 : PRINT "START OF COMBUSTION           / oCA"
2230 LOCATE 22,5 : PRINT "PLEASE WAIT"
2240 RETURN
2250 REM ====  INPUT DATA FROM SCREEN  ====================================
2260 LOCATE 22,5 : PRINT "PLEASE INPUT THE ABOVE REQUIRED DATA"
2270 LOCATE 6,30 : INPUT " ",INC
2280 LOCATE 10,40 : INPUT " ",VOLF    : VOLF=VOLF/(10^9)
2290 LOCATE 11,40 : INPUT " ",TF
2300 LOCATE 12,40 : INPUT " ",INPER
2310 LOCATE 13,40 : INPUT " ",NH
2320 LOCATE 14,40 : INPUT " ",DH     :DH=DH/1000
2330 LOCATE 15,40 : INPUT " ",SOI
2340 LOCATE 16,40 : INPUT " ",SOC
2350 LOCATE 22,5 : PRINT "PLEASE WAIT                                    "
2360 LOCATE 10,1 : PRINT "AIR SWIRL                          / revs/min    "
2370 LOCATE 11,1 : PRINT "SPRAY PENETRATION WITOUT SWIRL     / mm          "
2380 LOCATE 12,1 : PRINT "SPRAY PENETRATION WITH SWIRL       / mm          "
2390 LOCATE 13,1 : PRINT "TAN. DEFLECTION OF SPRAY TIP       / mm          "
2400 LOCATE 14,1 : PRINT "RAD. COMP. OF SPRAY VELOCITY       / m/s         "
2410 LOCATE 15,1 : PRINT "TAN. COMP. OF SPRAY VELOCITY       / m/s         "
2420 LOCATE 16,1 : PRINT "TAN. VELOCITY OF SWIRLING AIR      / m/s         "
2430 LOCATE 17,1 : PRINT "CROSS WIND VELOCITY                / m/s         "
2440 LOCATE 18,1 : PRINT "IMPINGEMENT VELOCITY               / m/s         "
2450 RETURN
2460 REM ====  PRINT CALCULATED RESULTS  ==================================
2470 LOCATE 7,30  : PRINT TIT                      : BOB(1)=TIT
2480 LOCATE 10,50 : PRINT WT*9.549296              : BOB(2)=WT*9.549296
2490 LOCATE 11,50 : PRINT XT*1000                  : BOB(3)=XT*1000
2500 LOCATE 12,50 : PRINT XTW*1000                 : BOB(4)=XTW*1000
2510 LOCATE 13,51 : PRINT USING "£.£££££";ST*1000: BOB(5)=ST*1000
2520 LOCATE 14,50 : PRINT XTWDOT                   : BOB(6)=XTWDOT
2530 LOCATE 15,50 : PRINT USING "££.£££££";STDOT : BOB(7)=STDOT
2540 LOCATE 16,50 : PRINT VA                       : BOB(8)=VA
2550 LOCATE 17,50 : PRINT VCW                      : BOB(9)=VCW
```

```
2550 LOCATE 17,50 : PRINT VCW                          : BOB(9)=VCW
2560 RETURN
2570 REM ====  TRANSFERING DATA TO PRINTER  ================================
2580 LPRINT : LPRINT : LPRINT : LPRINT
2590 LPRINT "=============================================================="
2600 LPRINT "      G   E   N   E   R   A   T   E   D       D   A   T   A"
2610 LPRINT "=============================================================="
2620 LPRINT
2630 LPRINT "DISC NUMBER                                          ",DISC$
2640 LPRINT : LPRINT
2650 LPRINT "ENGINE SPEED                          / revs/min     ",RPM
2660 LPRINT "COMPRESSION RATIO                                    ",CR
2670 LPRINT "NUMBER OF NOZZLE HOLES                               ",NH
2680 LPRINT "NOZZLE HOLE DIAMETER                  / mm           ",DH*1000
2690 LPRINT "START OF INJECTION                    / oCA          ",SOI
2700 LPRINT "INJECTION PERIOD                      / oCA          ",INPER
2710 LPRINT "START OF COMBUSTION                   / oCA          ",SOC
2720 LPRINT "IGNITION DELAY                        / oCA          ",SOC-SOI
2730 LPRINT : LPRINT
2740 LPRINT "=============================================================="
2750 LPRINT : LPRINT
2760 LPRINT "TOTAL MASS TRAPPED                    / g            ",Q*1000
2770 LPRINT
2780 LPRINT "TOTAL ANG. MOM. AT IVC                / kgm2/s       ",TOTMOM
2790 LPRINT
2800 LPRINT "SWIRL RATIO AT TDC                                   ",SWTDC/RPM
2810 LPRINT
2820 LPRINT "SQUISH AT BOWL RAD. AT TDC            / m/s          ",SQTDC
2830 LPRINT
2840 LPRINT "CRANK ANGLE AT IMPINGEMENT            / oCA          ",BOB(1)
2850 LPRINT
2860 LPRINT "SWIRL RATIO AT IMPINGEMENT                           ",BOB(2)/RPM
2870 LPRINT
2880 LPRINT "SQUISH AT BOWL RAD. AT IMP.           / m/s          ",SQIMP
2890 LPRINT
2900 LPRINT "SPRAY PENETRATION WITHOUT SWIRL       / mm           ",BOB(3)
2910 LPRINT
2920 LPRINT "SPRAY PENETRATION WITH SWIRL          / mm           ",BOB(4)
2930 LPRINT
2940 LPRINT "TAN. DEFLECTION OF SPRAY TIP          / mm           ",BOB(5)
2950 LPRINT
2960 LPRINT "RAD. COMP. OF SPRAY VELOCITY          / m/s          ",BOB(6)
2970 LPRINT
2980 LPRINT "TAN. COMP. OF SPRAY VELOCITY          / m/s          ",BOB(7)
2990 LPRINT
3000 LPRINT "IMPINGEMENT VELOCITY                  / m/s          ",VIMP
3010 LPRINT
3020 LPRINT "TAN. VELOCITY OF SWIRLING AIR         / m/s          ",BOB(8)
3030 LPRINT
3040 LPRINT "CROSS WIND VELOCITY                   / m/s          ",BOB(9)
3050 LPRINT : LPRINT : LPRINT : LPRINT
3060 END
```

Flow Chart for ITERAM

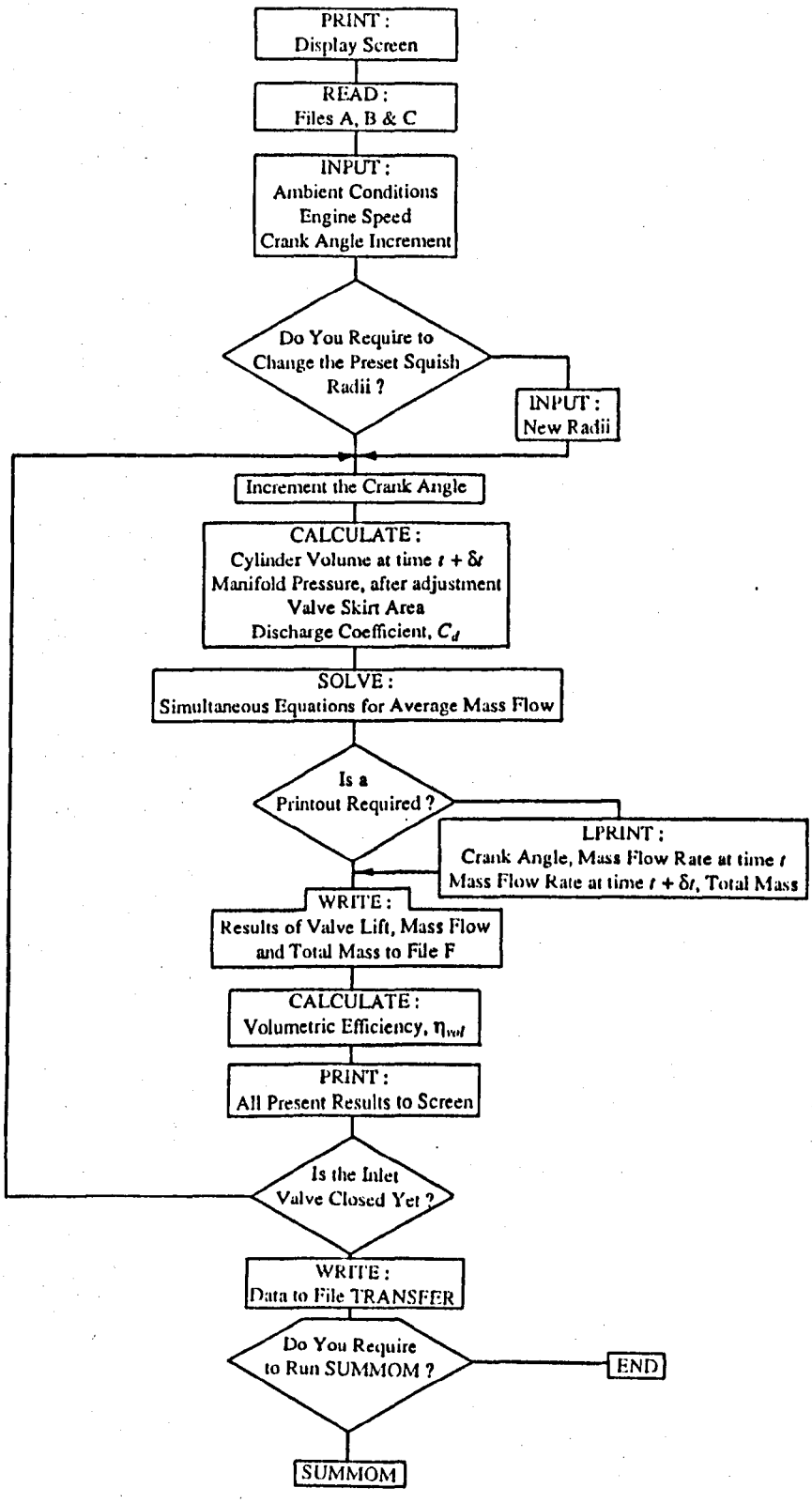

Flow chart for SUMMOM

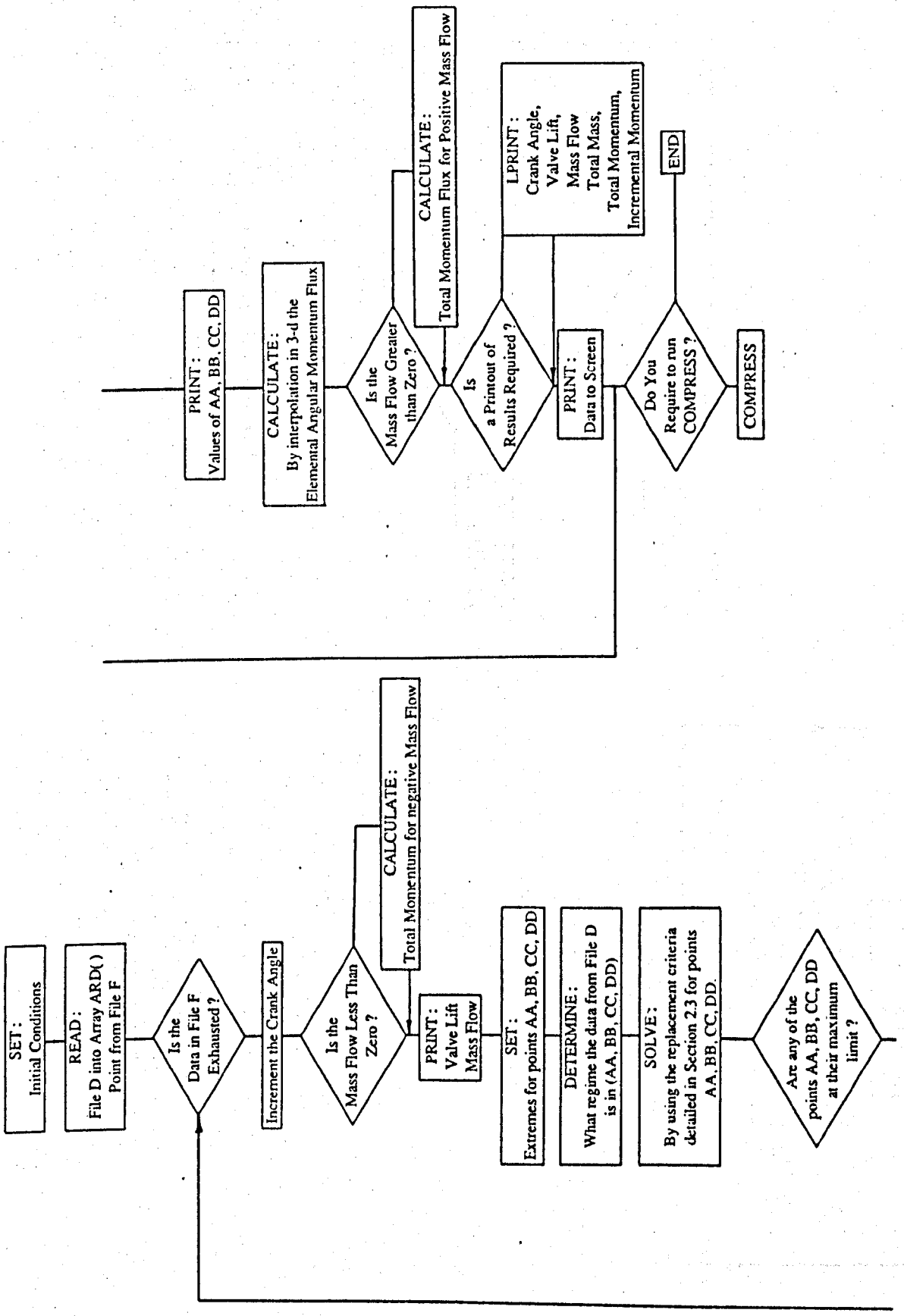

Flow Chart for COMPRESS

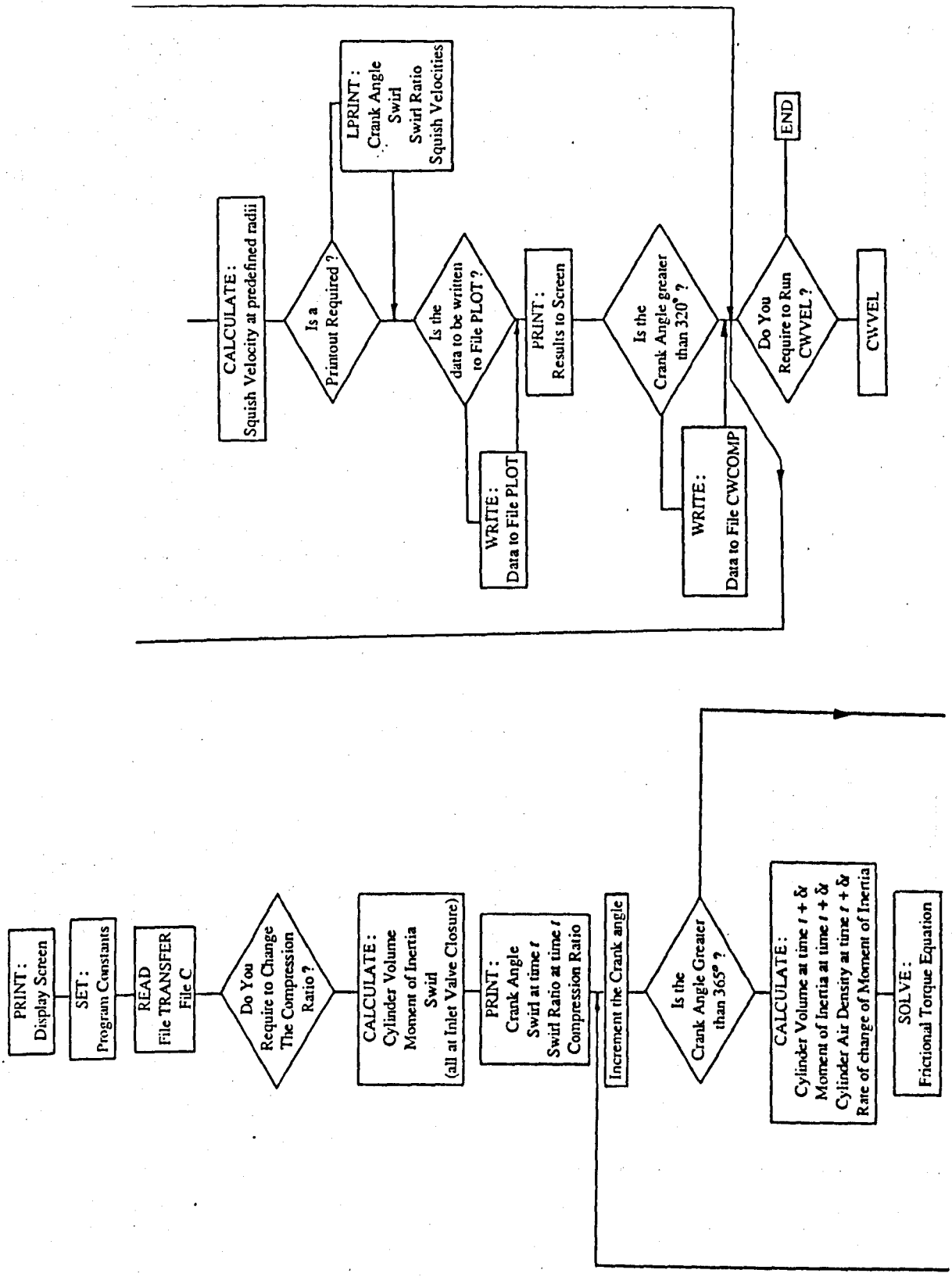

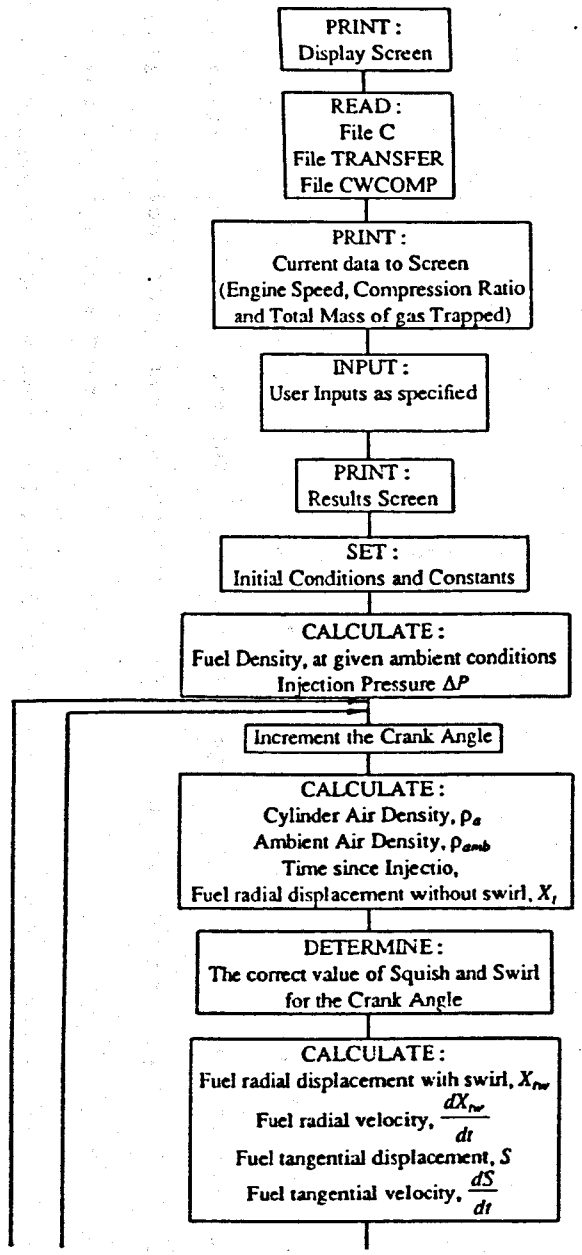
PRINT :
Display Screen
READ :
File C
File TRANSFER
File CWCOMP
PRINT :
Current data to Screen
(Engine Speed, Compression Ratio
and Total Mass of gas Trapped)
INPUT :
User Inputs as specified
PRINT :
Results Screen
SET :
Initial Conditions and Constants
CALCULATE :
Fuel Density, at given ambient conditions
Injection Pressure ΔP
Increment the Crank Angle
CALCULATE :
Cylinder Air Density, ρ_a
Ambient Air Density, ρ_{amb}
Time since Injectio,
Fuel radial displacement without swirl, X_f
DETERMINE :
The correct value of Squish and Swirl
for the Crank Angle
CALCULATE :
Fuel radial displacement with swirl, X_{fw}
Fuel radial velocity, $\frac{dX_{fw}}{dt}$
Fuel tangential displacement, S
Fuel tangential velocity, $\frac{dS}{dt}$

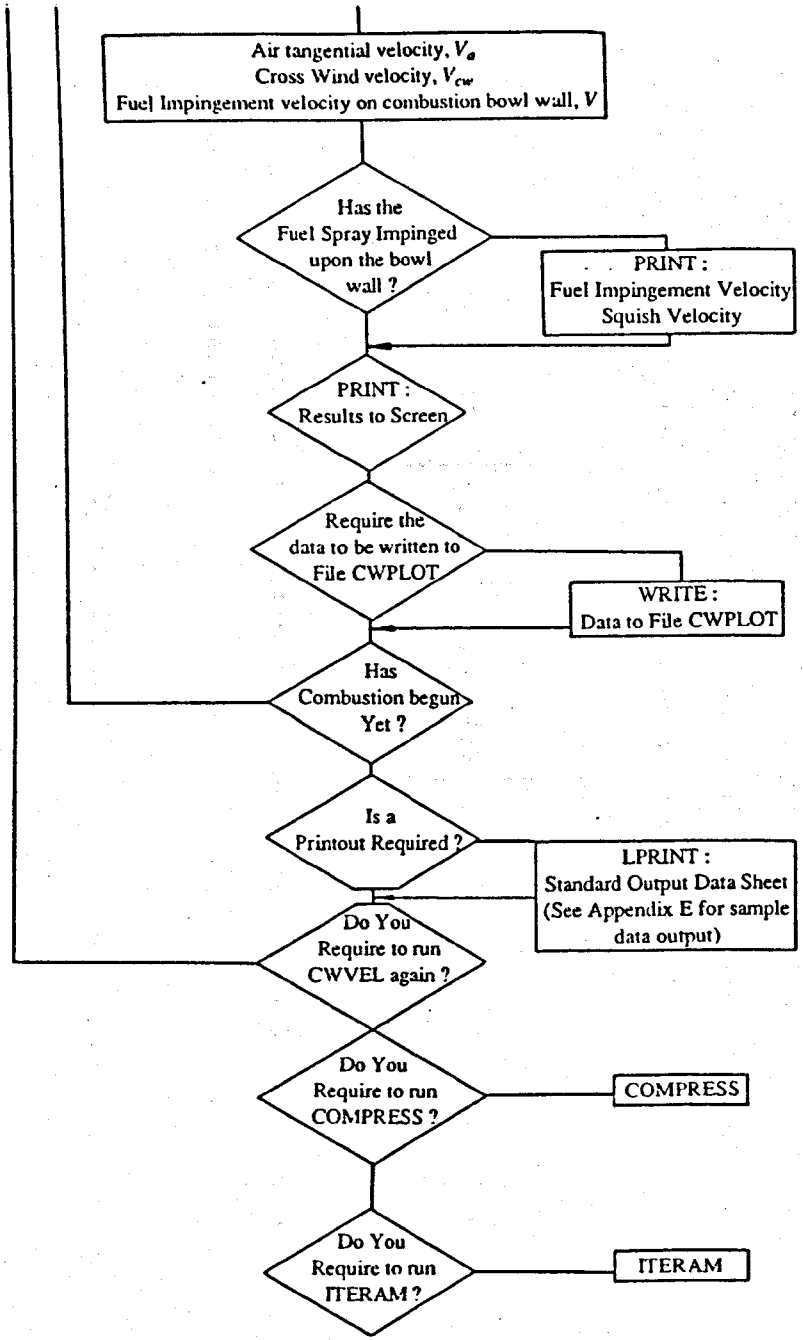
Air tangential velocity, V_a
Cross Wind velocity, V_{cw}
Fuel Impingement velocity on combustion bowl wall, V
Has the
Fuel Spray Impinged
upon the bowl
wall ?
PRINT :
Fuel Impingement Velocity
Squish Velocity
PRINT :
Results to Screen
Require the
data to be written to
File CWPLOT
WRITE :
Data to File CWPLOT
Has
Combustion begun
Yet ?
Is a
Printout Required ?
LPRINT :
Standard Output Data Sheet
(See Appendix E for sample
data output)
Do You
Require to run
CWVEL again ?
Do You
Require to run
COMPRESS ?
COMPRESS
Do You
Require to run
ITERAM ?
ITERAM

B.12 - **Effect of cylinder bore on the total moment of momentum at IVC and on the swirl speed during compression**

From section B.4 of this Appendix, the moment of momentum of the air admitted during the time interval δt is given by,

$$M = \left[2\pi\rho \int_0^{B/2} V_a \, \omega r^3 \, dr \right] \delta t \qquad \ldots\ldots \text{B.13}$$

As a first approximation, the effect of cylinder bore, B, can be illustrated by replacing,

$$V_a = \frac{\dot{m}_{av}}{\rho \pi (B/2)^2}$$

where $\dot{m}_{av}$ is the average air mass flow rate admitted by the engine over the interval δt. Also, assume that ω is not a function of radius, r; substituting in Eq B.13 and integrating gives,

$$M = \frac{\dot{m}_{av} \, \omega B^2 \, \delta t}{8}$$

Noting that the average air mass flow rate, $\dot{m}_{av}$, increases with increasing cylinder bore (at a given engine speed). It is clear from this equation that the moment of momentum increases rapidly with increasing cylinder bore.

However, the moment of inertia of the trapped mass rises with increasing bore and swept volume:

$$I = \frac{m_{ivc}}{2} \left[\frac{\frac{\pi (B/2)^4 s}{v} + (D/2)^2}{\frac{\pi (B/2)^2 s}{v} + 1} \right]$$

Assuming that there is no fluid friction (this assumption is made here only for illustration purposes), then:

$$\frac{d(I\omega_c)}{dt} = 0$$

$$I\,\omega_c = M$$

$$\omega_c = \frac{M}{I}$$

Therefore, the change in swirl speed, ω_c, with increasing cylinder bore B is dependebt on the ratio M / I. It is somewhat complicated to interpret mathematically the effect of the cylinder bore on each individual term in this ratio. However, this effect could be further ascertained using the models of Chapter 5, given suitable steady-flow rig data for the flow through the valve of a cylinder with larger bore.

Appendix C

Experimental Accuracy

This appendix presents the errors involved in the instrumentation, measured, and derived parameters. The errors calculated for the measured parameters were defined as: the smallest division on the scale of the instrument as a percentage of the range of the measured values. For example, the air inlet pressure range was 400-800 mmHg, where the smallest division on the manometer was 1mm, therefore:

Error = 1/800 x 100 = 0.125% to 1/400 x 100 = 0.25%

The errors for the derived parameters were calculated using the Binomial Approximation method, (Stone, 1985).

Measured Parameters	Range	Smallest Divisions	Percentage error
Atmospheric pressure (mmHg)	- 760	1	0.13
Cylinder gas pressure (bar)	- 80	1	1.25
Air inlet pressure (mmHg)	400 - 800	1	0.12-0.25
Exhaust back pressure (mmHg)	90 - 270	1	0.37-1.11
Air flow rate (g/s)	5 - 18	calib.	1 - 3
Fuel flow rate (g/s)	0.1 - 0.5	calib.	0.5 - 2
Engine speed (rev/min)	1000 - 3000	6	0.2 - 0.6
Engine load (lb)	20 - 24	1	4 - 5
Temperatures (K)	300 - 900	calib.	0.1 - 0.3
Crank angle (s)	200 - 1000	5	0.5 - 2.5
Smoke (Bosch unit)	2 - 10	0.2	2 - 10
NO_x (ppm)	2% full scale		2

Derived parameter	Proportional to:	Percentage error
BMEP	engine load	4 - 5
BSFC	engine load, fuel flow rate	4.5 - 7.0
BSAC	engine load, air flow rate	5 - 8
Vol. eff.	air flow rate, atm. press., temp.	1.23 - 3.43
Inj. timing	crank angle	0.5 - 2.5
Ign. Delay	crank angle	0.5 - 2.5
Start of comb.	crank angle	0.5 - 2.5
Air fuel ratio	air flow rate, fuel flow rate	1.5 - 5.0

REFERENCES

1 - **Abramovich G.N.**, THE THEORY OF TURBULENT JETS , MIT Press , 1963.

2 - **Adler D. and Lyn W.T.**, THE EVAPORATION AND MIXING OF A LIQUID FUEL SPRAY IN A DIESEL AIR SWIRL , Symp. on Diesel Engine Combustion, IMechE, 1970.

3 - **Aoyagi Y., Kamimoto T., Matsui Y. and Matsuoka S.**, A GAS SAMPLING STUDY ON THE FORMATION PROCESSES OF SOOT AND NO IN A DI DIESEL ENGINE, SAE Paper 800254, 1980.

4 - **ASTM D613**, RATING DIESEL FUELS BY TEH CETANE METHOD, 1963.

5 - **Barber J.R.**, VARRIABLE COMPRESSION RATIO PISTONS FOR HIGH OUTPUT DIESEL ENGINES, PhD Thesis, Brunel university, 1987.

6 - **Brandle F., Reverencic I., Cartellieri W. and Dent J.C.**, TURBULENT AIR FLOW IN THE COMBUSTION BOWL OF A DI DIESEL ENGINE AND ITS EFFECT ON ENGINE PERFORMANCE, SAE Paper 790040, 1979.

7 - **Bird R.B., Stewart W.E. and Lightfoot E.N.**, TRANSPORT PHENOMENTA, Published by Wiley Topman (1960).

8 - Chartered Mechanical Engineer, Diesel engien developements, Mechanical engineering publications, p81 Dec 1984.

9 - **Chiu W.S, Shahed S.M. and Lyn W.T.**, A TRANSIENT SPRAY MIXING MODEL FOR DIESEL COMBUSTION, SAE Paper 760128, 1976.

10 - **Dent J.C.**, TURBULENT MIXING RATE - ITS EFFECT ON SMOKE AND HYDROCARBON EMISSIONS FROM DIESEL ENGINES, SAE Paper 800092, 1980.

11 - **Dent J.C. and Derham J.A.**, AIR MOTION IN A FOUR-STROKE DIRECT INJECTION DIESEL ENGINE, Proc. IMechE Vol. 188 21/74 , 1974.

12 - **Etminan Y.**, INDUCTION TUNING OF A SINGLE CYLINDER DIESEL ENGINE, MPhil Thesis, Brunel university, 1989.

13 - Eureka magazine, VARIABLE PISTON INCREASES ENGINE EFFICIENCY, pp30-34, April 1989.

14 - **Fansler T.D.**, LASER VELOCIMETRY MEASUREMENTS OF SWIRL AND SQUISH FLOWS IN AN ENGINE WITH A CYLINDRICAL PISTON BOWL, SAE Paper 850124, 1985.

15 - **Fitzgeorge D. and Allison J.L.**, AIR SWIRL IN A ROAD-VEHICLE DIESEL ENGINE, Proc. IMechE (A.D) No. 4 , pp 151-177 , 1962-63.

16 - **Greeves G., Khan I.M., Wang C.H.T. and Fenne I.**, ORIGINS OF HYDROCARBON EMISSIONS FROM DIESEL ENGINES, SAE Paper 770259 , 1977.

17 - **Grundy J.R, Kiley L.R. and Brevick E.A.**, AVCR 1360-2 HIGH SPECIFIC OUTPUT VARIABLE COMPRESSION RATIO DIESEL ENGINE, SAE paper 760051, 1976.

18 - **Heywood J.B.**, INTERNAL COMBUSTION ENGINE FUNDAMENTALS, Published by McGraw-Hill, London, 1988.

19 - **Heap M.P., Carver G.P., Cornis C.M. and Taylor T.J.**, INVESTIGATION OF DIESEL COMBUSTION BY DIRECT IN-CYLINDER SAMPLING, SAE Paper 750850, 1975.

20 - **Igura S., Kadota T. and Hiroyasu H.**, SPONTANEOUS IGNITION DELAY FUEL SPRAY IN HIGH PRESSURE GASEOUS ENVIRONMENT, Trans. Japan Soc. Mech. Engrs., Vol. 41, No. 345, pp. 24-31, 1975.

21 - **Iijima T., and Bracco F.V.**, LDV MEASUREMENTS IN AN ENGINE WITH SQUARE AND CIRCULAR PISTON CUPS, SAE Paper 872973, 1987

22 - Internal combustion engine, US patent 4538557, 1985.

23 - **Kamimoto T., Aoyagi Y., Matsui Y. and Matsuoka S.**, THE EFFECT OF SOME ENGINE VARIABLES ON MEASURED RATES OF AIR ENTRAINMENT AND HEAT RELEASE IN A DI DIESEL ENGINE, SAE Paper 800253, 1980.

24 - **Kamo R.**, HIGHER BMEP PROSPECTS FOR VEHICULAR DIESELS, TURBOCHARGING AND TURBOCHARGERS, IMechE conference, London, pp107-114, 1978.

25 - **Khan I.M.**, FORMATION AND COMBUSTION ENGINE, Proc. IMechE, vol. 185 Pt. 3J, pp. 36-43, 1969-70.

26 - **Kuo T.W., Yu R.C. and Shahed S.M.**, A NUMERICAL STUDY OF THE TRANSIENT EVAPORATING SPRAY MIXING PROCESS IN THE DIESEL ENVIRONMENT, SAE Paper 831735, 1983.

27 - **Ladommatos N., Barber J.R. and Brown I.A.C.**, THEORETICAL AND EXPERIMENTAL INVESTIGATION OF A PRESSURE-RELIEF VALVE FOR VARIABLE-COMPRESSION-RATIO PISTON, Proc. IMechE 1989.

28 - **Ladommatos N., Stone R.S.**, DEVELOPMENT FOR DIRECT INJECTION DIESEL ENGINES, Proc. IMechE 1986.

29 - **Lyn W.T. and Valdmanis E.**, THE APPLICATION OF HIGH SPEED SCHLIEREN PHOTOGRAPHY TO DIESEL COMBUSTION RESEARCH, The Journal of Photographic Science, Vol. 10, 1962.

30 - **Mansfield W.P., Tryhorn D.W. and Thornycroft C.H.**, dEVELOPEMENT OF THE TURBOCHARGED DIESEL ENGINE TO HIGH MEAN EFFECTIVE PRESSURE WITHOUT MECHANICAL OR THERMAL LOADING, CIMAC conference, A6, pp1-18, 1965.

31 - **Mehta P.S. and Gupta A.K.**, MODELLING OF SPRAY-SWIRL INTERACTION IN DIRECT INJECTION DIESEL ENGINE COMBUSTION CHAMBER, Proc. IMechE, Vol. 199, No. D3, 1985.

32 - **McKinley T.L. and Primus R.J.**, THE INFLUENCE OF BOWL OFFSET ON AIR MOTION IN A DIRECT INJECTION DIESEL ENGINE, SAE Paper 881611, 1988.

33 - **Monaghan M.L.**, THE HIGH SPEED DIRECT INJECTION DIESEL ENGINE FOR PASSENGER CARS, SAE Paper 810477, 1981.

34 - **Monaghan M.L. and Pettifer H.F.**, AIR MOTION AND ITS EFFECT ON DIESEL PERFORMANCE AND EMISSIONS, SAE Paper 810255, 1981.

35 - **Morris C.J. and Dent J.C.**, THE SIMULATION OF AIR FUEL MIXING IN HIGH SWIRL OPEN CHAMBER DIESEL ENGINE, Proc. IMechE, Vol. 190, 47/76, 1976.

36 - **Osborne A.G.**, DIESEL ENGINE RESEARCH AT HIGH BMEP, Proc. IMechE, Vol. 199, No. A4, pp. 285-294, 1985.

37 - **Osborne A.G. and Bhinder F.S.**, INVESTIGATION INTO THE PERFORMANCE OF HIGHLY TURBOCHARGED DIESEL ENGINES, SAE Paper 820329, SP.514, 1982.

38 - **Pischinger R. and Cartellieri W.**, COMBUSTION SYSTEM PARAMETERS AND THEIR EFFECTS UPON DIESEL ENGINE EXHAUST EMISSIONS, SAE Paper 720756, 1972.

39 - **Rychter T.J. and Teodorczyk A.**, VR/LE ENGIEN WITH VARIABLE R/L DURING A SINGLE CYCLE, SAE paper 850206, 1985.

40 - **Scott W.M.**, LOOKING IN A DIESEL COMBUSTION, SAE Paper 690002, 1969.

41 - **Shimamoto Y. and Akiama K.**, A STUDY OF SQUISH IN OPEN COMBUSTION CHAMBERS OF A DIESEL ENGINE, Bull JSME, Vol. 13, no. 63, pp. 1096-1105, 1970.

42 - **Shiozaki T., Suzuki T. and Shimoda M.**, OBSERVATION OF COMBUSTION PROCESS IN DI DIESEL ENGINE VIA HIGH SPEED DIRECT AND SCHLIEREN PHOTOGRAPHY, SAE Paper 800025, 1980.

43 - **Spadoccini L.J. and TeVelda J.A.**, AUTOIGNITION CHARACTERISTICS OF AIRCRAFT-TYPE FUELS, Combust. Flame, Vol. 46, pp. 283-300, 1982.

44 - **Taylor C.F.**, THE INTERNAL COMBUSTION ENGINE IN THEORY AND PRACTICE, vol. 1 and 2, MIT Press, Cambridge, Mass., 1968.

45 - **Timoney D.J.**, A SIMPLE TECHNIQUE FOR PREDICTING OPTIMUM FUEL-AIR MIXING CONDITIONS IN A DIRECT INJECTION DIESEL ENGINE, SAE Paper 851543, 1985.

46 - **Tindal M.J.**, AN INVESTIGATION OF SWIRL AND TURBULENCE IN THE CYLINDERS OF DIRECT INJECTION DIESEL ENGINE, Proc. IMechE, C127/82, 1982.

47 - **Varde K.S., Popa D.M. and Varde L.K.**, SPRAY ANGLE AND ATOMISATION IN DIESEL SPRAYS, SAE Paper 841055, 1984.

48 - Variable displacement piston engone, US patent 4270495, 1981.

49 - Variable displacement reciprocating piston machine, US patent 4112826, 1978.

50 - **Wallace W.A. and Lux F.B.,** A VARIABLE COMPRESSION RATIO ENGINE DEVELOPEMENT, SAE paper 762A, 1963.

51 - **Walzer P., Adamis P., Heinrich H., Schumacher V.,** VARIABLE STENERZEITEN UND VARIABLE VERDICHTUNG BEIM OTTOMOTOR, MTZ Motortechnische Zeitschrift, 47 (1986)1.

52 - **Williams T.J. and Tindal M.J.,** GAS FLOW STUDIES IN DIRECT INJECTION DIESEL ENGINES WITH RE-ENTRANT COMBUSTION CHAMBERS, SAE Paper 800027, 1980.

53 - **Wirbeleit F., Binder K., Gwinner D.,** DEVELOPMENT OF PISTONS WITH VARIABLE COMPRESSION HEIGHT FOR INCREASING EFFICIENCY AND SPECIFIC OUTPUT OF COMBUSTION ENGINES, SAE paper 900229, 1990.

54 - **Youl A.J., Mo S.L., Tham S.Y. and Aval S.M.,** DIESEL SPRAY STRUCTURE, ICLASS-85, IIB/2/1-15

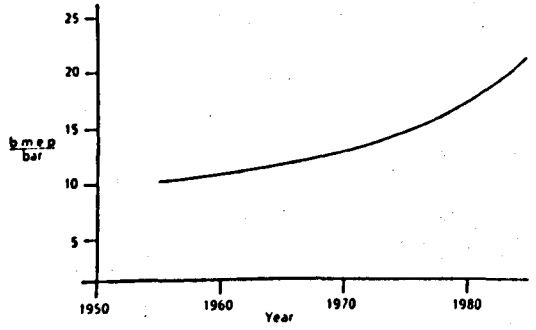

FIGURE 1.1
Increase in brake mean effective pressure (bmep) of medium speed diesel engines over the last 30 years. (Ladommatos and Stone, 1986)

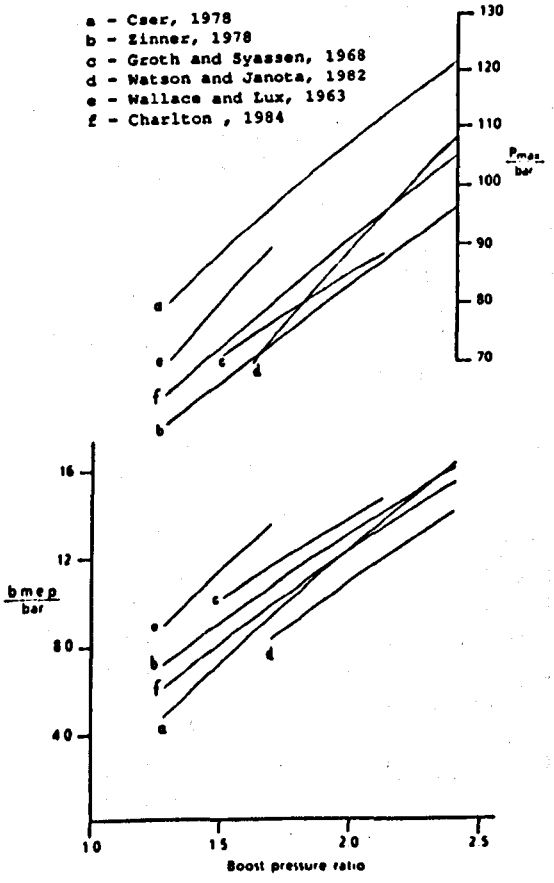

FIGURE 1.2
Increase in brake mean effective pressure (bmep) and firing pressure (P_{max}) with increasing boost pressure ratio. (Ladommatos and Stone, 1986)

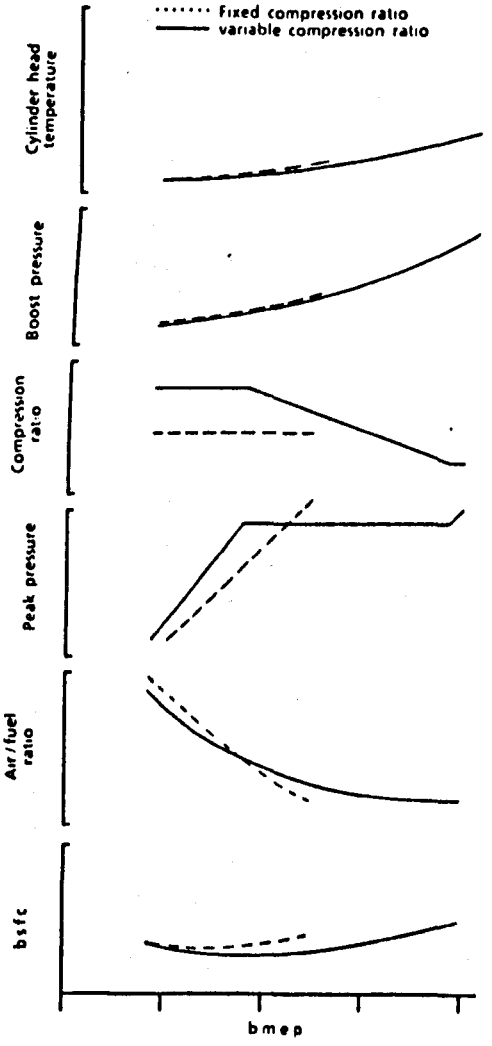

FIGURE 1.3
Comparison of expected diesel engine performance with fixed and variable compression ratio. (Ladommatos and Stone, 1986)

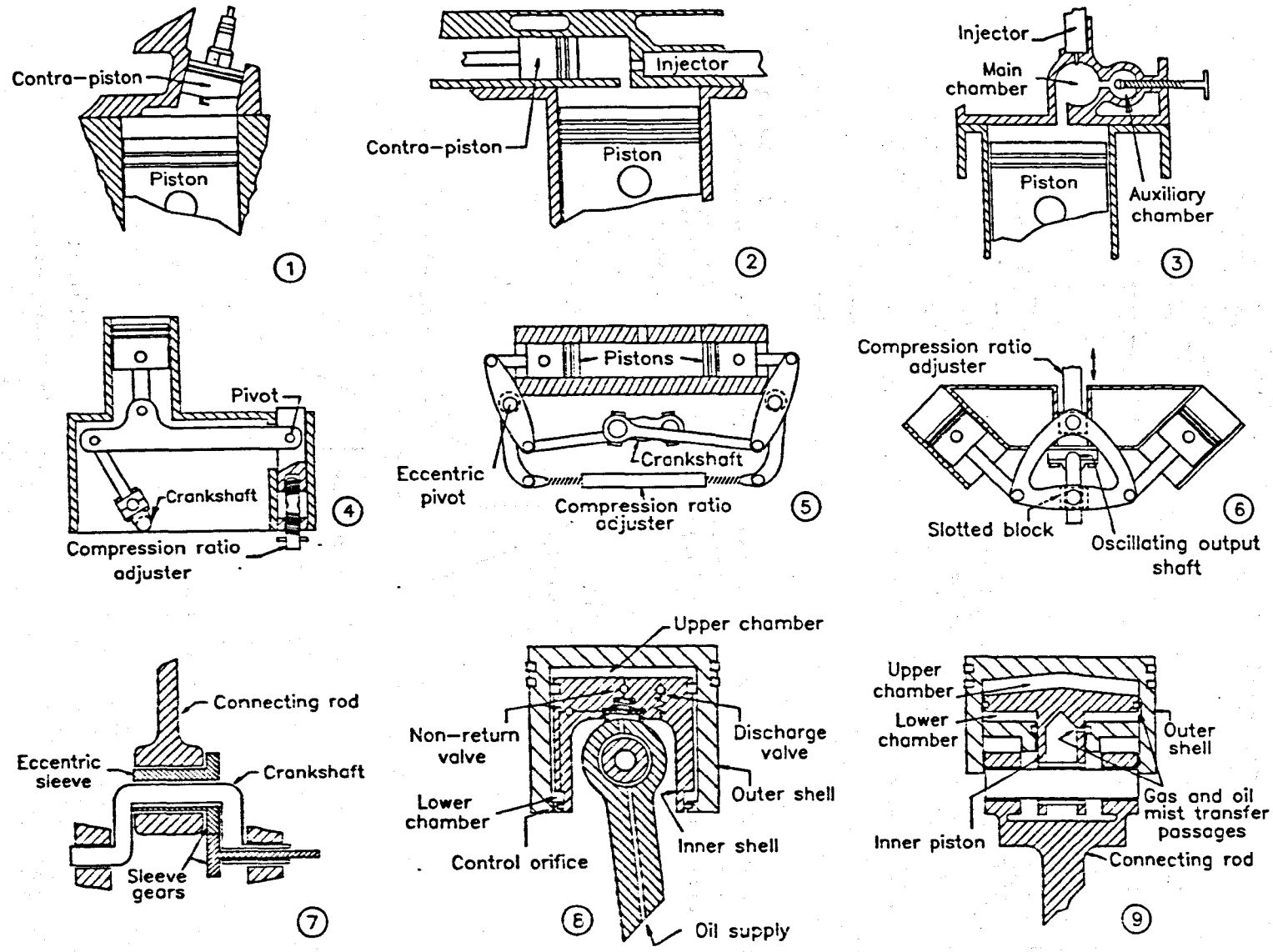

FIGURE 1.4
Cross-sectional views of a number of variable compression ratio (VCR) systems.

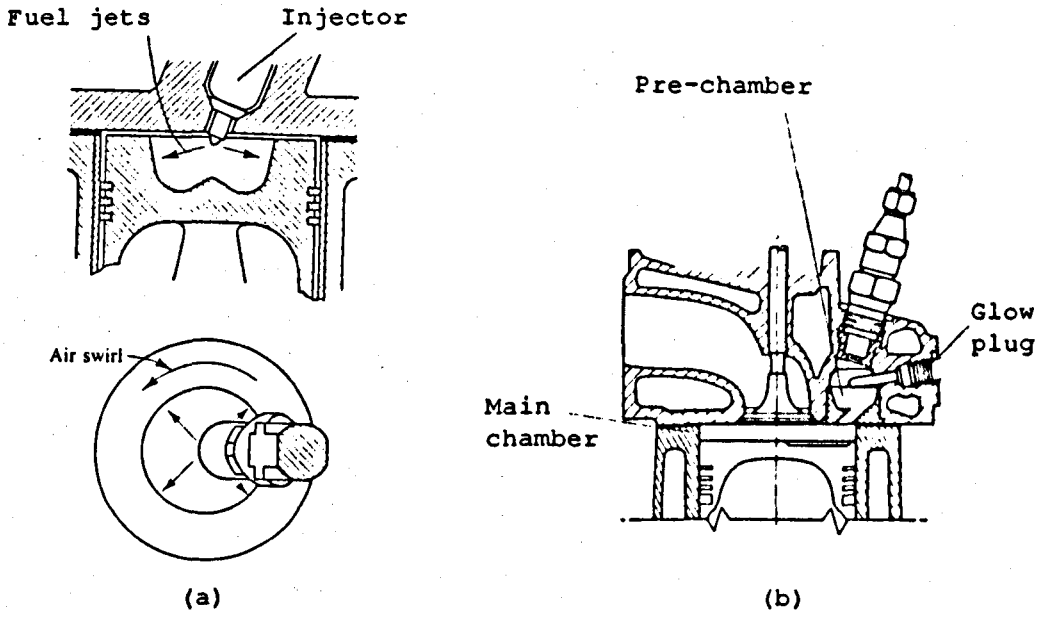

FIGURE 2.1
(a) Diesel engine bowl-in-piston combustion chamber with swirl and multihole nozzle; used in medium to small DI engine size range, (b) Small indirect-injection diesel engine combustion system (swirl prechamber type). (Heywood, 1988)

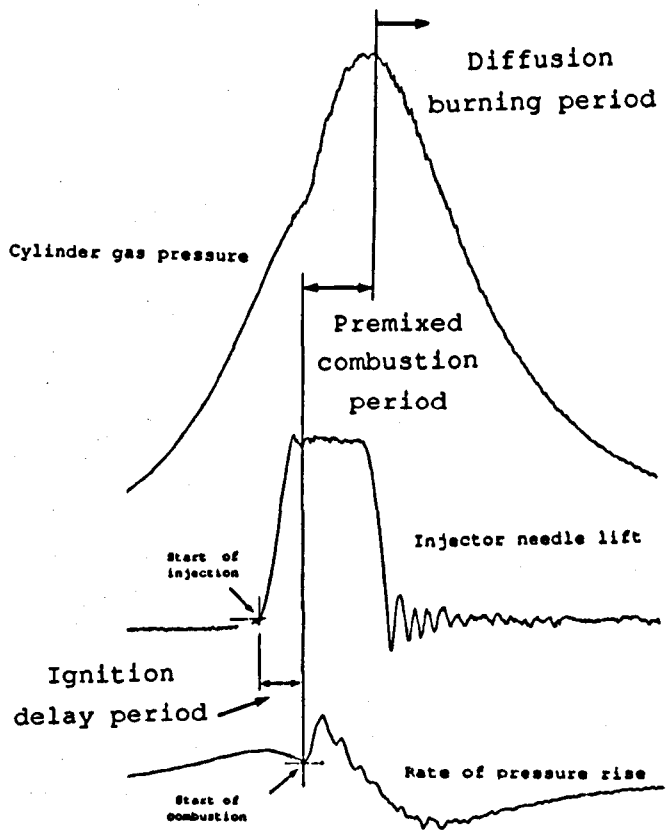

FIGURE 2.2
The three phases of diesel engine combustion.

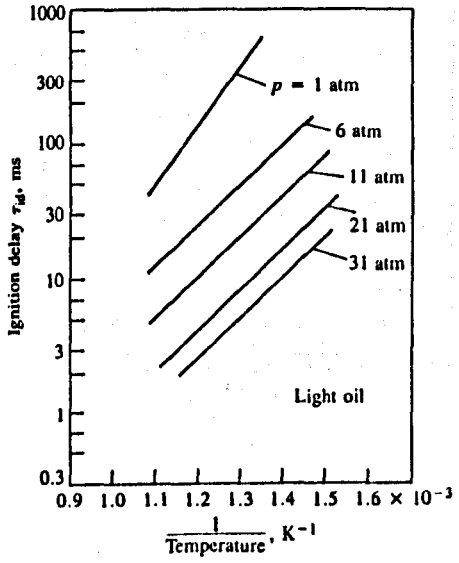

FIGURE 2.3
Ignition delay as function of reciprocal air temperature for light oil spray injected into constant volume combustion bomb. Injection pressure 9.8MPa (100atm). Air pressure indicated. (Igura et al, 1975)

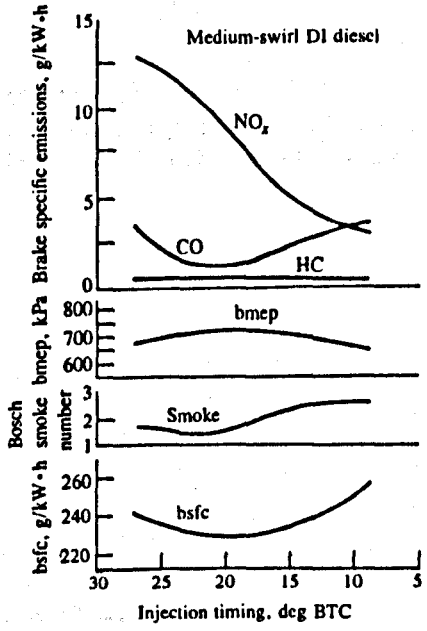

FIGURE 2.4
Effect of start-of-injection timing on diesel engine performance and emissions for a medium-swirl DI diesel engine with deep combustion bowl and four-hole injector nozzle, 2600 rev/min, fuel delivery 75mm^3/cycle. (Heywood, 1988)

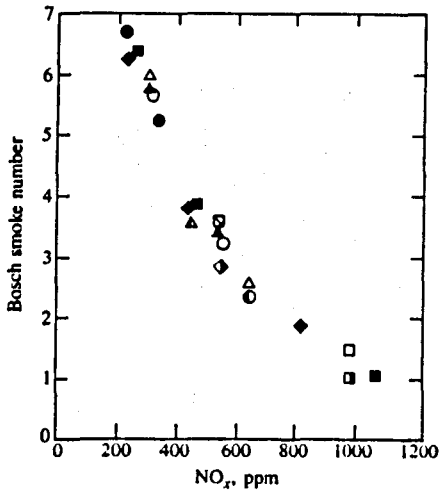

FIGURE 2.5
Tradeoff between NO_x and smoke emissions for a quiescient single-cylinder DI diesel engine with bore = 140mm , stroke = 152mm , CR = 14.3:1 , eight-hole injector nozzle. Various speeds, fueling rates, injection timings, injection pressures, % EGR; constant AFR = 25:1. (Heywood,1988)

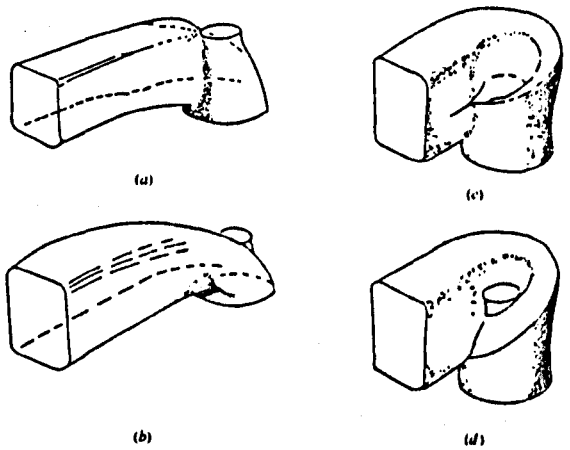

FIGURE 2.6
Different types of swirl-generating inlet ports: (a) deflector wall; (b) directed; (c) shallow ramp helical; (d) steep ramp helical. (Heywood 1988)

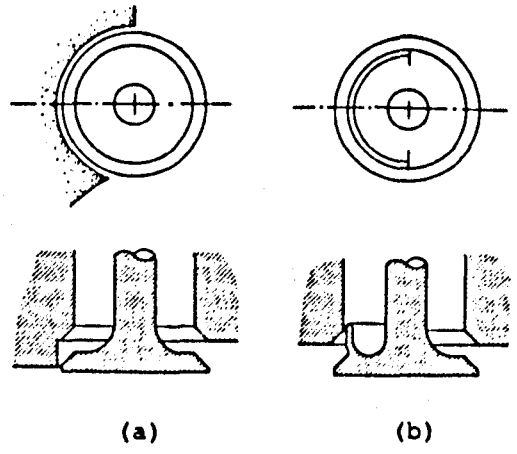

FIGURE 2.7
(a) Masked cylinder head and (b) shrouded inlet valve approaches for producing swirl during induction. (Heywood, 1988)

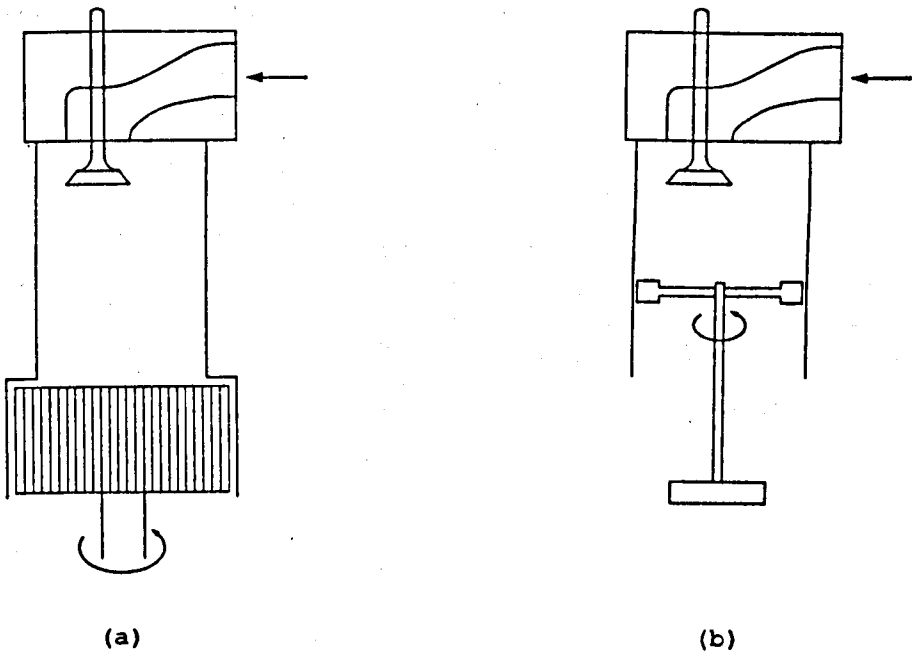

FIGURE 2.8
Schematic of steady-flow swirl meters: (a) impulse torque meter, (b) paddle wheel meter.

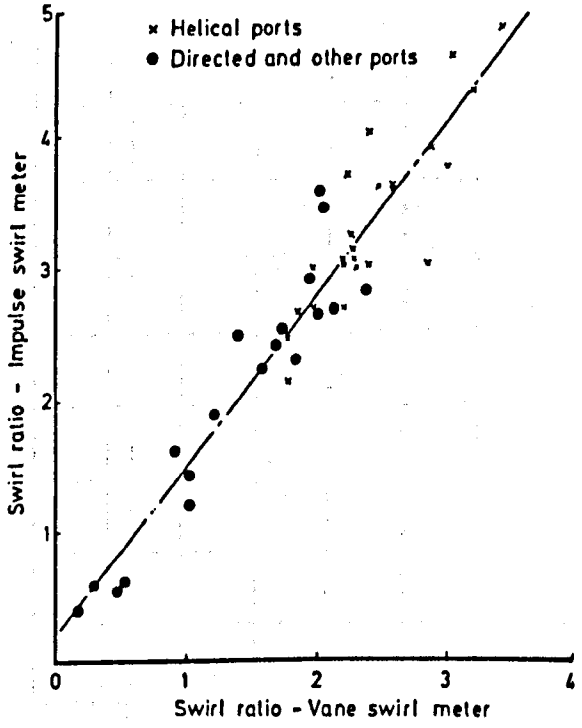

FIGURE 2.9
Comparison of impulse and paddle wheel swirl meter readings. (Monaghan and Pettifer, 1981)

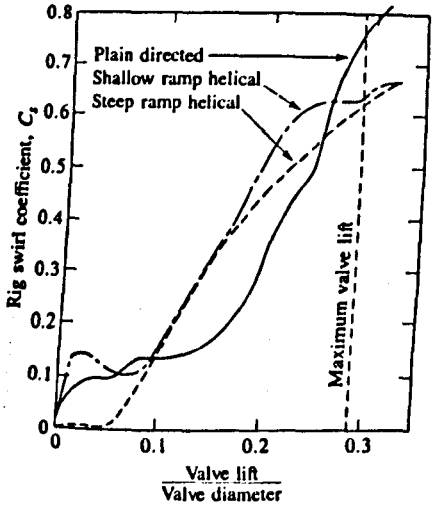

FIGURE 2.10
Steady-state torque meter swirl measurements of directed, shallow ramp helical, and steep ramp helical ports as a function of inlet valve lift/diameter ratio. (Heywood, 1988)

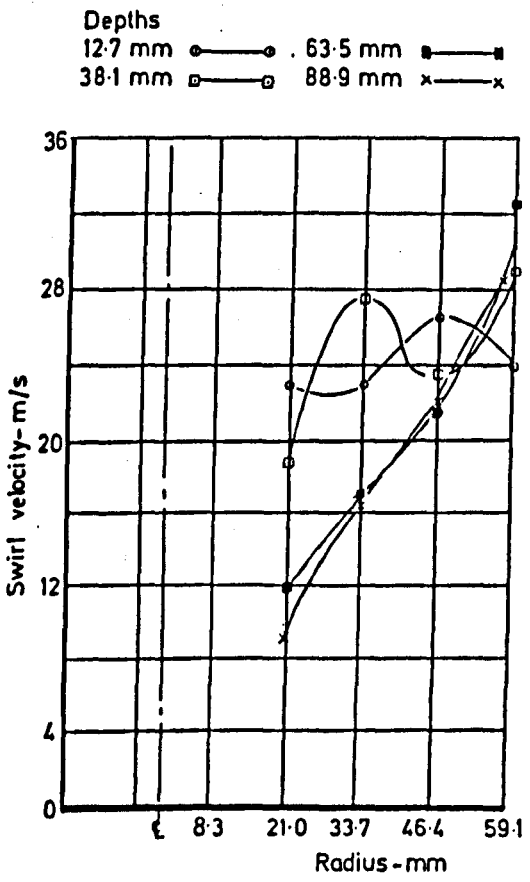

FIGURE 2.11
Variation of swirl velocity with radius at end of induction. Shallow ramp helical port, 24 rev/s. (Monaghan and Pettifer, 1981)

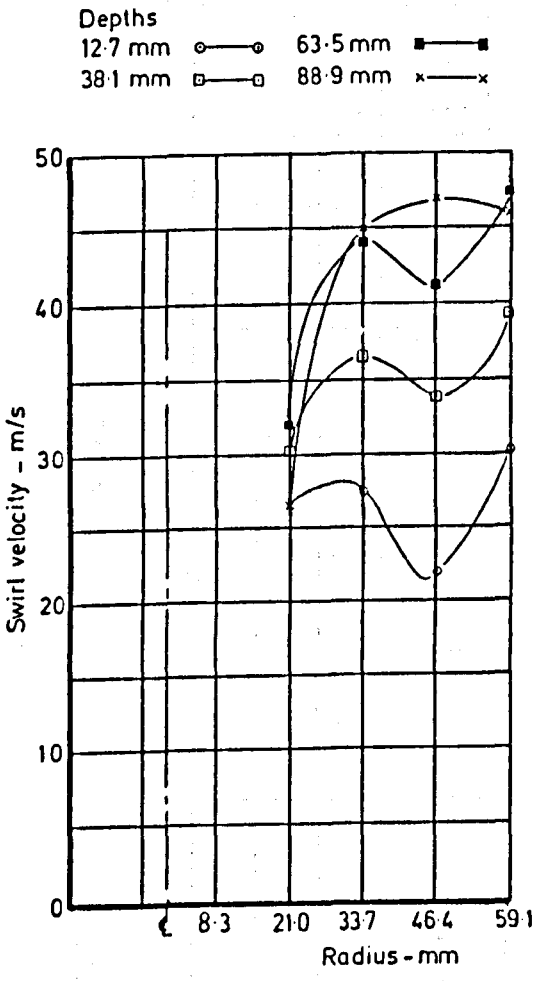

FIGURE 2.12
Variation of swirl velocity with radius at end of induction. Shallow ramp helical port, 40 rev/s. (Monaghan and Pettifer, 1981)

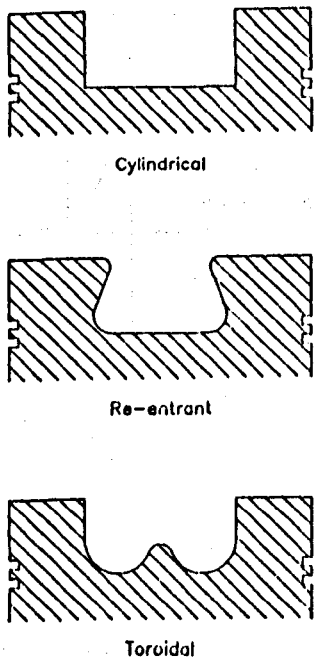

FIGURE 2.13
Three common designs of bowl-in-piston combustion chamber for DI diesel engines.

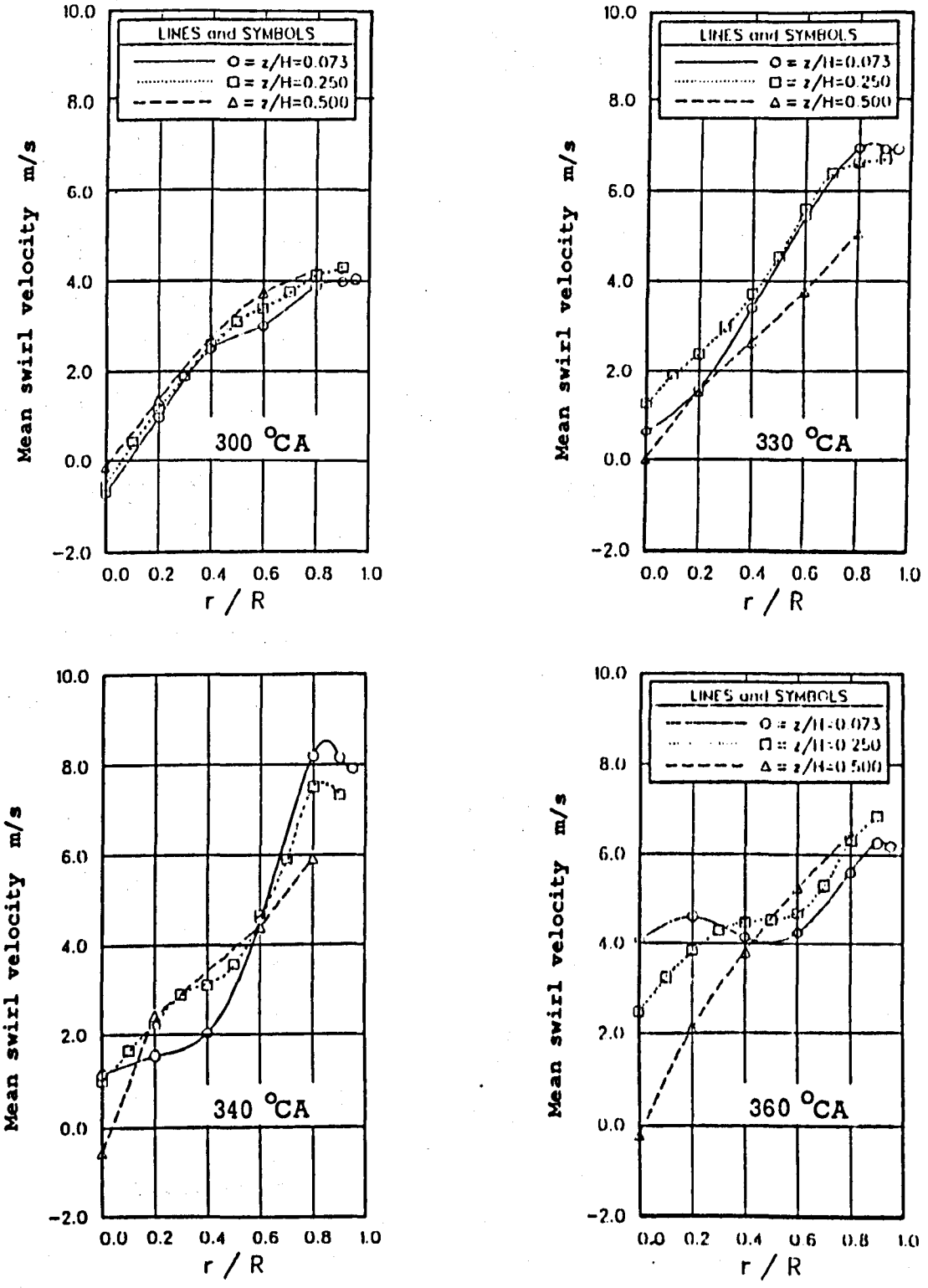

FIGURE 2.14
Radial profiles of mean swirl velocity at three depths. The cylinder axis is defined as the z-axis with the cylinder head as z = 0. H = 41.4 mm is the distance between the cylinder head and the bowl bottom when the piston is at TDC. r is the radial position of the LDV, and R = 28.3 mm is the piston bowl radius. The bump clearance at TDC is 1.1 mm. (Fansler, 1985)

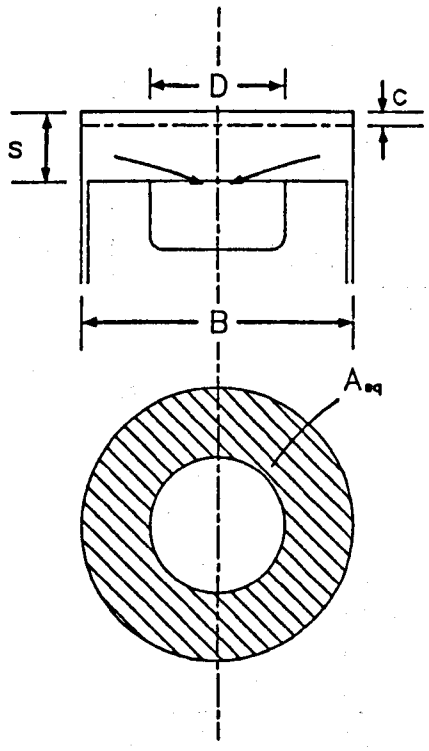

FIGURE 2.15
Schematic of axisymmetric bowl-in-piston combustion chamber.

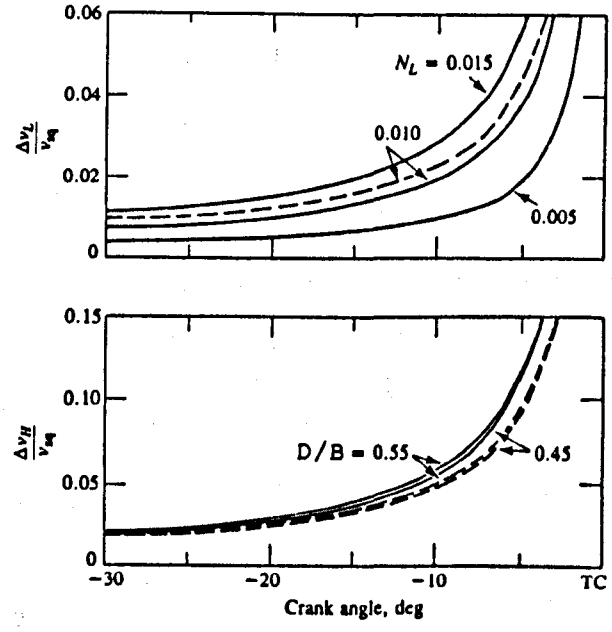

N_L = Dimensionless leakage number
D/B = 0.45 ———
D/B = 0.55 - - - -
c/L = 0.011
γ = 1.4

c/L = 0.011 ———
c/L = 0.027 - - - -
γ = 1.35

FIGURE 2.16
Values of squish velocity decrement, at 1500 rev/min, due to leakage ΔV_L and heat transfer ΔV_H, normalised by the ideal squish velocity, as a function of crank angle. B is the cylinder bore, D is the bowl diameter, c is the distance between the cylinder head and the piston crown when the piston is at TDC, and L is the stroke. (Shimamoto and Akiyama, 1970)

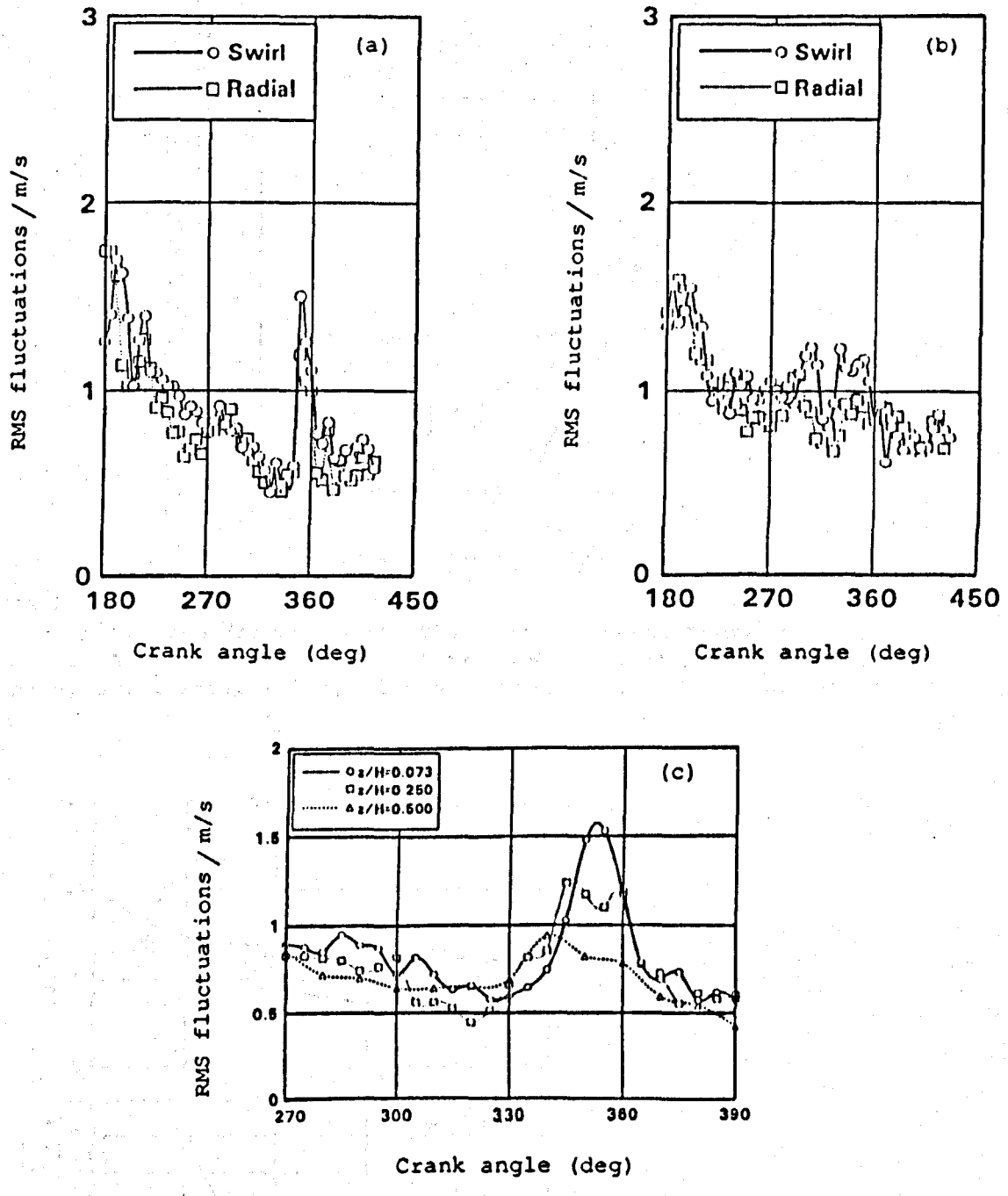

FIGURE 2.17
Results for ensemble-averaged rms velocity fluctuations at 600 rev/min; (a) near squish dominated region, r/R = 0.95, z/H = 0.073; (b) nearer the cylinder axis, r/R = 0.4, z/H = 0.073. (c) Ensemble-averaged rms velocity fluctuation intensity at three depths, r/R = 0.8. (Fansler, 1985)
z is the cylinder axis with the cylinder head as z = 0, H = 41.4 mm is the distance between the cylinder head and the bowl bottom when the piston is at TDC, r is the radial position of the LDV, and R = 23.8 mm is the piston bowl radius. The bump clearance at TDC is 1.1 mm.

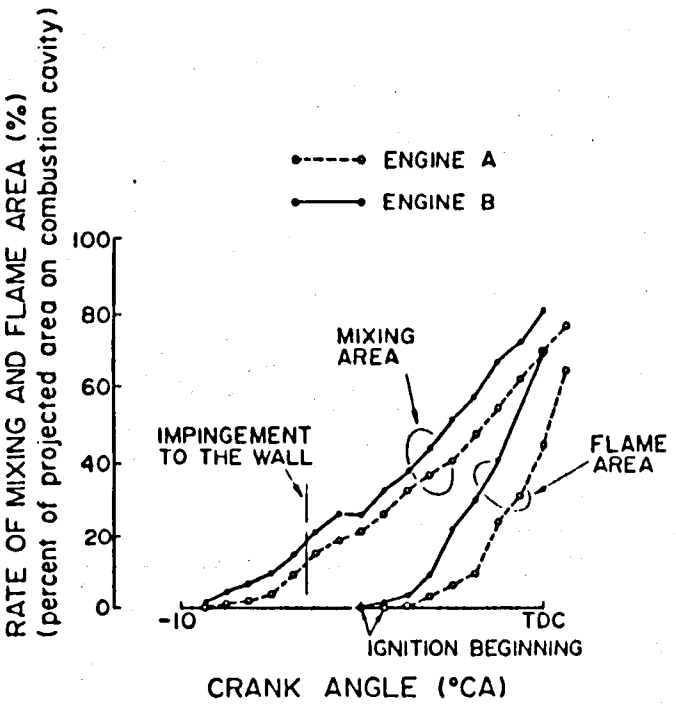

FIGURE 2.18
Process of mixture formation and flame development. Dynamic injection timing 10°CA BTDC. Engine A, swirl ratio = 2.6, with low turbulence; engine B, swirl ratio = 2.1, with high turbulence. (Shiozaki et al 1980)

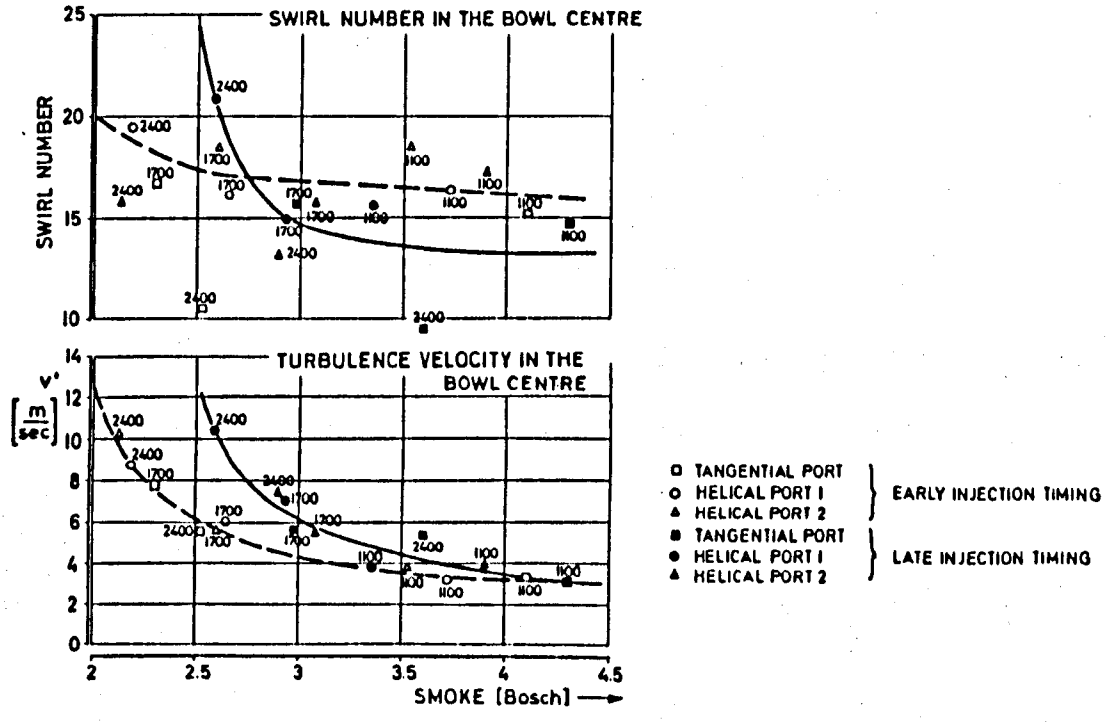

FIGURE 2.19
Swirl number and turbulence velocity, in the centre of the bowl, versus smoke. v' is an average figure over upper and lower part on the inner radius (bowl centre). (Brandl et al, 1979)

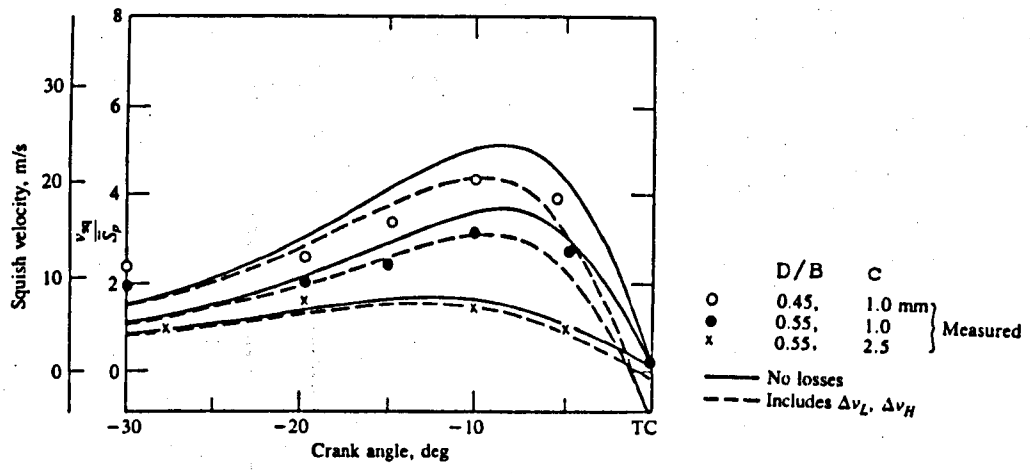

FIGURE 2.20
Comparison of measured squish velocities in bowl-in-piston combustion chambers, with different bowl diameter/bore ratios and clearance heights. B is the cylinder bore, D is the bowl diameter, c is the distance between the cylinder head and piston crown when the piston is at TDC, L is the stroke and S_p is the mean piston speed. See Fig 2.16 for definition of other terms. (Shimamoto and Akiyama, 1970)

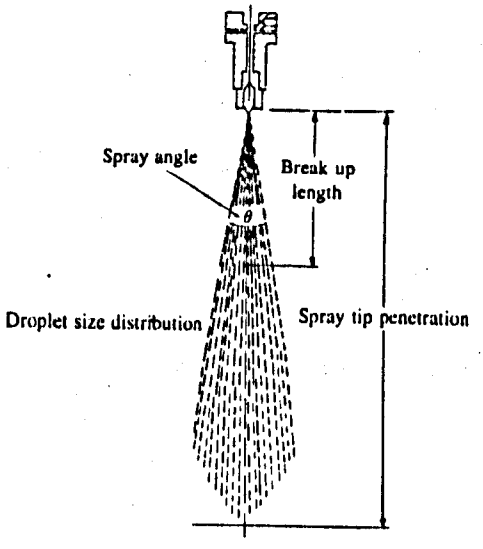

FIGURE 2.21
Schematic of diesel fuel spray defining its major parameters. (Heywood, 1988)

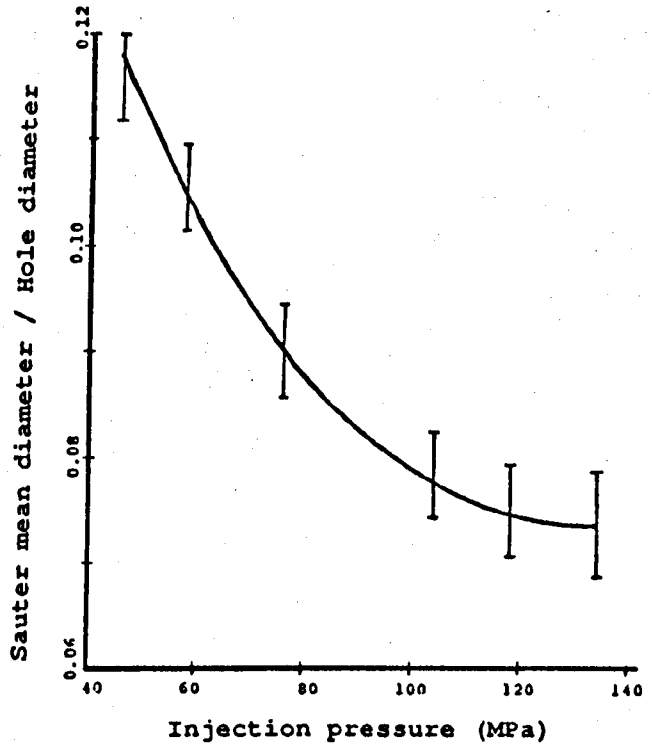

FIGURE 2.22
Effect of injection pressure on Sauter mean diameter. (Varde et al, 1984)

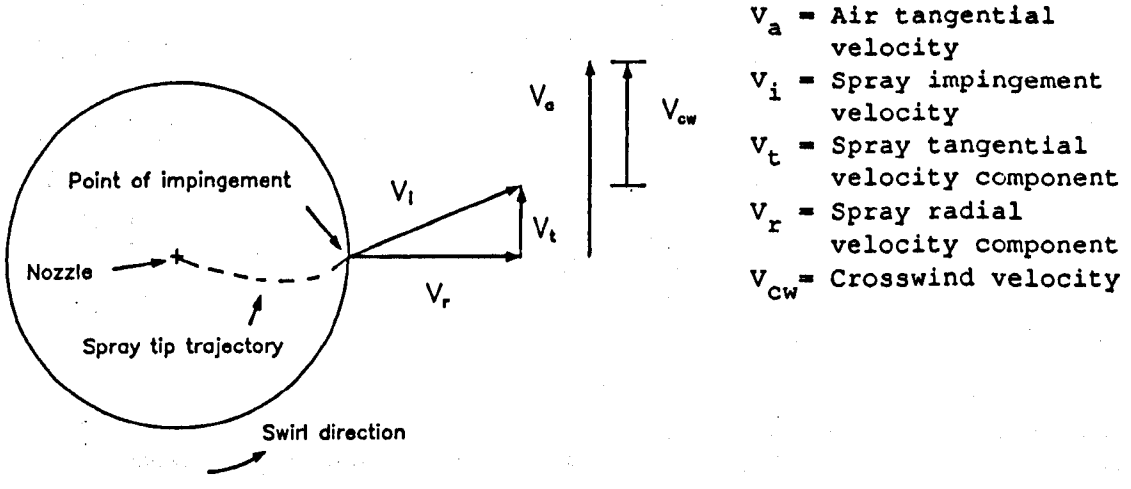

FIGURE 2.23
Interaction of fuel spray with swirling air at impingement, definition of crosswind velocity. (Timoney, 1985)

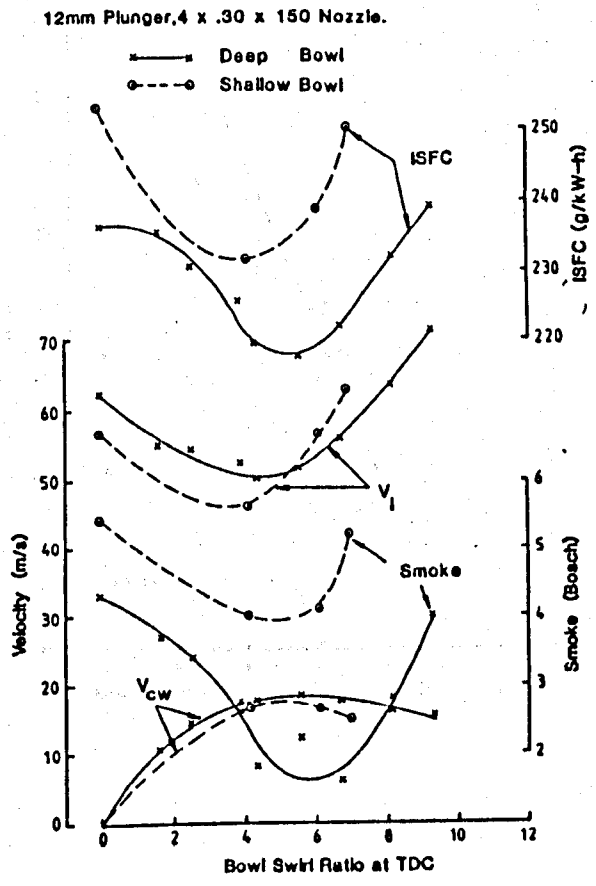

FIGURE 2.24
Correlation of spray impingement velocity, and crosswind velocity with ISFC and smoke. Ricardo E16, 40 rev/s, 19:1 AFR. (Timoney, 1985)
See Fig 2.23 for definition of terms.

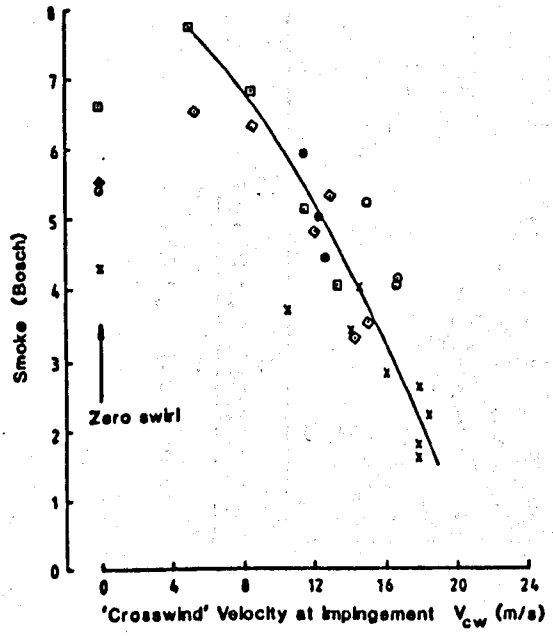

Deep Bowl, 12 mm Plunger.
Shallow Bowl, 12 mm Plunger.
Deep Bowl, 10 mm Plunger.
Shallow Bowl, 10 mm Plunger.
Deep Bowl, 8 mm Plunger.

FIGURE 2.25
Correlation between measured exhaust smoke and calculated crosswind velocity at impingement. Ricardo E16, 40 rev/s, 19:1 AFR. (Timoney, 1985)

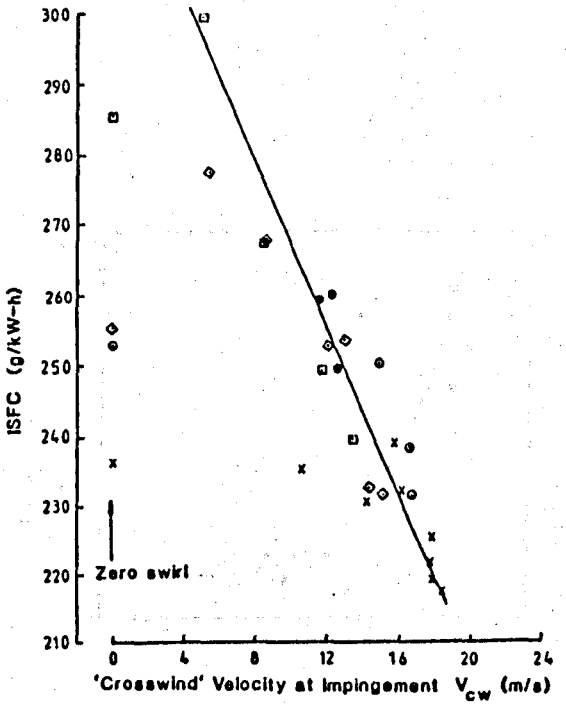

FIGURE 2.26
Correlation between measured ISFC and calculated crosswind velocity at impingement. Ricardo E16, 40 rev/s, 19:1 AFR, all swirl ratios. (Timoney, 1985)

× Deep Bowl, 12 mm Plunger.
• Shallow Bowl, 12 mm Plunger.
◆ Deep Bowl, 10 mm Plunger.
□ Shallow Bowl, 10 mm Plunger.
● Deep Bowl, 8 mm Plunger.

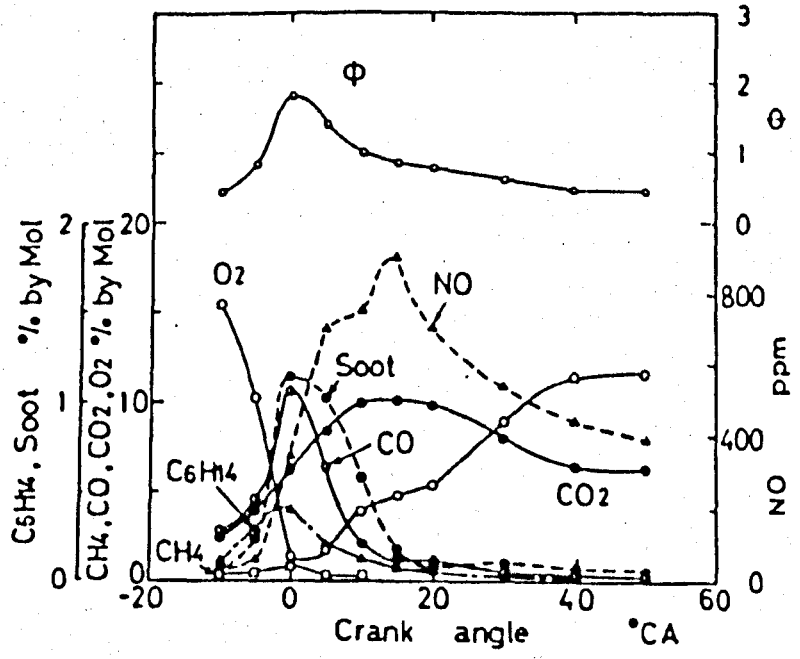

FIGURE 2.27
Time histories of equivalence ratio ϕ, and concentrations of oxygen and combustion products obtained by in-cylinder gas sampling. (Kamimoto et al, 1980)

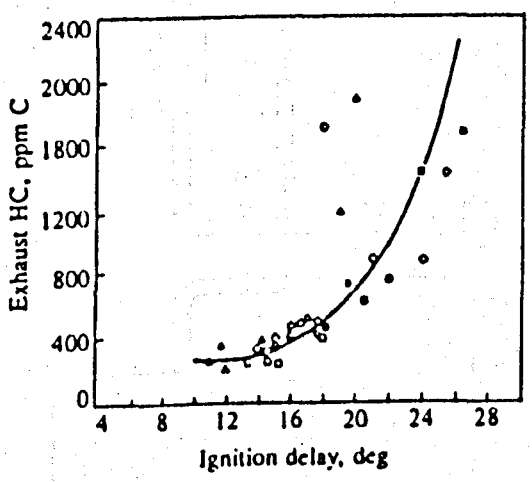

FIGURE 2.28
Influence of ignition delay on HC in the exhaust. (DI diesel engien at 2800 rev/min and various boost pressures, fuels, loads, injection timings). (Greeves et al, 1977)

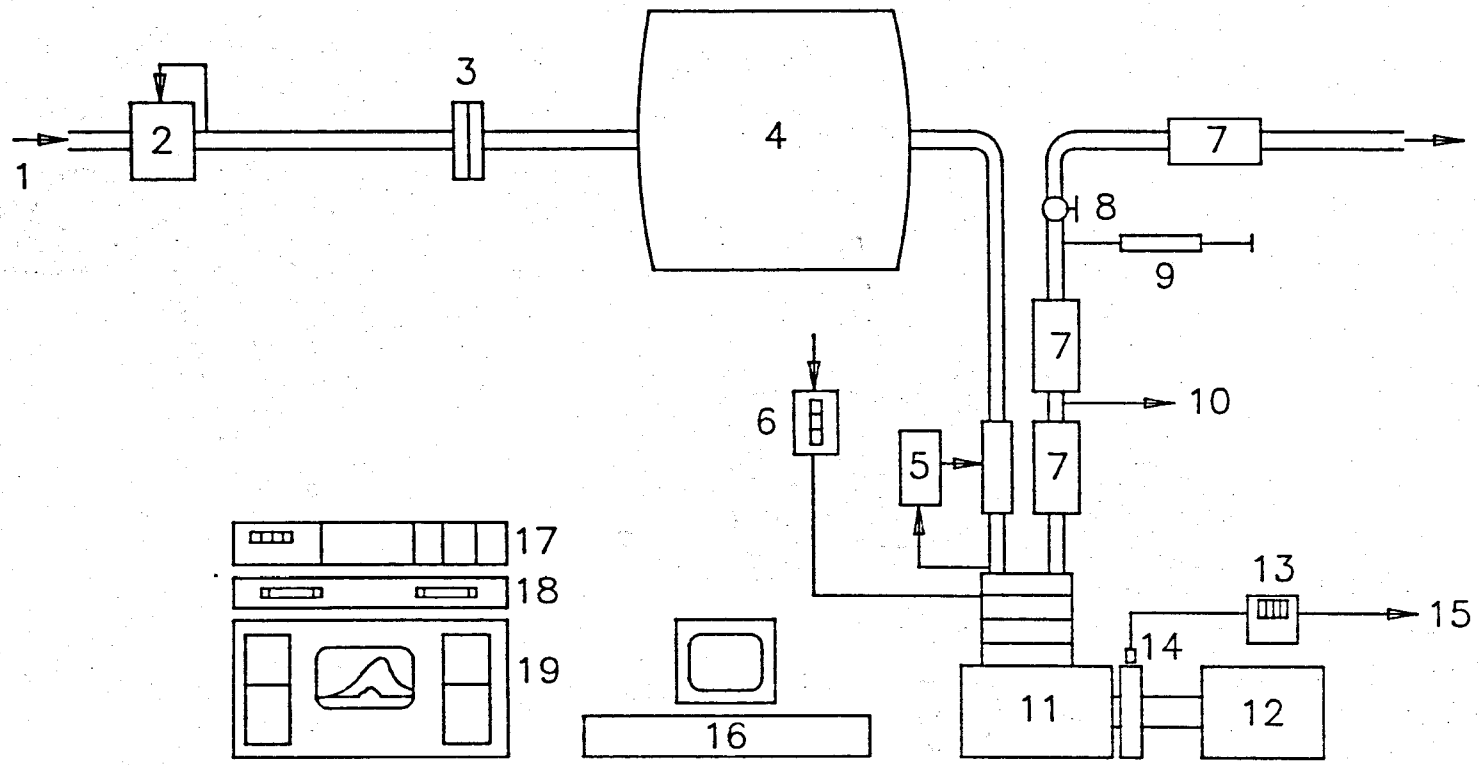

1. Air in
2. Pressure regulator
3. Orifice plate
4. Surge tank
5. Heater controller
6. Fuel flow meter
7. Silencer
8. Back–pressure valve
9. Bosch smoke meter
10. Exhaust–gas sample
11. Engine
12. Dynamometer
13. Speed meter
14. Crank angle sensor
15. To data acquisition
16. Microcomputer
17. Signal processing system
18. Disk drives
19. Data acquisition system

FIGURE 3.1
Schematic diagram of the experimental facilities.

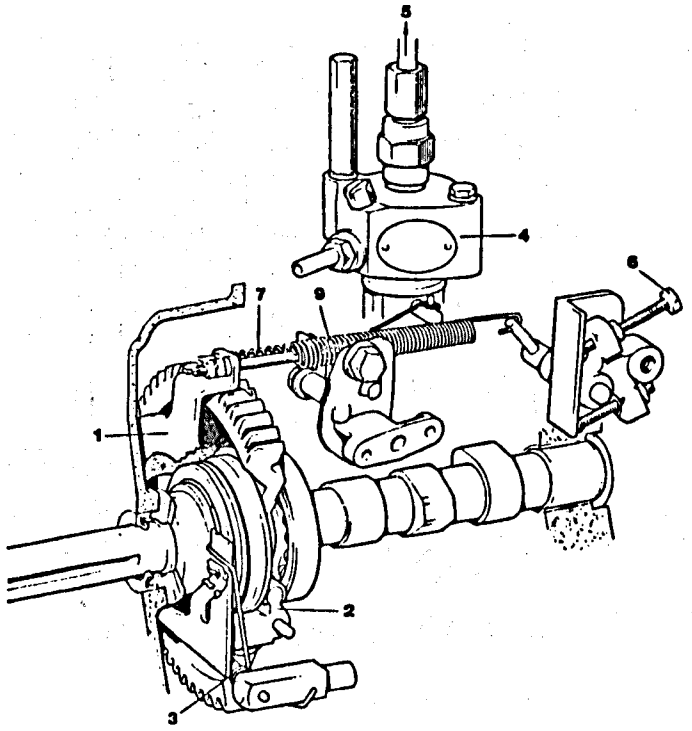

(a)

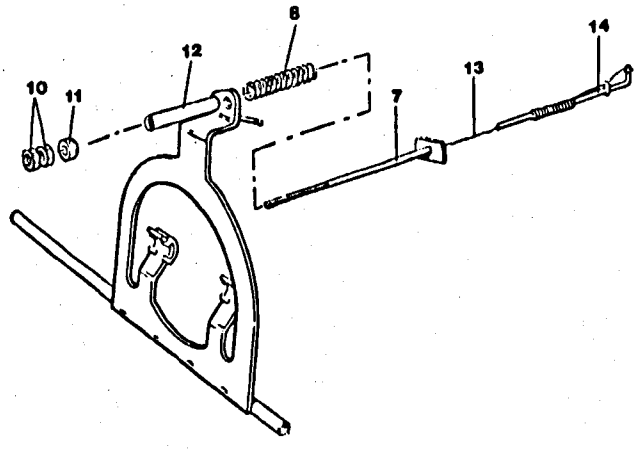

(b)

1. Governor Arm Plate
2. Governor Centrifugal Weights
3. Governor Spring
4. Fuel Pump
5. To Fuel Injector
6. Speed Setting Arm
7. Governor/Fuel Rack Link
8. Governor/Fuel Rack Link Spring
9. Speeder Spring
10. Governor/Fuel Rack Link Adjuster/Locknuts
11. Swivel Spacer
12. Governor Arm Plate Extension
13. Flexible Wire (Added)
14. Fuel Rack Link

FIGURE 3.2
Governor system: (a) installation; (b) detail and modifications.

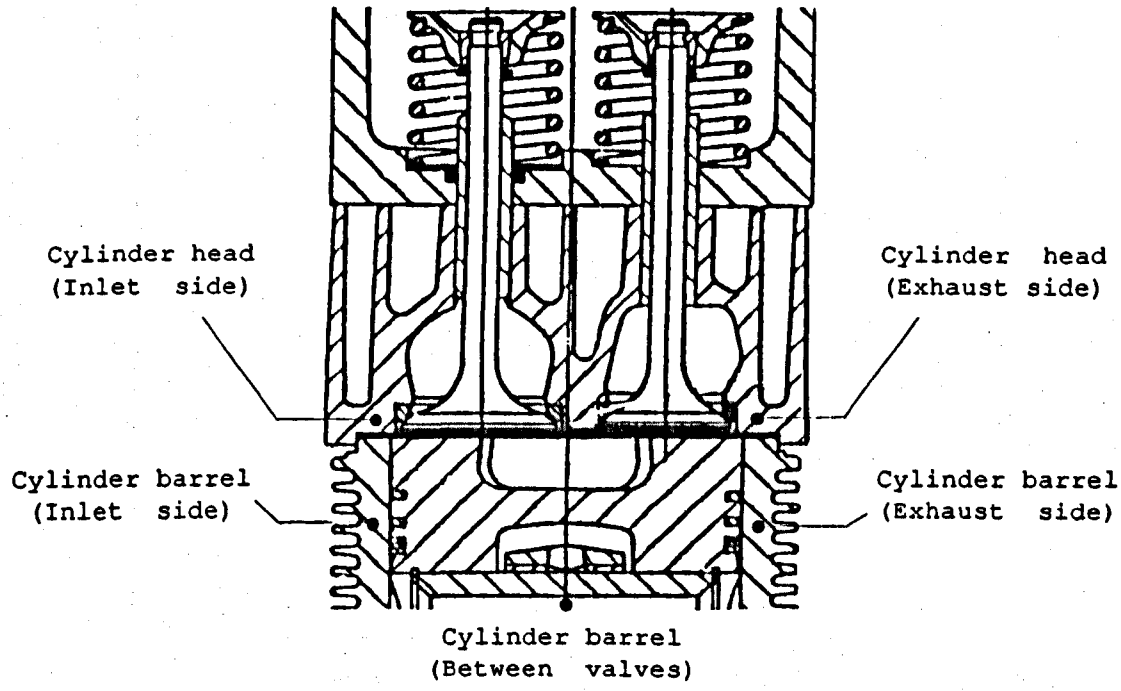

FIGURE 3.3
Location of thermocouples for the measurement of metal temperatures around the cylinder head and cylinder barrel.

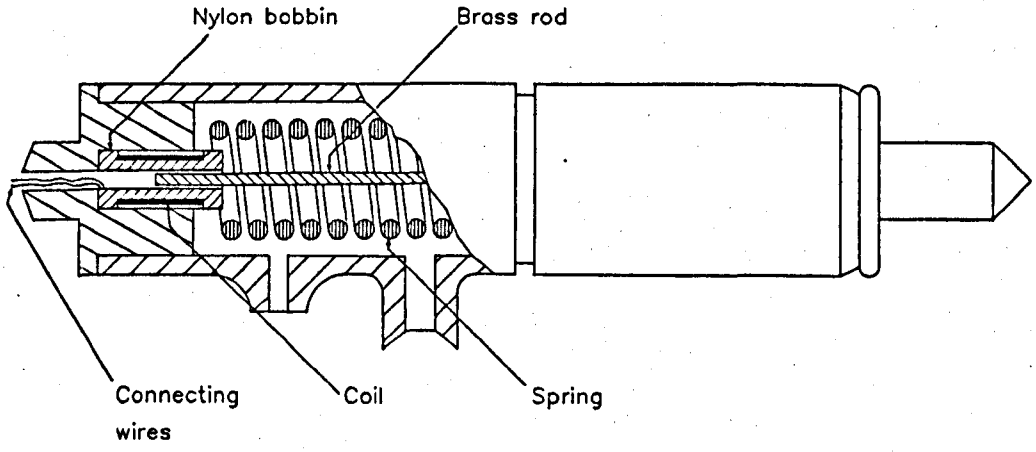

FIGURE 3.4
Diagram showing the installation of the injector needle-lift signal generating assembly.

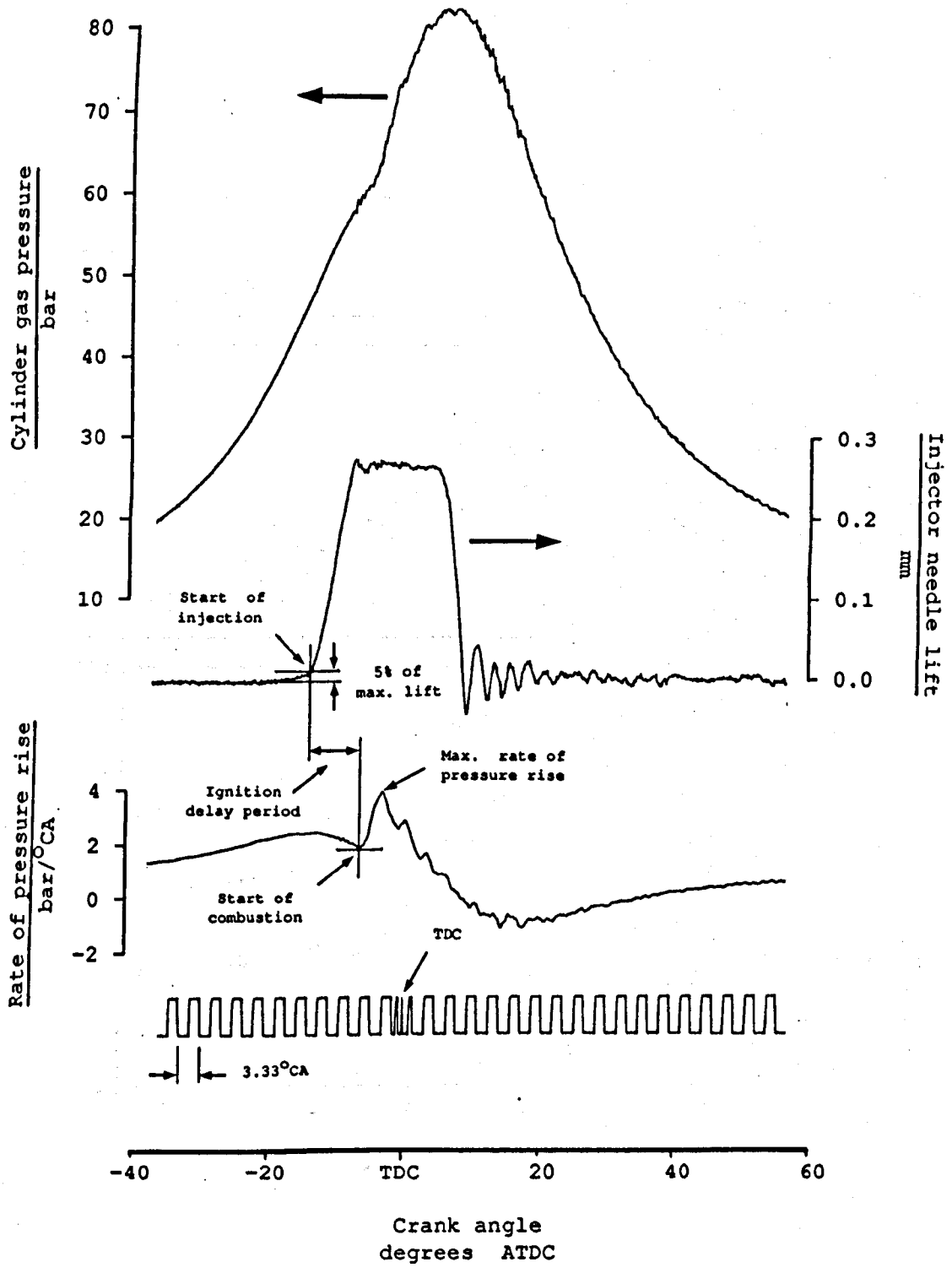

FIGURE 3.5
Typical signals of cyclic parameters and method used to determine start of injection, start of combustion, maximum rate of pressure rise, and maximum cylinder gas pressure.

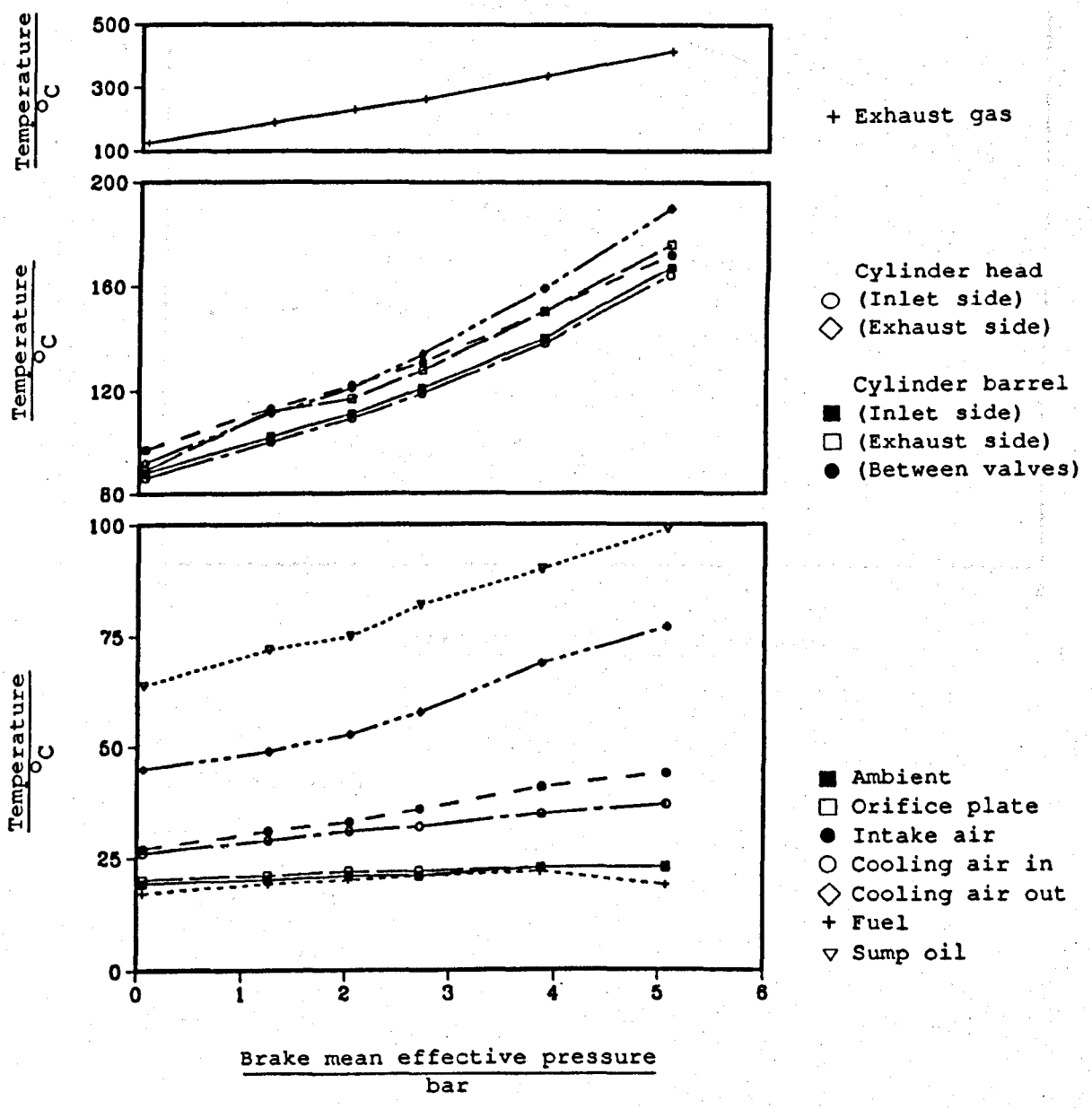

FIGURE 3.6
Variation of temperature at a number of locations with brake mean effective pressure at constant speed of 1300 rev/min. (baseline tests)

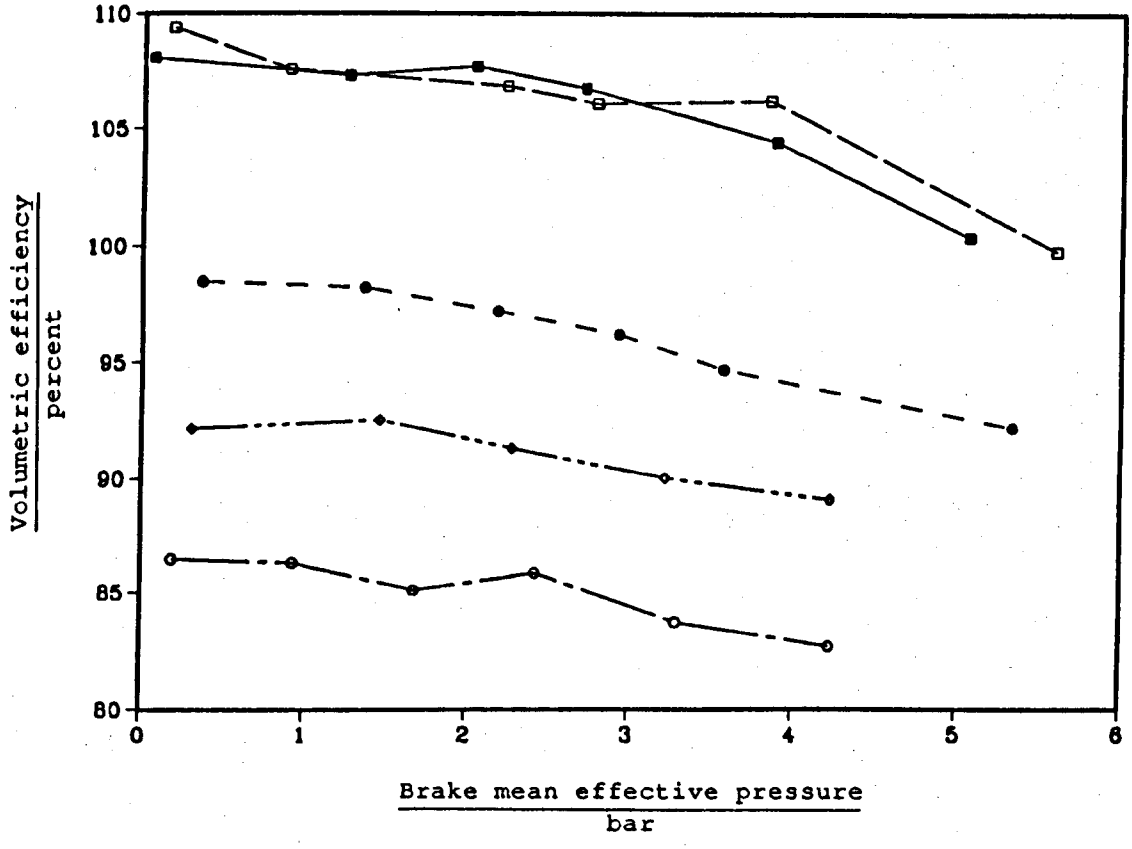

FIGURE 3.7
Effect of engine load and speed on the volumetric efficiency, (naturally aspirated conditions with the surge tank and the associated pipework connected).

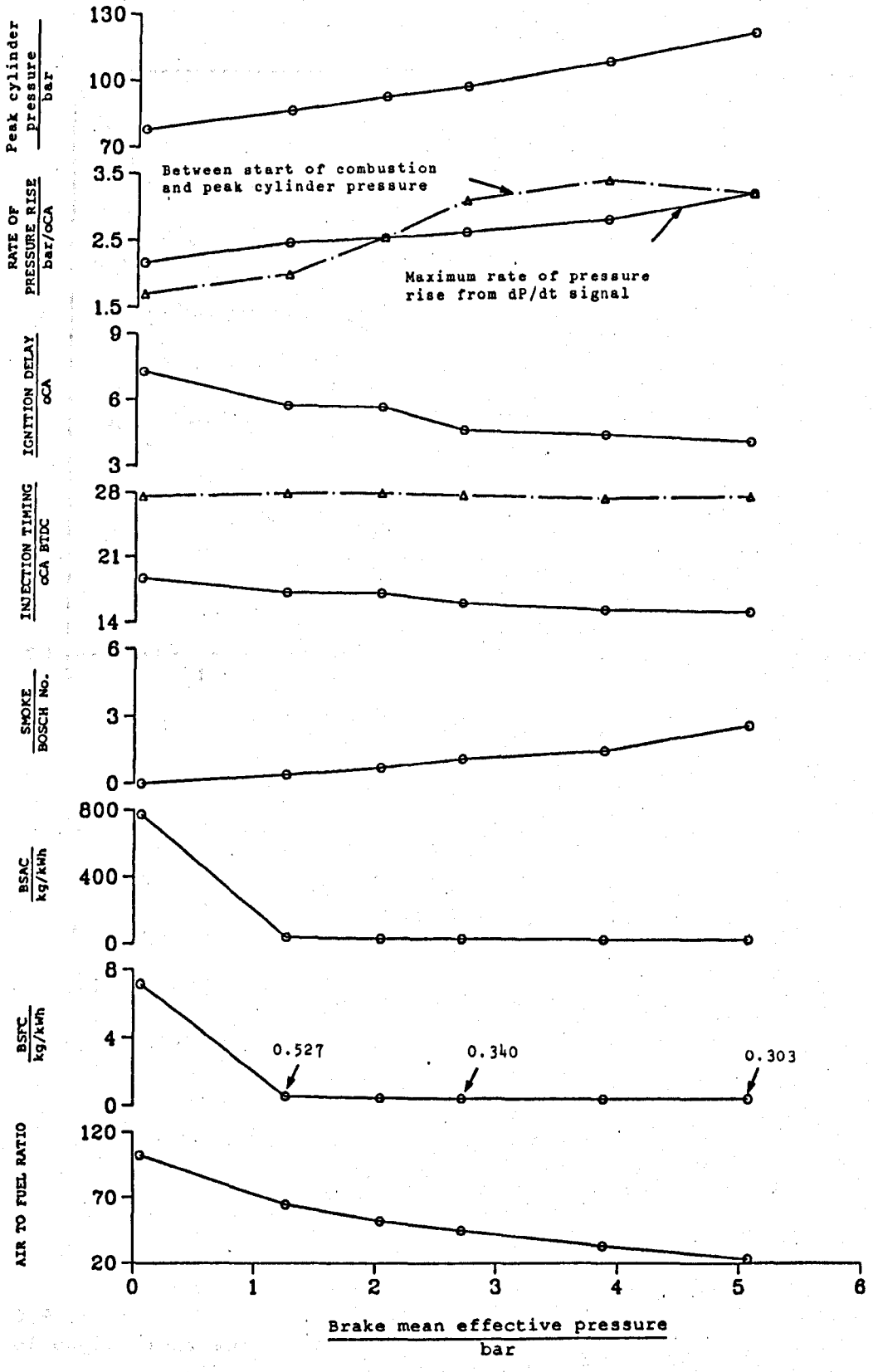

FIGURE 3.8
Typical results at 1300 rev/min obtained from the baseline tests.

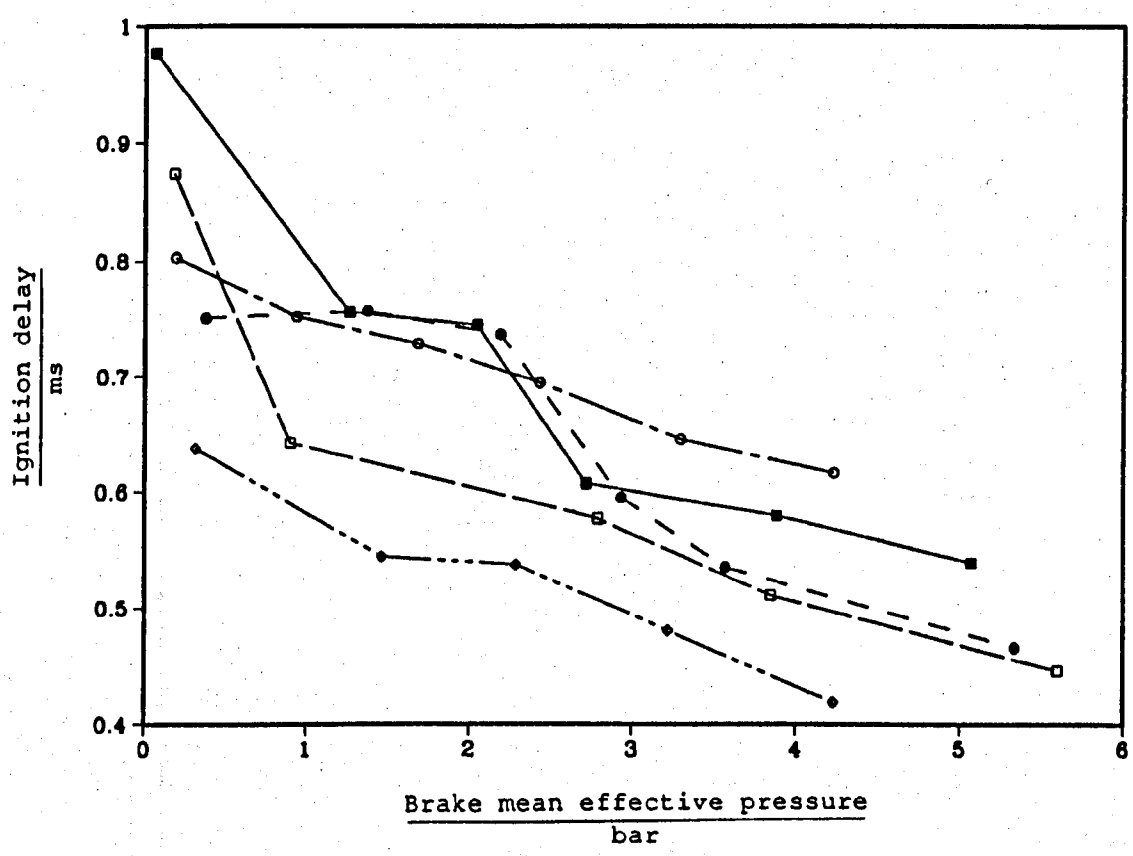

FIGURE 3.9
Effect of engine load and speed on ignition delay.

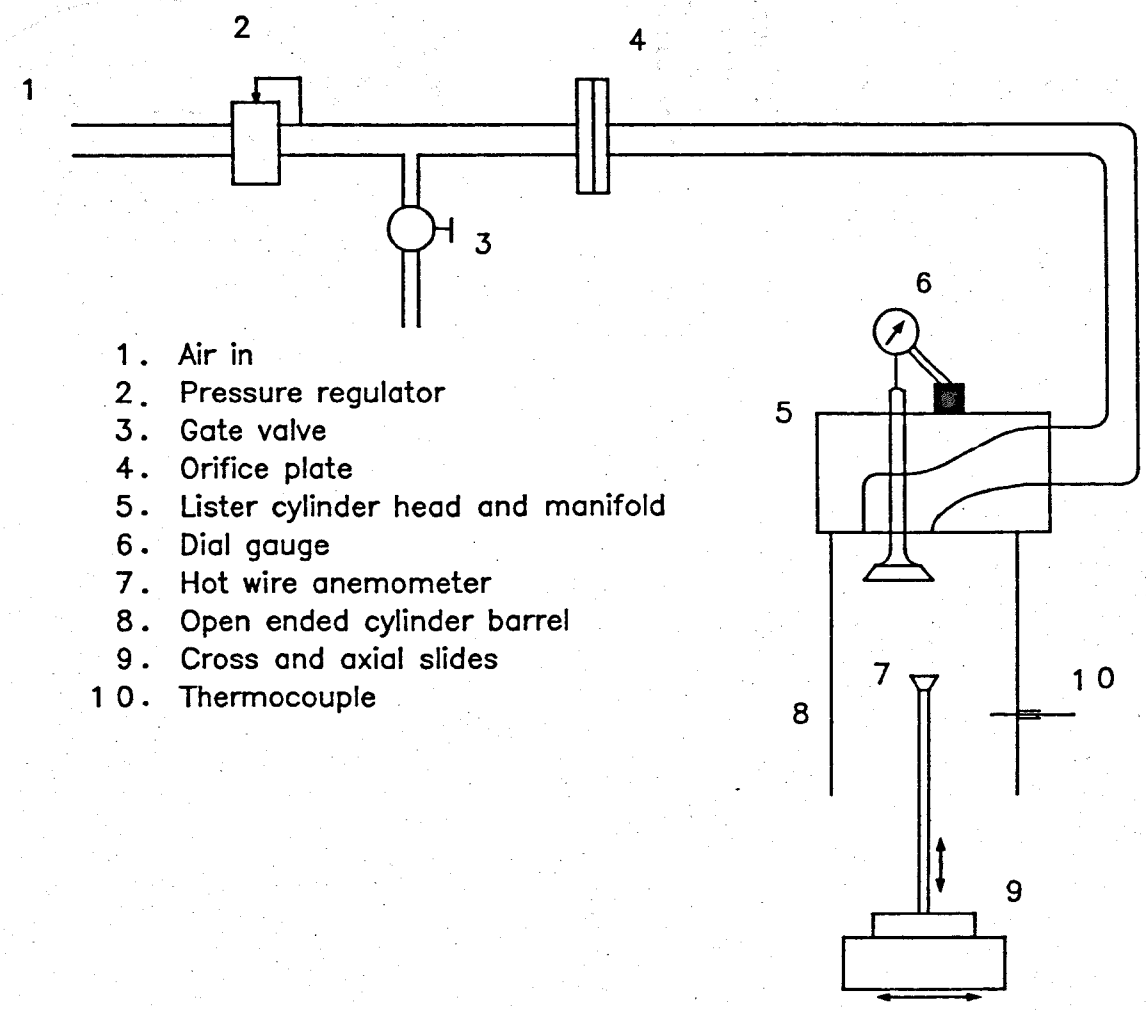

FIGURE 3.10
Schematic drawing of the steady flow rig.

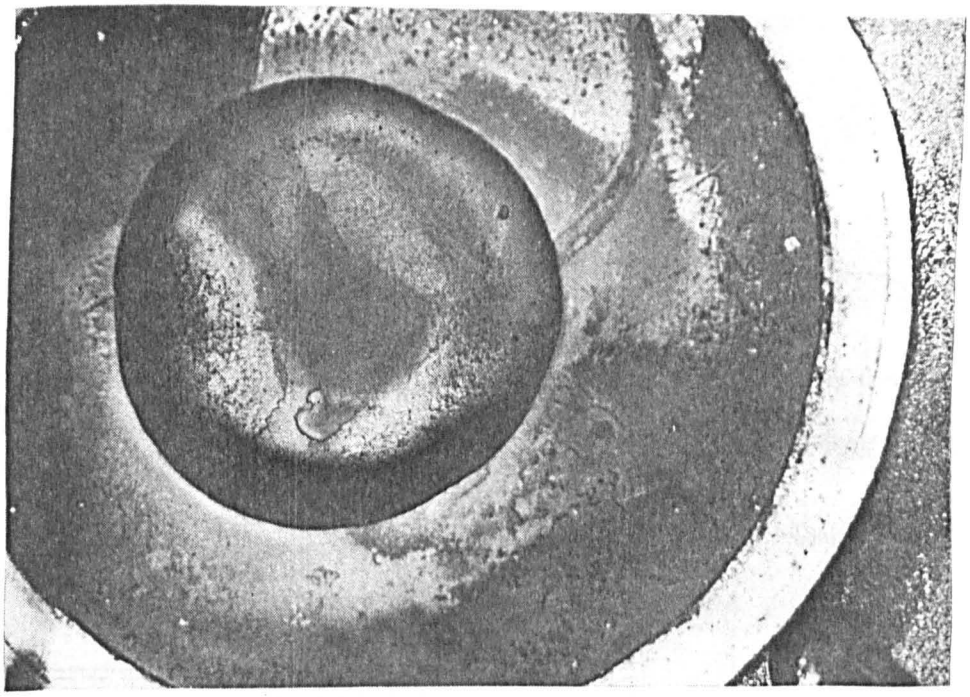

FIGURE 3.11
Photograph of the Lister piston crown showing carbon deposits due to fuel spray impingement; observed at the end of tests with the three-hole nozzle at 12.9:1 compression ratio.

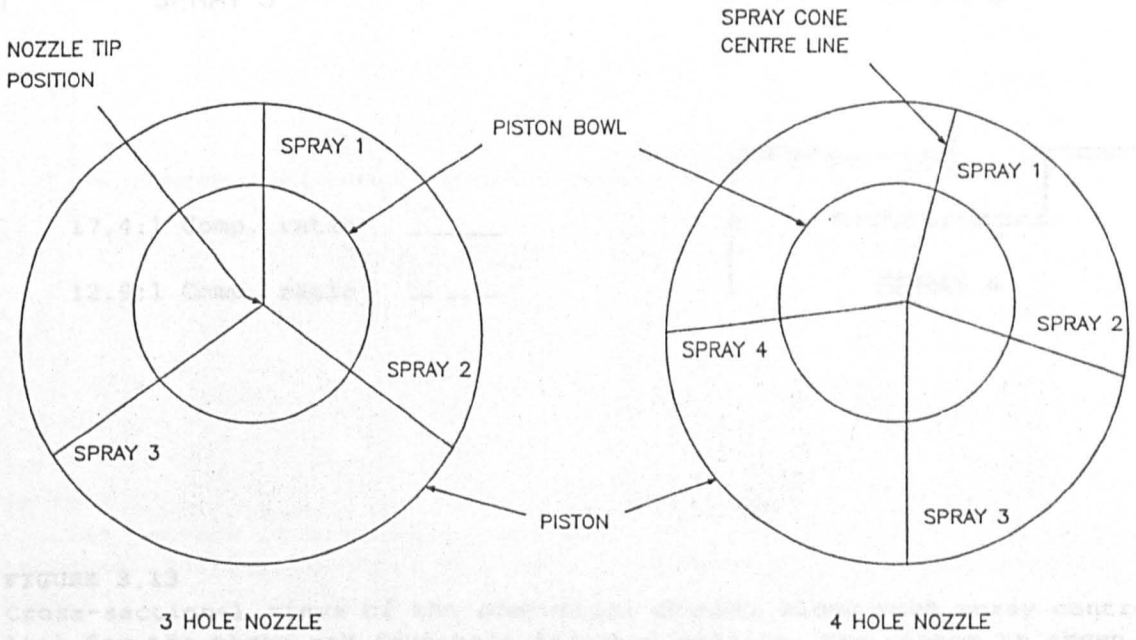

FIGURE 3.12
Diagram showing the piston crown, position of the injector, and fuel-spray centre-lines for the three and four-hole injector nozzles.

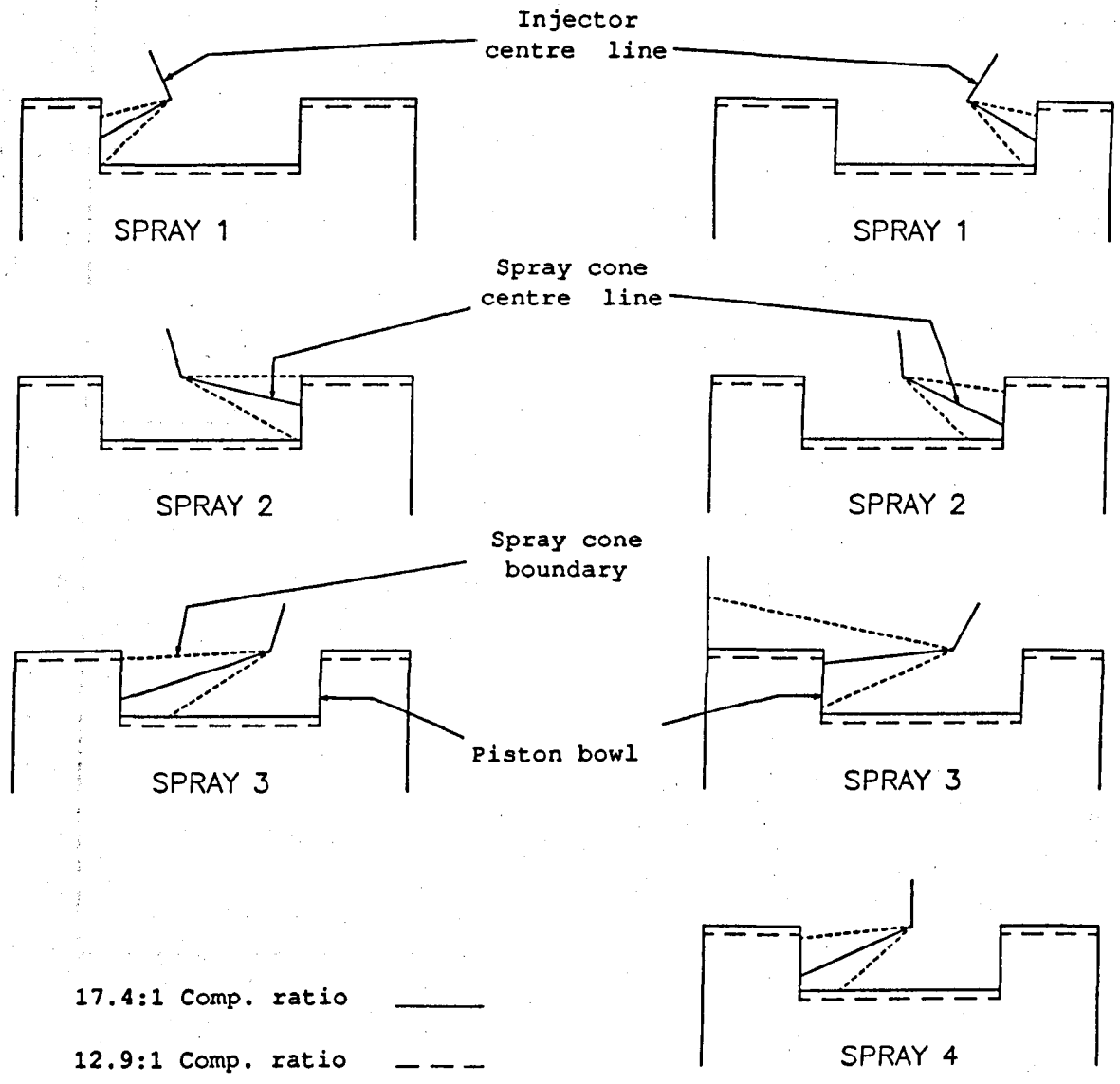

FIGURE 3.13
Cross-sectional views of the combustion chamber along each spray centre-line for the three and four-hole injector nozzles. The piston is shown at 15°CA BTDC, at compression ratios of 17.4 and 12.9:1. The spray cone angles were corrected to represent conditions at elevated pressure during injection.

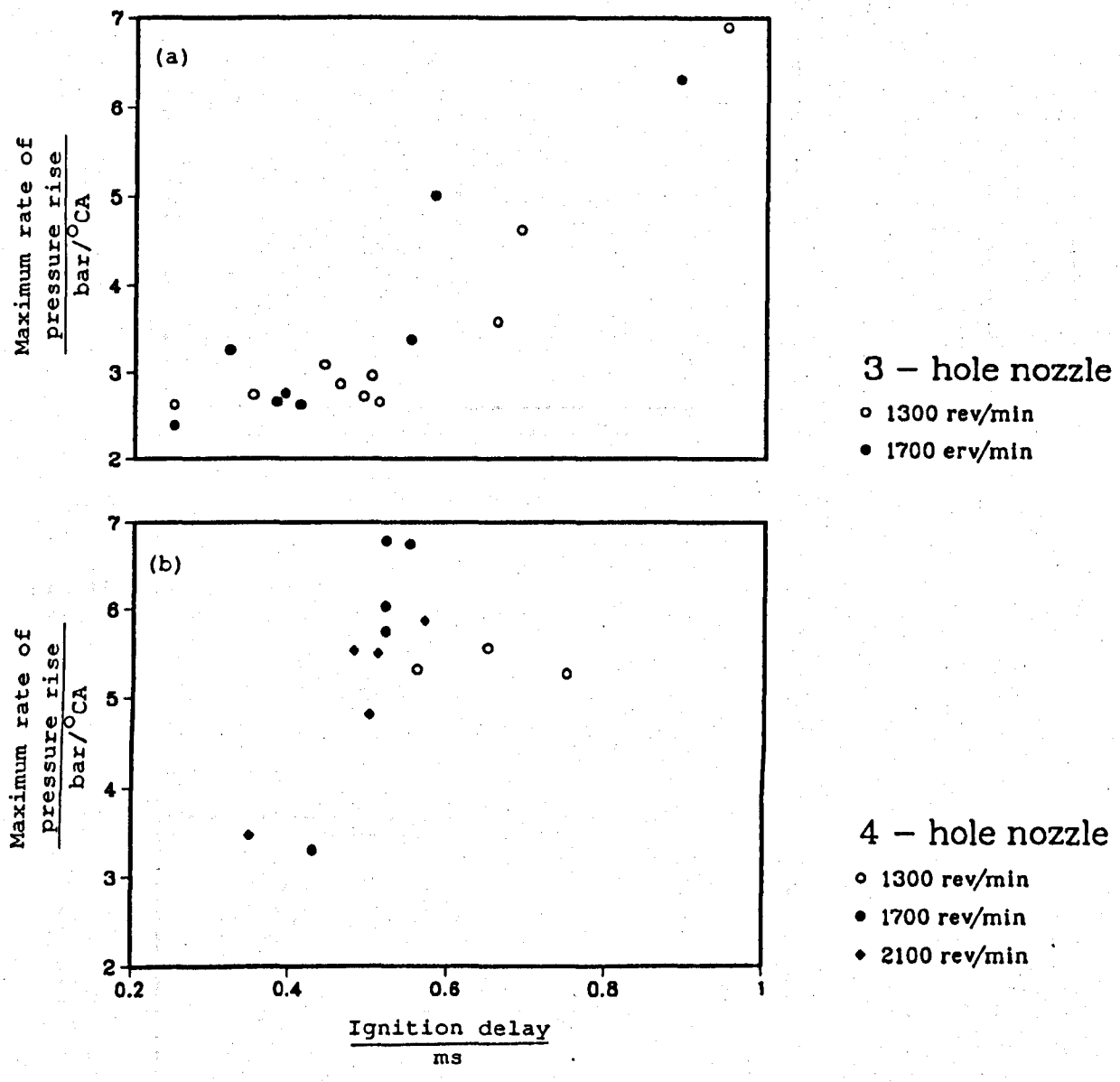

FIGURE 4.1
Relation between ignition delay and maximum rate of pressure rise: (a) Three-hole nozzle; (b) Four-hole nozzle. Results from all engine tests included.

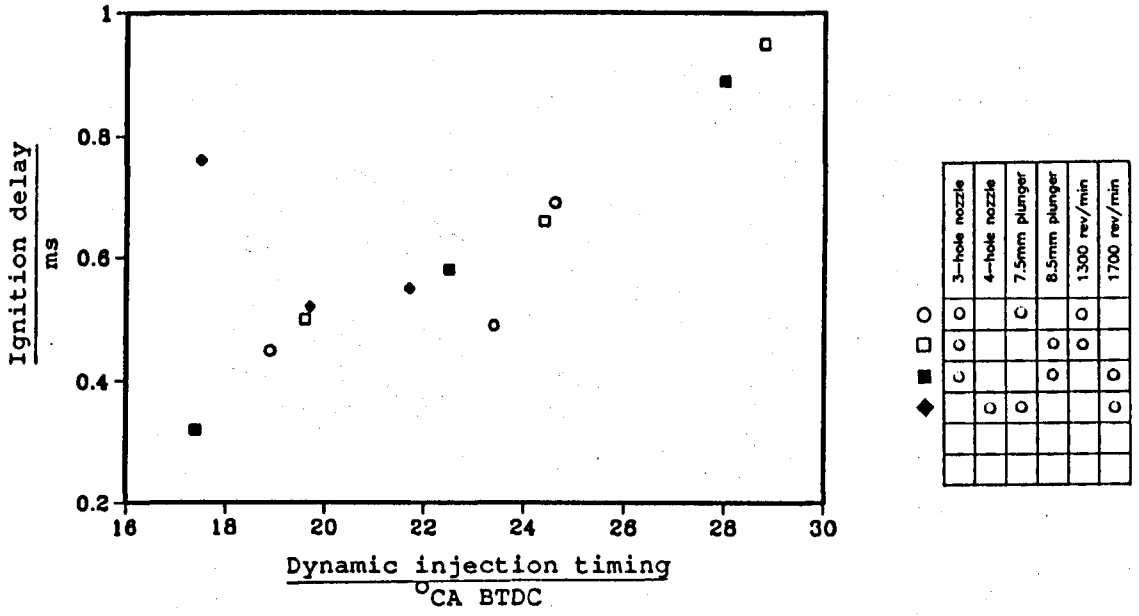

FIGURE 4.2
Effect of dynamic injection timing on ignition delay, (25:1 air fuel ratio).

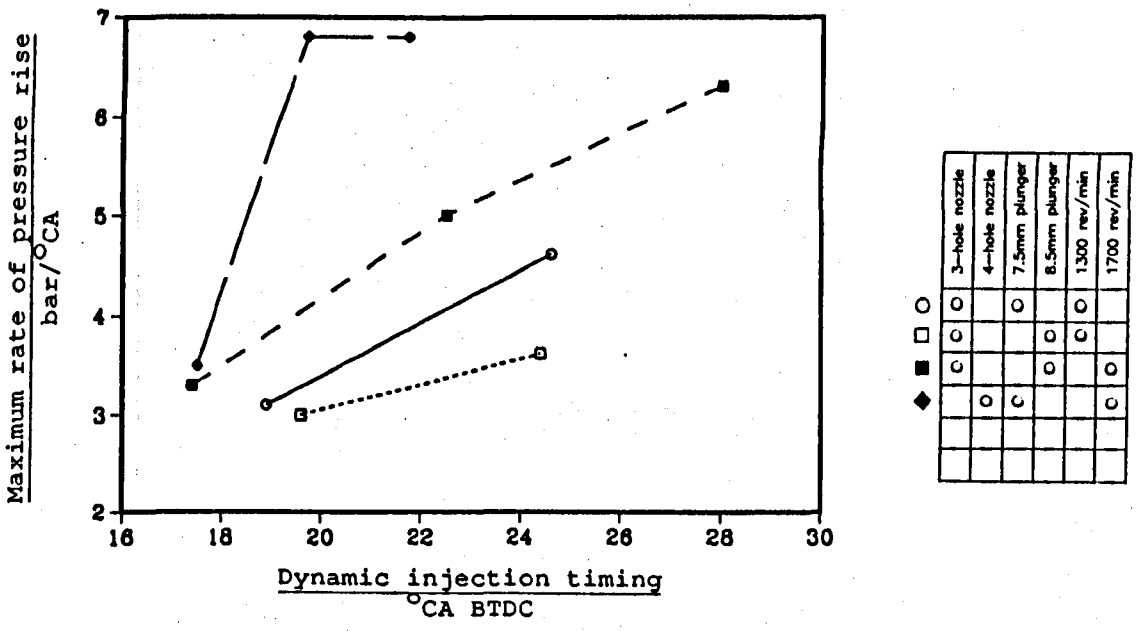

FIGURE 4.3
Effect of dynamic injection timing on maximum rate of pressure rise, (25:1 air fuel ratio).

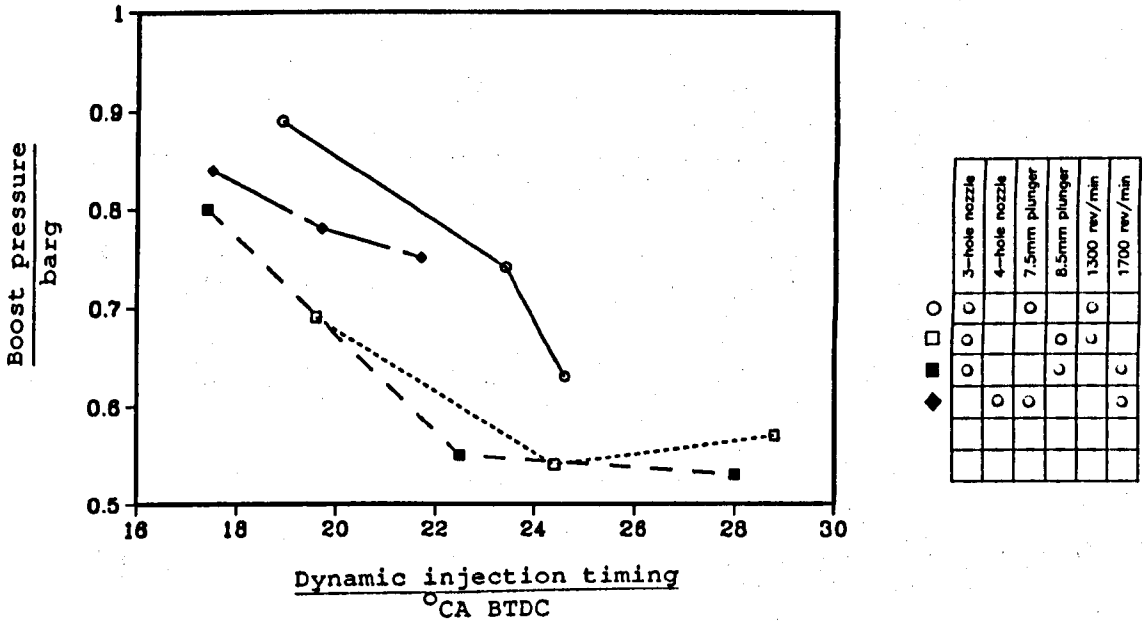

FIGURE 4.4
Effect of dynamic injection timing on boost pressure, (25:1 air fuel ratio).

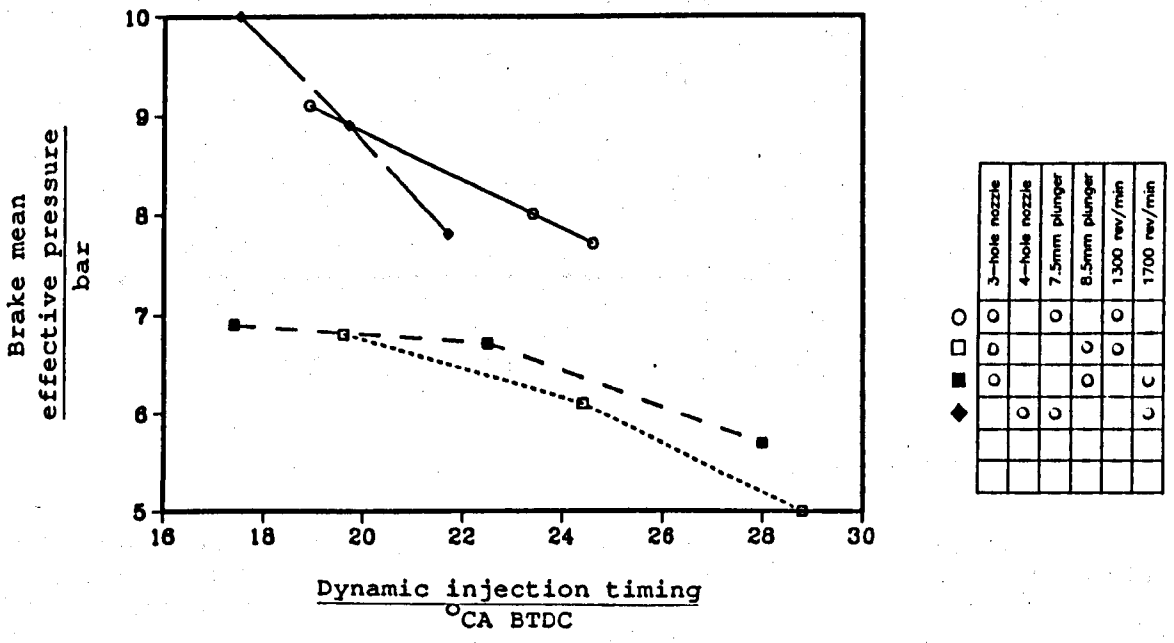

FIGURE 4.5
Effect of dynamic injection timing on brake mean effective pressure, (25:1 air fuel ratio).

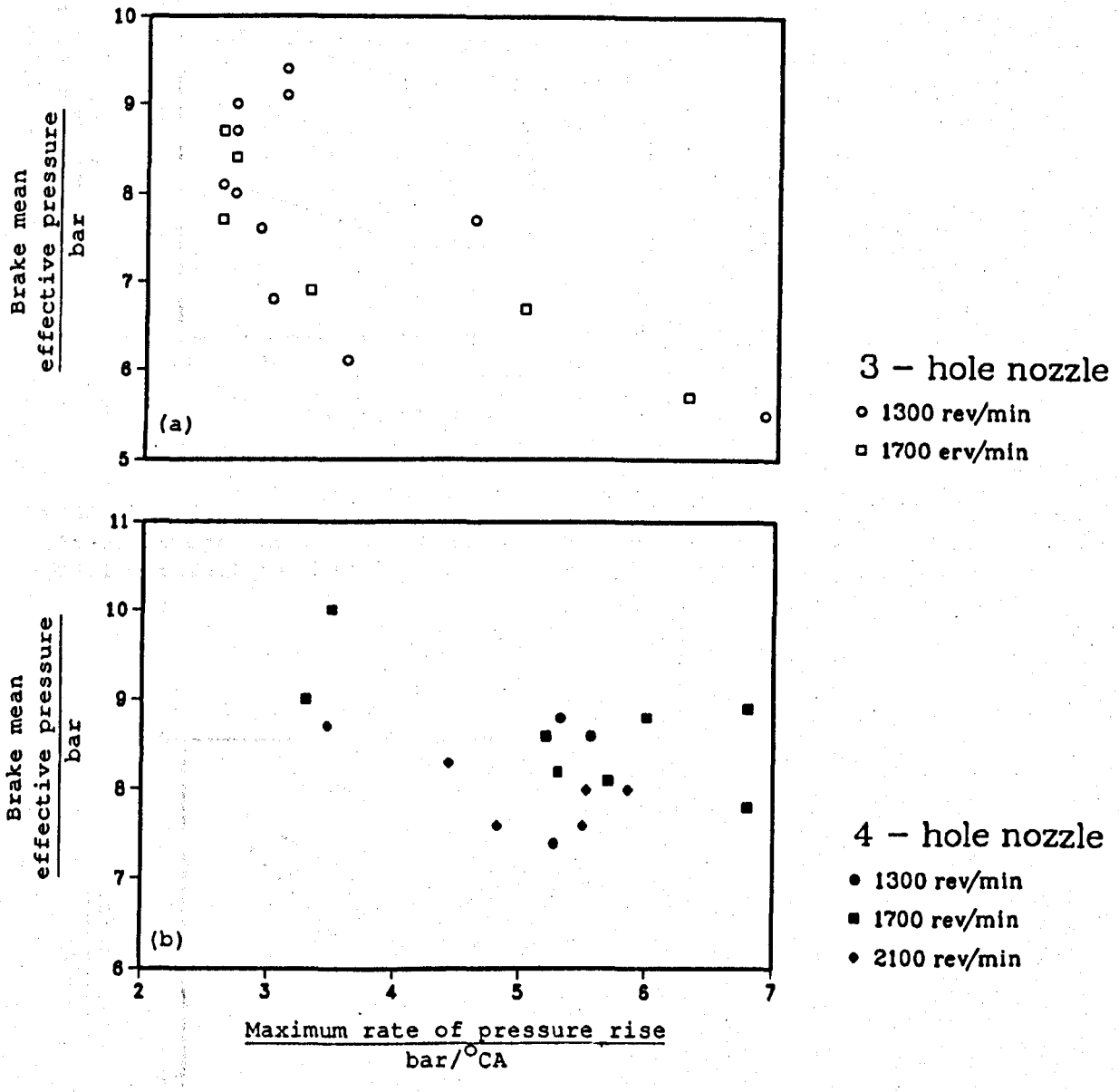

FIGURE 4.6
Effect of maximum rate of pressure rise on brake mean effective pressure: (a) Three-hole nozzle; (b) Four hole nozzle. Results from all engine tests included.

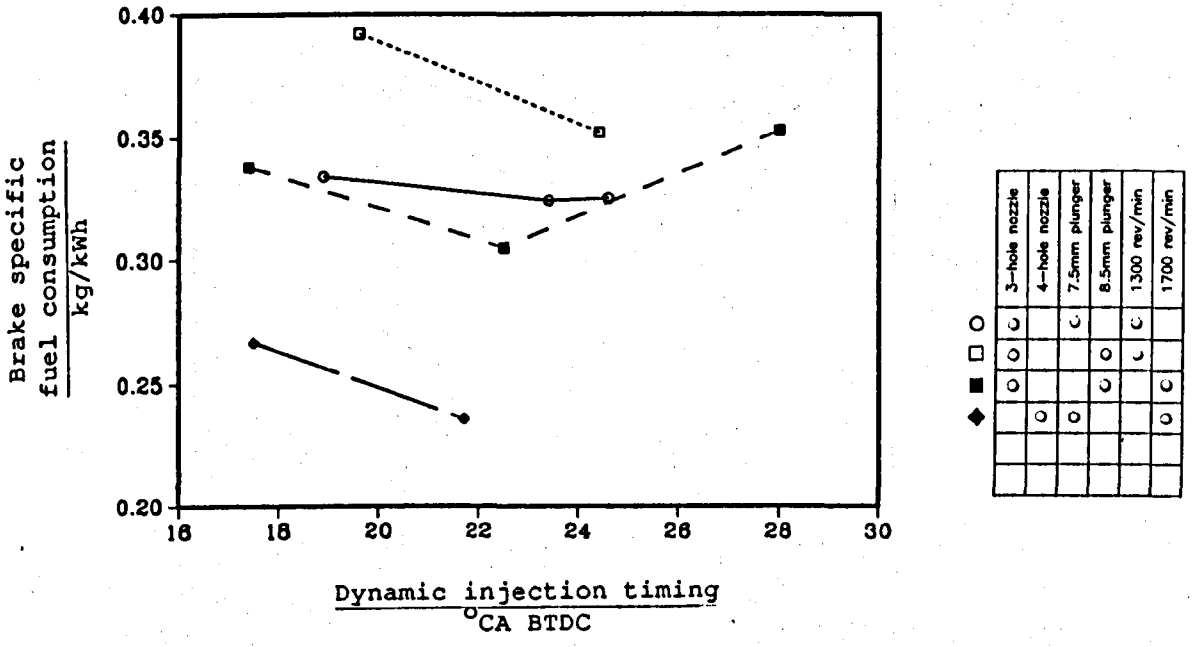

FIGURE 4.7
Effect of dynamic injection timing on brake specific fuel consumption, (25:1 air fuel ratio)

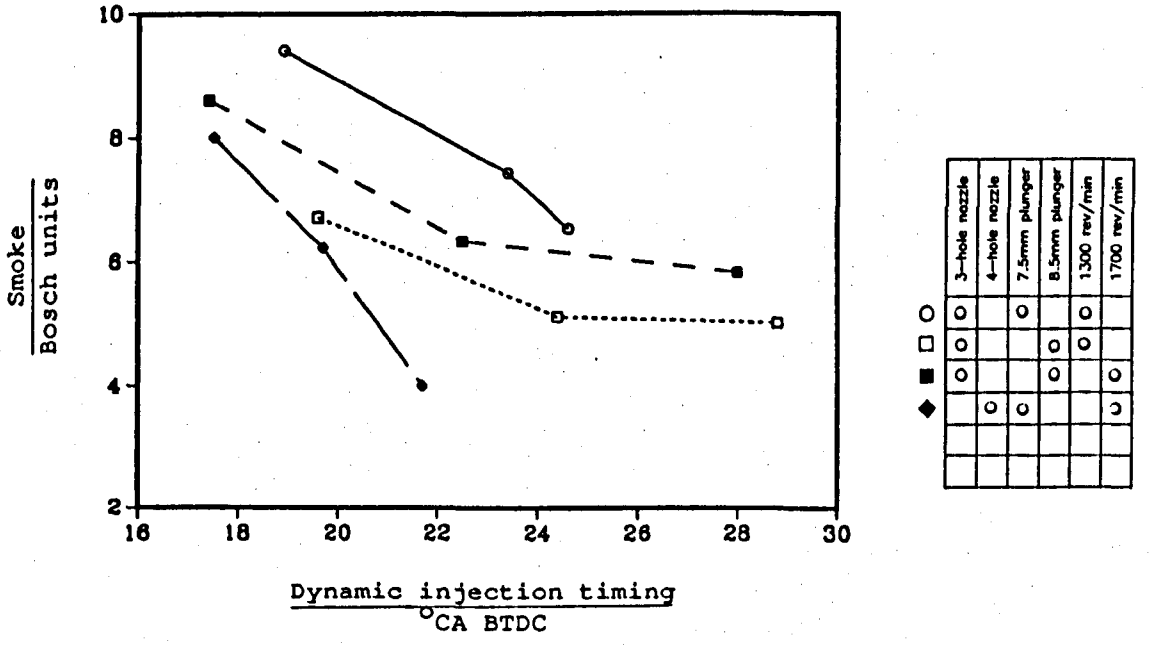

FIGURE 4.8
Effect of dynamic injection timing on exhaust smoke emission, (25:1 air fuel ratio).

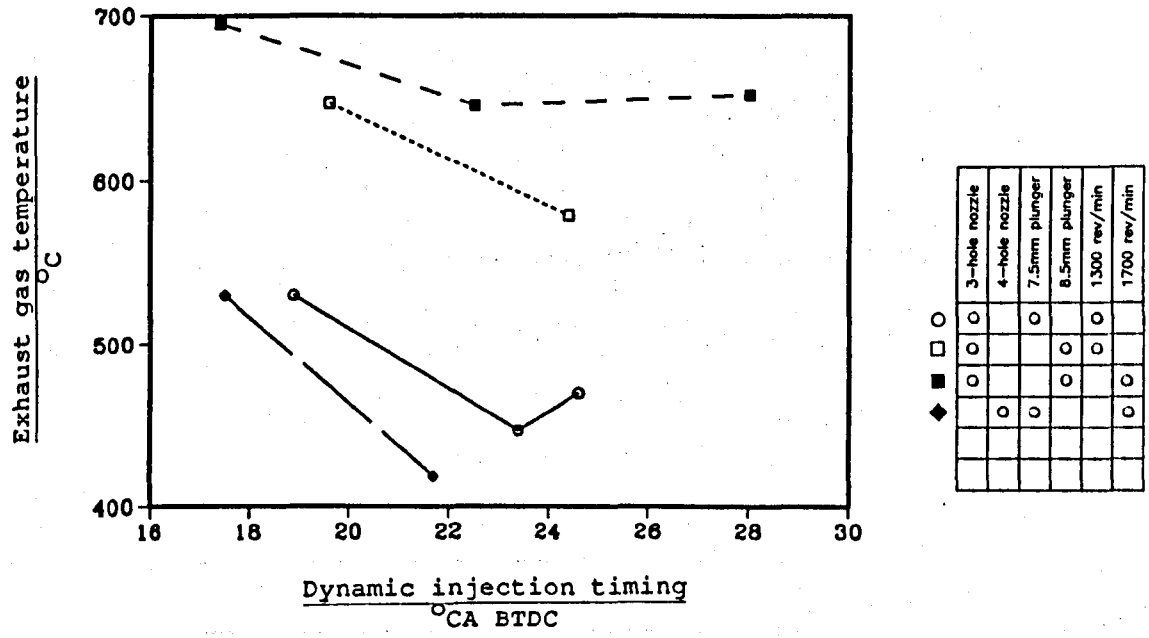

FIGURE 4.9
Effect of dynamic injection timing on exhaust gas temperature, (25:1 air fuel ratio).

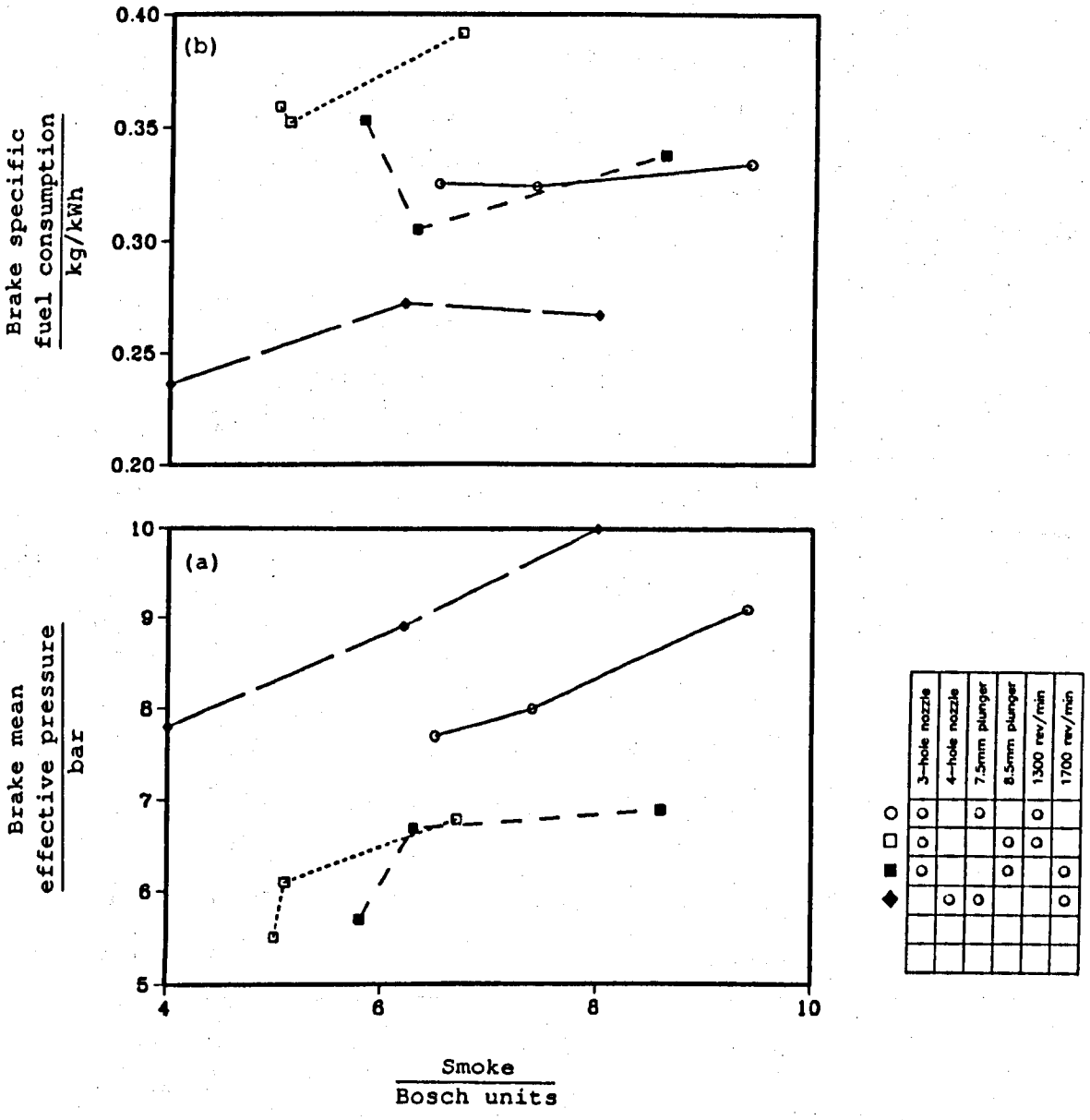

FIGURE 4.10
Tradeoffs between exhaust smoke emission and: (a) Brake mean effective pressure; (b) Brake specific fuel consumption, (constant 25:1 air fuel ratio and varying injection timing).

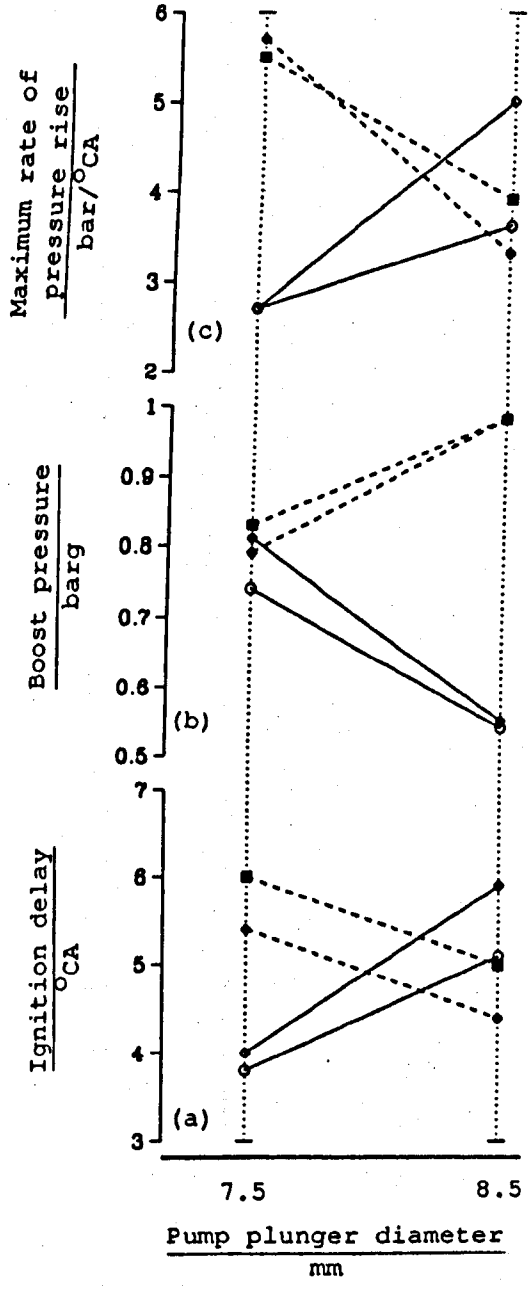

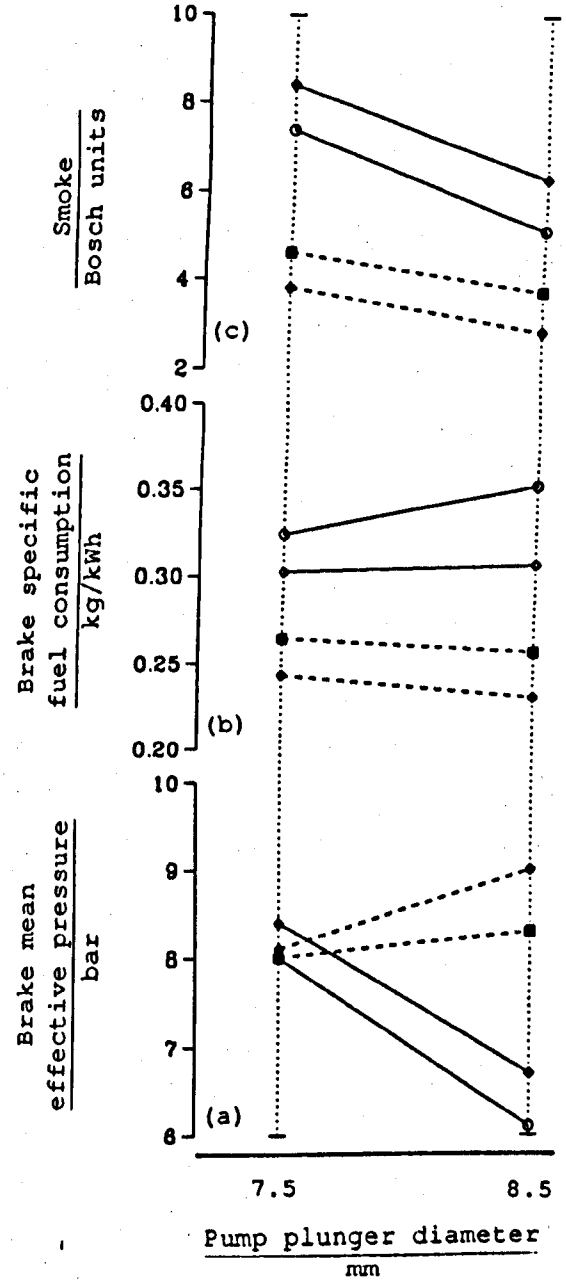

○ 3-hole nozzle, 25:1 air fuel ratio, 1300 rev/min
◇ 3-hole nozzle, 25:1 air fule ratio, 1700 rev/min
◆ 4-hole nozzle, 35:1 air fuel ratio, 1700 rev/min
■ 4-hole nozzle, 35:1 air fuel ratio, 2100 rev/min

FIGURE 4.11
Effect of increase in injection rate on: (a) ignition delay; (b) boost pressure; (c) maximum rate of pressure rise.

FIGURE 4.12
Effect of increase in injection rate on: (a) brake mean effective pressure; (b) brake specific fuel consumption; (c) smoke emission.

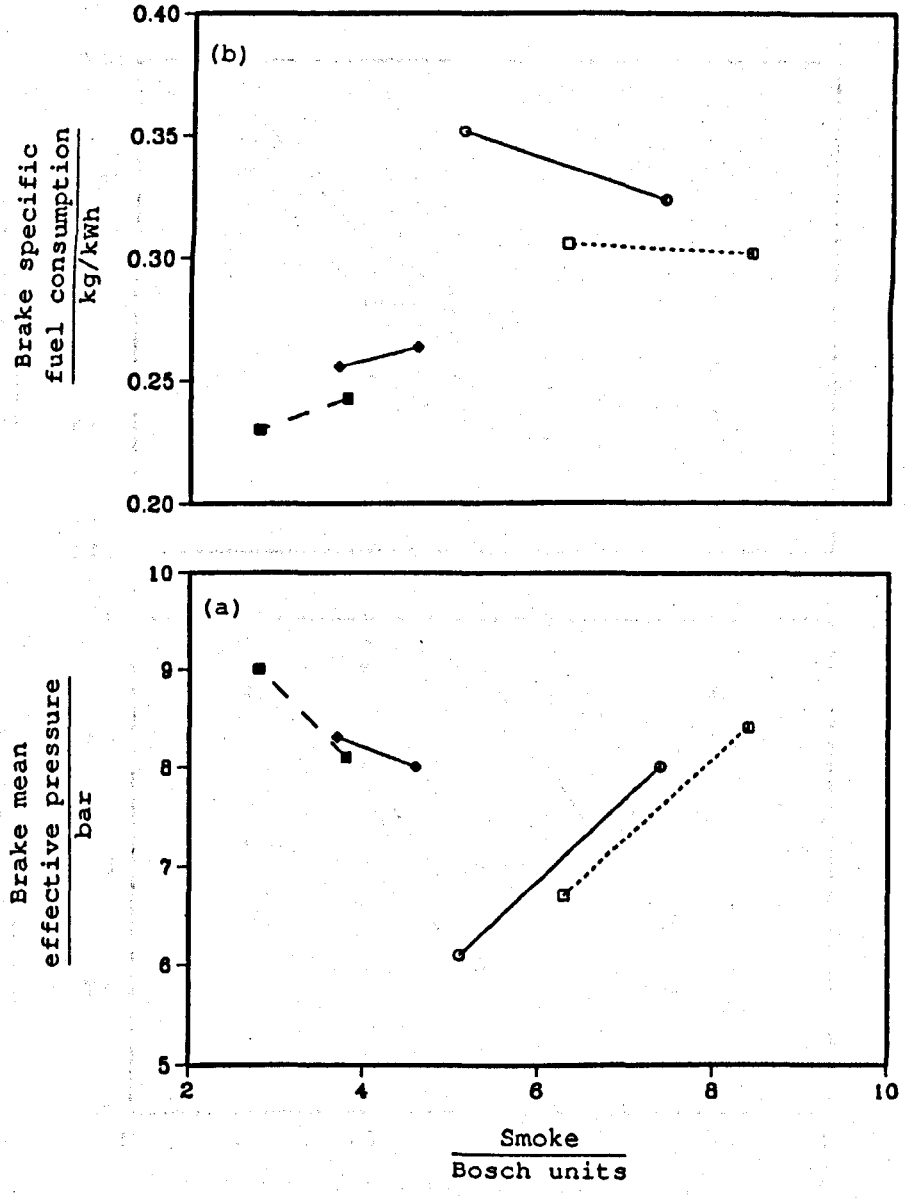

○ 3-hole nozzle, 25:1 air fuel ratio, 1300 rev/min
◇ 3-hole nozzle, 25:1 air fule ratio, 1700 rev/min
◆ 4-hole nozzle, 35:1 air fuel ratio, 1700 rev/min
■ 4-hole nozzle, 35:1 air fuel ratio, 2100 rev/min

FIGURE 4.13
Tradeoffs between exhaust smoke emission and: (a) brake mean effective pressure; (b) brake specific fuel consumption, (constant 25:1 air fuel ratio and varying injection rate).

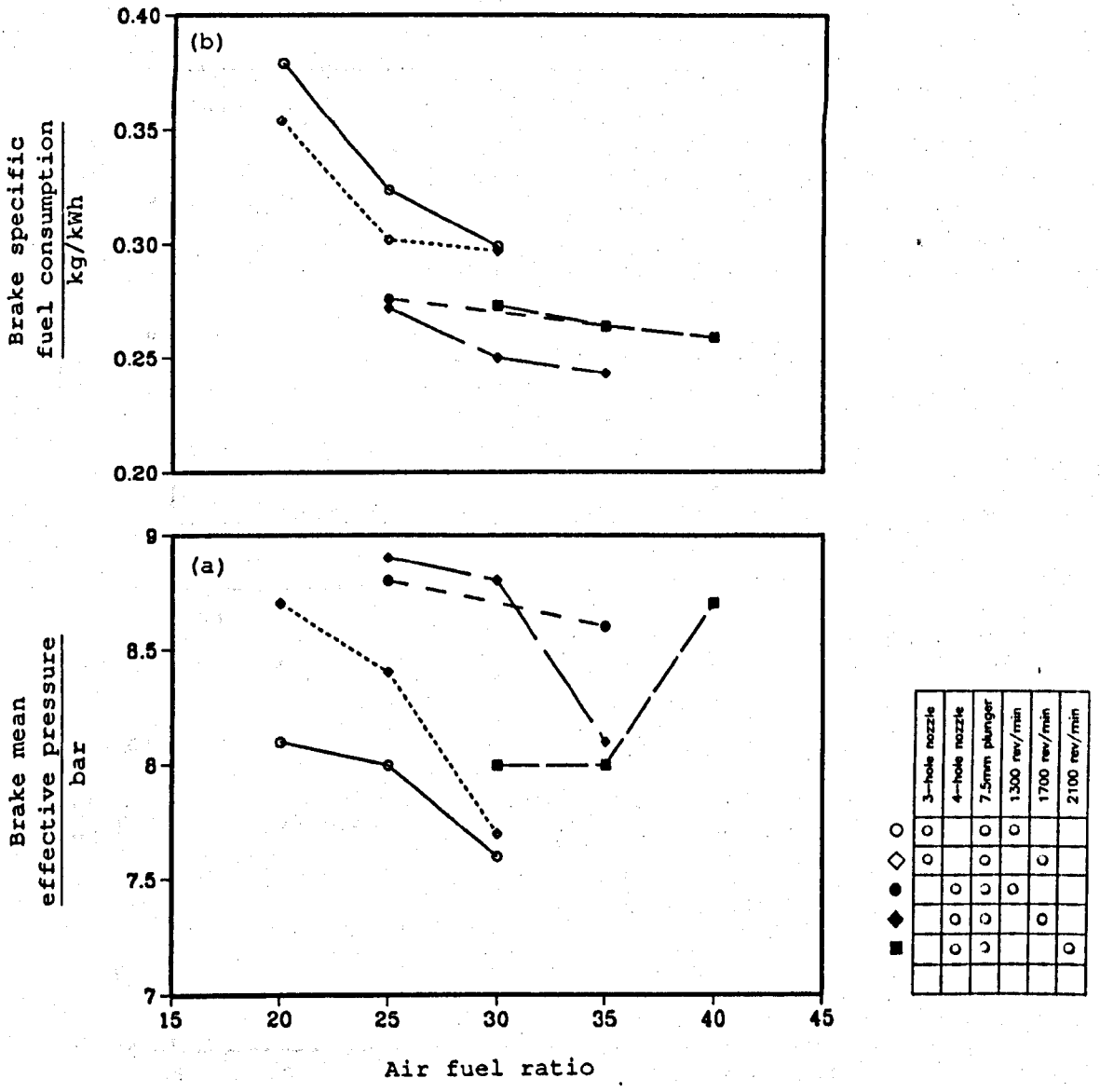

FIGURE 4.14
Effect of air fuel ratio on: (a) brake mean effective pressure; (b) brake specific fuel consumption, (constant static injection timing of 25°CA BTDC).

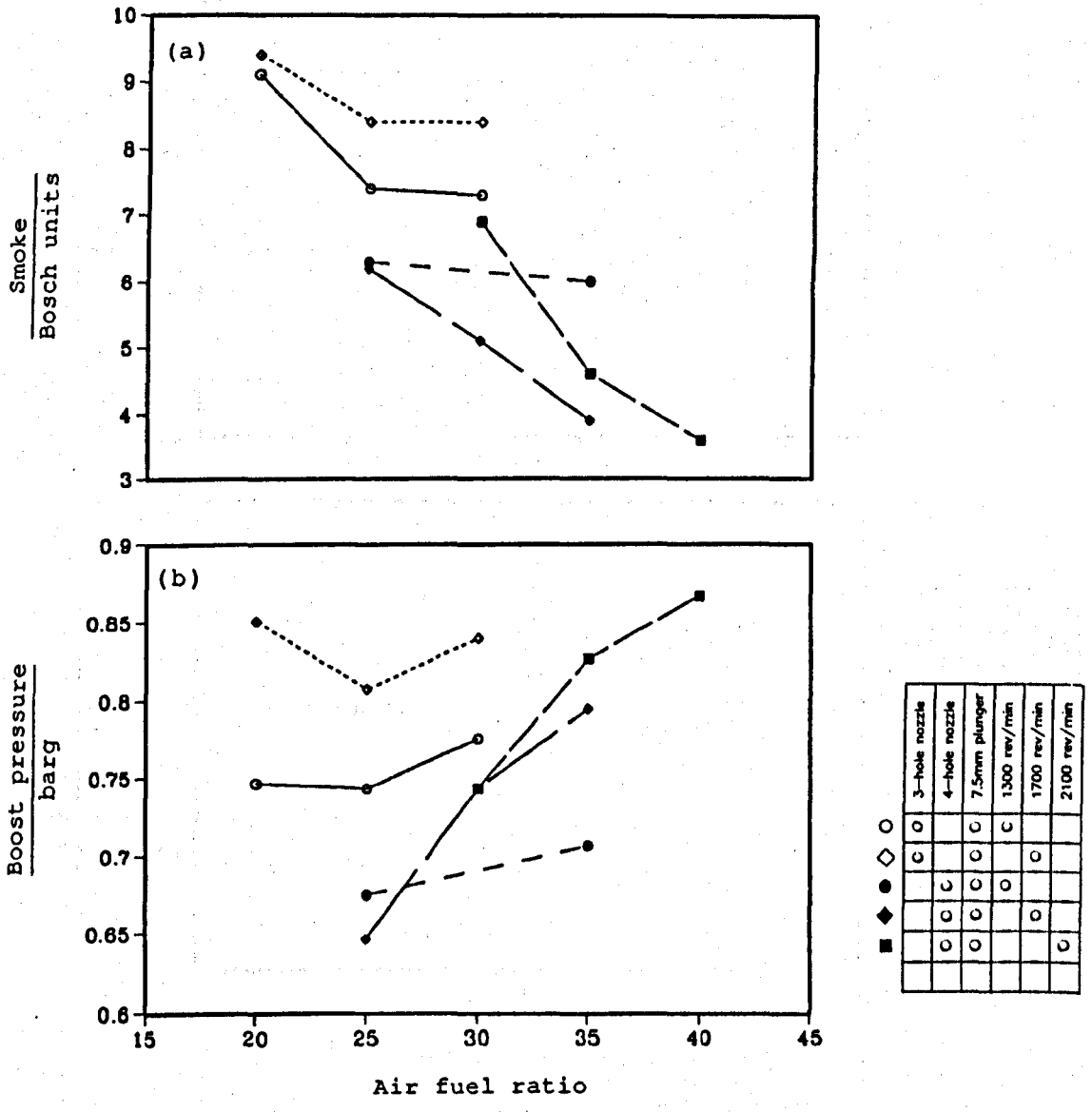

FIGURE 4.15
Effect of air fuel ratio on: (a) exhaust smoke emission; (b) boost pressure, (constant static injection timing of 25°CA BTDC).

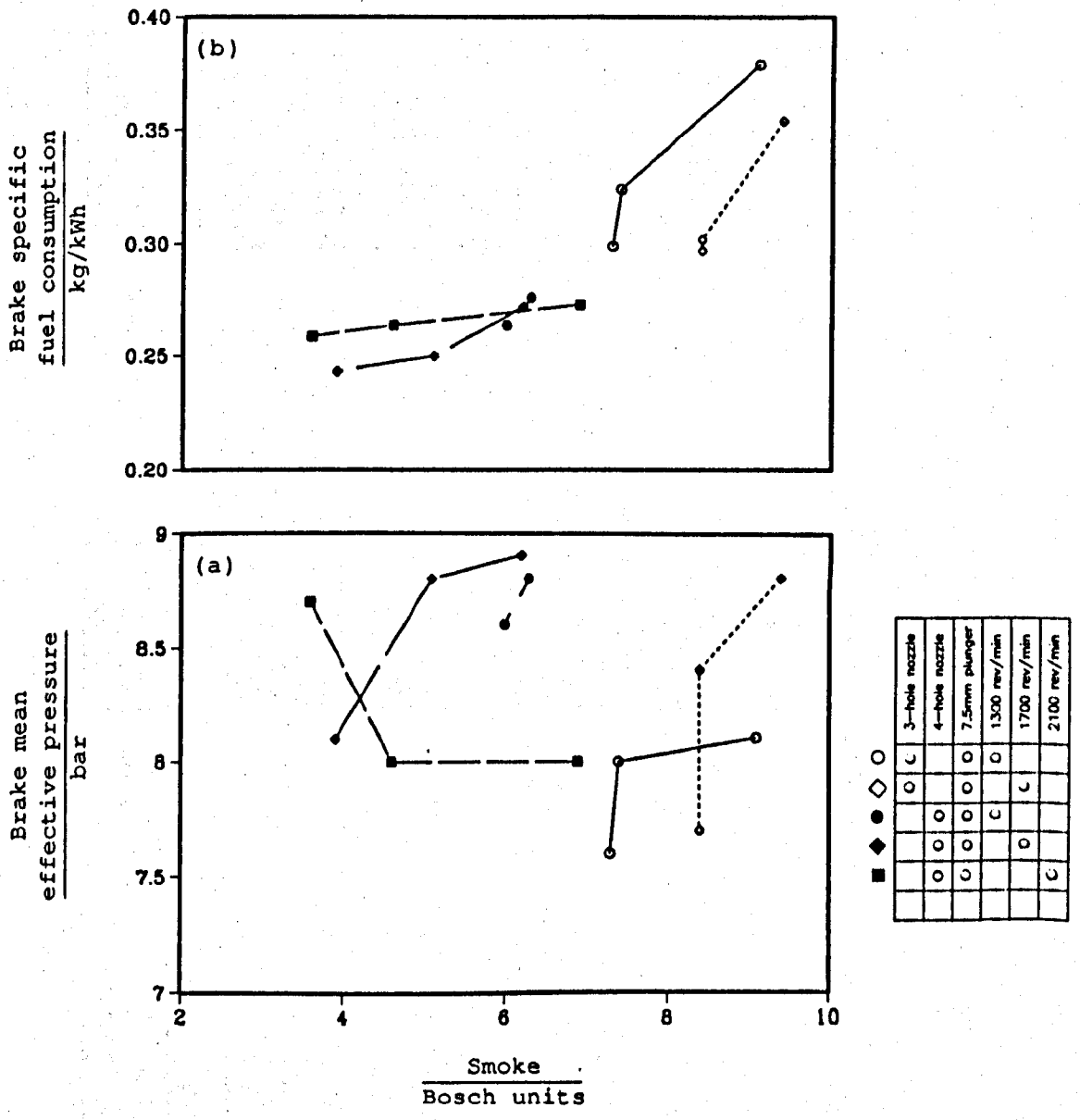

FIGURE 4.16
Tradeoffs between exhaust smoke emission and: (a) brake mean effective pressure; (b) brake specific fuel consumption, (constant static injection timing of 25°CA BTDC and varying air fuel ratio).

FIGURE 4.17
Comparison of engine performance parameters with and without intercooling at 1300 and 1700 rev/min with three-hole nozzle, 7.5mm pump plunger, 25:1 air fuel ratio, and static injection timing of 25°CA BTDC.

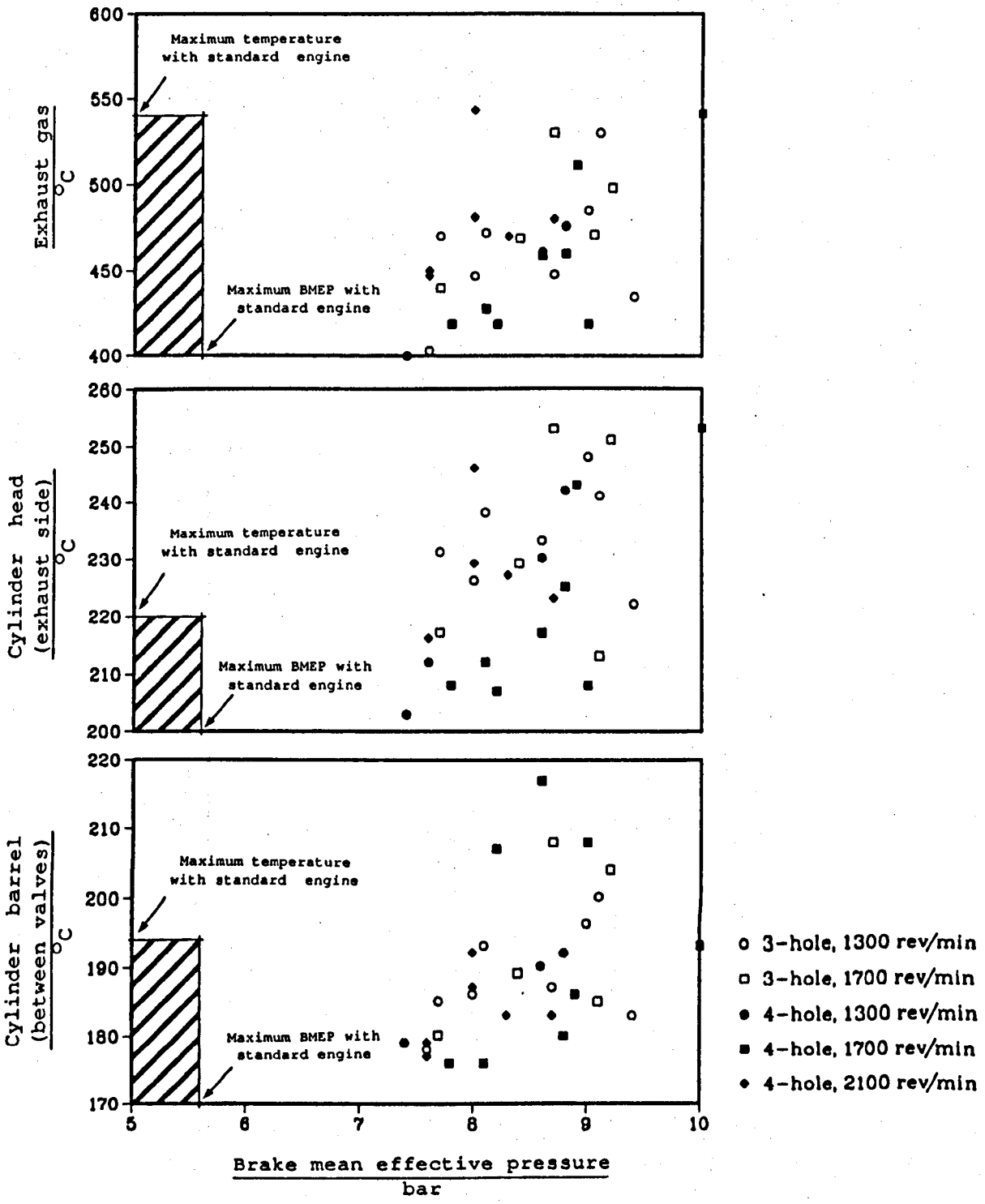

FIGURE 4.18
Effect of brake mean effective pressure on engine temperature at a number of locations, (results from all engine tests included).

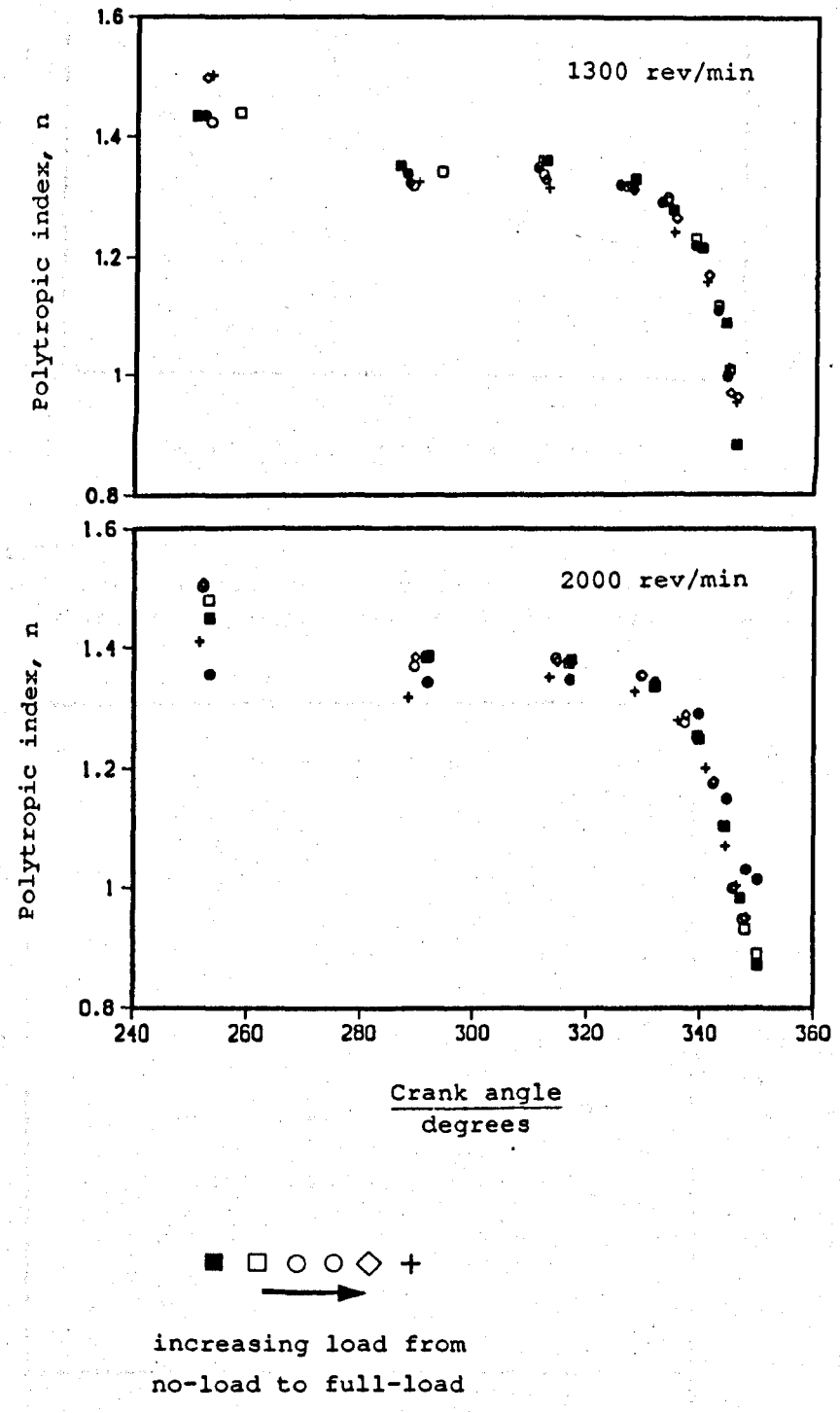

FIGURE 4.19
Variation of the polytropic index with crank angle during the compression stroke.

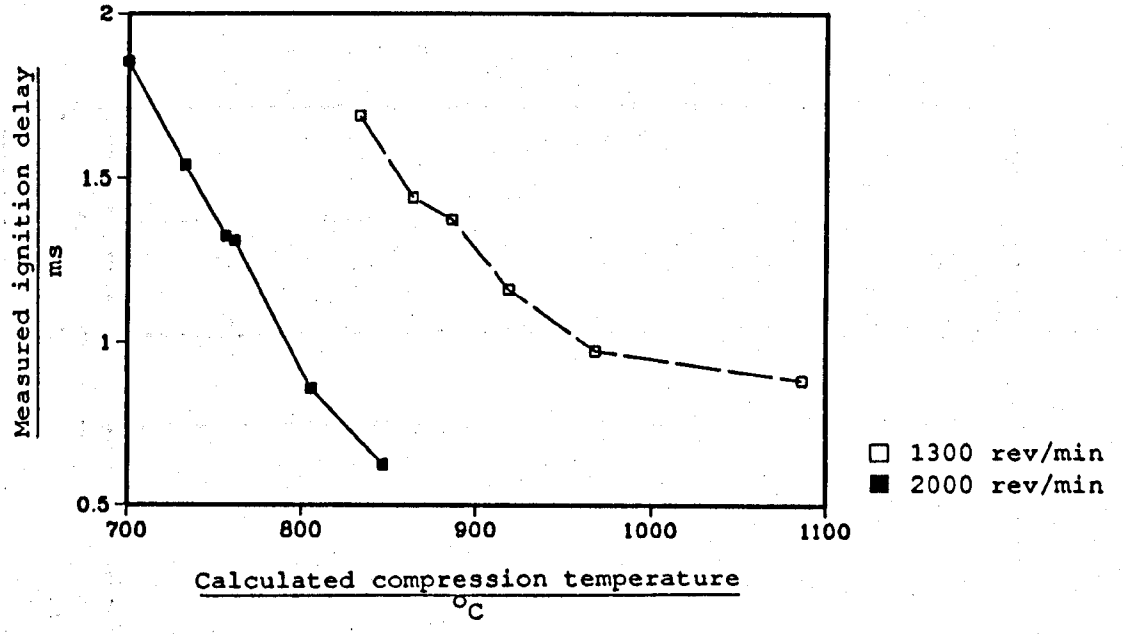

FIGURE 4.20
Relation between estimated compression temperature and measured ignition delay, (increasing engine load at constant speeds of 1300 and 2000 rev/min).

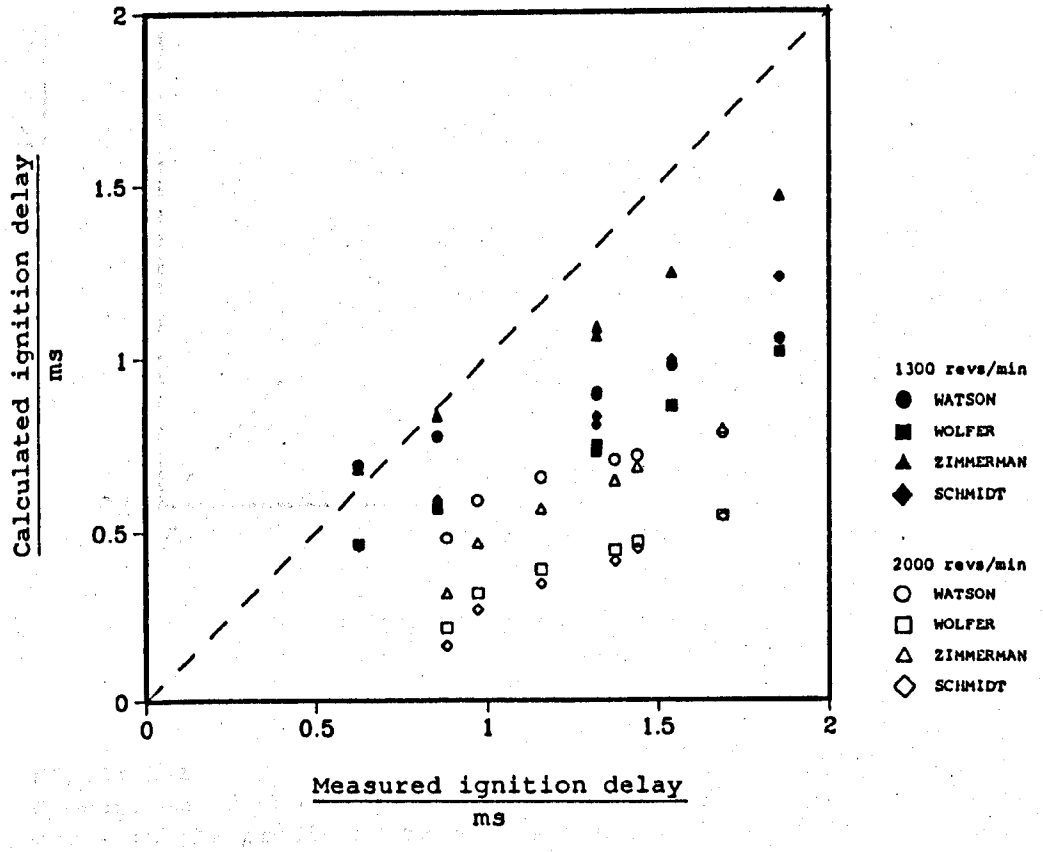

FIGURE 4.21
comparison between measured and calculated ignition delays.

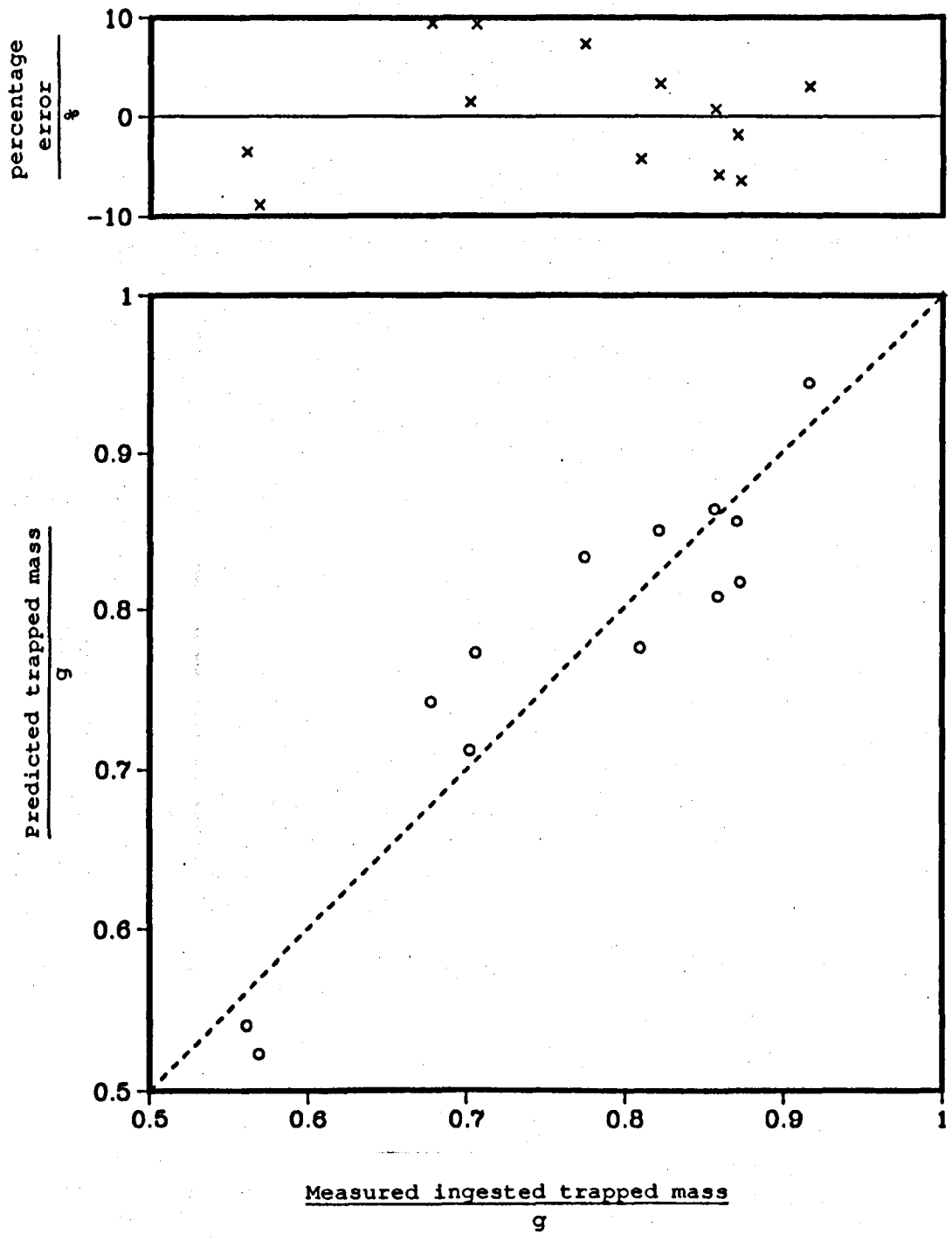

FIGURE 5.1
Comparison of the measured and the predicted trapped air mass, and the error in the predicted trapped air mass.

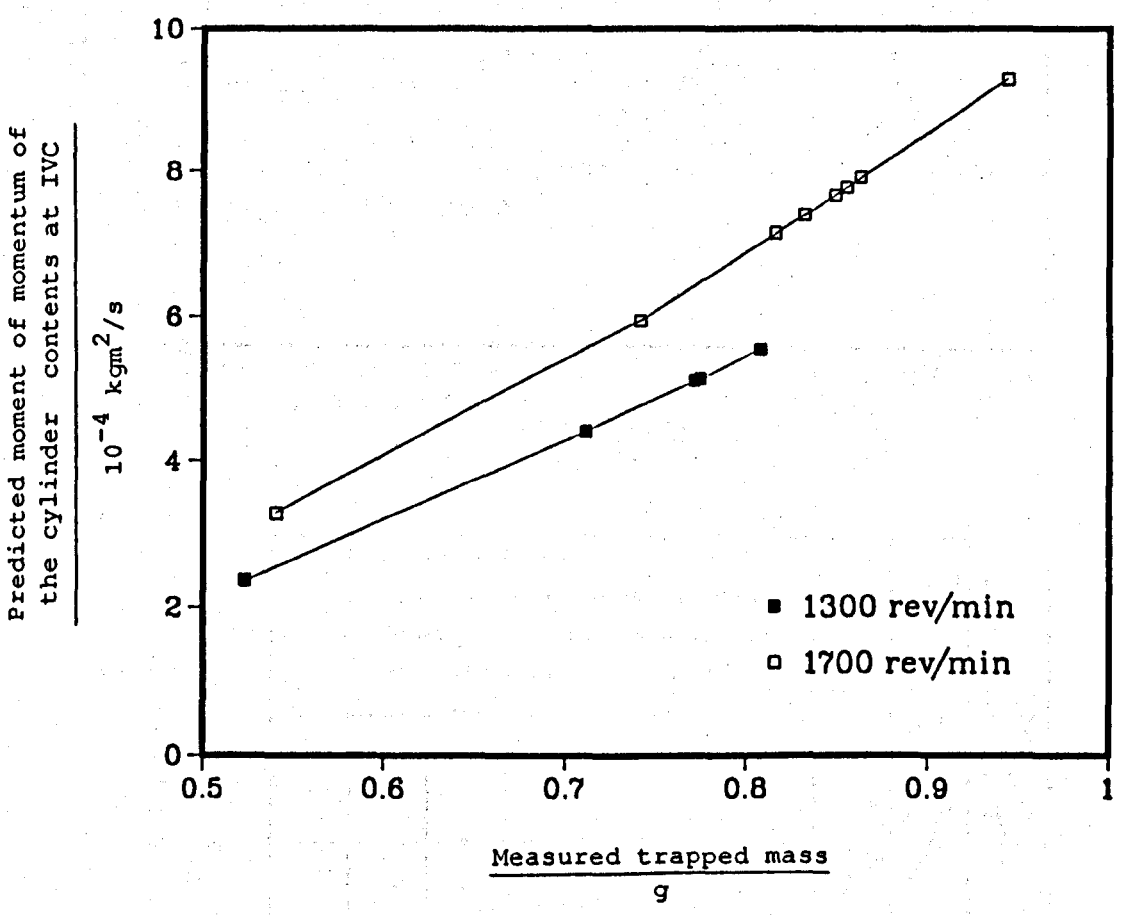

FIGURE 5.2
Relation between the predicted trapped air mass and the predicted total moment of momentum of the cylinder contents at inlet valve closure.

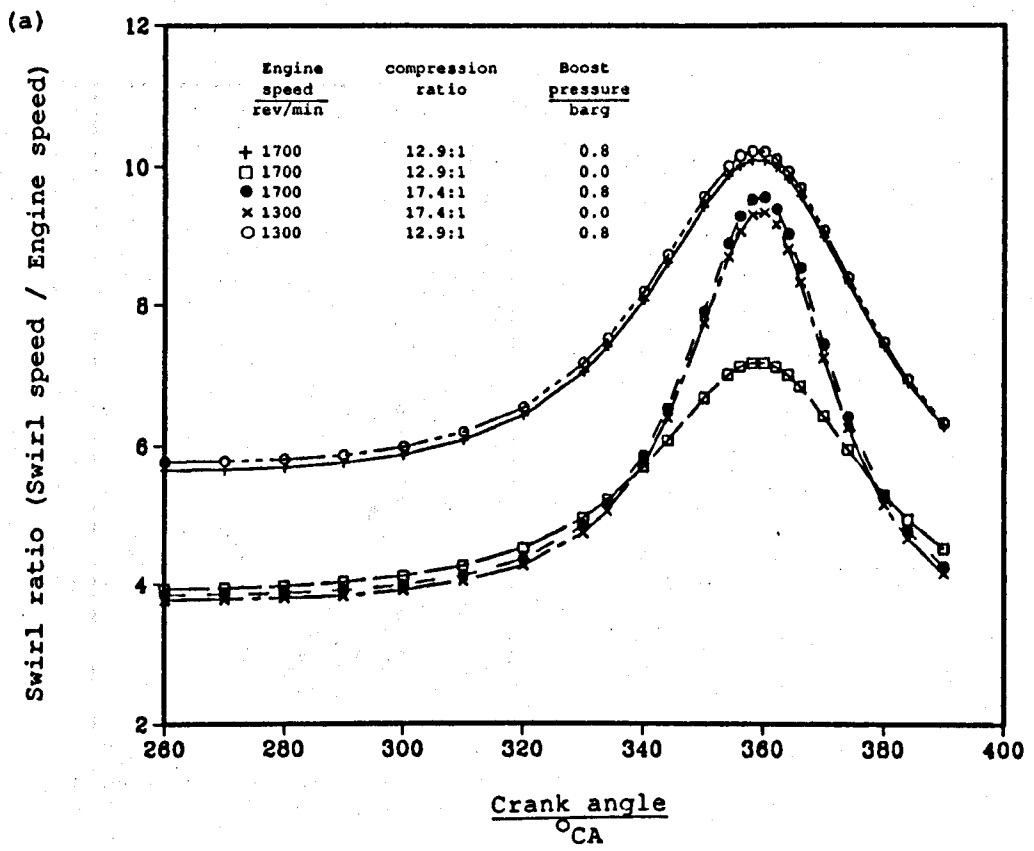

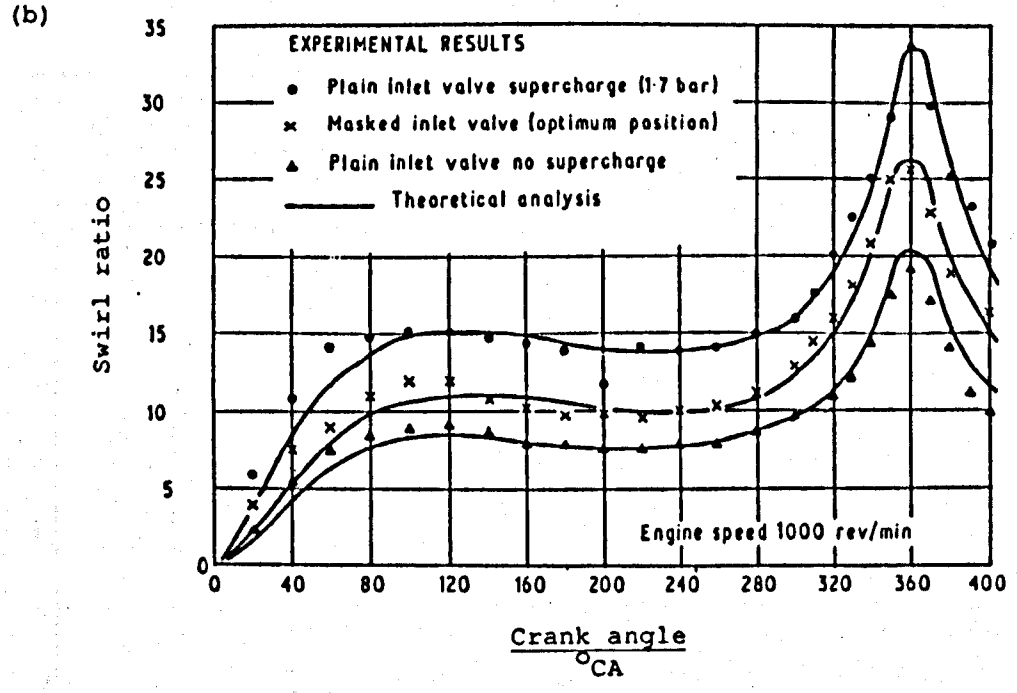

FIGURE 5.3
(a) Variation of the predicted swirl ratio of the trapped air during compression for the Lister engine, (b) variation of the swirl ratio during compression for the engine used by Dent and Derham (1974).

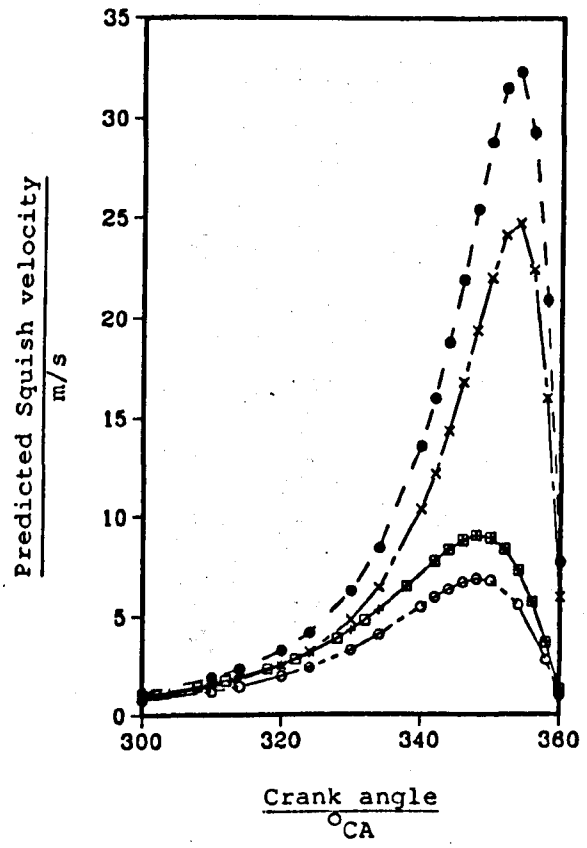

(a)

Engine speed rev/min	compression ratio	Boost pressure barg
+ 1700	12.9:1	0.8
□ 1700	12.9:1	0.0
● 1700	17.4:1	0.8
× 1300	17.4:1	0.0
○ 1300	12.9:1	0.8

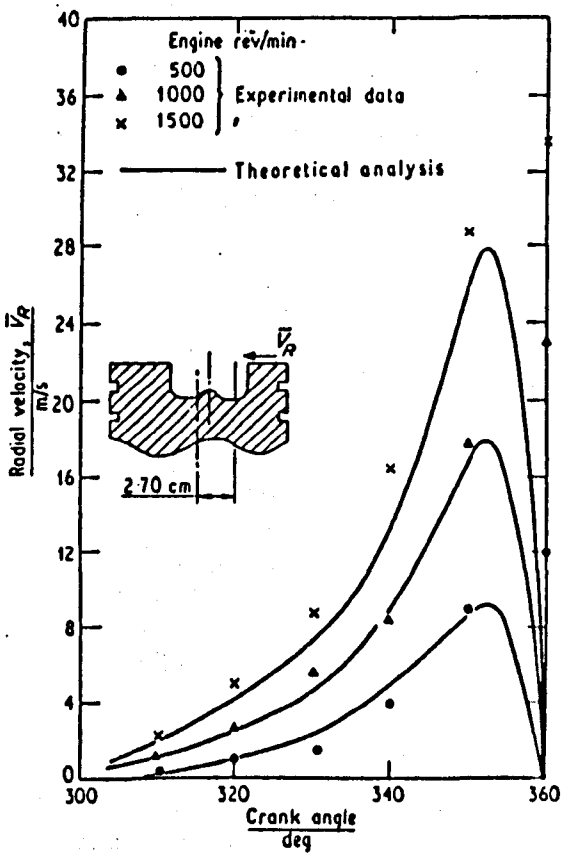

(b)

FIGURE 5.4
(a) Variation of the predicted air squish velocity during compression for the Lister engine, (b) variation of the squish velocity during compression for the engine used by Dent and Derham (1974).

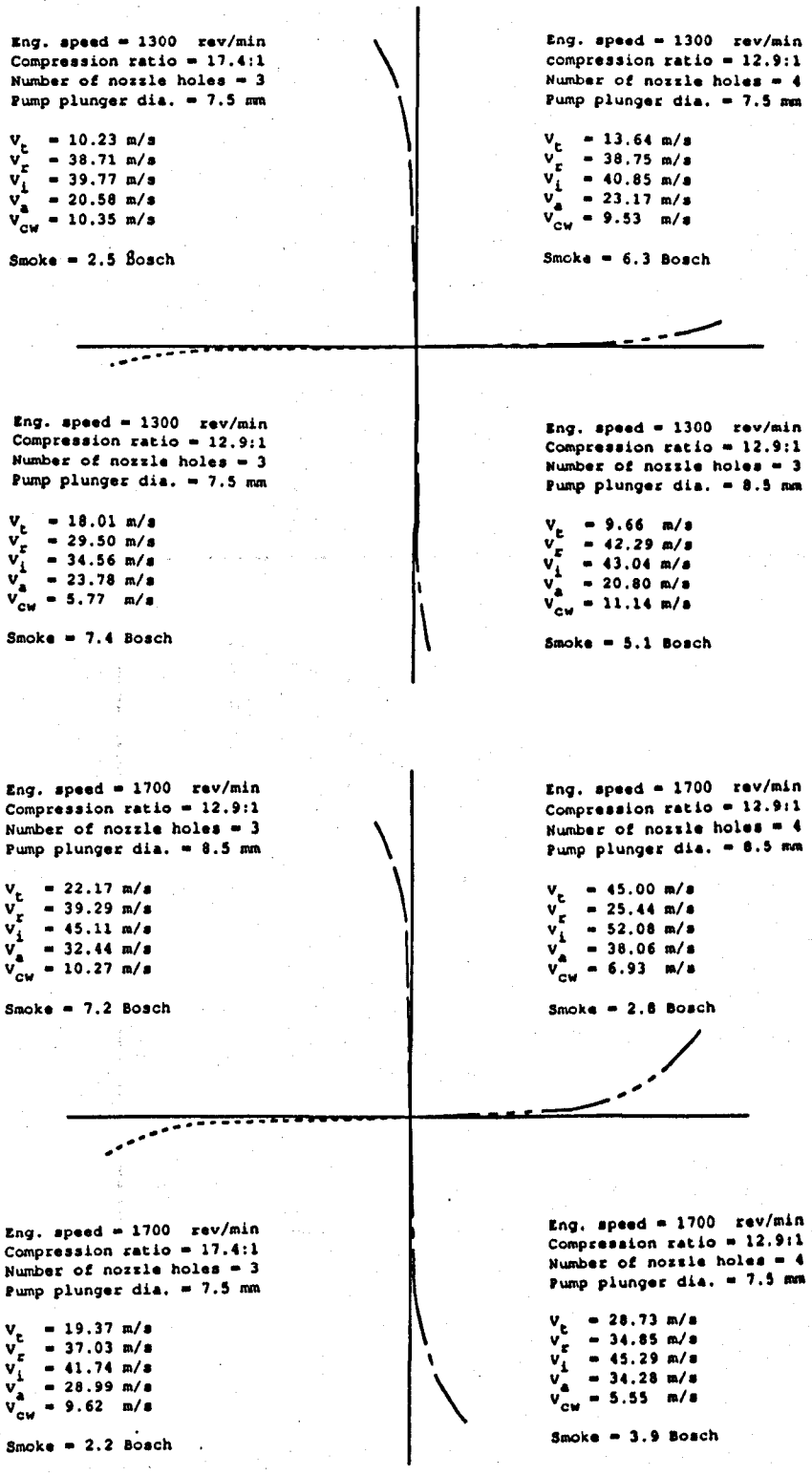

FIGURE 5.5
Predicted fuel spray tip trajectories at different engine running conditions.

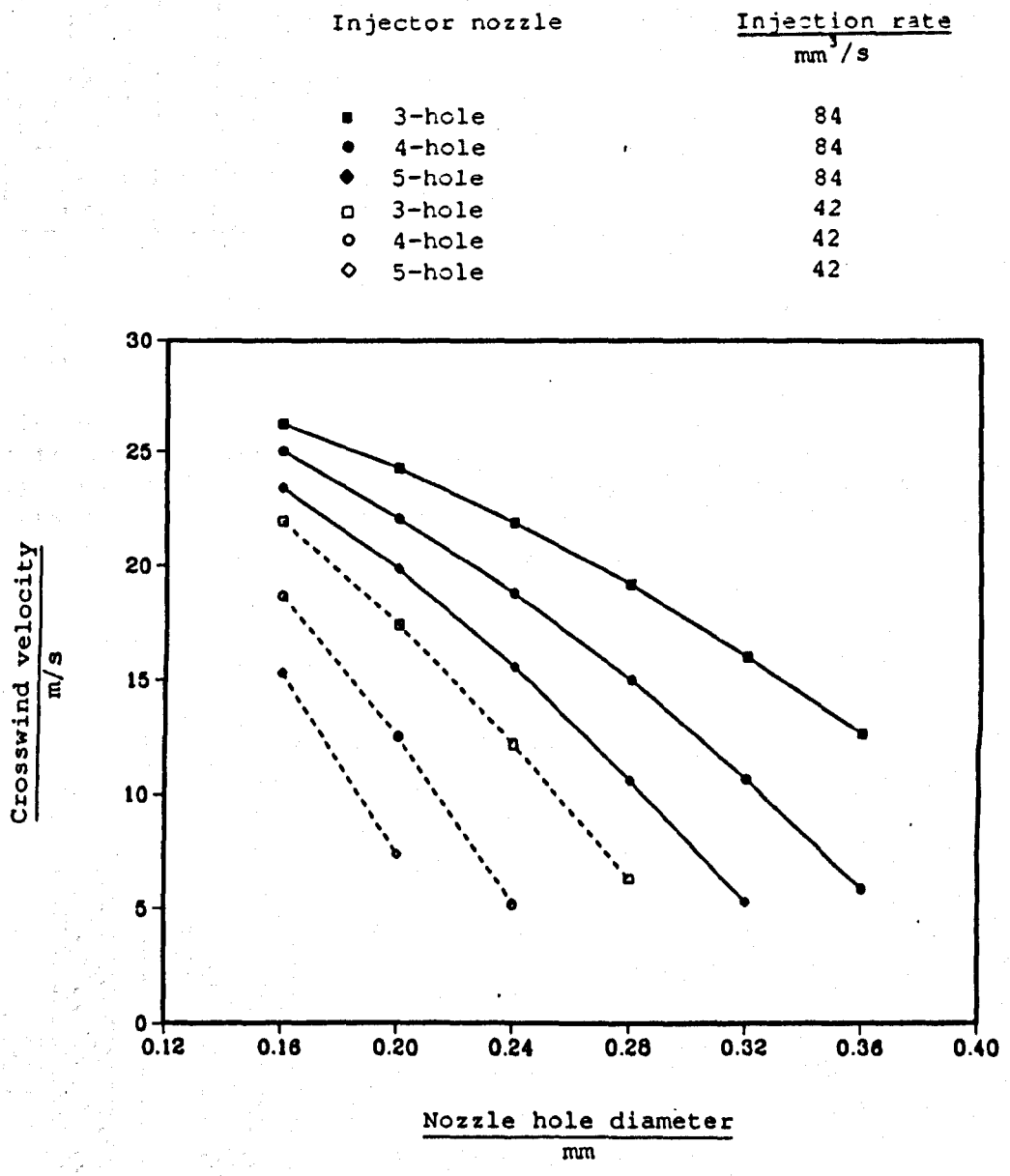

FIGURE 5.6
Effects of injector nozzle hole diameter, number of nozzle holes, and injection rate on crosswind velocity for the Lister engine; engine speed 2000 rev/min.

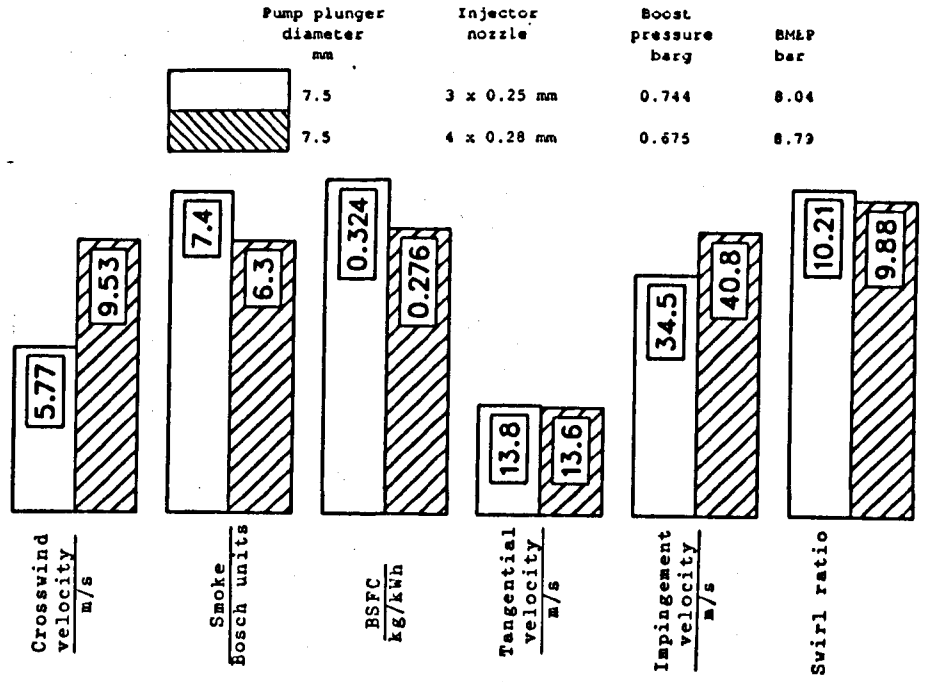

FIGURE 5.7
Results from the Lister engine tests at the low compression ratio (12.9:1) showing the effect on crosswind velocity and other performance parameters of the change in the injector nozzle from the 3-hole to the 4-hole unit; engine speed 1300 rev/min, air fuel ratio 25:1.

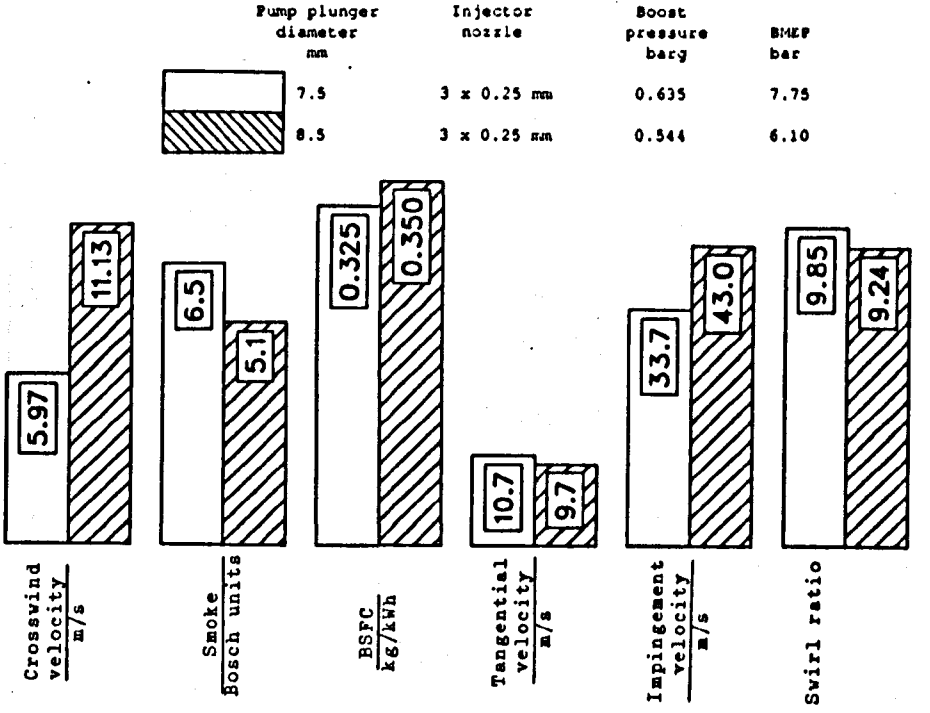

FIGURE 5.8
Results from the Lister engine tests at the low compression ratio (12.9:1) showing the effect on crosswind velocity and other performance parameters of an increase in the injection rate; engine speed 1300 rev/min, air fuel ratio 25:1.

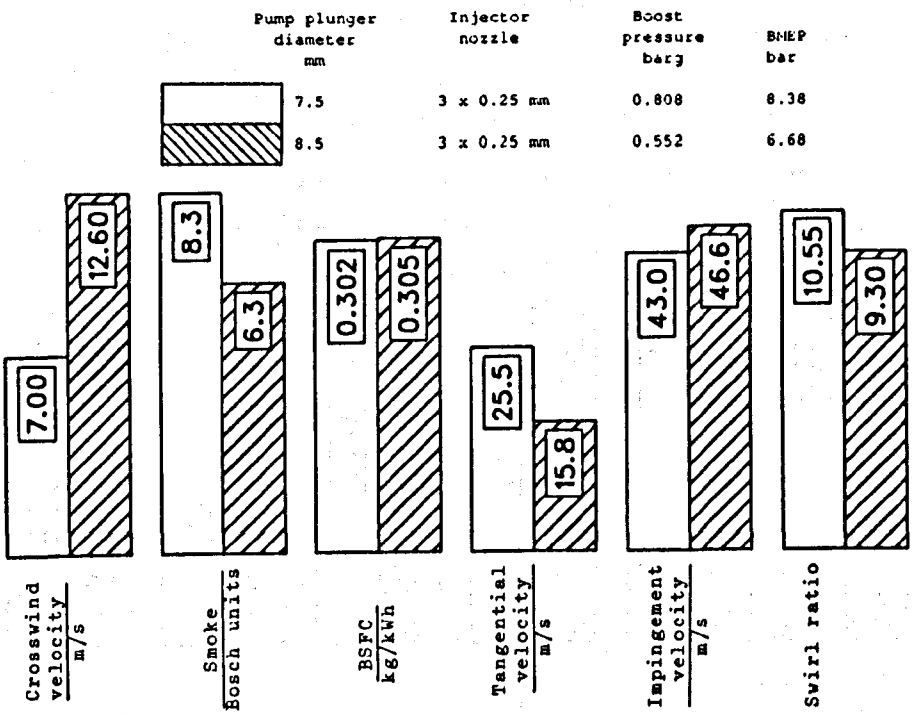

FIGURE 5.9
Results from the Lister engine tests at the low compression ratio (12.9:1) showing the effect on crosswind velocity and other performance parameters of an increase in the injection rate; engine speed 1700 rev/min, air fuel ratio 25:1.

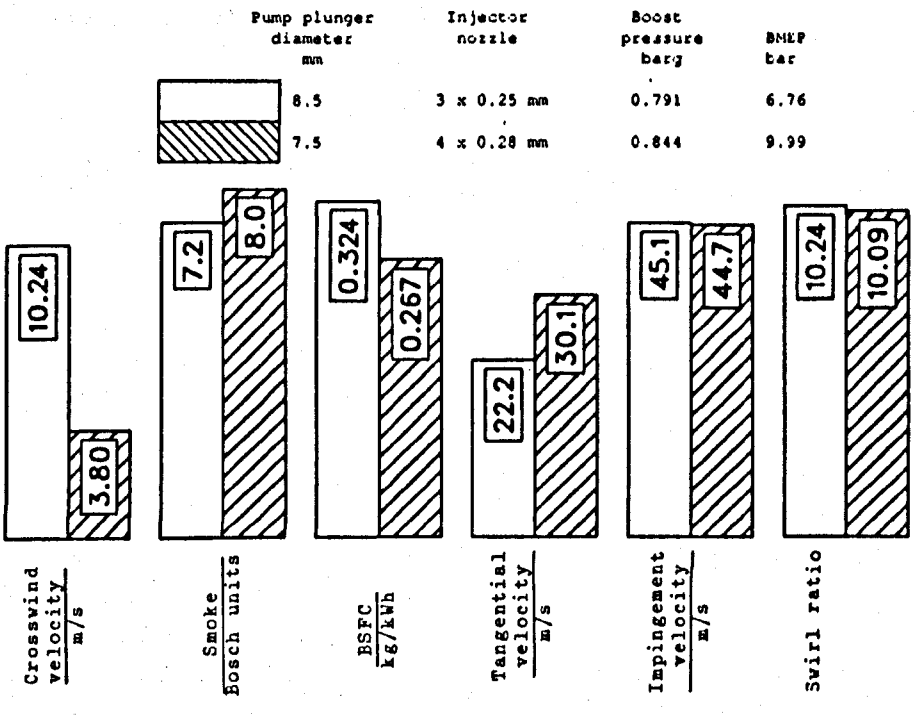

FIGURE 5.10
Results from the Lister engine tests at the low compression ratio (12.9:1) showing the effect on crosswind velocity and other performance parameters of changes in the injection rate and in the injector nozzle from the 3-hole to the 4-hole unit; engine speed 1700 rev/min, air fuel ratio 25:1.

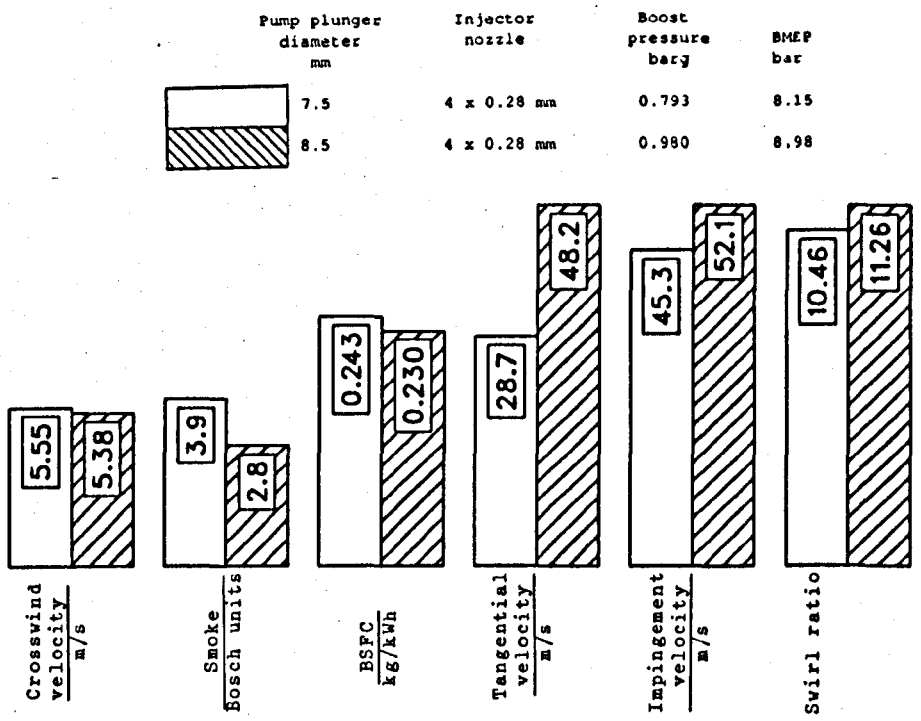

FIGURE 5.11
Results from the Lister engine tests at the low compression ratio (12.9:1) showing the effect on crosswind velocity and other performance parameters of an increase in the injection rate; engine speed 1700 rev/min, air fuel ratio 35:1.